PHENOMENOLOGICAL ASPECTS OF MODULAR SYMMETRY ON NEUTRINO MASS MODELS

MITESH KUMAR BEHERA

SCHOOL OF PHYSICS
UNIVERSITY OF HYDERABAD
SEPT, 2022

I dedicate this thesis to my family for extending their trust, love and affection.

हैदराबाद विश्वविद्यालय

University of Hyderabad

प्रतिष्ठित संस्थान

INSTITUTION OF EMINENCE

राष्ट्रीय अपेक्षाएँ, वैश्विक मानक

National Needs, Global Standards

Phenomenological aspects of modular symmetry on neutrino mass models

By

MITESH KUMAR BEHERA

REGD. NO. 17PHPH02

School of Physics
UNIVERSITY OF HYDERABAD
Hyderabad-500046, INDIA

A dissertation submitted to the University of Hyderabad in accordance with the requirements of the degree of DOCTOR OF PHILOSOPHY in the School of Physics.

SEPTEMBER 9, 2022

AUTHOR'S DECLARATION

I hereby declare that, this thesis titled **Phenomenological aspects of modular symmetry on neutrino mass models** submitted by me, under the guidance and supervision of **Prof. Rukmani Mohanta**, is a bonafide research work and is free from plagiarism. I also declare that it has not been submitted previously, in part or in full to this University or any other University or Institution, for the award of any degree or diploma. I hereby agree that my thesis can be deposited in Shodhganga/INFLIBNET.

A report on plagiarism statistics from the University Librarian is enclosed.

DATE: 09/09/2022

PLACE: HYDERABAD

MITESH KUMAR BEHERA

REGD. NO. 17PHPH02

CERTIFICATE

This is to certify that the thesis entitled **Phenomenological aspects of modular symmetry on neutrino mass models** submitted by **Mitesh Kumar Behera** bearing registration number **17PHPH02** in partial fulfilment of the requirements for award of Doctor of Philosophy in the School of Physics is a bonafide work carried out by him under my supervision and guidance.

This thesis is free from plagiarism and has not been submitted previously in part or in full to this or any other University or Institution for award of any degree or diploma.

Further, the student has the following publications before the submission of the thesis for adjudication.

[1] **M. K. Behera**, S. Mishra, S. Singirala and R. Mohanta, **"Implications of A_4 modular symmetry on Neutrino mass, Mixing and Leptogenesis with Linear Seesaw",**
Phys. Dark Univ. **36** (2022), 101027 doi:10.1016/j.dark.2022.101027 [arXiv:2007.00545 [hep-ph]].

[2] **M. K. Behera**, S. Singirala, S. Mishra and R. Mohanta,
"A modular A_4 symmetric scotogenic model for neutrino mass and dark matter",
J. Phys. G **49**, no.3, 035002 (2022) doi:10.1088/1361-6471/ac3cc2 [arXiv:2009.01806 [hep-ph]].

[3] **M. K. Behera** and R. Mohanta, **"Inverse seesaw in A_5' modular symmetry",**
J. Phys. G **49**, no.4, 045001 (2022) doi:10.1088/1361-6471/ac4d7a [arXiv:2108.01059 [hep-ph]].

[4] **M. K. Behera** and R. Mohanta, **"Linear Seesaw in A_5' Modular Symmetry With Leptogenesis",** Front. in Phys. **10**, 854595 (2022) doi:10.3389/fphy.2022.854595 [arXiv:2201.10429 [hep-ph]].

Certificate

Further, the student has passed the following courses towards fulfilment of coursework requirement for Ph.D:

Course Code	Name	Credits	Pass/Fail
PY801	Research Methodology	4	Pass
PY802	Advanced Quantum Mechanics	4	Pass
PY803	Advanced Experimental Techniques	4	Pass
PY804	Advanced Condensed Matter Physics	4	Pass

Rukmani Mohanta

Prof. Rukmani Mohanta

Thesis Supervisor

School of Physics

University of Hyderabad

Dr. Rukmani Mohanta
Professor
School of Physics
UNIVERSITY OF HYDERABAD
Hyderabad-500 046.

Date: 8/9/2022

Prof. K.C. James Raju

Dean

School of Physics

University of Hyderabad

DEAN
School of Physics
University of Hyderabad
HYDERABAD - 500 046

ACKNOWLEDGEMENTS

Procuring a doctorate and transcribing a dissertation is an extensive and challenging job, moreover, it is not done single handedly. It is quite regular to chalk down acknowledgements by declaring that there are an excessive number of obligations to reimburse but for me its a heartfelt emotion to express towards the people who were there with me in my journey. Firstly, I would like to express my deepest gratitude to my supervisor Prof. Rukmani Mohanta who has been a pinnacle of patience, perseverance, knowledge and wisdom guiding me in many unknown ways. I am not only getting a doctoral degree under her guidance but certain lessons for life too.

If supervisor is on one side of the balance scale than doctoral committee is on the other side of it, which kept my doctoral tenure on track. My committee members Dr. Soma Sanyal and Dr. Barilang Mawlong played a significant role by providing valuable comments and advice which impacted my research work extensively. They are without a doubt incredible scholarly investors: both of them are so rich mentally that no extra increase from this venture would appears to be ideal under conventional guidelines. Their intellect and perspective has helped me see things in a different light. I would like to express my thankfulness towards their support and motivation throughout.

It is well known that some people impact our lives passively, hence, I would like to extend my gratitude to Dean, SOP Prof. K.C. James Raju, our former Deans Prof. Ashok Chaterjee, Prof. V. Seshubai and Prof. Bindu A. Bambah. In addition, I would express my indebtedness to faculties with whom my interaction was for short period but impactful, they are, Prof. E. Harikumar, Prof. P. K. Suresh, Prof. Surajit Dhara, Prof. S. Srinath, Prof. Nirmal Kumar Viswanathan, Prof. P. Anantha Laxmi, Prof. Ashok Vudayagiri, Prof. B.V.R Tata, Dr. Pratap Kollu and others. A research scholar during his / her tenure financially survives on the fellowship/grants, for availing the facility the help was extended by administration officials of our physics department and institute. So I would like to thank Mr. Sudarshan, Ms. Sashikala, Mrs. Deepika, Mrs. Shailaja and Mr. Prashad for their assistance in all respects.

Producing some original work requires a lot of contemplations, discussions and literature survey. In this regard, I am deeply thankful to my seniors, Dr. Suchismita Sahoo, Dr. Soram Robertson Singh, Dr. Shivaramakrishna Singirala, Dr. Subhasmita Mishra and Dr. Monojit Ghosh from whom I learnt many things that helped me gain profound insights while working on different research problem. Their unremitting support, encouragement and non-judgemental behaviour helped me ask even the silliest question with fearlessness.

Acknowledgements

As research scholars we spend a substantial amount of time in our theoretical laboratories learning and deducing things for our research problems in order to simulate certain results. Therefore, having a healthy work environment is very essential because it impacts one's productivity, encourages risk taking, inspires creativity, broadens cooperation which in short contribute towards elevating our quality of research. In that regard, I would like to thank my colleagues cum friends Akshay Chatla, Atasi Ray, Aishwarya Bhatta, Dinesh Singha, Rudra Majhi, Priya Mishra, Papia Panda, Dhiren, Sambit and others for keeping the ambiance positive and vibrant around me.

Einstein once said, " Everybody is a genius. But if you judge a fish by its ability to climb a tree, it will live its whole life believing that it is stupid." My journey to pursue Ph.D. has been made possible due to a small coterie who believed and saw an inquisitive person within me. It is them whose faith acted like a catalyst during the tough times and helped me not to get distracted. The least I can do is to thank them for trusting and guiding me whenever needed. They are Mrs. Phalguni Moitra, Mrs. Poonam Shah, Mr. Sadashiv, Mr. Ambupani, Mr. Naidu, Ms. Rashmi, Mr. Shanti Bhushan Pandey, Mr. Chand, Mr. S Panda, Mrs. Arti Jha, Prof. Piyush Ranjan Das, Dr. Akhyaya K. Pattanaik, Dr. Ganeswar Nath, Dr. Santanu Sengupta, Dr. P. Lakshmi Praveen, Dr. Sunanda Kumari Patri and others. I would like to express my overwhelming gratitude and indebtedness towards one of my graduation lecturer Dr. Arundhati Mishra who has always encouraged me to aim for the high and filled me with her wisdom during my lows.

As we all know that education starts from home with father and mother being our first mentors and teachers. So, finally yet importantly, I would like to express my humblest and deepest gratitude towards my parents Mr. Pramod Chandra Behera and Mrs. Maunabati Behera who have celebrated my success as well as being the pillars of support during my failures. They too have struggled a lot to help me reach where I am today. My mother's wise words and father's soothing calmness has helped me get through different situations in life. They have always let me be myself and never burdened me with any fixed mindset. This helped me to think freely and seeded for the inquisitiveness I have today. I would also like to extend my gratitude towards my younger brother Preetesh Kumar Behera and my grandparents Late Brundaban Behera, Mrs. Lalita Behera, Mr. Chintamani Das, Mrs. Nishamani Das and others who helped me to be lively during tough times. When we move out in the world leaving our own soul circle we define new contours to the existing confinement by adding new people called friends. Hence I would take the privilege to thank Rekha, Subhranshu, Akash Tarai, Dinesh Sahu, Pooja Saini, Aman Jha, Subhankar, Sanjay, Jai, Sabdasmaran, Binay, Dr. Shilpa, Dr. Payal, Dr. Sumeet and others.

ABSTRACT

Standard model although has addressed and being successful regarding the fundamental particles and their interactions, but, is deficient in explaining certain experimental evidences. In support of the above statement, the list of things that standard model is sloppy about are dark matter, dark energy, baryon asymmetry of the Universe, massive neutrinos, strong CP problem. This becomes the drive for everybody contributing in this field to find some answers either theoretically or experimentally. Hence, in this thesis, we have made an attempt to address certain issues, left open, by the help of various prominent models.

So, to start with, we present a model, where we have included A_4 discrete symmetry in order to leap beyond the standard model (BSM). BSM physics helps us to accommodate right handed (RH) neutrinos which is successful in explaining the tiny neutrino mass via seesaw mechanism. Therefore, we take the advantage of linear seesaw which demands the inclusion of left handed (LH) neutrinos too. In the model we have also introduced modular symmetry due to which Yukawa couplings implicitly depends on modulus τ and explicitly on the dedekind eta function. Modular symmetry helps us in two aspects, one, reduces the usage of flavon fields, which otherwise would make the model complicated and less predictive. Second, modular weights helps us to avoid unwanted Lagrangian terms to an extend. However, a global symmetry i.e. $U(1)_X$ is included to avoid certain other Lagrangian terms which modular symmetry couldn't. All these gimmick leads to the specific structure of linear seesaw mass matrix, which after diagonalisation gives results in accordance with current neutrino oscillation data i.e. at 3σ level. This includes the reactor mixing angle i.e. $\sin^2\theta_{13}$, mass sum of the active neutrinos $\sum m_i$ which is well below the cosmological bound of 0.12 eV. Other parameters like $\sin^2\theta_{12}$ and $\sin^2\theta_{23}$ are also well within the 3σ limits. Introduction of right handed neutrinos, gave an idea that explanation of baryon asymmetry is also possible by the model. Hence, we explain leptogenesis using these RH neutrinos which gives us six doubly degenerate mass eigenstates. Therefore, to have a mass splitting we introduce a higher dimension mass term. By doing so, we obtain nonzero CP asymmetry from the decay of lightest heavy fermion. Also, this small mass difference between the two lighter heavy fermions enhances the self energy contribution. The coupled Boltzmann equations are solved to obtain the evolution of lepton asymmetry, which comes out to be order of $\approx 10^{-10}$, which is sufficient to explain the present baryon asymmetry of the Universe.

This successful attempt to explain neutrino mass and leptogenesis by implementing the new idea of modular symmetry motivated us to explore things for scotogenic scenario. So, the approach was to explain the neutrino mass at one loop level by suppressing the tree level contribution. This was done meticulously by defining the particle charges. Further in this model, we made an attempt to accommodate lepton flavor violations (LFVs) like $\mu \to e\gamma$, $\mu \to 3e$ and $\mu - e$ conversion. Hence, it was evident that our model is successful in doing the work and explaining LFVs well below the prescribed 3σ limits obtained from

the experiments. In addition, we also explain dark matter phenomenology of the lightest stable fermion spectrum. As there is no hold on the Yukawa couplings because of their dependence on the dedekind eta function. Even this stringent bound on the couplings allow us to get the correct relic density compatible to Planck data for particular benchmark values of the model parameters. We also realized that their is a contribution to relic density from the lepton - antilepton pair in the final state via η and Z' (U_{B-L} associated). However, as there is no direct coupling of η and Z' with the quarks, hence, the tree level direct detection is not possible. Till now modular symmetry has worked as charm for explaining different phenomenologies along with accurate predictions from the neutrino sector.

Hence, we make an attempt to take it further, by, working in a different discrete symmetry i.e. A_5' which is a double cover of A_5 symmetry. Previously, we have checked modular A_4 symmetry as being a promising candidate but freedom in regards to the number of irreducible representation is less. However, A_5' has more number of irreducible representations as compared to A_4 as well as A_5 modular symmetry. Therefore, we try to explain inverse seesaw using A_5' modular symmetry. In here, the permutation group $N = 5$ has 120 elements and under A_5' these 120 elements are categorized into nine conjugacy classes. Here, their are higher order Yukawa couplings which comes handy while writing the superpotential. Alongside of explaining the neutrino parameters at 3σ level we also discuss non-unitarity and lepton flavor violation of $\ell_i \to \ell_j \gamma$.

TABLE OF CONTENTS

Table of Contents

LIST OF TABLES

TABLE **Page**

LIST OF FIGURES

FIGURE **Page**

CHAPTER 1

INTRODUCTION

Since the beginning of time, homosapeins have been curious. We are the only species that asks "why" and "how" inquiries, which helped to spawn primitive science as we know it from history. Many others have also given their lives to bring the facts to light in the way we know them now. The preceding remark is true to its core since particle physics went through a lot of ups and downs in its early stages. Until now, the Standard Model (SM) has been our best hope for describing elementary matter particles, including quarks and leptons, in terms of three of the four fundamental forces: strong, weak, and electromagnetic. The fourth essential interaction, however, is missing: gravity. The initial work of constructing SM was taken by Glashow, who discovered, in 1961, a way to combine the electromagnetic and weak interactions into a single electroweak model ruled by an $SU(2) \times U(1)$ symmetry. Further, the $SU(3)$ symmetry called the Eightfold way, formulated in 1964, helped describe quarks and their interactions with strong force. However, later it was clubbed as a component of the SM, hence the formulation became $SU(3) \times SU(2) \times U(1)$ symmetry. In 1967, the concept of Higgs mechanism and its field came into picture, which was able to give masses to all the elementary particles via spontaneous symmetry breaking (SSB), as we all know it, the present standard model (SM). Many experiments were conducted and their observations were overwhelmingly in-accordance to the SM predictions. For instance, 1973, the discovery of neutral weak currents, caused by Z Bosons exchange. In 1983 the discovery of the W bosons themselves and not to forget the recent discovery of Higgs boson, in 2012. Myriad experiments added to the affirmation of SM as a successful theory that is staggeringly effective in depicting the interactions of elementary particle physics.

1.1 Standard model in a nutshell

As aforesaid, standard model (SM) of particle physics has been successful till now in describing the fundamental particles and forces of nature. The classification of the particles in SM is done based on the masses, spin and other quantum numbers. For instance, *fermions* are spin-$\frac{1}{2}$, *gauge bosons* are spin-1, but, *Higgs boson* is the only *scalar* particle being spin-0. Further, standard model is based on *local gauge theory*, which means the Lagrangian remains invariant under local transformations.

The gauge group describing SM is a 12-dimensional non-Abelian symmetry group,

$$G_{\mathrm{SM}} = SU(3)_C \otimes SU(2)_L \otimes U(1)_Y \,, \tag{1.1}$$

here, C stands for the color charge, L is for the left handed chirality, and Y represents weak hypercharge. $SU(3)_C$ is associated to the strong interactions expressed in QCD, which corresponds to eight generators given by $\mathbb{T}^{\mathsf{a}} = \frac{i\lambda^{\mathsf{a}}}{2}$, i.e. λ^{a} are the Gell-Mann matrices with $\mathsf{a} = \{1,2,3,\cdots,8\}$. These eight generators correlate to eight massless gluon fields as mediators of strong interaction. Further, the gauge group $SU(2)_L \times U(1)_Y$ represents the electroweak sector. This unification is described by Glashow, Weinberg, Salam (GWS) [1–3] theory, where, it is associated to four generators, three from $SU(2)_L$ i.e. $\mathbb{T}^{\mathsf{a}} = \frac{i\tau^{\mathsf{a}}}{2}$ (τ^{a} are three Pauli matrices with $\mathsf{a} = 1,2,3$) and fourth one from $U(1)_Y$ i.e $\mathbb{T}^{\mathsf{a}} = Y$. These three generators from $SU(2)_L$ are related to the massive gauge bosons ($W^{\pm}$ and Z^0), whereas, massless photon field is associated with the generator of the weak hypercharge $U(1)_Y$.

Symmetry \ **Particles**	u_R	d_R	e_R	$Q_L = (\nu_{e_L}, e_L)^T$	$L_L = (u_L, d_L)^T$
$SU(3)_C$	3	3	1	3	1
$SU(2)_L$	1	1	1	2	2
$U(1)_Y$	4/3	$-2/3$	-2	1/3	-1
I, I_3	0,0	0,0	0,0	$1/2, (1/2, -1/2)^T$	$1/2, (1/2, -1/2)^T$
$U(1)_Q = (2I_3 + Y)/2$	2/3	$-1/3$	-1	$(2/3, -1/3)^T$	-1

Table 1.1: Standard model particles and their gauge group charges.

As physicists, we are well aware that symmetry plays an important role in defining any physical phenomenology. In this regard, Emily Noether, stated, every symmetry is associated with a conservation law and vice-versa. Hence, SM of particle physics is no exception to the above statement as its formation is based on symmetries. As it is assumed that space and time are homogeneous, hence, the Lagrangian defined, of a closed system has to be invariant under space-time translations i.e. uniform also.

In support to above statement, the Lagrangian of a system mostly comprises of *kinetic*, *mass* and *interaction terms*. However, SM Lagrangian is a combination of four different parts

$$\mathscr{L}_{\rm SM} = \mathscr{L}_{\mathbb{G}} + \mathscr{L}_{\mathbb{F}} + \mathscr{L}_{\mathbb{H}} + \mathscr{L}_{\mathbb{Y}}. \tag{1.2}$$

Here, $\mathscr{L}_{\mathbb{G}}$ comprises of, kinetic and self interaction terms of the gauge bosons. Similarly, $\mathscr{L}_{\mathbb{F}}$ tells about the kinetic and gauge interaction terms of the fermions. Whereas, $\mathscr{L}_{\mathbb{H}}$ is associated with the kinetic, self interaction and gauge terms of the Higgs boson and $\mathscr{L}_{\mathbb{Y}}$ depicts all the interactions of the Higgs boson with leptons and quarks.

1. **Gauge term:** As it is evident from above discussion that twelve gauge bosons are associated to twelve generators of eqn. (1.1). The four bosons that corresponds to $\{SU(2)_L \times U(1)_Y\}$ are B boson from $U(1)_Y$ and $(\mathsf{W}^i, i = 1,2,3)$ i.e. triplet under $SU(2)_L$. When electroweak symmetry breaking takes place, a mixing between B and W^i occurs, which upon rediagonalization, gives rise to the physical bosons. These are $\mathsf{W}^{\pm}$ and Z massive bosons and γ a massless boson, where, the massive bosons help in mediating the charged and neutral weak current interactions. The other eight gauge bosons correspond to eight gluons G^{a} which mediates the strong force and are related to $SU(3)_C$ gauge group.

   A brief dialogue, above, further helps to understand the terms in the Lagrangian as shown in eqn. (1.2). The first term is related to the gauge fields given by

$$-\mathscr{L}_{\mathbb{G}} = \frac{1}{4}\mathsf{B}_{\mu\nu}\mathsf{B}^{\mu\nu} + \frac{1}{4}\mathsf{W}^{\mathsf{i}}_{\mu\nu}\mathsf{W}^{i,\mu\nu} + \frac{1}{4}\mathsf{G}^{\mathsf{a}}_{\mu\nu}\mathsf{G}^{\mathsf{a},\mu\nu}, \tag{1.3}$$

   where, $i = \{1,2,3\}$ and $\mathsf{a} \in \{1,2,3,\cdots,8\}$. The field strength tensors are given by

$$\mathsf{B}_{\mu\nu} = \partial_\mu \mathsf{B}_\nu - \partial_\nu \mathsf{B}_\mu, \tag{1.4}$$

$$\mathsf{W}^i_{\mu\nu} = \partial_\mu \mathsf{W}^i_\nu - \partial_\nu \mathsf{W}^i_\mu + \mathsf{g}\,\kappa^{ijk}\mathsf{W}^j_\mu \mathsf{W}^k_\nu, \tag{1.5}$$

$$\mathsf{G}^{\mathsf{a}}_{\mu\nu} = \partial_\mu \mathsf{W}^{\mathsf{a}}_\nu - \partial_\nu \mathsf{W}^{\mathsf{a}}_\mu + \mathsf{g}_3\,\epsilon^{\mathsf{abc}}\mathsf{W}^{\mathsf{b}}_\mu \mathsf{W}^{\mathsf{c}}_\nu, \tag{1.6}$$

   where, g and κ^{ijk} corresponds to the gauge coupling and structure constant under $SU(2)_L$ respectively, while, g_3 and ϵ^{abc} are that of $SU(3)_C$. As the gauge group are non-Abelian in nature, therefore, self interactions terms of W^i and G^{a} are required. In order to obtain massive gauge bosons EWSB (discussed later) is essential, as it is not possible directly to construct a gauge invariant mass terms for the gauge bosons.

2. **Fermion term:** Undoubtedly, electroweak transformation plays a major role in coupling of fermions to gauge fields in a gauge invariant way. Therefore, the second term of eqn.1.2 is related to fermions, describing the kinetic term of the fermions and their interactions with the gauge bosons as below

$$\mathscr{L}_{\mathbb{F}} = i\overline{\psi}\gamma^\mu D_\mu \psi. \tag{1.7}$$

In above, a covariant derivative D_μ is introduced by replacing ordinary derivative ∂_μ in order to maintain the gauge invariance which is defined as

$$D_\mu = \partial_\mu + ig\mathbb{A}^a_\mu \mathbb{T}^a_\mu, \tag{1.8}$$

Here, $\mathbb{T}^a_\mu$ are the generators associated associated with the gauge group and $\mathbb{A}^a_\mu$ represent the gauge fields. Therefore, when D_μ is replaced by its RHS from eqn.(1.8) in eqn.(1.7) it brings in a gauge interaction term shown below

$$\mathscr{L}_{int} = -g\overline{\psi}\gamma^\mu \mathbb{A}^a_\mu \mathbb{T}^a_\mu \tag{1.9}$$

Hence, the complete determination of the gauge interaction of the fermions takes place, once, the choice of gauge structure and the fermion representation is made appropriately.

3. **Higgs term:** One of the most important discovery in particle physics is the Higgs Field, which helped to solve the mystery how particles got their masses. Quite often, Higgs field is denoted by Φ which acquires the quantum number $\{2 \otimes \frac{1}{2}\}$ under $SU(2)_L \otimes U(1)_Y$.

   The third term in eqn. (1.2) defines Higgs term as follows

$$\mathscr{L}_{\mathbb{H}} = |D_\mu \Phi|^2 - V(\Phi), \tag{1.10}$$

   where, covariant derivative is from eqn. (1.8). In addition, the Higgs potential is given by,

$$V(\Phi) = \mu^2 \phi^\dagger \phi - \lambda(\phi^\dagger \phi)^2 \tag{1.11}$$

4. **Yukawa term:** The Yukawa interaction occurs when a scalar field interacts with the Dirac bilinear fields. The SM Lagrangian's Yukawa portion is further separated into leptonic and quark parts. The Yukawa interaction between leptons is,

$$-\mathscr{L}^{lepton}_{\mathbb{Y}} = Y_e^{ij} \overline{L}_{iL} \Phi e_{jR} + \text{h.c.}. \tag{1.12}$$

   The three physical parameters involved in this term are chosen to be the three charged lepton masses. The quark masses arise in the quark Yukawa interaction given by,

$$-\mathscr{L}^{quark}_{\mathbb{Y}} = Y_u^{ij} \overline{Q}_{iL} \tilde{\Phi} u_{jR} + Y_d^{ij} \overline{Q}_{iL} \Phi d_{jR} + \text{h.c.}, \tag{1.13}$$

   where, Y^{ij} are the Yukawa matrices, $\tilde{\Phi} = i\tau_2 \Phi^*$, τ_2 is the second pauli matrix, and $i, j \in \{1,2,3\}$ are the generation indices.

1.1.1 Higgs mechanism

Birth of our Universe was possible because of certain asymmetry, but, while writing out the Lagrangian for describing a physical phenomenon we make sure that it involves some symmetry. Breaking of the

symmetries can always be facilitated by involving certain terms that violate the symmetry. However, from theoretical perspective it will be bizzare, if symmetry breaking terms are present from the beginning, then the Lagrangian so constructed will be asymmetric. In contrast to above, interesting thing will be accessing a system which by itself breaks the symmetry called *spontaneous symmetry breaking* (SSB). The mechanism by which electroweak symmetry is broken

$$SU(3)_C \otimes SU(2)_L \otimes U(1)_Y \rightarrow SU(3)_C \otimes U(1)_Q, \tag{1.14}$$

and the gauge bosons Z and $W^{\pm}$ gain their masses is called *Brout-Englert-Higgs (BEH) mechanism*, where the minimum of the Higgs potential is deduced as

$$|\Phi|_0 = \sqrt{\frac{\mu^2}{\lambda}} \equiv v \approx 246\text{GeV}. \tag{1.15}$$

Hence, this minimum is called the vacuum expectation value (VEV), around which the excitation of the physical states take place. The expression for the Higgs field is given below

$$\Phi = \begin{bmatrix} \phi^+ \\ \frac{1}{\sqrt{2}}(h + i\phi + v) \end{bmatrix}, \tag{1.16}$$

here, h and ϕ represents real fields. In addition, $h + v$ is considered as the real part, where h behaves as the excitations around v. Further, SSB is acheived due to disobedience shown by the ground state of the field towards the $SU(2)_L$ symmetry, because of VEV gain. Therefore, gauge bosons gain masses as soon as Higgs field acquire VEV. The gauge interacting part of the eqn. (1.10) is given as follows

$$\mathscr{L}^{mass}_{gauge} = \frac{v^2}{8}\left\{g^2(\mathsf{W}^1_\mu)^2 + g^2(\mathsf{W}^2_\mu)^2 - (g\mathsf{W}^3_\mu - g'\mathsf{B}_\mu)^2\right\}, \tag{1.17}$$

where, g represents the gauge coupling of $SU(2)_L$, while, g' is that of $U(1)_Y$. The first two terms in eqn.(1.17) involving W^1 and W^2 have degenerate mass given by $m_{\mathsf{W}} = \frac{gv}{2}$. The third component which is linear combination of W^3 and B_μ represents Z_μ given as below

$$Z_\mu = \frac{1}{\left[g'^2 + g^2\right]^{\frac{1}{2}}}\left\{-g\mathsf{W}^3_\mu + g'\mathsf{B}_\mu\right\}, \tag{1.18}$$

this gives the mass for $Z_\mu = \frac{v}{2}\left[g'^2 + g^2\right]^{\frac{1}{2}}$. The orthogonal field combination

$$A_\mu = \frac{1}{\left[g'^2 + g^2\right]^{\frac{1}{2}}}\left\{g'\mathsf{W}^3_\mu + g\mathsf{B}_\mu\right\}, \tag{1.19}$$

represents the massless photon and is a gauge boson of $U(1)_Q$ gauge group. We know that $SU(2)_L \otimes U(1)_Y$ are associated with four generators out of which three are broken. Hence, intuitively those three must become Goldstone bosons [4], but in 1964 it was shown that due to *SSB* of the gauge symmetry, the extra degrees of freedom instead can become longitudinal polarizations of the gauge bosons. Therefore, it is said

that these components are eaten by the gauge boson fields. Hence, the left over component of the Higgs field becomes the physical boson called the Higgs boson which is a scalar particle. It is intereseting to observe that *BEH* mechanism doesn't affect the total number of degrees of freedom, as, massive gauge boson has an extra degree of freedom than a massless one.

The matrix involved in mixing of the B field and third component of W^i field i.e. W^3 into the Z and A fields is

$$\begin{bmatrix} \cos\theta_W & -\sin\theta_W \\ \sin\theta_W & \cos\theta_W \end{bmatrix}, \tag{1.20}$$

here, θ_W is called the *weak mixing angle* or *Weinberg angle*. It is expressed in terms of the gauge couplings g and g' i.e. $\tan\theta_W = g'/g$. This *Weinberg angle* also establishes the relation between the masses of W and Z boson i.e. $\cos\theta_W = \frac{m_Z}{m_W}$. Further, $W^i(i = 1,2)$ is rotated into the charged massive fields, expressed as

$$W^{\pm}_{\mu} = \frac{1}{\sqrt{2}}\left\{\mathrm{W}^1_{\mu} \mp i\mathrm{W}^2_{\mu}\right\}. \tag{1.21}$$

The Higgs mechanism is also successful in giving masses to the fermions. Due to ESWB the Yukawa sector will involve the following terms

$$\mathscr{L}^{mass}_{fermion} = m^{ij}\overline{\Psi}_{Li}\Psi_{Rj}, \tag{1.22}$$

where, the fermion mass matrix is given by $m^{ij} = \frac{v}{\sqrt{2}}\mathrm{Y}^{ij}$, although, the mass matrix isn't diagonal in general.

1.1.2 Downside of Standard Model

Inspite of all the success and being considered as a fundamental theory of particle physics, standard model, miserably fails in explaining certain sectors, which till date are a mystery for science. The baryon asymmetry of the universe, origin of the neutrino mass, neutrino oscillations, dark energy, dark matter, naturalness or hierarchy problem, quantization of gravity etc. are beyond the reach of SM.

1. All these years of meticulous and diligent work done by the high energy physics group across the globe has developed an understanding that SM has a *hierarchy or naturalness problem*. The problem is Higgs mass i.e. 125 GeV and gravitational scale i.e. around 10^{19} GeV is expected to be of same order. However there ratio boils down to about 10^{-17} order. Therefore, the question arises why this huge difference in the mass scale.

2. It is an interesting fact that during its voyage from source to detectors neutrinos oscillate from one neutrino family to another neutrino family which SM hasn't been able to describe till date.

3. Considering the ratio of the energy density of free space time (Λ) to Planck scale, as an output, a very small number is seen i.e. $\left(\frac{\Lambda}{M_{Planck}}\right)^4 \sim 10^{-120} \ll 1$. This leaves us with a query that why this ratio yields such a small number, it is also known as the cosmological constant problem.

4. We know that the ingredients that makes our universe is 4% of visible matter, 22% of dark matter and rest 74% is dark energy. However, to prove this, their is a deficiency of suitable candidate(s) which can act like dark matter within the SM.

There are so many unanswered problems in the standard model, hence, we make an attempt to deduce different parameters (i.e. mixing angles, sum of active neutrino masses, Jarlskog Invariant etc.) related neutrinos theoretically, suggestive from neutrino oscillations experimentally. As neutrinos don't have right handed partners in SM, so all model building is done beyond the standard model. Alongside, we also shed some light on the existence of dark matter through our models and discuss the issue of matter - antimatter asymmetry of the universe.

1.2 The phenomenon of neutrino oscillations

1.2.1 Insights and evidences from neutrino experiments

Indication about neutrino oscillations dates back to 1967, when efforts were made to measure the ν_e flux being produced by the Sun using a chlorine detector ($\nu_e + {}^{37}\text{Cl} \rightarrow e^- + {}^{37}\text{Ar}$). This pioneering work was lead by Raymond Davis, John N. Bahcall and their collaborators in Homestake mine [5], whose results clearly indicated that there is a difference between observed values from experiments and predicted values of standard solar model [6]. People were sceptical about oscillation hypothesis because compared to the quark mixing, neutrino oscillations required the involvement of large mixing angles. Although, within the standard model neutrinos were considered massless, but, neutrino oscillations implied that neutrinos are not massless. Experimental verifications done over the years by several experiments like GALLEX, Superkamiokande, T2K, SAGE etc. [7–13] cleared the clouds. This has motivated physicists across the globe to work and define frameworks beyond the standard model.

1.2.2 A theoretical background

It is very clear that neutrinos carry some mass as implied from oscillation experiments, and they oscillate between flavors i.e. observed from solar and atmospheric experiments. So let us first discuss the two flavor states of the neutrinos. Neutrinos of one generation is correspondingly produced along with the same generation charged leptons, as seen in the charge current weak interactions. Suppose a source produces neutrinos of flavor ν_α and undergoes oscillation to another flavor ν_β. Therefore, the mass eigenstate will be superposition of all the flavor states. Assuming the charged lepton diagonal basis, and the neutrino

charged current interaction is given as

$$L_W = \left[\frac{1}{2}\right]\left[\frac{g}{\sqrt{2}}\right] e^-_{iL}\gamma^\mu U_{ij}\nu_{jL}W^-_\mu + \text{ h.c.}, \tag{1.23}$$

where, the transformation from flavor eigenstate to mass eigenstate is given by $|\nu_{\alpha L}\rangle = U_{ij}\nu_{jL}$. For instance, if $|\nu_\alpha\rangle$ flavor state is produced at time $t = 0$ and during propagation transforms into another state ν_β such that it becomes necessary to calculate the probability of oscillation. So, a plane wave approximation helps resolve the thing where τ is proper time

$$i\frac{\partial|\nu_i(\tau_i)\rangle}{\partial t} = m_i|\nu_i(\tau_i)\rangle. \tag{1.24}$$

Hence, the evolution of the state is given by

$$|\nu_i(t)\rangle = e^{im_i\tau_i}|\nu_i(0)\rangle. \tag{1.25}$$

The oscillation amplitude at the time t for the neutrinos at flavor state $|\nu_\beta\rangle$ is given by

$$\mathscr{A}(\nu_\alpha \to \nu_\beta; t) = U_{\beta j}e^{-im_i\tau_i}U^*_{\alpha i}\langle\nu_j|\nu_i\rangle = U_{\beta j}e^{-im_j\tau_j}U^*_{\alpha j}. \tag{1.26}$$

Therefore, one can interpret that $U_{\alpha j}$ being the transformation amplitude and the exponential factor is due to the time evolution of neutrino mass eigenstate, and the probability of oscillation can be obtained as

$$P(\nu_\alpha \to \nu_\beta; t) = |\mathscr{A}(\nu_\alpha \to \nu_\beta; t)|^2 = |U_{\beta j}e^{-im_i\tau_i}U^*_{\alpha j}|^2 . \tag{1.27}$$

Assuming the Lorentz invariance, one can have

$$m_i\tau_i = p_\mu x^\mu = E_i t - p_i L_i . \tag{1.28}$$

Here,

$$p_i = \sqrt{E^2 - m_i^2} \approx E - \frac{m_i^2}{2E}. \tag{1.29}$$

Therefore. substituting eqn. 1.29 in eqn. 1.28, one can get

$$m_i\tau_i = Et - \left(E - \frac{m_i^2}{2E}\right)L = (E-t)L - \frac{m_i^2}{2E}L . \tag{1.30}$$

Looking carefully at the above equation, it is evident that the first term is a phase factor which can be redefined. Hence, the probability of oscillation in Eqn. 1.27 is written as

$$P(\nu_\alpha \in \nu_\beta; t) = \left|\delta_{\alpha\beta} + \Sigma_{j=2}^n U_{\beta j}U^*_{\alpha j}\left(e^{i\frac{\Delta m^2_{ji}}{2E}L} - 1\right)\right|^2 . \tag{1.31}$$

1.2.2.1 Two flavor oscillation

To understand the things we depict a simplistic scenario of two flavor oscillation case i.e. $\nu_e \to \nu_\mu$. The 2×2 mixing matirx utilized is given below

$$U = \begin{pmatrix} \cos\theta & \sin\theta \\ -\sin\theta & \cos\theta \end{pmatrix}. \tag{1.32}$$

Therefore, writing the mass eigenstates in terms of the flavor eigenstates are as follows

$$\begin{aligned} |\nu_1\rangle &= \cos\theta|\nu_e\rangle - \sin\theta|\nu_\mu\rangle, \\ |\nu_2\rangle &= \sin\theta|\nu_e\rangle + \cos\theta|\nu_\mu\rangle\,. \end{aligned} \tag{1.33}$$

The oscillation probability is then given by

$$P_{(\nu_e\to\nu_\mu)} = \sin^2 2\theta \sin^2(\pi\phi), \quad \phi = \frac{\Delta m^2_{12} L}{4E\pi}\,. \tag{1.34}$$

The oscillation is maximal at $\theta = \frac{\pi}{4}$ and minimal at $\theta = 0, \pi$.

1.2.2.2 Three flavor oscillation

Similarly, for three flavor neutrino oscillation the probability [14, 15] is given by

$$P_{(\nu_\alpha\to\nu_\beta)} = \delta_{\alpha\beta} - 4\sum_{i<j}\mathrm{Re}\left(U_{\alpha i}U_{\beta j}U^*_{\alpha j}U^*_{\beta i}\right)\sin^2\left(\Delta_{ij}\frac{L}{4E}\right) + 2\sum_{i<j}\mathrm{Im}\left(U_{\alpha i}U_{\beta j}U^*_{\alpha j}U^*_{\beta i}\right)\sin^2\left(\Delta_{ij}\frac{L}{4E}\right) \tag{1.35}$$

where, $\Delta_{ij} = (m^2_j - m^2_i)$ and $\delta_{\alpha\beta} = \sum_i U_{\alpha_i}U^*_{\beta i}$ being the unitarity relation. The standard parametrization of the three neutrino mixing matrix is given by

$$U_{PMNS} = \begin{bmatrix} c_{12}c_{13} & s_{12}c_{13} & s_{13}e^{-i\delta_{CP}} \\ -s_{12}c_{23} - c_{12}s_{23}s_{13}e^{i\delta} & c_{12}c_{23} - s_{12}s_{23}s_{13}e^{i\delta_{CP}} & s_{23}c_{13} \\ -s_{12}s_{23} + c_{12}c_{23}s_{13}e^{i\delta_{CP}} & c_{12}s_{23} + s_{12}c_{23}s_{13}e^{i\delta_{CP}} & -c_{23}c_{13} \end{bmatrix} \begin{bmatrix} 1 & 0 & 0 \\ 0 & e^{i\zeta_1/2} & 0 \\ 0 & 0 & e^{i\zeta_2/2} \end{bmatrix}, \tag{1.36}$$

where, $s_{jk} = \sin\theta_{jk}$, $c_{jk} = \cos\theta_{jk}$, δ_{CP} is the Dirac CP violating phase, $\zeta_{1,2}$ are the Majorana phases. Experiments based on neutrino oscillation predict two types of mass orderings, i.e. ($m_1 < m_2 < m_3$) called the normal hierarchy and ($m_3 < m_1 < m_2$) called the inverted hierarchy.

1.3 Dirac and Majorana neutrino mass terms

It is noticeable that Standard model (SM) is void of neutrino masses. However, neutrino oscillation experiments strongly suggest of neutrinos being massive. Therefore, it becomes important to theoretically justify the above fact.

Left handed chiral fermions voluntarily participate in the weak interactions, therefore, SM fields can be expressed in terms of their chiral fields. To do this Weyl fermions are defined as

$$\psi_{L,R} \equiv P_{L,R}\psi = \frac{1 \pm \gamma^5}{2}\psi\,, \tag{1.37}$$

ψ being the four-component Dirac spinor. Mass term in SM has the form $m\overline{\psi}_{L,R}\psi_{L,R}$ and it is evident only if opposite chirality spinors couple to each other. This gives rise to a possibility of having two kinds of mass terms [16, 17]

Dirac :

$$m_D\overline{\psi_L}\psi_R + \text{H.c.}, \tag{1.38}$$

Majorana :

$$M_L\overline{\psi_L}(\psi_L)^c + M_R\overline{(\psi_R)^c}\psi_R + \text{H.c.}, \tag{1.39}$$

where, $\psi^c \equiv C\overline{\psi}^T$ and C being the charge conjugation matrix. The nomenclature of the mass term is because they come into existence from the Dirac and Majorana type fields, where, $\psi = \psi_L + \psi_R$ and $\psi_{a,b} = \psi_{L,R} + \psi^c_{L,R}$ respectively.

Construction of Dirac mass term demands involvement of two distinct Weyl fermions. Therefore, we have to introduce chirally right handed neutrinos N_R into SM alongside of ν_L. As N_R are weak isospin singlets, hence can couple to ν_L and H (i.e. SM Higgs doublet) allowing us to write the Yukawa term i.e.

$$Y_\nu\bar{\ell_L}H\nu_R + \text{H.c.}. \tag{1.40}$$

1.4 Seesaw Mechanism

The seesaw mechanism gets its name from the interaction between the masses of sterile and active neutrinos. As the mass of the sterile neutrinos increases, the mass of the active neutrinos falls, like a seesaw. Hence, extending the SM with different symmetries helps us to constrict a theory with less random input parameters which for certain cases gives definite predictions. Hence, implementation of canonical seesaw, let us wonder if this unimpeded right handed neutrino sector can be estimated through these symmetries. This is interesting due to the fact that their is some link between seesaw parameters and lepton asymmetry of the universe i.e. leptogenesis. While constructing a model choice of symmetries are also governed by cosmological data. To realize the importance of symmetries, seesaw mechanism comes handy in establishing the connection between heavy RH neutrino mass matrix and the low-energy neutrino data, however, linking them is difficult as there are ample number of parameters to be fixed. Therefore, symmetry plays a crucial role in interrelating low-energy observables and the undetermined seesaw sector.

So shifting our focus towards seesaw mechanism and its beauty in explaining things which till now have been out of reach of standard model. In this regard, there are many variants aside from canonical i.e. type-II seesaw involving scalar triplets, type-III incorporating fermion triplets, linear and inverse seesaw

which are modified type-I seesaw. So, below we discuss only those relevant to my doctoral work i.e. linear and inverse seesaw.

1.4.0.1 Type-I seesaw

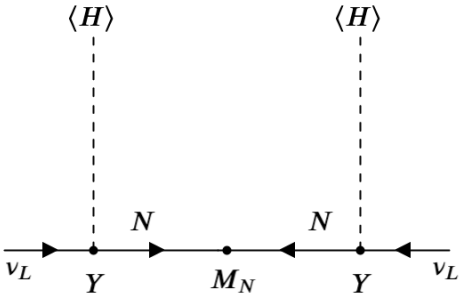

Figure 1.1: Feynman diagram showcasing neutrino mass through type-I seesaw.

Introduction of singlet RH neutrinos in the seesaw helps us write the Dirac mass term for neutrinos which was previously not possible. In MSSM only two right handed neutrinos are enough to generate a mass square splitting, but, adding one more RH neutrino to MSSM gives rise to two mass square splittings Δm^2_{ij}. Therefore, the Yukawa interaction term can be written as

$$\mathscr{L}_{\text{Yukawa}} = -Y_{ij}\overline{L_{iL}}N_{jR}\tilde{H} + \text{H.c.}, \tag{1.41}$$

where, Y_{ij} being the 3×3 coupling matrix and L_{iL} being the SM lepton doublet with $(i,j = 1,2,3)$, where, $\tilde{H} = i\sigma_2 H^*$ and $\langle H\rangle = \frac{v}{\sqrt{2}}$ being its VEV . The singlets RH neutrinos also allows us to write the Majorana mass term for neutrinos as well

$$\mathscr{L}_{\text{Maj}} = -\frac{1}{2}M_{N_{ij}}\overline{N}_{iL}N_{jR} + \text{H.c.}, \tag{1.42}$$

where, $\overline{N}_{iL} \equiv N_{iR}$ and ν_{iL} being the SM neutrino eigenstates, the neutrino mass matrix is written as

$$m_\nu = -\frac{1}{2}(\overline{\nu}_L \overline{N}_L)\begin{pmatrix} 0 & m_D \\ m_D^T & M_N \end{pmatrix}\begin{pmatrix} \nu_R \\ N_R \end{pmatrix}, \tag{1.43}$$

giving a neutrino mass in the form as shown below in eqn.(1.44) and is also pictorially depicted by the Feynman diagram as shown in Fig. 1.1.

$$m_\nu = m_D M_N^{-1} m_D^T \;\approx \left(\frac{v}{\sqrt{2}}\right)^2 \frac{Y^2}{M_N}. \tag{1.44}$$

with mixing between active (ν_{iL}) and heavy neutrinos (N_{iR})

$$\tan\theta \simeq \frac{m_D}{M_N} \simeq \sqrt{|m_\nu/M_N|}. \tag{1.45}$$

As there are no gauge interactions in N_{iR}, therefore, the 3×3 mixing matrix connecting the three neutrinos to the three charged leptons cannot be unitary. For $m_\nu \sim 1$ eV and $M_N \sim 1$ TeV, however, the violation of unitarity is of the order of 10^{-6}, which is far too tiny to be seen, but within the limit $M_N \to \infty$, lepton-number conservation is restored. To our surprise there exist modified canonical seesaw called the inverse and linear seesaw discussed in the sections below.

1.4.0.2 Inverse Seesaw

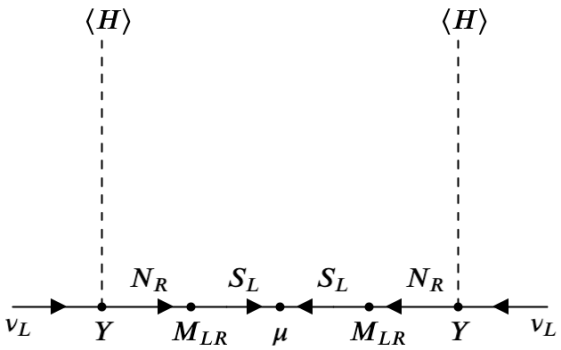

Figure 1.2: Neutrino mass generation through inverse seesaw.

This is a type of canonical seesaw where we include three singlet RH neutrinos (N_{iR}), three extra SM singlet neutral fermions (S_{iL}) along with three active neutrinos (ν_{iL}) with ($i = 1,2,3$). So this mechanism demands us to use these nine neutrinos to develop a Lagrangian by the implementation of some BSM symmetries and acquire the form given below

$$\mathscr{L}_{inv} = -Y\nu_L m_D N_R H - S_L^c M_{LR} N_R - \frac{1}{2}\mu S_L \overline{S_L^c} + H.c., \tag{1.46}$$

which indeed gives rise to 9×9 neutrino mass matrix in the basis of (ν, N_R, S_L) as follows,

$$m_\nu = \begin{pmatrix} 0 & m_D^T & 0 \\ m_D & 0 & M_{LR}^T \\ 0 & M_{LR} & \mu \end{pmatrix}. \tag{1.47}$$

The mass hierarchy utilized in the inverse seesaw is $\mu \ll m_D < M$ and the effective neutrino mass (m_ν) is given by

$$m_\nu = m_D^T (M_{LR}^{-1})^T \; \mu \; M_{LR}^{-1} \; m_D \, . \tag{1.48}$$

Due to the obvious twofold suppression by the mass scale associated with M_{LR}, such a scale can be substantially smaller than the one involved in the conventional seesaw mechanism. Standard neutrinos with masses in the sub-eV range have been confirmed for m_D at the electroweak scale, M_{LR} at the TeV

scale, and μ at the keV scale. In this instance, all six RH neutrinos may generate masses around the TeV scale, and the ratio $m_D M_{LR}^{-1}$ modulates their mixing with standard neutrinos. The crux of the inverse seesaw is that the tininess of neutrino masses is assured by assuming that the scale is small, and that it must be at the keV scale in order to get the RH neutrino masses down to the TeV scale [18, 19]. The mixing angle between the active and heavy fermion for the case of inverse seesaw is given as

$$\theta = \arctan\left(\frac{m_D}{M_{LR}}\right) \approx \sqrt{\left|\frac{m_\nu}{\mu}\right|} \tag{1.49}$$

For instance, if $m_\nu \sim 1$ eV and $\mu \sim 10$ keV consistent with the values of $m_D \sim 10$ GeV and $M_{LR} \sim 1$ TeV, hence, the mixing angle comes out to be $\mathcal{O}(10^{-2})$ which is quite appreciable thus can be probed in near future experiments.

1.4.0.3 Linear Seesaw

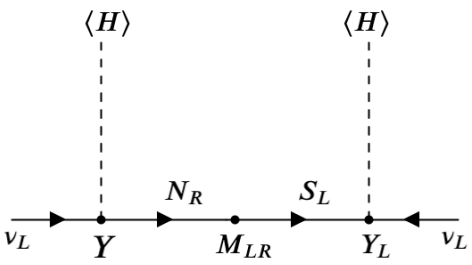

Figure 1.3: Neutrino mass generation in linear seesaw.

Similar to above, there exist another modified canonical seesaw called the linear seesaw which some striking differences in comparison to inverse seesaw. Here also we introduce six heavy neutrinos i.e. (N_{iR} and S_{iL}) as discussed above, but, the peculiarity arises by avoiding the 33 element and allowing the 13 and 31 element. This means we allow the mixing of (ν_{iL} and S_{iL}) while forbidding Majorana mass term for S_{iL}. The Lagrangian for linear seesaw is mentioned below as

$$\mathscr{L}_{linear} = Y H \overline{N_R} L + M_R \overline{N_R} S_L + Y_L H L S_L + \text{H.c.}\,. \tag{1.50}$$

Therefore, the 9×9 mass matrix in the basis of (ν_L, N_R^c, S_L) retains the structure as provided below

$$m_\nu = \begin{pmatrix} 0 & m_D^T & m_{LS}^T \\ m_D & 0 & M_{LR}^T \\ m_{LS} & M_{LR} & 0 \end{pmatrix}, \tag{1.51}$$

where, the mass hierarchy is considered to be $M_{LR} \gg m_D, m_{LS}$ leading to effective neutrino mass

$$m_\nu = \frac{m_D m_{LS}}{M_{LR}}\,. \tag{1.52}$$

The term “linear" tells that the effective neutrino mass formula as shown above in eqn. (1.52) is linear in m_D unlike canonical seesaw, where, it is quadratic in m_D.

1.5 An ingenious approach : Modular Symmetry

Inclusion of discrete symmetries in model building is escalated previously by many models of quark masses and mixing, and, currently due to the discovery of oscillations in neutrino sector. Back then discrete symmetries, were able to predict results that was in accordance to experimental results obtained, for instance, tri-bimaximal mixing of A_4 symmetry which yielded null value for reactor mixing angle. However, challenges increased for theoretical background as soon as the experiments improved and the results were more precise and stringent i.e. reactor mixing angle was obtained, departure of the atmospheric mixing angle from maximal value etc. Other drawbacks of conventional discrete symmetries, are, it requires quite a bunch of flavon fields in order to facilitate the symmetry breaking and deliberately involves non-renormalizable operators. Introduction of these higher dimensional operators reduces the predictability of the model. Therefore, modular symmetry was brought in for the rescue, where, finite modular groups Γ_N are introduced. One interesting thing about finite modular groups are: they are isomorphic to discrete symmetry groups like $\Gamma_2 \simeq S_3$, $\Gamma_3 \simeq A_4$, $\Gamma_4 \simeq S_4$, $\Gamma_5 \simeq A_5$, $\Gamma'_3 \simeq A'_4$, $\Gamma'_5 \simeq A'_5$ etc.

1.5.1 Defintions and examples

The modular group is defined as a group of 2×2 matrices having integer entries and determinant 1.

$$\mathrm{SL}_2(\mathbb{Z}) = \left\{ \begin{bmatrix} a & b \\ c & d \end{bmatrix} : a,b,c,d \in \mathbb{Z},\ ad - bc = 1 \right\}. \tag{1.53}$$

The generators of modular group being

$$T = \begin{bmatrix} 1 & 1 \\ 0 & 1 \end{bmatrix} \quad \text{and} \quad S = \begin{bmatrix} 0 & -1 \\ 1 & 0 \end{bmatrix}. \tag{1.54}$$

Therefore, the linear fractional transformation that acts on the modulus τ is given by

$$\begin{bmatrix} a & b \\ c & d \end{bmatrix}(\tau) = \frac{a\tau + b}{c\tau + d}, \qquad \mathscr{H} = \{\tau \in \mathbb{C},\ \mathrm{Im}(\tau) > 0\}, \quad \gamma = \begin{bmatrix} a & b \\ c & d \end{bmatrix} \in \mathrm{SL}_2(\mathbb{Z}), \tag{1.55}$$

where, $\mathscr{H}$ is defined as the upper half plane and is also recognized as one of the three connected surfaces of the Riemann surface. It is inferred from above that if $c \neq 0$, implies, $-d/c$ maps to ∞ and ∞ goes to a/c. However, if $c = 0$ then ∞ goes to ∞. Also, both $\pm$I gives identity transformation, where, I is identity matrix and in a more general perspective a pair of $\pm\gamma$ of matrices within $\mathrm{SL}_2(\mathbb{Z})$ yield a single transformation. In contrast to above, the generators of modular group as defined in eqn. (1.54) yield

$$S : \tau \to -\frac{1}{\tau} \qquad T : \tau \to \tau + 1\,. \tag{1.56}$$

1.5.1.1 Dedekind eta Function

The infinite product defines the Dedekind eta function $\eta(\tau)$ on the upper half plane given below

$$\eta(\tau) = e^{\frac{\tau i\pi}{12}} \prod_{n=1}^{\infty}(1-e^{2\pi i n\tau}), \tag{1.57}$$

where, $\mathrm{Im}(\tau) > 0$ is required for the convergence of the series. Jacobi's pioneering work "Fundamenta Nova" was the first to investigate this function. Jacobi assumed that $\mathrm{Im}(\tau) > 0$ in his research. In some of his unpublished writings, Riemann examined the behaviour of (τ) in the limiting condition $\mathrm{Im}(\tau) = 0$, which were edited by Dedekind and Weber in 1874 following Riemann's tragic death.

So following the transformation as expressed in eqn. (1.56) the Dedekind eta function tranforms as

$$S : \tau \to \tfrac{-1}{\tau}, \qquad \eta(\tau) = \sqrt{-i\tau}\,\eta(\tau), \tag{1.58}$$

$$T : \tau \to \tau + 1, \qquad \eta(\tau) = e^{\frac{-i\pi}{12}}\eta(\tau). \tag{1.59}$$

Extending the above transformations to $\eta(3\tau)$, $\eta(\tau/3)$, $\eta((\tau+1)/3)$, $\eta((\tau+2)/3)$ as they form a closed group under modular symmetry.

Under T generator the transformation are given as

$$\begin{aligned}
\eta(3\tau) &\to e^{i\frac{\pi}{4}}\eta(3\tau), \\
\eta\left(\frac{\tau}{3}\right) &\to \eta\left(\frac{\tau+1}{3}\right), \\
\eta\left(\frac{\tau+1}{3}\right) &\to \eta\left(\frac{\eta+2}{3}\right), \\
\eta\left(\frac{\tau+3}{3}\right) &\to e^{\frac{i\pi}{12}}\eta\left(\frac{\tau}{3}\right).
\end{aligned} \tag{1.60}$$

Under S generator they transform as

$$\begin{aligned}
\eta(3\tau) &\to \sqrt{\frac{1}{3}}\sqrt{-i\tau}\,\eta\left(\frac{\tau}{3}\right), \\
\eta\left(\frac{\tau}{3}\right) &\to \sqrt{3}\sqrt{-i\tau}\,\eta(3\tau), \\
\eta\left(\frac{\tau+1}{3}\right) &\to e^{\frac{-i\pi}{12}}\sqrt{-i\tau}\,\eta\left(\frac{\tau+2}{3}\right), \\
\eta\left(\frac{\tau+2}{3}\right) &\to e^{\frac{-i\pi}{12}}\sqrt{-i\tau}\,\eta\left(\frac{\tau+1}{3}\right).
\end{aligned} \tag{1.61}$$

The importance of these eta functions expressed in eqn.(1.60) and eqn.(1.61) more precise in further section where we discuss the A_4 modular symmetry because my doctoral work mostly involves it.

1.5.1.2 A_4 modular symmetry

In this section we mainly focus on the modular form of level 3, abiding the relation

$$f(\gamma\tau) = (c\tau + d)^{2k} f(\tau), \tag{1.62}$$

where,

$$\Gamma(3) = \left\{ \gamma = \begin{pmatrix} a & b \\ c & d \end{pmatrix} \in SL_2(\mathbb{Z}), \quad \begin{pmatrix} a & b \\ c & d \end{pmatrix} = \begin{pmatrix} 1 & 0 \\ 0 & 1 \end{pmatrix} \quad (\text{mod}(3)) \right\} \tag{1.63}$$

Therefore, their exists a quotient space for $\Gamma(3)$ i.e. $\mathscr{H}/\Gamma(3)$ purported by a fundamental domain $\mathscr{F}$, which implies to be a connected region of $\mathscr{H}$, suggesting that each point of $\mathscr{H}$ can be projected into $\mathscr{F}$ via $\Gamma(3)$ transformation. However, an interesting point to note is that no two points in the domain of $\mathscr{F}$ are related under $\Gamma(3)$. Therefore, $\mathscr{H}/\Gamma(3)$ is nothing but $\mathscr{F}$ with definite boundary points identified. Compatification of $\mathscr{H}/\Gamma(3)$ is made via adding certain points $i\infty, -1, 0, 1$ which forms the cusps and serve as the vertices of a tetrahedron, hence, $\Gamma(3)$ being isomorphic to A_4 discrete symmetry because cusps are related to the transformation $\Gamma_3 \approx \bar{\Gamma}/\bar{\Gamma}(3)$. The generators S and T help to generate A_4 symmetry while satisfying the relation:

$$S^2 = T^3 = (ST)^3 = 1\,. \tag{1.64}$$

The dimension of $\Gamma(3)$ being $2k+1$, for lower modular weight i.e. $k = 1$, their exist three linearly independent Yukawa coupling expressed in terms of Dedekind eta function expressed in appendix A in eqn. (B.1). However, for numerical calculation we use the q expansion form of the Yukawa couplings expressed as

$$\begin{aligned} Y_1(\tau) &= 1 + 12q + 36q^2 + 12q^3 + \cdots\,, \\ Y_2(\tau) &= -6q^{1/3}\left(1 + 7q + 8q^2 + \cdots\right)\,, \\ Y_3(\tau) &= -18q^{2/3}\left(1 + 2q + 5q^2 + \cdots\right). \end{aligned} \tag{1.65}$$

Also, $Y_i(\tau)$ satisfies the constraint relation given by

$$Y_2^2 + 2Y_1Y_3 = 0\,, \tag{1.66}$$

because it is necessary to recover the correct dimension of the linear space $M_{2k}(\Gamma(3))$.

1.5.1.3 A_5' modular symmetry

Here, we discuss the scenario for double cover of A_5 symmetry i.e. $\Gamma_5' \approx A_5'$. Unlike A_4 or A_5 double cover is advantageous because here we are able to have both even and odd weight modular forms. Moreover, exploring the geometrical aspect it seems clear that $\Gamma'(5) \approx A_5'$ resembles icosahedral which is a double cover of dodecahedron. However, a clear picture is established by discussing things in the domain of group theory. The basic properties and definitions are similar as discussed in section 1.5.1, but the peculiarity here being, three generators are involved i.e. along with S and T there is one more generator R given by

$$R = \begin{pmatrix} -1 & 0 \\ 0 & -1 \end{pmatrix}, \tag{1.67}$$

such that S, T and R satisfy the identities $S^2 = R$, $(ST)^3 = R^2 = I$ and $RT = TR$. This extra generator R helps in transforming matter fields in modular invariant theories as mentioned in refs. [20, 21]. Therefore, instead of $\overline{\Gamma}$ we have to use Γ as the symmetry group in such theories. Hence, for the finite double cover modular group, the definition goes as $\Gamma'_N \equiv \Gamma/\Gamma(N)$ utilizing the above identities.

Above preliminary discussion lays the foundation for A'_5 modular symmetry, where, A'_5 group consists of 120 elements for $N = 5$. These 120 elements are divided into nine conjugacy classes out of which **1**, **3**, $3'$, **4**, **5** with $R = I$ are the irreducible representations corresponding to dodecahedron symmetry. Similarly, $\hat{2}$, $\hat{2}'$, $\hat{4}$, $\hat{6}$ with $R = -I$ are the irreducible representations related to icosahedral. Therefore, the Kronecker product rules associated to these irreducible representations and relevant to my doctoral work are expressed in appendix C.

1.6 Leptogenesis – showcasing Universe's baryon asymmetry

The current cosmos is asymmetric in terms of matter-anti matter content, whereas it was previously acclimatised [22] with an equal amount of particle and antiparticle states. The value of the asymmetry has been demonstrated by results from BBN and CMBR as

$$\eta_B = \frac{n_B - n_{\bar{B}}}{n_\gamma} \approx (2.6 - 6.2) \times 10^{-10}. \tag{1.68}$$

Here, n_B ($n_{\bar{B}}$) is the (anti)baryon number density and n_γ being the photon number density. As a result, this has been a difficult problem with limited knowledge that will be resolved through further research. Sakharov [23], who insists on three requirements, has presented the most notable conditions explaining the production of asymmetry from a symmetric Universe given as : i) baryon number violation in the early Universe ii) C and CP violation iii) Out of equilibrium decay of heavy particles and discussed below.

1.6.1 Baryon number violation in early Universe

Baryon number violation in an earlier period is expected for the emergence of asymmetry in the baryon sector from a symmetric universe. This thing becomes obvious at the GUT scale where representations acquired by quark and leptons are same. Moreover, baryon and lepton number constitute accidental symmetries, hence, can be violated at tree level. Whereas, non-perturbative sphalerons may include $(B+L)$ violating processes expressed as

$$\begin{aligned} B &= \int J_0^B(x)\, d^3x\,, \\ L &= \int J_0^L(x)\, d^3x\,, \end{aligned} \tag{1.69}$$

where,

$$\begin{aligned} J^B_\mu &= \frac{1}{3}\sum_i \left(\overline{q_{L_i}}\gamma_\mu q_{L_i} - \overline{u^c_{L_i}}\gamma_\mu u^c_{L_i} - \overline{d^c_{L_i}}\gamma_\mu d^c_{L_i}\right), \\ J^L_\mu &= \sum_i \left(\overline{\ell_{L_i}}\gamma_\mu \ell_{L_i} - \overline{e_{L_i}}\gamma_\mu e_{L_i}\right). \end{aligned} \tag{1.70}$$

In here, J^B_μ is the baryonic current and J^L_μ represents leptonic current, also, q_L and ℓ_L represent the quark and lepton fields respectively in eqn. (1.70). Interesting thing to notice is that even if B and L are classically conserved but the triangle anomalies associated, generate a quantum mechanical divergent current given as

$$\partial_\mu J^B_\mu = \partial^L_\mu = \frac{1}{\left(4\sqrt{2}\pi\right)^2} n_F \left(g^2 W^a_{\mu\nu}\widetilde{W}^{a\mu\nu} - g'^2 B_{\mu\nu}\widetilde{B}_{\mu\nu}\right), \tag{1.71}$$

where, $SU(2)_L$ field strength is given by $W^a_{\mu\nu} = \partial_\mu W^a_\nu - \partial_\nu W^a_\mu$ and $U(1)_Y$ field strength is presented by $B_{\mu\nu} = \partial_\mu B_\nu - \partial_\nu B_\mu$ and n_F being the no. of fermion generations. It is quite clear from the equations presented above that $B+L$ is violated i.e. $\left(\partial^\mu J^B_\mu + \partial^\mu J^L_\mu \neq 0\right)$ being the divergent current which depends upon the topological charges identified as Chern-Simon numbers (N_{CS}) [24] and alters for different degenerate states of the vacuum in non-abelian theories. Additionally, B and L number are violated due to the transitions between different vacuum states i.e, $\Delta B = \Delta L = n_F \Delta N_{CS} = 3n$, with, n being an +ve integer. Therefore, yielding a lowest order operator

$$\mathcal{O}_{B+L} = \prod \left(q_{L_i} q_{L_i} q_{L_i} \ell_{L_i}\right). \tag{1.72}$$

There seems to be quantum tunneling effect between various vacua, called, instanton effects, which are exponentially suppressed at zero temperature with a probability of $e^{-\frac{4\pi}{\alpha}} \approx \mathcal{O}(10^{-165})$. However, when temperature is high enough it still will allow classical process and transition can lead through thermal fluctuations over barrier. As a result, the B + L violating process has a considerable rate of maintaining thermal balance at this scale. This transition rate is dictated by the sphalerons, an unstable solution of the gauge-Higgs system in finite temperature electroweak theory. Additionally, sphaleron transition rate per unit volume due to temperature below EWSB is given by $\frac{\Gamma_{B+L}}{V} \approx \frac{1}{e^{M_W/\alpha KT}}$ and is repressed exponentially, where, M_W being the mass of the W mass, k is the Boltzmann constant, and α being the fine structure constant. However, if the temperature is high enough then the transition rate is given by $\frac{\Gamma_{B+L}}{V} \approx (\alpha T)^4 \frac{\alpha}{\ln \alpha}$ which is a compelling result.

1.6.2 C and CP violation

To generate the B asymmetry CP violation plays a key role and is necessary. Let us demonstrate a toy model incorporating heavy exotic particles say χ_k which can interact with other particles say fermions ℓ_j and scalars η's through Yukawa terms

$$\mathcal{L} = h_{jk}\bar{\ell}_j \eta \chi_k + h.c., \tag{1.73}$$

where, h_{jk} is the complex coupling with $j,k = 1,2,\cdots$, where fig. 1.4 represents the tree level Feynman diagram related to the decay of χ_k. In general, let us consider that the decay $\chi_k \to \ell_j \eta$ as shown in fig. 1.4, gives a change of $\Delta B_\chi = +1$, while the decay of antiparticle $\bar{\chi}_k \to \bar{\ell}_j \bar{\eta}$ has $\Delta B_{\bar{\chi}} = -1$, then the CP asymmetry can be quantified w.r.t. the above decays as

$$\begin{aligned} \epsilon_{CP} &= \frac{\Delta_{B_\chi}\Gamma\left(\chi_k \to \ell_j \eta\right)}{\Gamma_{total}} + \frac{\Delta_{B_{\bar{\chi}}}\Gamma\left(\bar{\chi}_k \to \bar{\ell}_j \bar{\eta}\right)}{\Gamma_{total}} \\ &= \frac{(+1)\Gamma\left(\chi_k \to \ell_j \eta\right) + (-1)\Gamma\left(\bar{\chi}_k \to \bar{\ell}_j \bar{\eta}\right)}{\Gamma_{total}} \\ &= \frac{\Gamma - \bar{\Gamma}}{\Gamma + \bar{\Gamma}}\,, \end{aligned} \tag{1.74}$$

where the denominator expresses the total decay rate with $\Gamma \equiv \Gamma\left(\chi_k \to \ell_j \eta\right)$ and $\bar{\Gamma} \equiv \Gamma\left(\bar{\chi}_k \to \bar{\ell}_j \bar{\eta}\right)$. It is

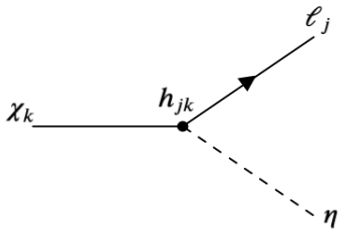

Figure 1.4: Tree level Feynman diagram for the heavy particle decay $\chi_k \to \ell_j \eta$

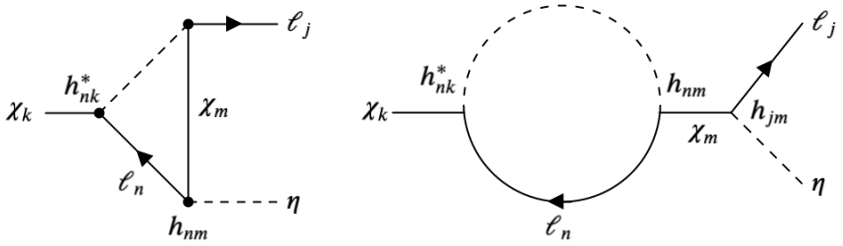

Figure 1.5: Left diagram represents the one loop vertex correction for the particle $\chi_k \to \ell_j \eta$ and right diagram showcases the corresponding one-loop self energy diagram.

clear from above expression that a difference in the decay of particle and antiparticle is a must which will allow to generate certain CP asymmetry in the baryon number. In order to achieve that one has to go beyond the lowest order and therefore the first non zero contribution to CP asymmetry comes from the mixing between the tree level and one-loop diagrams as shown in fig. 1.5

1.6.3 Departure from thermal equilibrium

The requirement of departing from thermal equilibrium in accordance with Sakharov's third condition is well justified by equilibrium thermodynamics. The number density of particles and anti-particles in

the thermal bath equilibrates through potential interactions such as decay, inverse decay, or annihilation in forward and backward directions. The particle decouples and the number density is diluted when the universe's expansion rate surpasses the interaction rate. Let us consider a heavy boson X existing in thermal equilibrium from the early epoch with $n_X = n_{\bar{X}} = n_\gamma$ for $T \geq m_X$ and $n_X = n_{\bar{X}} \simeq (m_X T)^{3/2} \ll n_\gamma$ for $T \simeq m_X$. In order to achieve an equilibrium number density of both X and $\bar{X}$, it demands the interactions taking part in the formation and decay of these bosons to be in counterpoise. As self quenching property is showcased by annihilation processes, therefore, decay processes are of great significance in equilibrium dynamics.

So to illustrate the third condition, we consider $\Gamma_D, \Gamma_{ID}, \Gamma_s$ being decay, inverse decay and scattering process of X and $\bar{X}$ bosons respectively expressed as

$$\Gamma_D = \alpha_{m_X} \begin{cases} m_x T^{-1}, \text{ when } T \geq m_X, \\ 1 \text{ when } T \leq m_X, \end{cases} \tag{1.75}$$

$$\Gamma_{ID} = \Gamma_D \begin{cases} 1 \text{ when } T \geq m_X, \\ (m_x/T)^{3/2}/e^{m_x/T} \text{ when } T \leq m_X, \end{cases} \tag{1.76}$$

$$\Gamma_s = \alpha^2 \left(\frac{T^{5/2}}{T^2 + m_x^2} \right)^2, \quad H = \frac{\sqrt{g_* T^4}}{M_{Pl}}, \tag{1.77}$$

where, $\alpha = g^2/4\pi$ represents the strength of coupling associated with boson X. Also, σ being the annihilation cross section at high temperature and is given as $\frac{\alpha^2}{T^2}$ and in low temperature it takes the value $\sigma \approx G_{\Delta B}^2 T^2$. Now for higher values of m_X, the effectiveness of the interaction rate is lowered as compared to Hubble expansion (H), depicted by expressing through a new parameter

$$K = \frac{\Gamma}{2H}\bigg|_{T=m_X} = \left[\frac{\alpha}{3.3\sqrt{g_*}} \right] \left[\frac{M_{Pl}}{m_X} \right]. \tag{1.78}$$

Above eqn. (1.78) defines the efficacy of decay or inverse decay depending upon $T \simeq m_X$ and $T \leq m_X$ respectively. Hence, when $K < 1$, the reaction rate is governed by the expansion and particle deviates from equilibrium, forbidding the backward reactions kinematically leading to over-abundance of X and $\bar{X}$. When the decay of X and $\bar{X}$ is completely done, $t \sim \Gamma_D^{-1}$ with $n_X = n_{\bar{X}} \simeq n_\gamma$ and $s \approx g_* n_\gamma$ called the entropy density. A simple relation for baryon asymmetry arises

$$Y_B = \frac{n_B}{s} \approx \frac{\epsilon n_\gamma}{g_* n_\gamma} \approx \frac{\epsilon}{g_*}. \tag{1.79}$$

As, $K < 1$ making inverse decay and scattering processes immaterial and allowing only decay process, hence, to have baryon symmetry of the order $\mathcal{O}(10^{-10})$, it is required to have $\epsilon_{CP} \simeq 10^{-8}$ with $g_* \simeq 10^2$. Taking the above considerations into account one can establish a Boltzmann equation to solve the number

density of X by incorporating decay and inverse decay as

$$\frac{dn_X}{dt} + 3H_X = -\Gamma_D \left(n_X - n_X^{eq}\right), \tag{1.80}$$

where, n_X indicates the equilibrium number density and Γ_D being thermally averaged decay rate X, where,

$$\begin{aligned} |M(X \to \mathrm{b}\mathrm{b})|^2 &= |M(\bar{\mathrm{b}}\bar{\mathrm{b}} \to X)|^2 = \frac{1+\epsilon}{2}|M_0|^2 , \\ |M(X \to \bar{\mathrm{b}}\bar{\mathrm{b}})|^2 &= |M(\mathrm{b}\mathrm{b} \to X)|^2 = \frac{1-\epsilon}{2}|M_0|^2 . \end{aligned} \tag{1.81}$$

Hence, the Boltzmann equation is modified by subtracting $n_{\bar{\mathrm{b}}}$ from n_b

$$\frac{dn_B}{dt} + 3Hn_B = \epsilon\Gamma_D(n_X - n_X^{eq}) - n_B\left(\frac{n_X^{eq}}{n_\gamma}\right) - 2n_B n_b \langle\sigma|v|\rangle . \tag{1.82}$$

As a result, the nonzero baryon asymmetry can only be obtained by departing from the thermal equilibrium and violating the baryon number, C and CP.

1.7 Dark Matter

In recent times, the presence of dark matter has become a hot topic, and the hunt for direct and indirect evidences remained unresolved. According to data from the WMAP and Planck satellites, dark matter and dark energy occupy around 23% and 73% of the universe, respectively, revealing a preponderance of the dark sector over the visible one [25, 26]. Unless Zwicky [27, 28] pointed out the existence of a dark sector, matter domination was still asserted until 1933. This was believed to be enormous, neutral, and stable, as indicated by its gravitational interaction [29, 30].

1.7.1 Galaxy rotation curves, CMBR and Gravitational lensing

Astronomy has provided proof of dark matter in an indirect way [31–33], as during 1978 Vera Rubin and colleagues meticulously studied flat rotation curves of spiral galaxies. The structure of spiral galaxies reveals that maximum mass is at the center forming a bulge. Therefore, stars rotational velocities are functions of radial distances. A simple equation demonstrates the validity of the above sentence given below:

$$\frac{mv^2(r)}{r} = \frac{GmM(r)}{r^2}. \tag{1.83}$$

Here, $v(r)$, r, m and $M(r)$, denote radial velocity, radial distance, mass of the star and mass enclosed in radius r respectively. To preserve the laws of physics the intuitive way being the decrease of velocity when r increase for a constant $M(r)$. But observation showed that the velocity being constant after a certain distance giving an indirect implication of the presence of dark matter. As an example we show the rotation curve plot for NCG 3198 in Fig. 1.6.

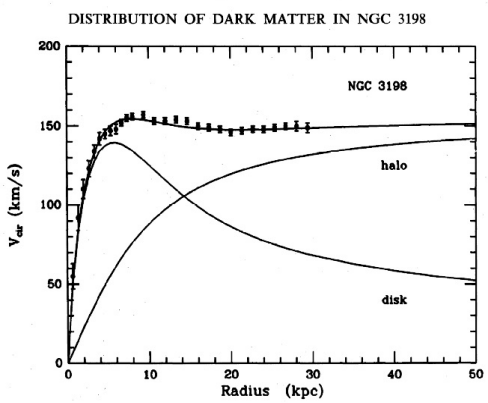

Figure 1.6: Velocity rotation curves for spiral galaxy NGC 3198.

The other perspective to admit the existence of dark matter is through Cosmological microwave background radiation (CMBR) where the observations from primodial nucleosynthesis predicted that the total density of luminous baryonic matter ($\Omega_B \approx 0.01$). This result is in disparity with the observed matter density $0.014 \leq \Omega_B \leq 0.16$ ruminating towards existence of a small amount of non-baryonic matter. Deeper insight regarding CMBR reveals the important role played by thermodynamics because during the early epoch, the temperature was high enough and matter was in plasma state making it difficult for photons streaming. But as temperature decreases (i.e. ≈ 0.1eV) and Universe cooled, matter-radiation decoupling took place bringing CMBR into existence. Wilkinson Microwave Anisotropy Probe (WMAP) made the discovery of CMBR and helped physicists to think deep and probe into the early Universe by setting new experiments. Before recombination epoch, weak interaction was inferior to Thomson scattering of photon interacting with electrons and baryons. However, the possibility of non-baryonic matter, which interacts solely through weak or gravitational interactions, is hinted at by the baryon acoustic oscillation. This creates a potential barrier for the baryon-photon fluid, forcing it to compress and expand in order to overcome it by creating a pressure difference. Photons in the most packed zone are high in temperature than those in the most dispersed area. As a consequence, minuscule anisotropies in the temperature of CMB photons from the surface of last scattering were formed, which revealed a lot more information about the universe than what was originally discovered by WMAP. Fig. 1.7 shows different peaks where the first peak corresponds to geometric structure of the universe, whereas, second one reveals the total baryon number density and the third one gives information

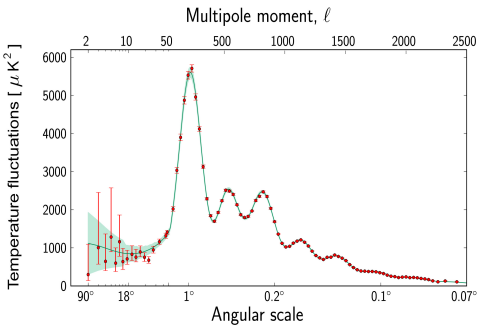

Figure 1.7: CMBR's power spectrum

about the existence of DM. Unlike CMBR, gravitational lensing i.e. bending of light makes a clear indirect inference towards the existence of dark matter. The support for above statement comes from calculating masses through scattered radial velocity, X-ray emission and gravitational lensing which signify that dark matter to visible matter is approximately 5 : 1. So, when a distant observer pinpoints a source such that the light reaching him/her has undergone bending having an massive obstruction proves general relativity right and helps in measuring the mass present because more the mass more the bending of light. Therefore, bullet cluster is best example which supports the presence of dark matter.

1.7.2 Dynamics of early Universe

Universe began being a charged soup which was extremely dense and hot, with particle interactions occurring far more often than they do today. Production and annihilation ensued at the same rate, sustaining the balance. This is known as 'thermal equilibrium' in statistical terms, and it occurs at a specific temperature. For most of the early Universe epochs, the thermal equilibrium description turns out to be a decent approximation. The expansion of the Universe, on the other hand, never results in a state of complete thermal equilibrium. Also, a nearly equilibrium state of the Universe is said to be maintained when $\Gamma \geq H$, where Γ is annihilation rate and H is Hubble expansion rate ($\approx \frac{\dot{a}}{a}$).

1.7.2.1 Thermodynamics at equilibrium

In thermodynamics a huge number of particles are involved to define a system and it is not feasible for anyone to calculate individual particle's physical observables. Therefore , statistical mechanics comes into picture where mainly all the properties of a system is revealed by incorporating one of the three mechanism i.e. for classical system we have Maxwell-Boltzmann statistics and for quantum system Fermi-Dirac or Bose-Einstein statistics is used. Two parameters play crucial role, one is temperature (T) and second is chemical potential (μ) in writing the distribution function

$$\bar{n}(\epsilon) = \frac{1}{\exp\left(\frac{\epsilon-\mu}{K_B T}\right) \pm 1}\,, \tag{1.84}$$

where, ϵ represents the energy of the particle with +1 taken for fermions and -1 for bosons. Also, defining the number and energy densities as below

$$\begin{aligned} n &= \frac{g}{(2\pi)^3}\int d^3\epsilon\; \bar{n}(\epsilon)\,, \\ \rho &= \frac{g}{(2\pi)^3}\int d^3\epsilon\; \epsilon\bar{n}(\epsilon)\,. \end{aligned} \tag{1.85}$$

where, g implies the internal d.o.f. of the particle. If we omit the chemical potential of the particles, we get

$$\begin{aligned} n &= \frac{g}{2\pi^2}\int_m^\infty \epsilon d\epsilon\; \frac{(\epsilon^2-m^2)^{1/2}}{e^{\frac{\epsilon}{K_B T}} \pm 1}\,, \\ \rho &= \frac{g}{2\pi^2}\int_m^\infty \epsilon^2 d\epsilon\; \frac{(\epsilon^2-m^2)^{1/2}}{e^{\frac{\epsilon}{K_B T}} \pm 1}\,. \end{aligned} \tag{1.86}$$

Using the relations of ζ and Γ functions

$$\begin{aligned}\int_0^\infty \frac{v^n}{e^v-1}dv &= \zeta(n+1)\Gamma(n+1)\,,\\ \int_0^\infty v^n e^{-v^2}dv &= \frac{1}{2}\Gamma\left(\frac{n+1}{2}\right).\end{aligned} \tag{1.87}$$

we can have the relativistic limit ($m \ll T$)

$$n = \left(\zeta(3)/\pi^2\right) gT^2 \begin{cases} 1, \text{ boson} \\ \frac{3}{4}, \text{ fermion,} \end{cases} \qquad \rho = \left(\frac{\pi^2}{30}\right) gT^4 \begin{cases} 1, \text{ boson} \\ \frac{7}{8}, \text{ fermion.} \end{cases} \tag{1.88}$$

However, the non-relativistic limit ($m \gg T$) results for n and ρ

$$n = g\left(\frac{2\pi}{mT}\right)^{-3/2} e^{-m/T}, \quad \rho = mg\left(\frac{2\pi}{mT}\right)^{-3/2} e^{-m/T}\,. \tag{1.89}$$

At low temperature, the number density of heavy particles is exponentially suppressed, as shown above in eqn. (1.89). As a result, the number density of any heavy particle today will be minimal, as the Universe has progressed from a hot dense phase to the current cooling state. We now address non-equilibrium thermodynamics to explain dark matter abundance since its density endures throughout the Universe.

1.7.2.2 Delving into thermodynamics at non-equilibrium - Relic density

Let us consider a stable dark matter particle n_ϕ with lifetime more than the age of the Universe. When interaction rate (Γ) > Hubble expansion rate (H) particles remain in equilibrium and for vice-versa they decouple

$$\begin{aligned}\frac{dn_\phi}{dt} + 3Hn_\phi = -\int d\prod_\phi\, d\prod_{\bar\phi}\, d\prod_\chi\, d\prod_{\bar\chi} \times (2\pi)^4\delta^4(p_\phi + p_{\bar\phi}) \times \\ \left[|M|^2_{\phi\bar\phi\to\chi\bar\chi} f_\phi f_{\bar\phi}(1\pm f_\chi)(1\pm f_{\bar\chi}) - |M|^2_{\chi\bar\chi\to\phi\bar\phi} f_\chi f_{\bar\chi}(1\pm f_\phi)(1\pm f_{\bar\phi})\right].\end{aligned} \tag{1.90}$$

Here, $d\prod = \frac{g}{(2\pi)^3}\frac{d^3p}{2\epsilon}$, $1+f$ is applicable for boson and $1-f$ for fermion expressing the Bose enhancement and Pauli blocking respectively. When $T < \epsilon_i$, Maxwell-Boltzmann statistics becomes applicable to all species with $f_i = e^{\epsilon_i/T}$, also, $1 \pm f \approx 1$. Now, if we consider CP invariance i.e. $|M|^2_{\phi\bar\phi\to\chi\bar\chi} = |M|^2_{\chi\bar\chi\to\phi\bar\phi}$, it simplifies the Boltzmann equation as

$$\frac{dn_\phi}{dt} + 3Hn_\phi = -\int d\prod_\phi\, d\prod_{\bar\phi}\, d\prod_\chi\, d\prod_{\bar\chi} \times (2\pi)^4\delta^4(p_\phi + p_{\bar\phi}) \times |M|^2 \left[f_\phi f_{\bar\phi} - (1\pm f_{\bar\phi})\right]. \tag{1.91}$$

So, now if the outgoing particles ($\chi, \bar\chi$) are in equilibrium, i.e.,

$$f_\chi = e^{-\epsilon_\chi/T}\,, \qquad f_{\bar\chi} = e^{-\epsilon_{\bar\chi}/T}\,. \tag{1.92}$$

The energy conservation is imposed by the δ-function, therefore

$$f_\chi f_{\bar\chi} = e^{-(\epsilon_\chi+\epsilon_{\bar\chi})/T} = e^{-(\epsilon_\phi+\epsilon_{\bar\phi})/T} = f^{eq}_\phi f^{eq}_{\bar\phi}\,. \tag{1.93}$$

So, the Boltzmann equation modifies as

$$\frac{dn_\phi}{dt} + 3Hn_\phi = -\langle\sigma|v|\rangle\left[\left(n_\phi + n_\phi^{eq}\right)\left(n_\phi - n_\phi^{eq}\right)\right], \tag{1.94}$$

where,

$$\langle\sigma|v|\rangle = \frac{1}{\left(n_\phi^{eq}\right)^2}\int d\prod_\phi\, d\prod_{\bar{\phi}}\, d\prod_\chi\, d\prod_{\bar{\chi}} \times (2\pi)^4\delta^4\left(p_\phi + p_{\bar{\phi}} - p_\chi - p_{\bar{\chi}}\right)|M|^2 e^{-(\epsilon_\phi+\epsilon_{\bar{\phi}})/T}. \tag{1.95}$$

Let us suppose a dimensionless parameter $Y_\phi = n_\phi/s$, where, $s = \frac{2\pi^2T^3}{45}g_{*s}$ denoting the entropy density. Therefore, above equation takes the form given below, where, entropy density is treated constant i.e. (sa^3 = const.) in a co-moving volume

$$\frac{dY_\phi}{dt} = -s\langle\sigma|v|\rangle\left[\left(Y_\phi + Y_\phi^{eq}\right)\left(Y_\phi - Y_\phi^{eq}\right)\right]. \tag{1.96}$$

Introducing another massless parameter $x = m_\phi/T$, where, there is temperature dependence interaction. Moreover, in a radiation dominated era t and x satisfy

$$t = \log 2 * \frac{M_{Pl}}{\sqrt{T^4 g_*}} = \log 2 * M_{Pl}\frac{x^2}{m_\phi^2\sqrt{g_*}}, \tag{1.97}$$

where, m_ϕ represents the dark matter mass, $M_{Pl} = 1.22 * 10^{19}$ GeV and g_* accounts for total massless dependent relativistic degree of freedom mentioned below

$$g_*(T) = \sum_{i=bosons} g_i\left(\frac{T_i}{T}\right)^4 + \frac{7}{8}\sum_{i=fermions} g_i\left(\frac{T_i}{T}\right)^4. \tag{1.98}$$

As their is a clear temperature dependence in the above equation, hence, g_* value comes to be 106.75 for $T \geq 300$GeV. This is due to the fact that above this temperature, all SM particles acquire relativistic nature. If we consider present scenario of the universe only photons and neutrinos come under the relativistic particles with $g_* = 3.36$ and $T < 1$ MeV. Hence, again the Boltzmann equation modifies as

$$\begin{aligned}\frac{dY_\phi}{dt} &= -\frac{xs}{H(m)}\langle\sigma|v|\rangle\left[\left(Y_\phi - Y_\phi^{eq}\right)\left(Y_\phi + Y_\phi^{eq}\right)\right] \\ &= -\left(\frac{2\pi^2}{45}\right)\left(\frac{g_{*s}}{H(m)}\right)m_\phi^3\langle\sigma|v|\rangle\left[\left(Y_\phi - Y_\phi^{eq}\right)\left(Y_\phi + Y_\phi^{eq}\right)\right],\end{aligned} \tag{1.99}$$

with $H(m) = 1.67\sqrt{g_{*s}}\frac{m_\phi^2}{M_{Pl}}$.

At equilibrium,

$$Y_\phi^{eq} = \frac{n_\phi^{eq}}{s} = 0.145 * \frac{g}{g_{*s}}x^{3/2}e^{-x}, \;\; n_\phi^{eq} = g\left(\frac{m_\phi T}{2\pi}\right)e^{-\frac{m_\phi}{T}}. \tag{1.100}$$

Their is no analytical solution that can be obtained from eqn. (1.99), as it impersonates a specific form of Riccati equation, to its rescue, the solutions can be obtained via approximations. Moreover, velocity dependence acts as a catalyst for annihilations cross-section, therefore, for non-relativistic speices $\sigma|v| \approx$

$\sigma_0 x^{-n}$. If the value of $n = 0$, it accounts for s-wave, whereas, $n = 1$ is for p wave annihilation. Hence, the modified eqn. 1.99 becomes

$$\frac{dY_\phi}{dt} = -\lambda x^{-(n+2)} \left[\left(Y_\phi - Y_\phi^{eq} \right) \left(Y_\phi + Y_\phi^{eq} \right) \right]. \tag{1.101}$$

Here,

$$\lambda = \frac{2\pi^2 g_{*s} \sigma_0 m_\phi^3}{45 x^2 H(m)} = 0.264 \sigma_0 \left(\frac{g_{*s}}{\sqrt{g}_*} \right) M_{Pl} m_\phi \,. \tag{1.102}$$

Proceeding further and bringing in another new quantity $\Delta_\phi = Y_\phi - Y_\phi^{eq}$, therefore eqn. (1.101) can be written as

$$\Delta'_\phi = -\frac{dY_\phi^{eq}}{dx} - \lambda x^{-(n+2)} \Delta_\phi (2Y_\phi^{eq} + \Delta_\phi) \,. \tag{1.103}$$

So, eqn. (1.103) further transforms when, $x < \left(x_f = \frac{m_\phi}{T_f} \right)$, if this is the case then Y_ϕ superimposes Y_ϕ^{eq} and hence the above differential equation of Δ_ϕ becomes negligible and reduces to

$$\Delta_\phi \approx \frac{x^{n+2}}{2\lambda} \,. \tag{1.104}$$

But when the case becomes $x \gg x_f$, it gives $\Delta_\phi \simeq Y_\phi \gg Y_\phi^{eq}$, hence

$$\Delta'_\phi = -\lambda x^{-(n+2)} \Delta_\phi^2 \,. \tag{1.105}$$

When we take out the integration from limits $\{x_f, \infty\}$, it yields

$$Y_\infty = \Delta_\infty = \frac{1}{\lambda} \frac{x_f^{n+1}}{(n+1)^{-1}} \,. \tag{1.106}$$

All this painstacking to calculate the relic density computed as

$$\Omega_\phi = \frac{\rho}{\rho_0} = m_\phi \frac{Y_\infty s_0}{\rho_0} = 1.07 * 10^9 * (n+1) * x_f^{n+1} \left(\frac{\sqrt{g_*}}{g_{*s}} \right) \left(h^2 M_{Pl} \sigma_0 \right)^{-1} \mathrm{GeV}^{-1}. \tag{1.107}$$

Here, $\rho_0 = \frac{3H_0^2}{8\pi G}$ called the critical density, $H_0 = 100h \frac{\mathrm{Km}}{\mathrm{sec} * \mathrm{Mpc}}$ and G being the gravitational constant. The void of annihilation process due to freeze-out reduces the number density and present abundance is estimated as

$$\Omega h^2 = \frac{1.07 * 10^9}{\sqrt{g_*} M_{Pl} J_f} \mathrm{GeV}^{-1} \,, \tag{1.108}$$

where, $J_f = \int_{x_f}^{\infty} \frac{\langle \sigma v \rangle x}{x^2}$ and $\langle \sigma v \rangle x$ is given by

$$\langle \sigma v \rangle (x) = \left(\frac{x}{8} \right) \frac{1}{m_\phi^5 K_2^2(x)} \int_{4m_\psi^2}^{\infty} \sigma \left(s - 4m_\phi^2 \right) s^{1/2} K_1 \left(\frac{x s^{1/2}}{m_\phi} \right) ds. \tag{1.109}$$

Here, K_i and s being the modified Bessel function and center of mass energy respectively.

1.8 Thesis overview

In this chapter, a concise recap of the standard model of elementary particles is made, shedding light on scientific proof that cannot be explained within this framework. We carried out a comprehensive review of the origins of these crucial challenges and give a brief sense of the current experimental restrictions because this thesis work focuses largely on the phenomenological implications of neutrino masses and mixing, dark matter, and leptogenesis. With the observed low mass from neutrino oscillation and multiple seesaw scenarios, the masslessness of neutrinos in the standard model is addressed along-with its observed tiny mass arising from various seesaw.

In **chapter 2**, we introduce a model where we incorporate three heavy right handed neutrinos (N_{R_i}) and three heavy left handed sterile neutrinos (S_{L_i}) along with a weighton field (ρ) in presence of discrete A_4 modular symmetry and global $U(1)_\chi$ was introduced to eliminate some of the unwanted terms in the superpotential. The charges are so defined for the particles under $SU(2)_L \times U(1)_Y \times U(1)_\chi \times A_4$ with k_I as the modular weight, hence, they acquire the linear seesaw mass structure. Further as the heavy neutrinos are within few TeV range, therefore, we are able to explore Baryon asymmetry of the Universe i.e Leptogenesis. Also, we are able to make a brief discussion on flavored leptogenesis as the mass range of heavy right handed fermions suggested so.

In **chapter 3**, we make an exploration of radiative seesaw framework. In here, the neutrino mass is generated at one-loop level by introducing an inert doublet in the particle gamut. Moreover, local $U(1)_{B-L}$ is introduced to block the unwanted terms. Further, we also discuss lepton flavor violating processes i.e. $\mu \to e\gamma$, $\mu \to 3e$ and $\mu - e$ conversion in the nucleus. We have also discussed the dark matter (DM) scenario by considering the lightest Dirac fermion as DM candidate where it has scalar as well as gauge boson Z' mediated annihilations channels. Hence, we are able to obtain the relic density obeying Planck data and included a brief note on collider bounds.

In **chapter 4**, we includes a model based on A_5' modular symmetry which is a double cover of A_5 symmetry in a inverse seesaw framework. The interesting thing about inverse seesaw is that the correct order for the active neutrinos mass comes from the Majorana term (μ) in the mass structure. It means that in regular seesaw the heaviness of the right handed neutrino decides the correct order of the active neutrinos, but in inverse seesaw the smallness of the μ term governs the correct order. Additionally, we discuss the lepton flavor violation i.e. $\ell_i \to \ell_j \gamma$ and as $U(1)_{B-L}$ is involved in the model, therefore, a comment on the collider bounds is included on the Z' mass.

Chapter 5 is interesting because it makes use of linear seesaw framework in A_5' modular symmetry. Unlike A_4 symmetry which has only three Yukawa couplings for utilization, A_5' modular symmetry has plethora of higher weight Yukawa couplings which provide us a free-hand on there usage to get correct neutrino phenomenology. In this model, we include six heavy fermions and also include a local $U(1)_{B-L}$ which helps to forbid certain terms in the superpotential to showcase a definite mass structure. We also

allow an higher dimension term to have a small mass splitting such that we are able to incorporate resonant case for the leptogenesis where this splitting enhances the CP asymmetry such that it gives correct baryon asymmetry.

Chapter 6 summaries the complete work alongside gives an insight regarding my future prospects.

CHAPTER 2

IMPLICATIONS OF A_4 MODULAR SYMMETRY ON NEUTRINO MASS, MIXING AND LEPTOGENESIS WITH LINEAR SEESAW

2.1 Introduction

Neutrino oscillation data obtained from various experiments support the fact that neutrinos are not completely massless but have some minuscule mass [34–40]. Hence, standard model (SM) falls short in acknowledging the above claims from different experiments. Further, evidences were gathered from these experiments regarding the mixing of neutrinos and it was inferred that two of them have non-zero masses [41]. Simultaneously, it is very well known from theory and experiments that neutrinos are void of their right-handed (RH) counterparts in the SM, hence, Dirac mass term cannot be written for neutrinos, like other charged fermions, nonetheless, dimension-five operator [42–44] is useful in providing them masses. Astonishingly, the origin and flavour structure of this operator are debatable. As a result, obtaining non-zero masses for neutrinos requires examining possibilities beyond the standard model (BSM) [45]. There are various models throughout the literature that explain the observed data from various neutrino oscillation experiments, as well as the lightness of the neutrino masses, such as the most popular seesaw mechanism [46–48], radiative mass generation [49, 50], extra-dimensions [51], etc. The existence of sterile neutrinos, which are SM gauge singlets, commonly regarded right-handed neutrinos, couple to the standard active neutrinos by Yukawa interactions, is a common characteristic of many BSM theories that illuminate the origin of non-zero neutrino masses. In support to above, their masses and interaction strengths can vary over wide orders of magnitude, which helps towards explaining many observable phenomena. For instance, in the type-I seesaw framework, to accomodate the eV-scale light

neutrinos, the right handed neutrino mass is expected to be $\mathcal{O}(10^{15})$ GeV, which is clearly beyond the reach of existing and future investigations. However, its low scale variants like inverse seesaw [52–54] linear seesaw [55], extended seesaw [56], etc., where the heavy neutrino mass can be in the TeV range, which makes them experimentally verifiable.

The non-abelian discrete flavour symmetry group A_4 brings a great relief in serving as an underlying symmetry for getting the neutrino mass matrix [57], however this results in a vanishing reactor mixing angle θ_{13}. Despite this, it is nevertheless extensively employed to characterise neutrino mixing phenomenology with the addition of a simple alteration by introducing extra flavon fields that are SM singlets but transform non-trivially under the flavour symmetry group, resulting in a non-zero reactor mixing angle. As a consequence of the unique vacuum alignment they acquire, the flavons become a significant feature in manifesting the observed pattern in neutrino mixing, which plays a crucial role in spontaneous breaking of the discrete flavour symmetry [58]. Flavons are usually required in large numbers to actualize certain phenomenological characteristics within the scope of such flavour symmetry. However, there are several disadvantages to this technique, such as the fact that higher-dimensional operators can undermine the discrete flavour symmetry prediction. Furthermore, flavour symmetry is typically used to confine mixing angles, although neutrino masses are unknown except in a few cases. In contrast to above, using a modular invariance technique [59], these flaws are remedied.

Presently, pioneering work on modular flavor symmetries is proposed [36, 59, 60] to bring predictable flavor structures into the spotlight. Utilizing the approach many effective models were designed and published [61–64], by avoiding the usage of flavon fields apart from modulus τ, which breaks the flavor symmetry after it gains VEV. Therefore, we solely require a mechanism to set the modulus τ and avoid the usage of vacuum alignment which is rather very confusing. To put it another way, these couplings occur as a result of a non-trivial representation of a non-Abelian discrete flavour symmetry approach, which can substitute for the employment of flavon fields, which are not necessary or minimised in the realisation of the flavour structure. In the above context, it was realised after reading various texts that there are many groups available, such as the basis defined under the modular group of A_4 [60, 65–69], S_4 [70–73], A_5 [74, 75], larger groups [76], various other modular symmetries and double covering of A_4 [77–79], prediction of masses, mixing, and CP phases peculiar to quarks and/or leptons are done.

As aforesaid, modular invariance plays a crucial role in neutrino mass models involving only few coupling strengths, hence, establishing a correlation between neutrino masses and mixing parameters. However, there is an extension of above formalism to combine it with the generalized CP symmetry [67, 80–84]. As we know that, S and T representation are symmetric, so the modular form multiplets, if normalized aptly, acquire complex conjugation under CP transformation. As an outcome, all couplings in a modular invariant model are required to be real [81] due to generalised CP symmetry, and the model prediction power is reduced. To put the above into practice, the use of modular symmetry in constructing a

model for neutrino mass generation, as well as the indications of new physics via the observables in the neutrino sector, is quite exciting [85].

In this article, we diligently work to illuminate the benefits of A_4 modular symmetry by applying it to linear seesaw framework. The linear seesaw mechanism entails three LH neutral fermions S_{Li} in addition to three right handed ones N_{Ri} ($i = 1,2,3$) and produces a neutrino mass matrix which is intricate enough, and has been studied in the context of A_4 symmetry in [86–88]. Additionally, S_{Li} & N_{Ri} are allocated as triplets under A_4 symmetry and Yukawa couplings are defined in terms of modular form by which the neutrino mass matrix attains a confined structure. Consequently, numerical analysis is performed to scan for free parameters in the model and find an area that fits neutrino data. Neutrino sector observables are expected after adjusting for the allowable parameters.

The following is the outline for this chapter, in Sec. 2.2 we describe the well known linear seesaw mechanism with discrete A_4 modular flavor symmetry and its appealing feature resulting in simple mass structure for the charged leptons and neutral leptons including light active neutrinos and other two types of sterile neutrinos. We then provide a discussion for the light neutrino masses and mixing in this framework. In Sec. 2.3 numerical correlational study between observables of neutrino sector and model input parameters is established. We also present a brief discussion of the non-unitarity effect. Leptogenesis in the context of the present model is discussed in Sec. 2.4 and in Sec. 2.6, we conclude our results.

2.2 Model Framework

This model represents the simplistic scenario of linear seesaw, where the particle content and group charges are provided in Table 2.1. We prefer to extend with discrete A_4 modular symmetry to explore the neutrino phenomenology and a global $U(1)_X$ symmetry is imposed to forbid certain unwanted terms in the superpotential. The particle spectrum is enriched with six extra singlet heavy fermion superfields (N_{Ri} and S_{Li}) and one weighton field (ρ). The extra supermultiplets of the model transform as triplet under the A_4 modular group. The A_4 and $U(1)_X$ symmetries are considered to be broken at a scale much higher than the electroweak symmetry breaking [89]. The extra superfields acquire masses by assigning non-zero vacuum expectation value to the singlet weighton. The modular weight is assigned to all the particles and denoted as k_I. Further, it is evident that the breaking of $U(1)_X$ symmetry takes places by singlet ρ acquiring VEV. Therefore, a massless Goldstone boson comes into picture which does not have dangerous interaction among the SM particles but interact only with Higgs and contributes to the dark radiation [90, 91]. The importance of A_4 modular symmetry is the requirement of less number of flavon or weighton fields unlike the usual A_4 group, since the Yukawa couplings have the non-trivial group transformation. Assignment of group charge and modular weight to the Yukawa coupling is provided in Table 2.2.

Fields	e_R^c	μ_R^c	τ_R^c	L_L	N_R	S_L^c	$H_{u,d}$	ρ
$SU(2)_L$	1	1	1	2	1	1	2	1
$U(1)_Y$	1	1	1	$-\frac{1}{2}$	0	0	$\frac{1}{2},-\frac{1}{2}$	0
$U(1)_X$	1	1	1	-1	1	-2	0	1
A_4	1	$1'$	$1''$	$1,1'',1'$	3	3	1	1
k_I	1	1	1	-1	-1	-1	0	0

Table 2.1: Particle content of the model and their charges under $SU(2)_L \times U(1)_Y \times A_4$ where k_I is the number of modular weight.

Yukawa coupling	A_4	k_I
Y	**3**	**2**

Table 2.2: Modular weight of the Yukawa coupling $\mathbf{Y}$ and its transformation under A_4 symmetry.

2.2.1 Dirac mass term for charged leptons (M_ℓ)

In order to have a simplified structure for charged leptons mass matrix, we consider the three generations of left-handed doublets ($L_{e_L}, L_{\mu_L}, L_{\tau_L}$) transform as $\mathbf{1}, \mathbf{1''}, \mathbf{1'}$ respectively under the A_4 symmetry. They are assigned the $U(1)_X$ charge of -1 for each generation. The right-handed charged leptons follow a transformation of $\mathbf{1}, \mathbf{1'}, \mathbf{1''}$ under A_4 and singlets in $U(1)_X$ symmetries respectively. All of them are assigned with a modular weight of 1. The VEVs of Higgs superfields i.e. $\langle H_u \rangle = v_u/\sqrt{2}, \langle H_d \rangle = v_d/\sqrt{2}$ are related to SM Higgs VEV as $v_H = \sqrt{v_u^2 + v_d^2}$ and the ratio of their VEVs is expressed as $\tan\beta = (v_u/v_d) = 5$ [92, 93]. The relevant superpotential term for charged leptons is given by

$$\mathcal{W}_{M_\ell} = y_\ell^{ee} L_{e_L} H_d \; e_R^c + y_\ell^{\mu\mu} L_{\mu_L} H_d \; \mu_R^c + y_\ell^{\tau\tau} L_{\tau_L} H_d \; \tau_R^c \, . \tag{2.1}$$

The charged lepton mass matrix is found to be diagonal and the couplings can be adjusted to achieve the observed charged lepton masses. The mass matrix takes the form

$$M_\ell = \begin{pmatrix} y_\ell^{ee} v_d/\sqrt{2} & 0 & 0 \\ 0 & y_\ell^{\mu\mu} v_d/\sqrt{2} & 0 \\ 0 & 0 & y_\ell^{\tau\tau} v_d/\sqrt{2} \end{pmatrix} = \begin{pmatrix} m_e & 0 & 0 \\ 0 & m_\mu & 0 \\ 0 & 0 & m_\tau \end{pmatrix}. \tag{2.2}$$

Here, m_e, m_μ and m_τ are the observed charged lepton masses.

2.2.2 Dirac and pseudo-Dirac mass terms for the small neutrinos

Along with the transformation of lepton doublets mentioned previously, the right-handed fermion superfields transform as triplets under A_4 modular group with $U(1)_X$ charge of +1 and modular weight -1. Since, with these charge assignments we cannot write the standard interaction term, we introduce the Yukawa couplings to transform non-trivially under the A_4 modular group (triplets) and assign with modular weight of 2, as represented in Table 2.2. We use the modular forms of the coupling as $\boldsymbol{Y}(\tau) = (y_1(\tau), y_2(\tau), y_3(\tau))$, which can be written in terms of Dedekind eta-function $\eta(\tau)$ and its derivative [59], expressed in Eq. A.8 (Appendix A). Therefore, the invariant Dirac superpotential involving the active and right-handed fermion superfields can be written as

$$\mathcal{W}_D = \alpha_D L_{e_L} H_u \, (\boldsymbol{Y} N_R)_1 + \beta_D L_{\mu_L} H_u \, (\boldsymbol{Y} N_R)_{1'} + \gamma_D L_{\tau_L} H_u \, (\boldsymbol{Y} N_R)_{1''}. \tag{2.3}$$

Here, the subscript for the operator $\boldsymbol{Y} N_R$ indicates A_4 representation constructed by the product and $\{\alpha_D, \beta_D, \gamma_D\}$ are free parameters. The resulting Dirac neutrino mass matrix is found to be

$$M_D = \frac{v_u}{\sqrt{2}} \begin{bmatrix} \alpha_D & 0 & 0 \\ 0 & \beta_D & 0 \\ 0 & 0 & \gamma_D \end{bmatrix} \begin{bmatrix} y_1 & y_3 & y_2 \\ y_2 & y_1 & y_3 \\ y_3 & y_2 & y_1 \end{bmatrix}_{LR} . \tag{2.4}$$

As we also have the extra sterile fermion superfields S_{Li}, which transform analogous to N_{Ri} under A_4 modular symmetry, the pseudo-Dirac term for the light neutrinos is allowed, and the corresponding super-potential is given as

$$\mathcal{W}_{LS} = \left[\alpha'_D L_{e_L} H_u \, (\boldsymbol{Y} S_L^c)_1 + \beta'_D L_{\mu_L} H_u \, (\boldsymbol{Y} S_L^c)_{1'} + \gamma'_D L_{\tau_L} H_u \, (\boldsymbol{Y} S_L^c)_{1''} \right] \frac{\rho^3}{\Lambda^3} , \tag{2.5}$$

where, the subscript for the operator $(\boldsymbol{Y} S_L^c)$ indicates A_4 representation constructed by the product and $\{\alpha'_D, \beta'_D, \gamma'_D\}$ are free parameters. The flavor structure for the pseudo-Dirac neutrino mass matrix takes the form,

$$M_{LS} = \frac{v_u}{\sqrt{2}} \left(\frac{v_\rho}{\sqrt{2}\,\Lambda} \right)^3 \begin{bmatrix} \alpha'_D & 0 & 0 \\ 0 & \beta'_D & 0 \\ 0 & 0 & \gamma'_D \end{bmatrix} \begin{bmatrix} y_1 & y_3 & y_2 \\ y_2 & y_1 & y_3 \\ y_3 & y_2 & y_1 \end{bmatrix}_{LR} . \tag{2.6}$$

2.2.3 Mixing between the heavy fermions N_R and S_L

Following the transformation of the heavy fermion superfields under the imposed symmetries, it can be noted that the usual Majorana mass terms are not allowed. But one can have the interactions leading to

the mixing between these additional superfields as follows

$$\begin{aligned} \mathcal{W}_{M_{RS}} &= [\alpha_{NS}\mathbf{Y}(S_L^c N_R)_{sym} + \beta_{NS}\mathbf{Y}(S_L^c N_R)_{Anti-sym}]\rho \\ &= \alpha_{NS}[y_1(2S_{L_1}^c N_{R_1} - S_{L_2}^c N_{R_3} - S_{L_3}^c N_{R_2}) + y_2(2S_{L_2}^c N_{R_2} - S_{L_1}^c N_{R_3} - S_{L_3}^c N_{R_1}) \\ &+ y_3(2S_{L_3}^c N_{R_3} - S_{L_1}^c N_{R_2} - S_{L_2}^c N_{R_1})]\rho \\ &+ \beta_{NS}[y_1(S_{L_2}^c N_{R_3} - S_{L_3}^c N_{R_2}) + y_2(S_{L_3}^c N_{R_1} - S_{L_1}^c N_{R_3}) + y_3(S_{L_1}^c N_{R_2} - S_{L_2}^c N_{R_1})]\rho\,, \end{aligned} \tag{2.7}$$

where the first and second terms in the first line correspond to symmetric and anti-symmetric product for $S_L^c N_R$ making triplet representation of A_4 with α_{NS}, β_{NS} being the free parameters. Using $\langle\rho\rangle = v_\rho/\sqrt{2}$, the resulting mass matrix is found to be,

$$M_{RS} = \frac{v_\rho}{\sqrt{2}}\left(\frac{\alpha_{NS}}{3}\begin{bmatrix} 2y_1 & -y_3 & -y_2 \\ -y_3 & 2y_2 & -y_1 \\ -y_2 & -y_1 & 2y_3 \end{bmatrix} + \beta_{NS}\begin{bmatrix} 0 & y_3 & -y_2 \\ -y_3 & 0 & y_1 \\ y_2 & -y_1 & 0 \end{bmatrix}\right). \tag{2.8}$$

It should be noted that $\frac{\alpha_{NS}}{3} \neq \beta_{NS}$, otherwise the matrix M_{RS} becomes singular, which eventually spoils the intent of linear seesaw. The masses for the heavy fermions can be found in the basis $(N_R, S_L^c)^T$, which can be written as

$$M_{Hf} = \begin{pmatrix} 0 & M_{RS} \\ M_{RS}^T & 0 \end{pmatrix}. \tag{2.9}$$

Therefore, one can have six doubly degenerate mass eigenstates for the heavy super-fields upon diagonalization.

2.2.4 Linear Seesaw mechanism for light neutrino Masses

Within the present model invoked with A_4 modular symmetry, the complete 9 × 9 mass matrix in the flavor basis of $\left(\nu_L, N_R, S_L^c\right)^T$ is given by

$$\mathbb{M} = \left(\begin{array}{c|ccc} & \nu_L & N_R & S_L^c \\ \hline \nu_L & 0 & M_D & M_{LS} \\ N_R & M_D^T & 0 & M_{RS} \\ S_L^c & M_{LS}^T & M_{RS}^T & 0 \end{array}\right). \tag{2.10}$$

The linear seesaw mass formula for light neutrinos is given with the assumption $M_{RS} \gg M_D, M_{LS}$ as,

$$m_\nu = M_D M_{RS}^{-1} M_{LS}^T + \text{transpose}\,. \tag{2.11}$$

Apart from the small neutrino masses, other relevant parameters in the neutrino sector are Jarlskog invariant and the effective neutrino mass which play a key role in neutrinoless double beta decay and can

be computed from the mixing angles and phases of PMNS matrix elements as following :

$$J_{CP} = \mathrm{Im}[U_{e1}U_{\mu 2}U_{e2}^{*}U_{\mu 1}^{*}] = s_{23}c_{23}s_{12}c_{12}s_{13}c_{13}^{2}\sin\delta_{CP}, \tag{2.12}$$

$$|m_{ee}| = |m_{\nu_1}\cos^2\theta_{12}\cos^2\theta_{13} + m_{\nu_2}\sin^2\theta_{12}\cos^2\theta_{13}e^{i\alpha_{21}} + m_{\nu_3}\sin^2\theta_{13}e^{i(\alpha_{31}-2\delta_{CP})}|\,. \tag{2.13}$$

Many dedicated experiments are looking for neutrinoless double beta signals, for details please refer to [94]. The sensitivity limits on $|m_{ee}|$ by the current experiments such as GERDA is (102–213) meV [95] and CUORE is (90–420) meV [96]. The future generation experiments, like LEGEND-200 can probe 35–73 meV [94] and KamLAND-Zen (61–165) meV [97].

2.3 Numerical analysis

For numerical analysis we consider the global fit neutrino oscillation data at 3σ interval from [98] as follows:

$$\begin{aligned} &\mathrm{NO}: \Delta m^2_{\mathrm{atm}} = [2.431, 2.622]\times 10^{-3}\ \mathrm{eV}^2,\ \Delta m^2_{sol} = [6.79, 8.01]\times 10^{-5}\ \mathrm{eV}^2, \\ &\sin^2\theta_{13} = [0.02044, 0.02437],\ \sin^2\theta_{23} = [0.428, 0.624],\ \sin^2\theta_{12} = [0.275, 0.350]. \end{aligned} \tag{2.14}$$

Here, we numerically diagonalize the neutrino mass matrix eqn. 2.11 through the relation $U^{\dagger}\mathcal{M}U = diag(m_1^2, m_2^2, m_3^2)$, where $\mathcal{M} = m_\nu m_\nu^{\dagger}$ and U is an unitary matrix, from which the neutrino mixing angles can be extracted using the standard relations:

$$\sin^2\theta_{13} = |U_{13}|^2, \quad \sin^2\theta_{12} = \frac{|U_{12}|^2}{1-|U_{13}|^2}\,, \quad \sin^2\theta_{23} = \frac{|U_{23}|^2}{1-|U_{13}|^2}\,. \tag{2.15}$$

To fit to the current neutrino oscillation data, we chose the following ranges for the model parameters:

$$\begin{aligned} &\mathrm{Re}[\tau]\in[-0.5, 0.5],\ \ \mathrm{Im}[\tau]\in[1,2],\ \ \{\alpha_D, \beta_D, \gamma_D\}\in 10^{-5}\,[0.1, 1],\ \ \{\alpha'_D, \beta'_D, \gamma'_D\}\in 10^{-2}\,[0.1, 1], \\ &\alpha_{NS}\in[0, 0.5], \quad \beta_{NS}\in[0, 0.0001], \quad v_\rho\in[10, 100]\,\mathrm{TeV}, \quad \Lambda\in[100, 1000]\,\mathrm{TeV}. \end{aligned}$$

The input parameters are randomly scanned over the above mentioned ranges and the allowed regions for those are initially filtered by the observed 3σ limit of solar and atmospheric mass squared differences and mixing angles which are further constrained by the observed sum of active neutrino masses $\sum m_i \leq$ 0.12 eV [40]. The typical range of modulus τ is found to be $-0.5 \lesssim \mathrm{Re}[\tau] \lesssim 0.5$ and $1 \lesssim \mathrm{Im}[\tau] \lesssim 2$ for normally ordered neutrino masses. Thus, the modular Yukawa couplings as function of τ (Eq. A.8 in Appendix) are found to vary in the region $0.99 \lesssim y_1(\tau) \lesssim 1$, $0.1 \lesssim y_2(\tau) \lesssim 0.8$ and $0.01 \lesssim y_3(\tau) \lesssim 0.3$. The variation of those Yukawa couplings with the real and imaginary parts of τ are represented in the top left and top right panels of Fig. 2.1 respectively, whereas, bottom panel shows the allowed region of $\mathrm{Re}(\tau)$ and $\mathrm{Im}(\tau)$ which abides all the constraints used to deduce the neutrino oscillation parameters. Variation of the mixing angles with the sum of active neutrino masses, consistent with the allowed 3σ range are obtained,

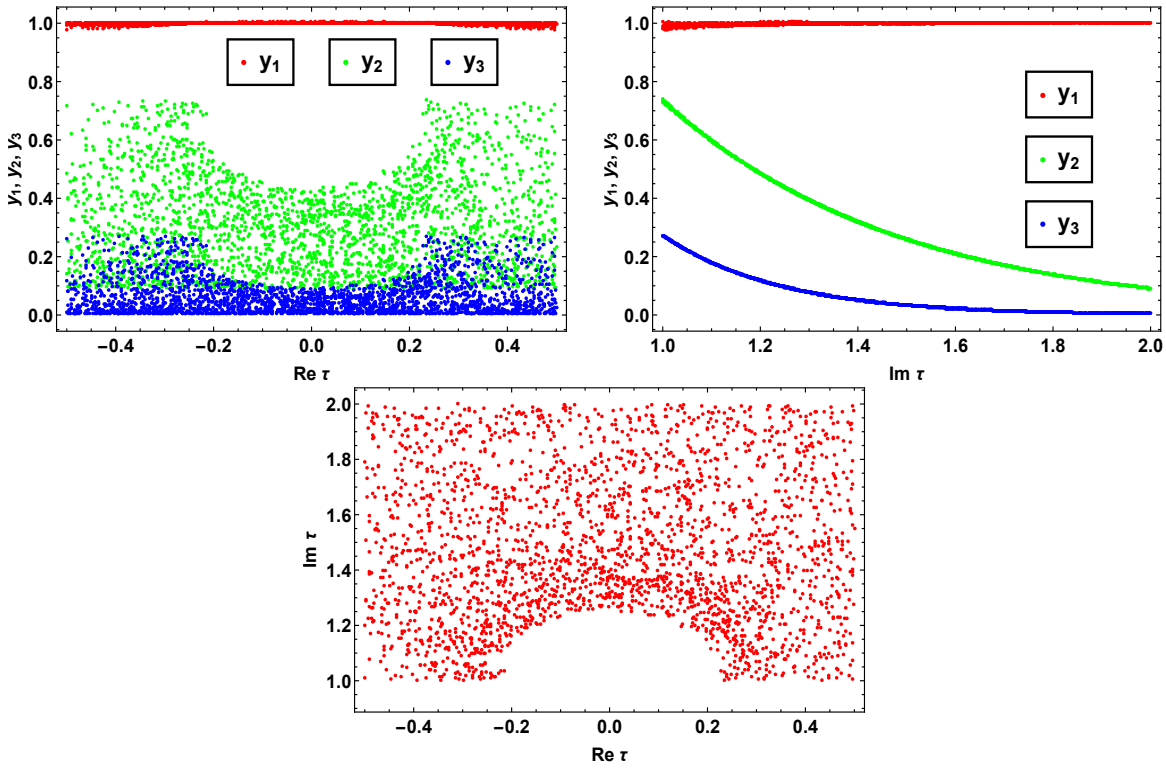

Figure 2.1: Top left and top right panel signify the correlation of the modular Yukawa couplings (y_1, y_2, y_3) with the real and imaginary parts of modulus τ respectively. The bottom panel represents the allowed region of the Re(τ) and Im(τ) abiding all the constraints and within the range of its fundamental domain.

as shown in Fig. 2.2. In the left panel of Fig. 2.3, we show the correlation of Jarlskog CP invariant with the reactor mixing angle allowed by the neutrino oscillation data, which is found to be of the order of $\mathcal{O}(10^{-3})$. The right panel of Fig. 2.3, signifies the full parameter space for Yukawa couplings as per the observed sum of active neutrino masses. In Fig. 2.4, we have displayed a correlation of the Yukawa couplings y_1 with y_2 and y_2 with y_3 in the left and right panels respectively. The effective neutrinoless double beta decay mass parameter $|m_{ee}|$ for both normal and inverted orderings is found to have a maximum value of 55 meV from the variation of observed sum of active neutrino masses, which is presented in the left panel of Fig. 2.5. The results for normal and inverted hierarchies are shown by the blue and red points. The horizontal pink and cyan bands represent the 3σ sensitivity limits of current GERDA and the future LEGEND-200 experiments respectively. It should be noted from the figure that the model predictions for $|m_{ee}|$ are within the reach of the future generation experiments and the inverted hierarchical region is more favored. The right panel represents the correlation between heavy fermion masses M_2 and M_3.

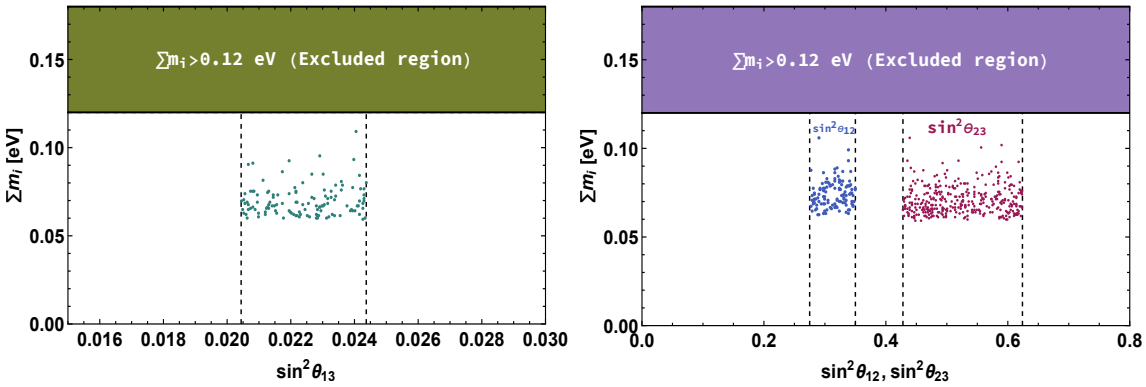

Figure 2.2: Left (Right) panel represents the correlation between $\sin^2\theta_{13}$ ($\sin^2\theta_{12}$ and $\sin^2\theta_{23}$) with the sum of active neutrino masses.

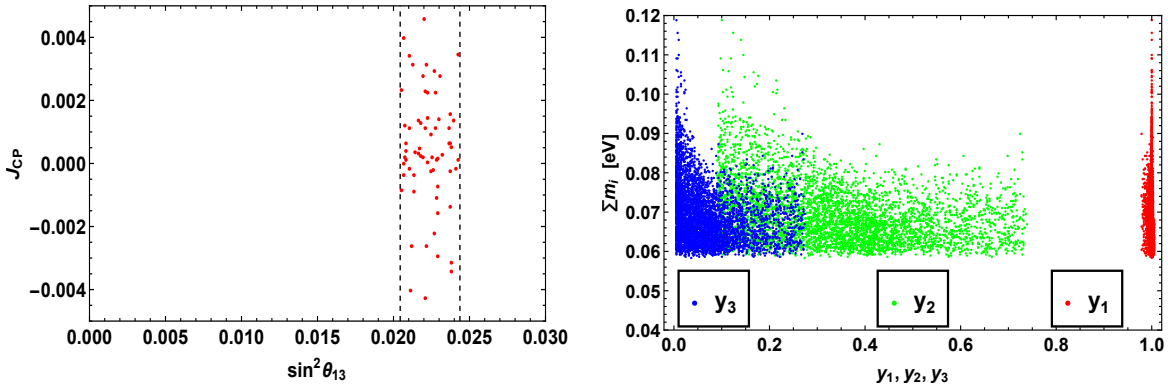

Figure 2.3: Left panel displays the correlation of Jarlskog invariant with the reactor mixing angle and right panel reflects the variation of modular Yukawa couplings with the sum of active neutrino masses.

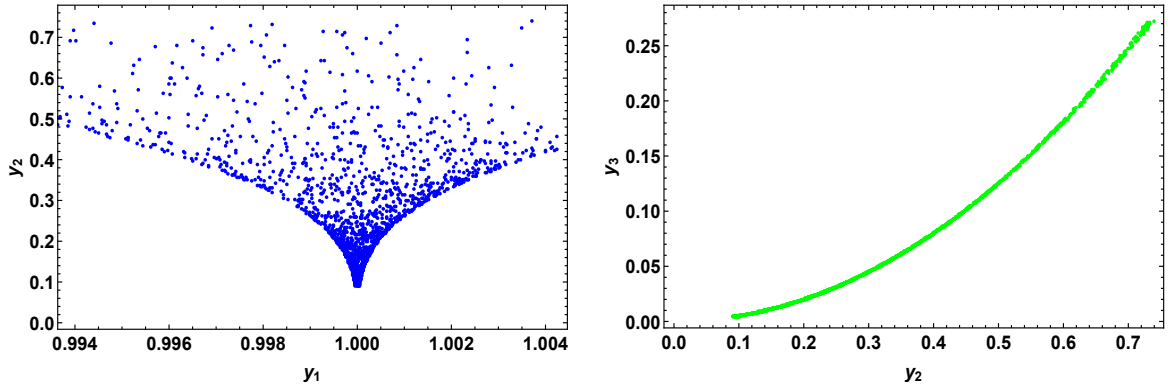

Figure 2.4: Left (Right) panel displays the correlation between y_1 and y_2 (y_2 and y_3).

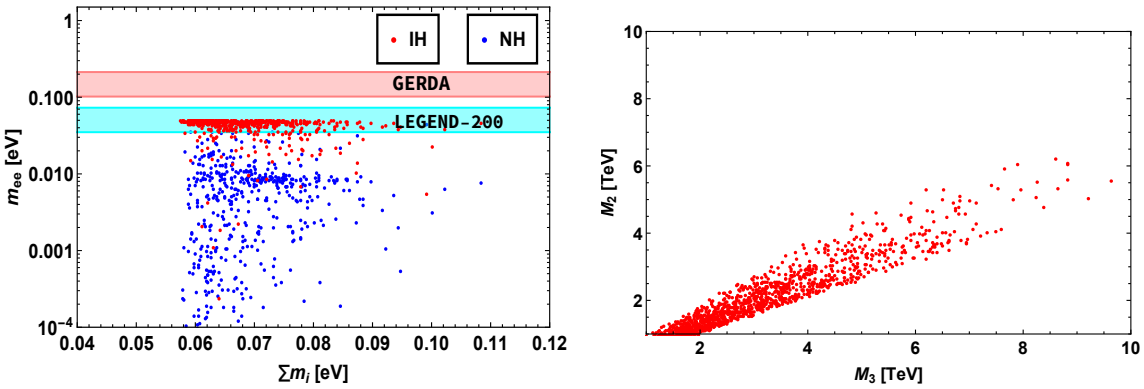

Figure 2.5: Left panel shows the correlation of effective neutrino mass of neutrinoless double beta decay with the sum of active neutrino masses, where the blue and red points correspond to normal and inverted hierarchies. The horizontal pink band corresponds to the 3σ sensitivity limit of currently running GERDA experiment and the cyan band represents the 3σ limit of the future LEGEND-200 experiment. Right panel depicts correlation between the heavy fermion masses M_2 and M_3.

Comment on non-unitarity

Here, we briefly comment on non-unitarity of neutrino mixing matrix $U'_{\rm PMNS}$ in the presence of heavy fermions. The standard parametrization for the deviation from unitarity in a small scale can be expressed as following [99]

$$U'_{\rm PMNS} \equiv \left(1 - \frac{1}{2}FF^{\dagger}\right) U_{\rm PMNS}. \tag{2.16}$$

Here, $U_{\rm PMNS}$ is the PMNS mixing matrix which diagonalises the mass matrix of the three light neutrinos and F is the mixing of active neutrinos with the heavy fermions and approximated as $F \equiv (M_{NS}^{T})^{-1} M_D \approx \frac{\alpha_D v}{\alpha_{NS} v_\rho}$, which is a hermitian matrix. The global constraints on the non-unitarity parameters [100–102], are found via several experimental results such as the W boson mass M_W, the Weinberg angle θ_W, several ratios of fermionic Z boson as well as its invisible decay, electroweak universality, CKM unitarity bounds, and lepton flavor violations. In our model framework, we consider the following approximated normalized order for the Dirac, pseudo-Dirac and heavy masses to correctly generate the observed mass-squared differences as well as the sum of active neutrino masses of desired order:

$$\left(\frac{m_\nu}{0.1\ \text{eV}}\right) \approx \left(\frac{M_D}{10^{-3}\ GeV}\right)\left(\frac{M_{RS}}{10^{3}\ GeV}\right)^{-1}\left(\frac{M_{LS}}{10^{-4}\ GeV}\right). \tag{2.17}$$

Therefore, with the chosen order masses, we obtain an approximated non-unitary mixing for the present model as

$$|FF^{\dagger}| \leq \begin{bmatrix} 4.5\times10^{-13} & 2.3\times10^{-13} & 6.2\times10^{-13} \\ 2.3\times10^{-13} & 2.08\times10^{-12} & 4.5\times10^{-12} \\ 6.2\times10^{-13} & 4.5\times10^{-12} & 5.6\times10^{-12} \end{bmatrix}. \tag{2.18}$$

Since, the mixing between the active and heavy fermions in our model is found to be very small, it leads to a negligible contribution to the non-unitarity.

Comment on lepton flavor violation

Here, we will briefly discuss about the prospect of lepton flavor violation (LFV) effect, in particular $\ell_i \to \ell_j \gamma$ decays, in the context of present model. Lepton flavor violating decays are strictly forbidden in the SM and are known to be induced in models with extended lepton sectors. The current limit on these branching ratios are: $\mathrm{B}r(\mu \to e\gamma) < 4.2 \times 10^{-13}$ from MEG Collaboration [103], $\mathrm{B}r(\tau \to e\gamma) < 3.3 \times 10^{-8}$ [104] and $\mathrm{B}r(\tau \to \mu\gamma) < 4.4 \times 10^{-8}$ from Belle collaboration [105].

In this model, the lepton flavor violating decays ($\ell_i \to \ell_j \gamma$) can occur via exchange of heavy fermions at one loop level [106, 107], as there is mixing between the light and heavy fermions and the corresponding dominant one-loop contribution to the branching ratios for these decays is given as [99, 108]

$$\mathrm{Br}(\ell_i \to \ell_j \gamma) = \frac{\alpha_W^3 s_W^2}{256\pi^2} \frac{m_{\ell_i}^5}{M_W^4} \frac{1}{\Gamma_{\ell_i}} |G_{ij}^W|^2, \tag{2.19}$$

where G_{ij}^W is loop functions whose analytic form is

$$\begin{aligned} G_{ij}^W &= \sum_{k=1}^{3} F_{ik} F_{jk}^\dagger G_\gamma^W \left(\frac{M_{N_k}^2}{M_W^2} \right), \quad \text{with} \\ G_\gamma^W(x) &= \frac{1}{12(1-x)^4} (10 - 43x + 78x^2 - 49x^3 + 4x^4)\,. \end{aligned} \tag{2.20}$$

Here, M_{N_k} represents heavy neutrino superfields and F characterises the mixing of active neutrinos with the heavy fermions leading to non-unitarity effect. Since in the present model, the non-unitarity parameters are found to be extremely small (2.18), the branching ratios of the LFV decays are highly suppressed. Thus, for TeV scale heavy fermions M_{N_k}, the branching ratios for different LFV decays are found to be

$$\begin{aligned} \mathrm{B}r(\mu \to e\gamma) &\le 8.9 \times 10^{-33} \left(\frac{|(FF^\dagger)_{\mu e}|}{4.25 \times 10^{-14}} \right)^2, \\ \mathrm{B}r(\tau \to e\gamma) &\le 4.2 \times 10^{-33} \left(\frac{|(FF^\dagger)_{\tau e}|}{6.9 \times 10^{-14}} \right)^2, \\ \mathrm{B}r(\tau \to \mu\gamma) &\le 1.2 \times 10^{-30} \left(\frac{|(FF^\dagger)_{\tau \mu}|}{1.14 \times 10^{-12}} \right)^2, \end{aligned} \tag{2.21}$$

which are beyond the reach of any of the future experiments.

2.4 Leptogenesis

Leptogenesis has proven to be one of the most preferred way to generate the observed baryon asymmetry of the Universe. The standard scenario of resonant enhancement in CP asymmetry has brought down

the scale as low as TeV [109–112]. The present model includes six heavy states with doubly degenerate masses for each pair Eq. 2.9. But one can introduce a higher dimensional mass term for the heavy neutrino superfield (S_L^c) as

$$L_M = -\alpha_R Y S_L^c S_L^c \frac{\rho^4}{\Lambda^3}\,. \tag{2.22}$$

This leads to a small mass splitting between the heavy superfields, there by enhancing the CP asymmetry to generate required lepton asymmetry [113, 114]. Thus, one can construct the right-handed Majorana mass matrix as follows

$$M_R = \frac{\alpha_R v_\rho^4}{6\Lambda^3}\begin{pmatrix} 2y_1 & -y_3 & -y_2 \\ -y_3 & 2y_2 & -y_1 \\ -y_2 & -y_1 & 2y_3 \end{pmatrix}. \tag{2.23}$$

The coupling α_R is chosen to be extremely small to retain the linear seesaw structure of the mass matrix Eq. 2.10, i.e., $M_D, M_{LS} \gg M_R$ and such inclusion does not affect the previous results. However, this term introduces a small mass splitting and the 2×2 submatrix of Eq. 2.10 in the (N_R, S_L^c) basis, now can be written as

$$M = \begin{pmatrix} 0 & M_{RS} \\ M_{RS}^T & M_R \end{pmatrix}. \tag{2.24}$$

This matrix can have a block diagonal structure in the limit $\beta_{NS} \ll \alpha_{NS}$ by the unitary matrix $\frac{1}{\sqrt{2}}\begin{pmatrix} I & -I \\ I & I \end{pmatrix}$ as

$$M' = \begin{pmatrix} M_{RS} + \frac{M_R}{2} & -\frac{M_R}{2} \\ -\frac{M_R}{2} & -M_{RS} + \frac{M_R}{2} \end{pmatrix} \approx \begin{pmatrix} M_{RS} + \frac{M_R}{2} & 0 \\ 0 & -M_{RS} + \frac{M_R}{2} \end{pmatrix}. \tag{2.25}$$

Therefore, the mass eigenstates ($N^\pm$) are related to N_R and S_L^c through

$$\begin{pmatrix} S_{Li}^c \\ N_{Ri} \end{pmatrix} = \begin{pmatrix} \cos\theta & -\sin\theta \\ \sin\theta & \cos\theta \end{pmatrix}\begin{pmatrix} N_i^+ \\ N_i^- \end{pmatrix}. \tag{2.26}$$

Assuming a maximal mixing, we can have

$$N_{Ri} = \frac{(N_i^+ + N_i^-)}{\sqrt{2}},\;\; S_{Li}^c = \frac{(N_i^+ - N_i^-)}{\sqrt{2}}, \tag{2.27}$$

Thus, the interaction superpotential in Eq. 2.3 can be written in the new basis $N_i^\pm$ as

$$\begin{aligned} \mathcal{W}_D \;=\; & \alpha_D L_{e_L} H_u \left[\boldsymbol{Y}\left(\frac{(N_i^+ + N_i^-)}{\sqrt{2}}\right)\right]_1 + \beta_D L_{\mu_L} H_u \left[\boldsymbol{Y}\left(\frac{(N_i^+ + N_i^-)}{\sqrt{2}}\right)\right]_{1'} \\ & + \gamma_D L_{\tau_L} H_u \left[\boldsymbol{Y}\left(\frac{(N_i^+ + N_i^-)}{\sqrt{2}}\right)\right]_{1''}. \end{aligned} \tag{2.28}$$

Analogously, the pseudo-Dirac interaction term Eq. 2.5 becomes

$$\begin{aligned} \mathcal{W}_{LS} &= \alpha'_D L_{e_L} H_u \left[\boldsymbol{Y} \left(\frac{(N_i^+ - N_i^-)}{\sqrt{2}} \right) \right]_1 \frac{\rho^3}{\Lambda^3} + \beta'_D L_{\mu_L} H_u \left[\boldsymbol{Y} \left(\frac{(N_i^+ - N_i^-)}{\sqrt{2}} \right) \right]_{1'} \frac{\rho^3}{\Lambda^3} \\ &\quad + \gamma'_D L_{\tau_L} H_u \left[\boldsymbol{Y} \left(\frac{(N_i^+ - N_i^-)}{\sqrt{2}} \right) \right]_{1''} \frac{\rho^3}{\Lambda^3}. \end{aligned} \tag{2.29}$$

The mass eigenvalues for the new states N^+ and N^- can be obtained by diagonalizing the block diagonal form of heavy superfield masses, expressed as

$$M_{RS} \pm \frac{M_R}{2} = \left(\frac{\alpha_{NS} v_\rho}{\sqrt{2}} \pm \frac{\alpha_R v_\rho^4}{4\Lambda^3} \right) \begin{pmatrix} 2y_1 & -y_3 & -y_2 \\ -y_3 & 2y_2 & -y_1 \\ -y_2 & -y_1 & 2y_3 \end{pmatrix}. \tag{2.30}$$

In the above, the anti-symmetric part in M_{RS} is neglected because β_{NS} is small compared with α_{NS}. The above matrix can be diagonalized through $(M^\pm)_{diag} = U_{TBM} U_R \left(M_{RS} \pm \frac{M_R}{2} \right) U_R^T U_{TBM}^T$, with mass eigenvalues

$$\begin{aligned} M_1^\pm &\approx \frac{1}{6} \left(\frac{\alpha_{NS} v_\rho}{\sqrt{2}} \pm \frac{\alpha_R v_\rho^4}{4\Lambda^3} \right) \left(y_1 + 2y_2 - \sqrt{9y_1^2 + 12y_1 y_2 + 12y_2^2} \right), \\ M_2^\pm &\approx \frac{1}{6} \left(\frac{\alpha_{NS} v_\rho}{\sqrt{2}} \pm \frac{\alpha_R v_\rho^4}{4\Lambda^3} \right) \left(y_1 + 2y_2 + \sqrt{9y_1^2 + 12y_1 y_2 + 12y_2^2} \right), \\ M_3^\pm &\approx \frac{1}{3} \left(\frac{\alpha_{NS} v_\rho}{\sqrt{2}} \pm \frac{\alpha_R v_\rho^4}{4\Lambda^3} \right) (y_1 + 2y_2). \end{aligned} \tag{2.31}$$

Here, U_{TBM} is the tribimaximal mixing matrix [115, 116] and

$$U_R \approx \begin{pmatrix} B_- & \frac{1}{\sqrt{X_-}} & 0 \\ 0 & 0 & 1 \\ B_+ & \frac{1}{\sqrt{X_+}} & 0 \end{pmatrix}, \tag{2.32}$$

with

$$\begin{aligned} B_\pm &= -\frac{y_1 + 2y_2 \pm \sqrt{9y_1^2 - 12y_1 y_2 + 12y_2^2}}{2\sqrt{2}(y_1 - y_2)}, \text{ and} \\ X_\pm &= \sqrt{1 + B_\pm^2}. \end{aligned} \tag{2.33}$$

As noticed from Eq. 2.31, we get three sets of nearly degenerate mass states after diagonalization. We further assume that the lightest pair with TeV scale masses dominantly contribute to the CP asymmetry.[1]

[1] We also have heavier fermions i.e., $N_2^\pm$ and $N_3^\pm$, whose decays can also generate lepton asymmetry. But these heavy fermions decouple early and moreover the asymmetry can be washed out from the inverse decays of lighter fermion mass eigenstates i.e., $\ell H \to N_1^\pm$. Even though we consider the asymmetry generated from other fermions (i.e., $N_2^\pm, N_3^\pm$), the final asymmetry hardly changes up to a maximum of 3 times the asymmetry generated from $N_1^\pm$ in one flavor approximation, which does not really make any appreciable difference in the final result.

$\epsilon^e_{N^-}$	$\epsilon^\mu_{N^-}$	$\epsilon^\tau_{N^-}$	ϵ_{N^-}	ΔM (GeV)
-9×10^{-5}	-2.13×10^{-4}	-2.42×10^{-4}	-5.45×10^{-4}	2.94×10^{-5}

Table 2.3: CP asymmetries and mass splitting obtained from the allowed range of model parameters which satisfy neutrino oscillation data.

The small mass splitting between the lightest states implies the contribution from one loop self energy of heavy particle decay dominates over the vertex diagram. The expression for CP asymmetry is given by [109, 117]

$$\epsilon_{N_i^-} \approx \frac{1}{32\pi^2 A_{N_i^-}} \mathrm{Im}\left[\left(\frac{\tilde{M}_D}{v_u}-\frac{\tilde{M}_{LS}}{v_u}\right)^\dagger\left(\frac{\tilde{M}_D}{v_u}+\frac{\tilde{M}_{LS}}{v_u}\right)^2\left(\frac{\tilde{M}_D}{v_u}-\frac{\tilde{M}_{LS}}{v_u}\right)^\dagger\right]_{ii}\frac{r_N}{r_N^2+4A^2_{N_i^-}}. \tag{2.34}$$

Here, $\tilde{M}_D = M_D U_{TBM} U_R$, $\tilde{M}_{LS} = M_{LS} U_{TBM} U_R$ and $\Delta M = M_i^+ - M_i^- \approx M_R$. The parameters r_N and A_{N^-} are expressed as

$$\begin{aligned} r_N &= \frac{(M_i^+)^2-(M_i^-)^2}{M_i^+ M_i^-} = \frac{\Delta M(M_i^+ + M_i^-)}{M_i^+ M_i^-}\,, \\ A_{N^-} &\approx \frac{1}{16\pi}\left[\left(\frac{\tilde{M}_D}{v_u}-\frac{\tilde{M}_{LS}}{v_u}\right)\left(\frac{\tilde{M}_D}{v_u}+\frac{\tilde{M}_{LS}}{v_u}\right)\right]_{ii}. \end{aligned} \tag{2.35}$$

It should be noted that because of the imposition of modular symmetry, which plays the role of eliminating the usage of extra flavon fields, the CP asymmetry parameter crucially depends on the Yukawa couplings $\mathbf{Y} = (y_1, y_2, y_3)$, apart from other free parameters of the model and the flavon VEV v_ρ. However, essentially there is no freedom in the choice of how much can be the numerical values of the Yukawa couplings as they depend on the real and imaginary part of the modulus τ, which are constrained by the neutrino oscillation data. In the top left (right) panel of Fig. 2.6, we show the variation of CP asymmetry with the magnitude (argument) of the Yukawa coupling y_1 and bottom left panel projects its behavior with r_N. It should be noted that, the CP symmetry in the context of the present model is broken by the vacuum expectation value of the modulus τ. As this vacuum expectation value is related to the CP phases in the PMNS matrix and the CP asymmetry of leptogenesis, it is generally anticipated that there should be a non-trivial correlation between these observables. In the bottom right panel of Fig. 2.6, we show the correlation plot between the Dirac CP violating phase δ_{CP} and the CP asymmetry of leptogenesis, which depicts no appreciable correlation between these observables. In Table 2.3, we provide benchmark values that satisfy both neutrino mass and required CP asymmetry for leptogenesis [118, 119] (to be discussed in the next subsection).

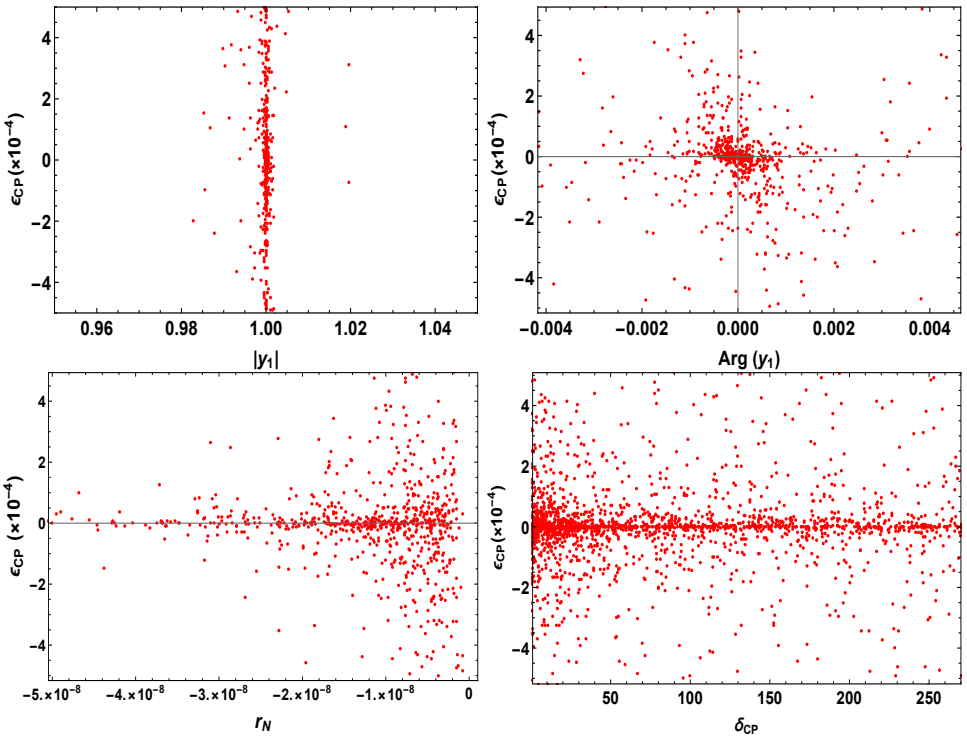

Figure 2.6: Top left and right panels represent the variation of CP asymmetry with the magnitude and argument of Yukawa coupling respectively. Bottom left panel shows its dependence with parameter r_N. Whereas, the bottom right plot represents the correlation between CP asymmetry and the CP violating phase δ_{CP}.

2.4.1 One flavor approximation

The evolution of lepton asymmetry can be deduced from the dynamics of relevant Boltzmann equations. Sakharov criteria [23] demand the decay of parent fermion to be out of equilibrium to generate the lepton asymmetry. To impose this condition, one has to compare the Hubble rate with the decay rate as follows.

$$K = \frac{\Gamma_{N_1^-}}{H(T = M_1^-)} \,. \tag{2.36}$$

Here, $H = \frac{1.67\sqrt{g_\star}\, T^2}{M_{\rm Pl}}$, with $g_\star = 106.75$, $M_{Pl} = 1.22 \times 10^{19}$ GeV. We consider the coupling strength $\left(\approx \left(\frac{\sqrt{2}M_D}{v} U_{TBM} U_R\right)_{ij}\right)$ roughly around 10^{-6}, where the minimum order of coupling parameters are taken from the numerical analysis section, consistent with neutrino oscillation data. The Boltzmann equations for the evolution of the number densities of right-handed superfield and lepton, written in terms of yield parameter (ratio of number density to entropy density) are given by [119–123]

$$\begin{aligned}
\frac{dY_{N^-}}{dz} &= -\frac{z}{sH(M_1^-)} \left[\left(\frac{Y_{N^-}}{Y_{N^-}^{eq}} - 1 \right) \gamma_D + \left(\left(\frac{Y_{N^-}}{Y_{N^-}^{eq}} \right)^2 - 1 \right) \gamma_S \right], \\
\frac{dY_{B-L}}{dz} &= -\frac{z}{sH(M_1^-)} \left[\epsilon_{N^-} \left(\frac{Y_{N^-}}{Y_{N^-}^{eq}} - 1 \right) \gamma_D - \frac{Y_{B-L}}{Y_\ell^{eq}} \frac{\gamma_D}{2} \right],
\end{aligned} \tag{2.37}$$

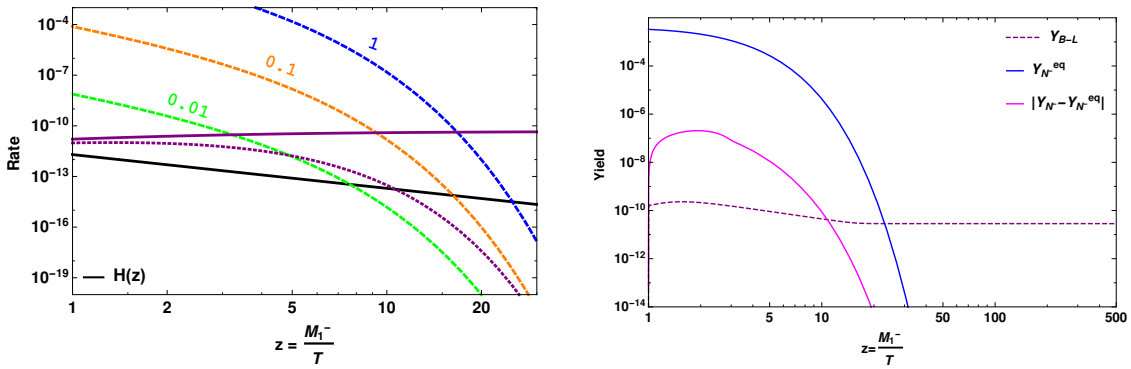

Figure 2.7: Left panel projects the comparison of interaction rates with Hubble expansion, where purple lines correspond to decay (solid), inverse decay (dotted) and scattering rates plotted for various values of Majorana coupling (green, orange, blue). Right panel projects the evolution of Y_{B-L} (dashed) as a function of $z = M_1^-/T$.

where s denotes the entropy density, $z = M_1^-/T$ and the equilibrium number densities are given by [118]

$$Y_{N^-}^{eq} = \frac{45 g_{N^-}}{4\pi^4 g_\star} z^2 K_2(z), \quad Y_\ell^{eq} = \frac{3}{4}\frac{45\zeta(3) g_\ell}{2\pi^4 g_\star}. \tag{2.38}$$

Here, $K_{1,2}$ denote modified Bessel functions, $g_\ell = 2$ and $g_{N^-} = 2$ denote the degrees of freedom of lepton and right-handed superfields respectively. The decay rate γ_D is given by

$$\gamma_D = s Y_{N^-}^{eq} \Gamma_D, \tag{2.39}$$

where, $\Gamma_D = \Gamma_{N^-}\frac{K_1(z)}{K_2(z)}$. γ_S denotes the scattering rate of the decaying particle i.e., $N_1^- N_1^- \to \rho\rho$ [123].[2] The Boltzmann equation for Y_{B-L} is free from the subtlety of asymmetry getting produced even when N_1^- is in thermal equilibrium i.e., by subtracting the on-shell N_1^- exchange contribution ($\frac{\gamma_D}{4}$) from the $\Delta L = 2$ process [121].

The interaction rates are compared with Hubble expansion in the left panel of Fig. 2.7. The decay (Γ_D) and inverse decay $\left(\Gamma_D \frac{Y_{N^-}^{eq}}{Y_\ell^{eq}}\right)$ rates are plotted in purple with the coupling strength $\sim 10^{-6}$. The scattering rate $\left(\frac{\gamma_S}{s Y_{N^-}^{eq}}\right)$ for $N_1^- N_1^- \to \rho\rho$ is projected for various set of values for coupling (of Eq. 2.7), consistent with neutrino oscillation study. For larger Majorana coupling, the scattering process makes N_1^- to stay longer in thermal soup and hence, number density of N_1^- depletes in annihilation rather than decay, generating lesser lepton asymmetry. In one-flavor approximation, the solution of Boltzmann eqn. 2.37 using the benchmark given in Table 2.3 is projected in the right panel of Fig. 2.7 with the inclusion of decay and scattering rates. Once the out-of-equilibrium criteria is satisfied, the decay proceeds slow (over abundance), Y_{N^-} does not trace $Y_{N^-}^{eq}$ (magenta curve) and the lepton asymmetry (dashed curve) is

[2]
$$\gamma(ab \leftrightarrow cd) = \frac{T}{64\pi^4}\int_{s_{min}}^{\infty} ds\, \hat{\sigma}(s')\sqrt{s'} K_1\left(\frac{\sqrt{s'}}{T}\right),$$
where, $s_{min} = Max[(m_a + m_b)^2, (m_c + m_d)^2]$ and $\hat{\sigma}(s')$ is the reduced cross section with s' denoting the center of mass energy.

generated. The obtained lepton asymmetry gets converted to the observed baryon asymmetry through sphaleron transition, given by [124]

$$Y_B = \left(\frac{8N_f + 4N_H}{22N_f + 13N_H}\right) Y_{B-L}. \tag{2.40}$$

Here, N_f denotes the number of superfields generations and N_H is the number of Higgs doublets. The observed baryon asymmetry is quantified in terms of baryon to photon ratio [40]

$$\eta = \frac{\eta_b - \eta_{\bar{b}}}{\eta_\gamma} = 6.08 \times 10^{-10}. \tag{2.41}$$

Based on the relation $Y_B = (7.04)^{-1}\eta$, the current bound on baryon asymmetry is $Y_B \sim 0.86 \times 10^{-10}$.

We observe the same Yukawas i.e. $\mathbf{Y} = (y_1, y_2, y_3)$ are involved in both Dirac as well as Majorana masses and hence, appear not only in the neutrino phenomenology but also in computation related to leptogenesis. But the values of these couplings are strongly constrained from the real and imaginary part of the complex modulus τ. Thus, the free parameters play an important role in adjusting the parameter space to generate a successful leptogenesis.

2.4.2 Flavor consideration

One flavor approximation is probable at high scale ($T > 10^{12}$ GeV), where all the Yukawa interactions are out of equilibrium. But for temperatures below 10^{12} GeV, various charged lepton Yukawa couplings come into equilibrium and hence flavor effects play a crucial role in generating the final lepton asymmetry. For temperatures below 10^5 GeV, all the Yukawa interactions are in equilibrium and the asymmetry is stored in the individual lepton sector. The detailed investigation of flavor effects in type-I leptogenesis can be found in the literature [125–130].

The Boltzmann equation for generating the lepton asymmetry in each flavor is [126]

$$\frac{dY^{\alpha}_{B-L_\alpha}}{dz} = -\frac{z}{sH(M_1^-)}\left[\epsilon^{\alpha}_{N^-}\left(\frac{Y_{N^-}}{Y^{eq}_{N^-}} - 1\right)\gamma_D - \left(\frac{\gamma^{\alpha}_D}{2}\right)\frac{A_{\alpha\alpha}Y^{\alpha}_{\mathrm{B-L}_\alpha}}{Y^{eq}_{\ell}}\right], \tag{2.42}$$

where, $\epsilon^{\alpha}_{N^-}$ represents the CP asymmetry in each lepton flavor and

$$\gamma^{\alpha}_D = sY^{eq}_{N^-}\Gamma^{\alpha}_{N^-}\frac{K_1(z)}{K_2(z)}, \quad \gamma_D = \sum_{\alpha}\gamma^{\alpha}_D\,,$$

The matrix A is given by [127],

$$A = \begin{pmatrix} -\frac{221}{711} & \frac{16}{711} & \frac{16}{711} \\ \frac{16}{711} & -\frac{221}{711} & \frac{16}{711} \\ \frac{16}{711} & \frac{16}{711} & -\frac{221}{711} \end{pmatrix}.$$

From the benchmark shown in Table 2.3, we project the $B-L$ yield with flavor consideration in the left panel of Fig. 2.8. It is clear that a notable enhancement in $B-L$ asymmetry is obtained in case of flavor

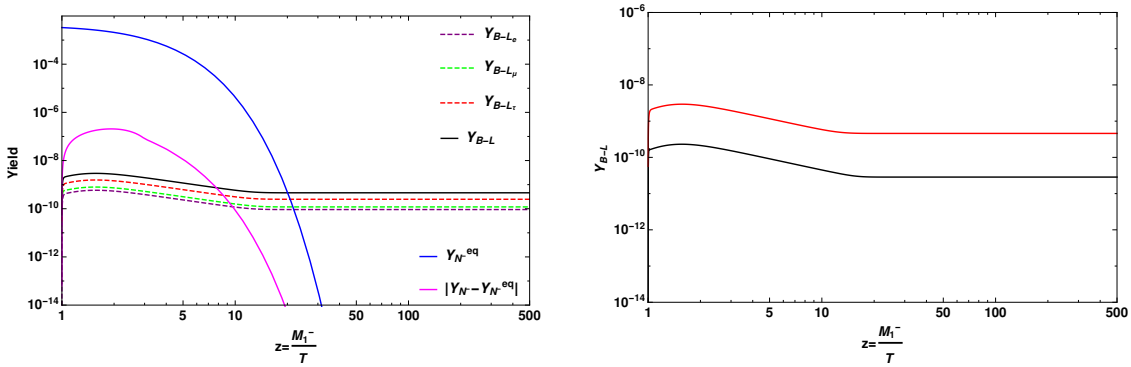

Figure 2.8: The left panel displays yield with inclusion of flavor effects. The right panel shows the enhancement in the yield due to three-flavor calculation (red curve) over one-flavor approximation (black curve).

consideration (red curve) over one flavor approximation (black curve), as displayed in the right panel. This is because, in one flavor approximation the decay of heavy fermion to a specific lepton flavor final state can get washed out by the inverse decays of any flavor unlike the flavored case [128].

2.5 Comment on collider studies

Here, we briefly comment on the most promising collider signature of heavy pseudo-Dirac neutrinos without going into any detailed estimation, in the context of the present model. In the linear seesaw scenario the M_{LS} is the lepton number violating term [131] therefore its mass scale is naturally small. Also the effective Majorana neutrino mass matrix as shown in eqn. 2.11 for active neutrino where the smallness of m_ν is attributed due to M_{LS} being the pseudo-Dirac neutrino mass term and further suppressed by the ratio of M_D and M_{RS}. Hence, the seesaw scale can be lowered to TeV range which is experimentally accessible at LHC. The trilepton plus missing energy process as mentioned in eqn. 2.43, which can be studied at colliders, is an interesting mechanism involving heavy pseudo-Dirac neutrinos [132]:

$$\sigma(pp \to N\ell^\pm \to \ell^\pm\ell^\pm + \not{E}) = \sigma(pp \to W \to N\ell^\pm) \times \mathrm{Br}(N \to \ell^\pm\ell^\pm + \not{E}). \tag{2.43}$$

where it is assumed that the heavy neutrinos are heavier than the W boson, so that the two-body decay process $N \to \ell W$ is kinematically allowed, followed by the on-shell W decaying into SM leptons. Its viability is essentially determined by firstly, large mixing between active–sterile neutrinos i.e. $\theta_{\nu RS} \simeq \sqrt{m_\nu / M_{RS}} \leq 10^{-6}$ [133], secondly, masses of heavy pseudo-Dirac neutrinos ranging from few [GeV–TeV], and finally its production mechanism.

2.6 Conclusion

We have emphasized on showcasing the importance of A_4 modular symmetry that avoids the complications associated while using the multiple flavons. The model we have dealt with intakes three right-handed and three left-handed heavy superfields to explore neutrino phenomenology within a choosen framework of linear seesaw in super-symmetric context. The role played by conventional flavon fields are now taken over by the modular Yukawa couplings. Hence, giving up a specific flavor structure to the neutrino mass matrix and provides a scope to study neutrino mixing. Further, we take the path of numerical diagonalization of the neutrino mass matrix by finding a suitable parameter-space which accommodates all the observables found in 3σ range of the oscillation data. Proceeding further, makes us realize that flavor structure of heavy superfields leads to three doubly degenerate mass eigenvalues. Therefore, in order to have hands on leptogenesis we bring in a higher dimensional term to develop a small mass splitting. All this gimmick pave the way to get a non-zero CP asymmetry from the decay of lightest heavy fermion eigenstate and also a self energy contribution is slightly enhanced as an advantage of utilizing the small mass splitting in between the two lighter heavy fermion superfields. The coupled Boltzmann equations are handled by utilizing a specific benchmark values of the model parameters which is also validated in oscillation data and as an outcome, lepton symmetry is of the order of 10^{-10} self explaining the baryon asymmetry seen in the Universe. As we are dealing with TeV scale heavy fermion superfields, hence, flavor considerations are also discussed. The promising collider signature of the heavy pseudo-Dirac neutrinos is the trilepton plus missing energy, which depend crucially on the mixing between the light active and pseudo-Dirac neutrinos, mass of these heavy neutrinos and their production mechanism.

CHAPTER 3

A MODULAR A_4 SYMMETRIC SCOTOGENIC MODEL FOR NEUTRINO MASS AND DARK MATTER

3.1 Introduction

Various experimental observations over the last few decades have conclusively established the robustness of the Standard Model (SM). Nonetheless, there are a few issues demonstrating the presence of physics beyond the SM, for example, the nature and existence of dark matter (DM) [134–139], small but non-vanishing neutrino masses [40, 140, 141], observed baryon asymmetry of the Universe [23, 118, 119, 122, 142], origin of flavor structure, etc. Therefore, apprehending the nature of physics beyond the standard model (BSM) gets inescapable, and in this context, symmetry is assumed to play a significant role, e.g., ensuring the appropriate mechanism for achieving the tiny neutrino masses, stability of DM, confining flavour structure, and so on. It is thus, intriguing to build models beyond the SM adopting new symmetries.

The Scotogenic model, proposed by Ma [143] is probably the simplest model that generates the small neutrino masses at one-loop level and also simultaneously accounts for the dark matter (both inert scalar and fermionic), see for example a legion of works in the literature [144–149] and references therein. Various other works have realized neutrino mass at one-loop [150–154]. Further, the pioneering work of introducing modular flavor symmetries to quark and neutrino sectors is seen in the literature of [36, 59, 60] to highlight predictable flavor structures. The basic idea behind the use of modular symmetry is to minimize the necessity of the inclusion of extra flavon fields having specific vacuum expectation value (VEV) alignments. The breaking of flavor symmetry takes place when the complex modulus τ acquires VEV.

The main issue of the perplexing vacuum alignment is avoided, the only requirement is a certain kind of mechanism which can fix the modulus τ. Resultantly, this has prompted a restoration of the possibility that modular symmetries are symmetries of the extra dimensional space-time with Yukawa couplings dictated by their modular weights [155]. Hence, they transform systematically under this framework, where there is a functional dependence of these couplings on modular forms, which verily are holomorphic function of τ. To put it in a different way, these couplings come from a non-trivial representation of a non-Abelian discrete flavor symmetry approach [62], to such an extent that it can remunerate the utilization of flavon fields, which undoubtedly are not required in understanding the flavor structure. In reference to above, it was fathomed that there are numerous groups accessible i.e., basis characterized under modular group of A_4 [60, 65–69, 156], S_4 [70–73, 157], A_5 [75, 158, 159], larger groups [76], various other modular symmetries and double covering of S_4 [21], predictions regarding masses, mixing [160, 161], and CP phases distinctive to quarks and/or leptons are made.

This chapter pertains to scotogenic model [162–166], constructed, based on modular A_4 symmetry in which mass generation for neutrinos is done at one-loop level alongside it also provides a stable DM candidate. The model can be appreciated by using the modular forms for the Yukawa couplings with weight-2, while the other couplings of the model with higher weights, can be constructed from the triplet Yukawa couplings. The radiative neutrino mass generation in the context of A_4 modular symmetry has been investigated in [167, 168]. However, our proposed model is different from these studies in terms of the field contents as well as model predictions. Our model encompasses two different sets of SM singlet heavy neutrinos i.e., N_{Ri} & S_{Li}, $(i = 1,2,3)$, which transform as triplets under A_4, with modular weight $k_I = -1$ and $+1$ respectively. Likewise, the inert scalar doublet is allocated a non-zero modular weight as $k_I = -2$. Interestingly, modular weights help in impersonating the additional Z_2 symmetry, ensuring the stability of DM. The present work remains unique from the earlier models in the context of avoiding multiple flavon fields and their vacuum alignment. Furthermore, without the requirement of any ad-hoc discrete symmetry, we discuss dark matter phenomenology. The gauge parameter space that gives correct relic density (Planck), will be shown to be consistent with the collider (LEP-II and ATLAS) constraints as well, which can be hardly seen in literature incorporated with modular symmetry. In view of the above, the present work gives a new picture of phenomenological study, made simple yet rich.

The layout of this chapter is as follows. We introduce modular A_4 in section-3.2, followed by model description and its appealing feature resulting in simple mass structure for the charged and neutral leptons with two types of sterile neutrinos. We then provide a brief discussion on the generation of light neutrino masses and their mixing in section 3.4. In section 3.5 numerical correlational study between observables of neutrino sector and input model parameters is established. Comment on lepton flavour violating decays $\mu \to e\gamma$, $\mu \to 3e$ and $\mu - e$ conversion in nuclei is presented in section 3.6. Further, Sec. 3.7 comprises the discussion on fermionic dark matter followed by collider constraints in section 3.8. We

summarize the results in section 3.9.

3.2 Model with A_4 modular symmetry

Here, we present a brief discussion on modular symmetry which manifests the invariance under linear fractional transformations (LFTs) γ acting on the complex variable τ as follows:

$$\gamma : \tau \to \gamma(\tau) = \frac{a\tau + b}{c\tau + d}\,, \tag{3.1}$$

with, $ad - bc = 1$, where a, b, c, d are integers (Z). Modular group (Γ) forms a group of these LFTs acting on upper half complex plane ($\mathrm{Im}(\tau) > 0$). Moreover, it shows isomorphism to $PSL(2,Z)$ (projective special linear group) of 2×2 matrices with unit determinant and integers (Z) being the elements. S and T are the generators of the modular group given by,

$$S = \begin{pmatrix} 0 & 1 \\ -1 & 0 \end{pmatrix}; \qquad T = \begin{pmatrix} 1 & 1 \\ 0 & 1 \end{pmatrix}. \tag{3.2}$$

These generators satisfy the relation $S^2 = I$ and $(ST)^3 = I$, under which τ transforms as:

$$S : \tau \to -\frac{1}{\tau}, \qquad T : \tau \to \tau + 1\,. \tag{3.3}$$

Group definition for $\Gamma(N)$, where $N = 1, 2, 3, 4, \cdots$ is given as

$$\Gamma(N) = \left\{ \begin{pmatrix} a & b \\ c & d \end{pmatrix} \in SL(2,Z), \quad \begin{pmatrix} a & b \\ c & d \end{pmatrix} = \begin{pmatrix} 1 & 0 \\ 0 & 1 \end{pmatrix} \mod(N) \right\}, \tag{3.4}$$

such that $\Gamma(1) = \mathrm{SL}(2,\mathrm{Z})$. Considering the case for $N = 3$, i.e. $\Gamma_3 \simeq A_4$ which is the non linear realization of A_4 discrete symmetry. The dimension for the A_4 modular symmetry is $2k + 1$. For $k = 1$, it yields three Yukawa couplings, i.e., $\mathbf{Y} = (y_1, y_2, y_3)$ expressed in modular form (see Eqn.(B.1)) which are linearly independent forming a triplet of A_4 having a modular weight 2. Also modular forms of higher weights are expressed in terms of the modular forms of weight 2 given in Eqn.(B.3) and Eqn.(B.4). The Yukawa couplings can be expressed in terms of Dedekind eta function $\eta(\tau)$ (see appendix B.1), which has the form,

$$\eta(\tau) = q^{1/24} \sum_{n=1}^{\infty} (1 - q^n)\,, \tag{3.5}$$

where, $q = e^{2i\tau\pi}$ plays a crucial role in building the modular forms. However, for numerical simplicity the q-expansion forms are utilized presented in Eqn. (B.2). Due to its simplistic nature modular A_4 symmetry plays a key role in the one loop framework.

3.3 Model Framework

Here, we take the privilege of introducing the model framework, investigating the impact of A_4 modular symmetry on neutrino and dark matter phenomenology. The SM particle spectrum is enriched with three right-handed (N_R) and three left-handed (S_L) heavy fermions to meet the purpose. We impose a local $U(1)_{B-L}$ symmetry to avoid certain unwanted interactions and a scalar singlet ρ to break it spontaneously. The $U(1)_{B-L}$ charges are assigned in such a way that the model is free from triangle gauge anomalies. The scalar sector is extended with an inert scalar doublet η, to realize neutrino mass at one-loop. The assigned modular weight mimics Z_2 symmetry by playing a vital role in forbidding the neutrino mass at tree-level and also in stabilizing the fermionic dark matter. The representation of different fields of the model under $SU(2)_L \times U(1)_Y \times U(1)_{B-L} \times A_4$ symmetries and their modular weights are given in the Table 3.1. In addition, the non-trivial transformation of Yukawa and scalar couplings and their modular weights are furnished in Table 3.2.

	Fermions						Scalars		
	e_R	μ_R	τ_R	$\overline{L}_L$	N_R	S_L	H	η	ρ
$SU(2)_L$	1	1	1	2	1	1	2	2	1
$U(1)_Y$	-1	-1	-1	$\frac{1}{2}$	0	0	$\frac{1}{2}$	$\frac{1}{2}$	0
$U(1)_{B-L}$	-1	-1	-1	$+1$	-1	0	0	0	-1
A_4	1	$1'$	$1''$	$1, 1'', 1'$	3	3	1	1	1
k_I	-1	-1	-1	1	-1	1	0	-2	-2

Table 3.1: Particle content of the model and their charges under $SU(2)_L \times U(1)_Y \times U(1)_{B-L} \times A_4$, where k_I is the modular weight.

Couplings	A_4	k_I
$\mathbf{Y} = (y_1,\ y_2,\ y_3)$	**3**	**2**
λ_η	**1**	**8**
λ'_η	**1**	**4**

Table 3.2: Transformation of the Yukawa and quartic couplings under A_4 symmetry and their corresponding modular weights shown in Appendix A.

The scalar potential of the model is given by

$$\begin{aligned} \mathcal{V} \;=\; & \mu_H^2(H^\dagger H) + \lambda_H (H^\dagger H)^2 + \lambda'_\eta \Big[\mu_\eta^2 (\eta^\dagger \eta) + \mu_\rho^2 (\rho^\dagger \rho) + \zeta_3 (H^\dagger H)(\eta^\dagger \eta) \\ & + \zeta_4 (H^\dagger \eta)(\eta^\dagger H) + \frac{\zeta_5}{2} \big((H^\dagger \eta)^2 + (\eta^\dagger H)^2 \big) + \zeta' (H^\dagger H)(\rho^\dagger \rho) \Big] \\ & + \lambda_\eta \Big[\zeta_\eta (\eta^\dagger \eta)^2 + \zeta_\rho (\rho^\dagger \rho)^2 + \zeta'' (\rho^\dagger \rho)(\eta^\dagger \eta) \Big] + \text{H.}c. \end{aligned} \tag{3.6}$$

Here, $H = \begin{pmatrix} 0 & (v+h)/\sqrt{2} \end{pmatrix}^T$ is the SM Higgs doublet, $\eta = \begin{pmatrix} \eta^+ & (\eta_R + i\eta_I)/\sqrt{2} \end{pmatrix}^T$ denotes the inert doublet and the complex scalar $\rho = \frac{1}{\sqrt{2}}(v_\rho + h_\rho + iA_\rho)$ breaks the $U(1)_{B-L}$ local gauge symmetry spontaneously. The mass mode of A_ρ is eaten up by the $U(1)_{B-L}$ associated gauge boson Z', attains the mass $M_{Z'} = g_{BL} v_\rho$. In the above potential, ζ_i's ($i = 3,4,5$), ζ', ζ_ρ, ζ_η, ζ'' are the free parameters and the scalar couplings λ'_η, λ_η are singlets under A_4 with modular weight 4, 8 respectively, which can be expressed in terms of the components of weight-2 triplet Yukawa couplings [59],

$$\begin{aligned} \lambda'_\eta &= y_1^2 + 2y_2 y_3, \\ \lambda_\eta &= (y_1^2 + 2y_2 y_3)^2. \end{aligned} \tag{3.7}$$

For simplicity, we assume there is no $H-\rho$ mixing i.e., $\zeta' = 0$. The mass spectrum of scalar sector [169] can be written as follows:

$$\begin{aligned} M_h^2 &= 2\lambda_H v^2, \\ M_\rho^2 &= 2\lambda_\eta \zeta_\rho v_\rho^2, \\ M_{\eta^\pm}^2 &= \lambda'_\eta \left[\mu_\eta^2 + \zeta_3 \frac{v^2}{2} \right] + \lambda_\eta \zeta'' \frac{v_\rho^2}{2}, \\ M_{\eta_R,\eta_I}^2 &= \lambda'_\eta \left[\mu_\eta^2 + (\zeta_3 + \zeta_4 \pm \zeta_5) \frac{v^2}{2} \right] + \lambda_\eta \zeta'' \frac{v_\rho^2}{2}. \end{aligned} \tag{3.8}$$

In order to construct a simplified version of charged leptons mass matrix, left-handed doublets (i.e., three generations ($\overline{L}_{e_L}, \overline{L}_{\mu_L}, \overline{L}_{\tau_L}$)) are considered to transform as $\mathbf{1}, \mathbf{1}'', \mathbf{1}'$ respectively under the A_4 symmetry with assignment of modular weight, $k_I = 1$ for each generation. Analogously, the right-handed charged leptons (e_R, μ_R, τ_R) transform under A_4 as $\mathbf{1}, \mathbf{1}', \mathbf{1}''$, and carry a modular weight, $k_I = -1$. The SM Higgs is uncharged under the new symmetries, to make the scenario a bit simplistic.

The charged leptons interaction Lagrangian is given by

$$L_{M_\ell} = y_\ell^{ee} \overline{L}_{e_L} H e_R + y_\ell^{\mu\mu} \overline{L}_{\mu_L} H \mu_R + y_\ell^{\tau\tau} \overline{L}_{\tau_L} H \tau_R + \text{H.}c.. \tag{3.9}$$

The mass matrix for charged leptons achieves a diagonal structure, following, the spontaneous breaking of electroweak gauge symmetry. Moreover, one can obtain the observed masses for the charged leptons by adjusting the Yukawa couplings. Hence, the obtained mass matrix is represented as follows

$$M_\ell = \begin{pmatrix} y_\ell^{ee} v/\sqrt{2} & 0 & 0 \\ 0 & y_\ell^{\mu\mu} v/\sqrt{2} & 0 \\ 0 & 0 & y_\ell^{\tau\tau} v/\sqrt{2} \end{pmatrix} = \begin{pmatrix} m_e & 0 & 0 \\ 0 & m_\mu & 0 \\ 0 & 0 & m_\tau \end{pmatrix}, \tag{3.10}$$

where m_e, m_μ and m_τ are the observed charged lepton masses.

3.3.1 Dirac and pseudo-Dirac interaction terms for the neutrinos

The right (left) handed heavy fermions contrary to SM leptons are considered as triplet under A_4 modular group with a $U(1)_{B-L}$ charge of $-1(0)$ and modular weight $k_I = -1(+1)$. The usual Dirac interactions of neutrinos with SM Higgs cannot be realized with the aforesaid charges. The introduction of modular Yukawa couplings with transformation represented in Table 3.2 along with inert scalar doublet η are necessary to write such interactions. Moreover, the Yukawa couplings $\mathbf{Y}(\tau) = (y_1(\tau), y_2(\tau), y_3(\tau))$, are expressed in terms of Dedekind eta-function $\eta(\tau)$ and its derivative, as discussed in (Appendix of [59]). Hence, the invariant interaction Lagrangian, involving the active neutrinos along with the right and left-handed heavy fermions, can be represented in the following forms:

$$L_D = \alpha_D \overline{L}_{e_L} \widetilde{\eta} (\mathbf{Y} N_R)_1 + \beta_D \overline{L}_{\mu_L} \widetilde{\eta} (\mathbf{Y} N_R)_{1'} + \gamma_D \overline{L}_{\tau_L} \widetilde{\eta} (\mathbf{Y} N_R)_{1''} + \text{H.}c., \tag{3.11}$$

$$L_{LS} = \left[\alpha'_D \overline{L}_{e_L} \widetilde{\eta} (\mathbf{Y} S^c_L)_1 + \beta'_D \overline{L}_{\mu_L} \widetilde{\eta} (\mathbf{Y} S^c_L)_{1'} + \gamma'_D \overline{L}_{\tau_L} \widetilde{\eta} (\mathbf{Y} S^c_L)_{1''} \right] \frac{\rho}{\Lambda} + \text{H.}c.. \tag{3.12}$$

Hence, the nature of the light neutrino mass could be of Majorana type, due to presence of small lepton number violating terms as shown in eqn. (3.12). Adjacently, the A_4 and $U(1)_{B-L}$ charges for heavy fermions are imposed in such a way that their usual Majorana mass terms are forbidden. However, the mixing between the additional leptons are allowed, which can be written as follows [156]

$$\begin{aligned} L_{M_{RS}} &= \left[\alpha_{NS} \mathbf{Y} (\overline{S_L} N_R)_{\text{sym}} + \beta_{NS} \mathbf{Y} (\overline{S_L} N_R)_{\text{Anti-sym}} \right] \rho^\dagger + \text{H.c.} \\ &= \alpha_{NS} \left[y_1 (2\bar{S}_{L_1} N_{R_1} - \bar{S}_{L_2} N_{R_3} - \bar{S}_{L_3} N_{R_2}) + y_2 (2\bar{S}_{L_2} N_{R_2} - \bar{S}_{L_1} N_{R_3} - \bar{S}_{L_3} N_{R_1}) \right. \\ &\quad \left. + y_3 (2\bar{S}_{L_3} N_{R_3} - \bar{S}_{L_1} N_{R_2} - \bar{S}_{L_2} N_{R_1}) \right] \rho^\dagger + \beta_{NS} \left[y_1 (\bar{S}_{L_2} N_{R_3} - \bar{S}_{L_3} N_{R_2}) \right. \\ &\quad \left. + y_2 (\bar{S}_{L_3} N_{R_1} - \bar{S}_{L_1} N_{R_3}) + y_3 (\bar{S}_{L_1} N_{R_2} - \bar{S}_{L_2} N_{R_1}) \right] \rho^\dagger + \text{H.c.}, \end{aligned} \tag{3.13}$$

where, α_{NS} and β_{NS} are the free parameters and $(\overline{S_L} N_R)_{\text{sym}}$ and $(\overline{S_L} N_R)_{\text{Anti-sym}}$ represent the triplet symmetric ($\mathbf{3}_s$) and anti-symmetric ($\mathbf{3}_a$) product of $\bar{S}_L N_R$ under A_4. Using $\langle \rho \rangle = v_\rho / \sqrt{2}$, the resulting mass matrix is found to be

$$M_{RS} = \frac{v_\rho}{\sqrt{2}} \left(\frac{\alpha_{NS}}{3} \begin{bmatrix} 2y_1 & -y_3 & -y_2 \\ -y_3 & 2y_2 & -y_1 \\ -y_2 & -y_1 & 2y_3 \end{bmatrix} + \beta_{NS} \begin{bmatrix} 0 & y_3 & -y_2 \\ -y_3 & 0 & y_1 \\ y_2 & -y_1 & 0 \end{bmatrix} \right). \tag{3.14}$$

As the mass matrix (3.14) is not symmetric, for simplicity we consider in our numerical analysis $\alpha_{NS} \gg \beta_{NS}$, i.e., the symmetric term gives the dominant contribution compared to the anti-symmetric term. The mass matrix for the six heavy leptons, in the basis $(N_R, S_L)^T$, can be given as

$$M_{Hf} = \begin{pmatrix} 0 & M_{RS} \\ M_{RS}^T & 0 \end{pmatrix}. \tag{3.15}$$

Here, the diagonal entries i..e., Majorana mass terms of S_L and N_R are forbidden. Diagonalization of the mass matrix (3.15) yields three doubly degenerate heavy fermions, with mass eigenvalues $M_i^{\pm}$, $(i = 1,2,3)$

$$\begin{aligned}
M_1^{\pm} &\approx \pm\Big(\frac{\alpha_{NS} v_\rho}{6}\Big)\Big(y_1+y_2+y_3-\sqrt{9(y_1^2+y_2^2+y_3^2)-6y_2y_3-6y_1(y_2+y_3)}\Big),\\
M_2^{\pm} &\approx \pm\Big(\frac{\alpha_{NS} v_\rho}{6}\Big)\Big(y_1+y_2+y_3+\sqrt{9(y_1^2+y_2^2+y_3^2)-6y_2y_3-6y_1(y_2+y_3)}\Big),\\
M_3^{\pm} &\approx \pm\Big(\frac{\alpha_{NS} v_\rho}{3}\Big)(y_1+y_2+y_3).
\end{aligned} \tag{3.16}$$

The eigenvalues are obtained upon the rotation $M_i^{\pm} = U_R U_{\rm TBM} M_{RS} (U_R U_{\rm TBM})^T$, where

$$U_{TBM} = \begin{pmatrix} -\sqrt{\frac{2}{3}} & \sqrt{\frac{1}{3}} & 0 \\ \sqrt{\frac{1}{6}} & \sqrt{\frac{1}{3}} & -\sqrt{\frac{1}{2}} \\ \sqrt{\frac{1}{6}} & \sqrt{\frac{1}{3}} & \sqrt{\frac{1}{2}} \end{pmatrix}, \quad U_R = \begin{pmatrix} \frac{A}{N_-} & \frac{A}{N_+} & -\frac{1}{\sqrt{1+A^2}} \\ \frac{B}{N_-} & \frac{B}{N_+} & 0 \\ \frac{1}{N_-} & \frac{1}{N_+} & \frac{1}{\sqrt{1+A^2}} \end{pmatrix}, \tag{3.17}$$

with,

$$\begin{aligned}
B_- &= \frac{1}{\sqrt{6}(y_2-y_3)}\Big[y_1+y_2+y_3+\sqrt{9y_1^2+9y_2^2+9y_3^2-6y_2y_3-6y_1(y_2+y_3)}\Big],\\
B_+ &= \frac{1}{\sqrt{6}(y_2-y_3)}\Big[y_1+y_2+y_3-\sqrt{9y_1^2+9y_2^2+9y_3^2-6y_2y_3-6y_1(y_2+y_3)}\Big],\\
A &= \frac{2y_1-y_2-y_3}{\sqrt{3}(y_2-y_3)},\\
N_- &= \sqrt{1+B_-^2+A^2},\\
N_+ &= \sqrt{1+B_+^2+A^2}.
\end{aligned} \tag{3.18}$$

3.4 Radiative Neutrino mass

Since, the usual Dirac mass terms of neutrinos with SM Higgs are forbidden by the assigned symmetries, one can generate light neutrino masses at one-loop level and the corresponding Feynman diagram is displayed in Fig. 3.1.

The expression of the neutrino mass[1] from one loop radiative corrections is written as [143, 170]

$$(\mathcal{M}_\nu)_{ij} = \sum_k \frac{(\tilde{Y}_D)_{ik}(\tilde{Y}_{LS})_{jk}}{32\pi^2}\left[\frac{M_{\eta_R}^2}{M_{\eta_R}^2-M_k^2}\ln\frac{M_{\eta_R}^2}{M_k^2}-\frac{M_{\eta_I}^2}{M_{\eta_I}^2-M_k^2}\ln\frac{M_{\eta_I}^2}{M_k^2}\right]. \tag{3.19}$$

Here, M_k is the mass of the heavy fermions ($M_i^{\pm}$, with $i = 1,2,3$) inside the loop, the couplings $\tilde{Y}_D$ and $\tilde{Y}_{LS}$ are related to the Yukawa coupling matrices (Y_D and Y_{LS}), characterizing the interactions of light

[1] We write the correct expression by including the appropriate factor, which is missing in many references of scotogenic model along with the original paper [143].

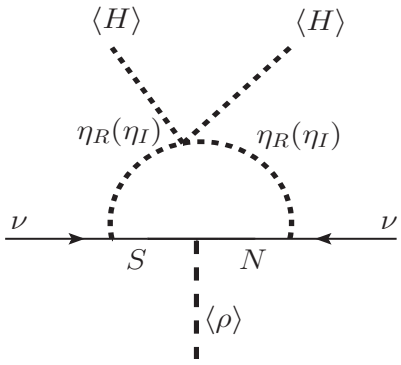

Figure 3.1: Feynman diagram for radiatively neutrino mass generation.

neutrinos with N_R and S_L respectively and are given by

$$\tilde{Y}_D = Y_D U_{\rm TBM} U_R\,, \quad \text{with} \quad Y_D \;= \begin{bmatrix} \alpha_D & 0 & 0 \\ 0 & \beta_D & 0 \\ 0 & 0 & \gamma_D \end{bmatrix} \begin{bmatrix} y_1 & y_3 & y_2 \\ y_2 & y_1 & y_3 \\ y_3 & y_2 & y_1 \end{bmatrix}_{LR}, \tag{3.20}$$

$$\tilde{Y}_{LS} = Y_{LS} U_{\rm TBM} U_R\,, \quad \text{with} \quad Y_{LS} \;= \frac{v_\rho}{\Lambda\sqrt{2}} \begin{bmatrix} \alpha'_D & 0 & 0 \\ 0 & \beta'_D & 0 \\ 0 & 0 & \gamma'_D \end{bmatrix} \begin{bmatrix} y_1 & y_3 & y_2 \\ y_2 & y_1 & y_3 \\ y_3 & y_2 & y_1 \end{bmatrix}_{LS}. \tag{3.21}$$

The mass matrix in eqn.(3.19), can be reduced to the simplified form (see Appendix B.2) as follows with the assumption $M_k^2 \simeq m_0^2$, where $m_0^2 = (M_{\eta_R}^2 + M_{\eta_I}^2)/2$:

$$(\mathcal{M}_\nu)_{ij} = \frac{\zeta_5 \lambda'_\eta}{2(4\pi)^2} \left(\frac{v}{\sqrt{2}}\right)^2 \sum_k \frac{(\tilde{Y}_D)_{ik} (\tilde{Y}_{LS})_{jk}}{M_k}, \tag{3.22}$$

where, we have used $M_{\eta_R}^2 - M_{\eta_I}^2 = \zeta_5 \lambda'_\eta v^2$, with, $\zeta_5 \approx \mathcal{O}(10^{-7})$. When specific mass ranges are considered for M_{η_R}, M_{η_I} and M_k, one can generate both linear seesaw and inverse seesaw [107, 171, 172]. The neutrino mass matrix (3.22) is numerically diagonalized through the relation $U\mathbb{M}U^\dagger = {\rm d}iag(m_1^2, m_2^2, m_3^2)$, where $\mathbb{M} = \mathcal{M}_\nu^\dagger \mathcal{M}_\nu$ and U is an unitary matrix. Thus, the neutrino mixing angles can be extracted from the matrix elements of the diagonalizing matrix U, through the generic expressions:

$$\sin^2\theta_{13} = |U_{13}|^2, \quad \sin^2\theta_{12} = \frac{|U_{12}|^2}{1-|U_{13}|^2}, \quad \sin^2\theta_{23} = \frac{|U_{23}|^2}{1-|U_{13}|^2}. \tag{3.23}$$

Next, we attempt to determine the Jarlskog invariant (J_{CP}) as well as the effective Majorana mass

parameter ($\langle m_{ee} \rangle$) through the following relations [94]:

$$
\begin{aligned}
&J_{CP} = \mathrm{Im}[U_{e1} U_{\mu 2} U_{e2}^{*} U_{\mu 1}^{*}] = s_{23} c_{23} s_{12} c_{12} s_{13} c_{13}^{2} \sin\delta_{CP}, \\
&\left| \langle m_{ee}^{\mathrm{NO}} \rangle \right| \simeq \left| \sqrt{\Delta m_{21}^{2}} \sin^{2}\theta_{12} \cos^{2}\theta_{13} + \sqrt{\Delta m_{31}^{2}} \sin^{2}\theta_{13} \sin^{2}\theta_{13} e^{i(\alpha_{32} - 2\delta)} \right|, \\
&\left| \langle m_{ee}^{\mathrm{IO}} \rangle \right| \simeq \sqrt{|\Delta m_{32}^{2}|} \cos^{2}\theta_{13} \sqrt{1 - \sin^{2} 2\theta_{12} \sin^{2}\left(\frac{\alpha_{21}}{2}\right)}.
\end{aligned}
\tag{3.24}
$$

where, $s_{ij} = \sin\theta_{ij}$ and $c_{ij} = \cos\theta_{ij}$, while α_{ij} denote the Majorana phases.

3.5 Numerical Analysis

For constraining the model parameters, we use the current 3σ limit on neutrino mixing parameters for normal ordering (NO) from global-fit [173–175], which are given as

$$
\begin{aligned}
&\Delta m^{2}_{\mathrm{atm}} = [2.431, 2.622] \times 10^{-3}\ \mathrm{eV}^{2}, \quad \Delta m^{2}_{sol} = [6.79, 8.01] \times 10^{-5}\ \mathrm{eV}^{2}, \\
&\sin^{2}\theta_{13} = [0.02044, 0.02437], \ \ \sin^{2}\theta_{23} = [0.428, 0.624], \ \ \sin^{2}\theta_{12} = [0.275, 0.350]\,.
\end{aligned}
\tag{3.25}
$$

For inverted ordering (IO),

$$
\begin{aligned}
&\Delta m^{2}_{\mathrm{atm}} = [2.37, 2.53] \times 10^{-3}\ \mathrm{eV}^{2}, \quad \Delta m^{2}_{sol} = [6.79, 8.01] \times 10^{-5}\ \mathrm{eV}^{2}, \\
&\sin^{2}\theta_{13} = [0.02018, 0.02424], \ \ \sin^{2}\theta_{23} = [0.433, 0.608], \ \ \sin^{2}\theta_{12} = [0.275, 0.350]\,.
\end{aligned}
\tag{3.26}
$$

The model parameters are so chosen, as to fit the current neutrino oscillation data given in Eqn. (3.25), as follows:

$$
\begin{aligned}
&\mathrm{Re}[\tau] \in [-0.5, 0.5], \ \ \mathrm{Im}[\tau] \in [1, 2], \ \ \{\alpha_D, \beta_D, \gamma_D\} \in [0.1, 1.0], \ \ \{\alpha'_D, \beta'_D, \gamma'_D\} \in \ [0.1, 1.0], \\
&\alpha_{NS} \in [0.01, 0.1], \quad \beta_{NS} \in [10^{-5}, 10^{-4}], \quad v_\rho \in [7, 300]\ \mathrm{TeV}, \quad \frac{v_\rho}{\Lambda} \in [0.001, 0.01].
\end{aligned}
$$

The parameters used are randomly looked over the above mentioned ranges and the allowed regions for those are first constrained by the observed 3σ range of mass squared differences, mixing angles and sum of active neutrino masses 0.058 (0.098) eV $\sum m_i < 0.12$ eV [40, 176] for NO (IO) case. Furthermore, the range of modulus τ helps in validating the model with experimental results of neutrino masses is found to be $-0.5 \lesssim \mathrm{Re}[\tau] \lesssim 0.5$ and $1 \lesssim \mathrm{Im}[\tau] \lesssim 2$. Hence, a very narrow range is satisfied by the modular Yukawa couplings, which are functions of τ (please refer Appendix of [59]) and their regions of validation are found as: $0.99 \lesssim y_1(\tau) \lesssim 1$, $0.1 \lesssim y_2(\tau) \lesssim 0.75$ and $0.1 \lesssim y_3(\tau) \lesssim 0.25$, as visible from Fig. 3.2. We know that in conventional models, we have a control on the value of the Yukawa couplings, that satisfies the neutrino phenomenology. However, in modular frameworks, the Yukawa couplings exhibit q expansion form (see Eqn (B.2)) and are dependent on modulus τ. After obtaining the range of Yukawa couplings and by suitably fixing the free parameters, one can explain the desired neutrino oscillation parameters. Proceeding further, Fig. 3.3 and Fig. 3.4 depict the parameter space consistent with neutrino mass squared

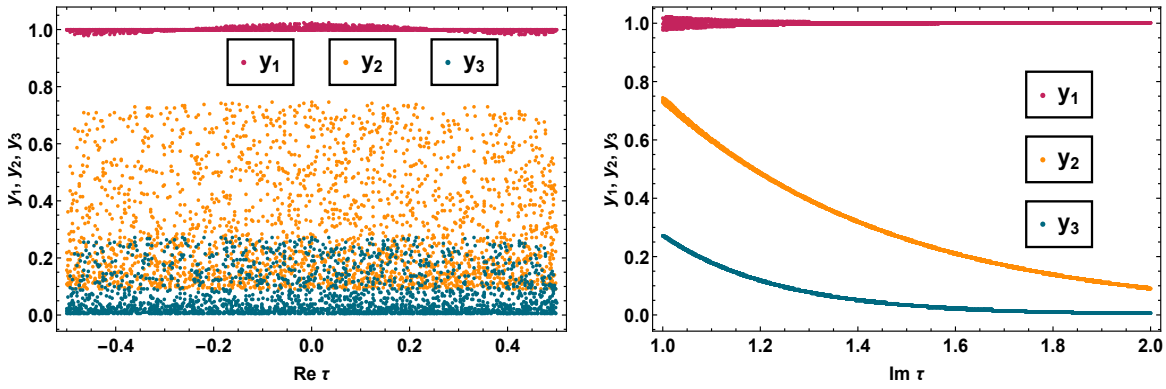

Figure 3.2: Left panel indicates the interdependence of the modular Yukawa couplings (y_1, y_2, y_3) with the real part while right panel presents the imaginary part of modulus τ.

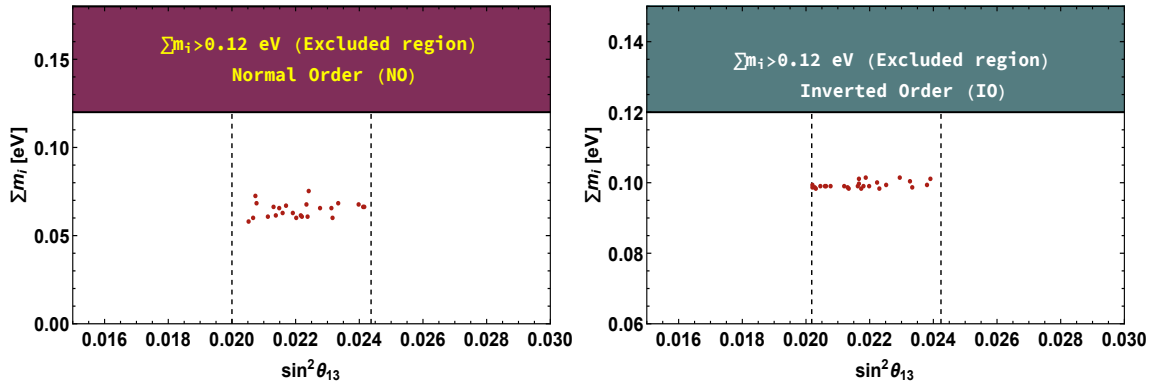

Figure 3.3: Left (right) panel represents the plot of Σm_i with $\sin^2\theta_{13}$ for both NO (IO). Here, the vertical dashed line represents the 3σ range of the respective mixing angles for NO (IO) case.

differences of 3σ region in the plane of sum of total neutrino masses and mixing angles in NO and IO case. Here, it is evident that we obtain the sum of the total neutrino masses within cosmological bound (0.050 eV $\leq \Sigma m_i \leq 0.07$ eV) and the mixing angles meet their corresponding 3σ region of oscillation data i.e., $0.02051\ (0.02024) \leq \sin^2\theta_{13} \leq 0.02412\ (0.0237)$, $0.275\ (0.276) \leq \sin^2\theta_{12} \leq 0.340\ (0.345)$, $0.429\ (0.434) \leq \sin^2\theta_{23} \leq 0.588\ (0.587)$ for NO (IO) case. In other words, the model is able to satisfy all the current neutrino oscillation parameters in their respective 3σ regions simultaneously. In Fig. 3.5 we show the plot in the plane of $\sin^2\theta_{12} - \sin^2\theta_{13}$ (left panel) and $\sin^2\theta_{12} - \sin^2\theta_{23}$ (right panel) in NO case. We do not include the same for IO, as they are pretty similar to NO case. Fig. 3.6 projects the range of Yukawa couplings abiding 3σ of all neutrino mixing parameters, plotted with the sum of active neutrino masses. As mentioned in Sec. 3.4, Fig. 3.7, helps us to have a glimpse of how Jarlskog CP invariant fits in the whole scenario, and found to be ranging from $[-0.007, 0.007]$, its connection with the reactor mixing angle is depicted in the left panel for NO case. Right panel depicts the same for inverted ordering case where J_{CP} ranges from $[-0.006, 0.005]$. Fig. 3.8 shows the plot of Jarlskog invariant with sum of active neutrino mass for normal

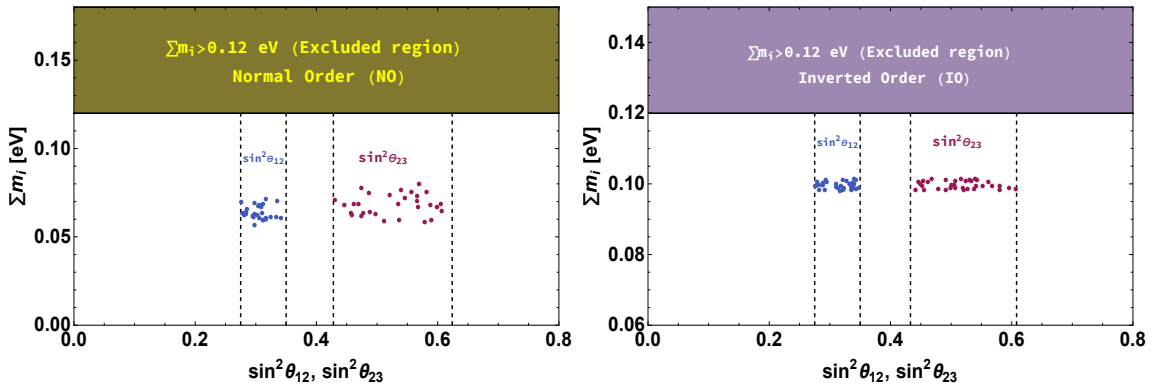

Figure 3.4: Left (right) panel represents the plot of Σm_i with $\sin^2\theta_{12}$ and $\sin^2\theta_{23}$ for NO (IO) cases respectively. Here, the vertical dashed line represents the 3σ range of the respective mixing angles for NO (IO) case.

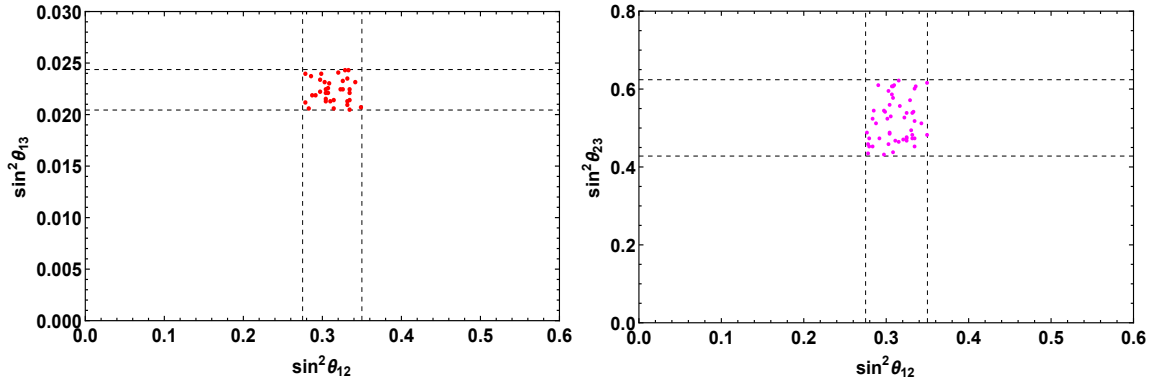

Figure 3.5: Left panel represents a plot in a mutual space between $\sin^2\theta_{12}$ with $\sin^2\theta_{13}$ and right panel stands for $\sin^2\theta_{12}$ with $\sin^2\theta_{23}$ with dashed lines implying the respective 3σ ranges.

(left panel) and inverted (right panel) ordering.

Advancing further, in Fig. 3.9, the correlation between the effective neutrino-less double beta decay (NDBD) mass parameter m_{ee} and the sum of neutrino masses is shown in the left (right) panel for NO (IO) case. Also, in Fig. 3.10 the left (right) panel shows its dependence with the lightest neutrino mass m_1 (m_3) for normal (inverted) ordering. From the model perspective, one should note that the upper limit of m_{ee} could be as large as 0.05 eV and the lightest neutrino mass should be $m_1(m_3) \leq 0.015$ eV. It is also evident that the effective neutrino mass parameter of our model reaches the sensitivity of LEGEND-200 [94]. In addition, we have also shown in the left (right) panel of Fig. 3.11 the plot between the CP violating phase δ_{CP} with the reactor mixing angle θ_{13} for normal (inverted) ordering, which provides the constraint on δ_{CP} as $0 \leq \delta_{CP} \leq 284^\circ$ for NO and and $0 \leq \delta_{CP} \leq 250^\circ$ for IO. In the left (right) panel of Fig. 3.12, we display the correlation of the two Majorana phases i.e. α_{21} and α_{31} for normal (inverted) ordering, which are involved in the determination of the effective mass of NDBD process.

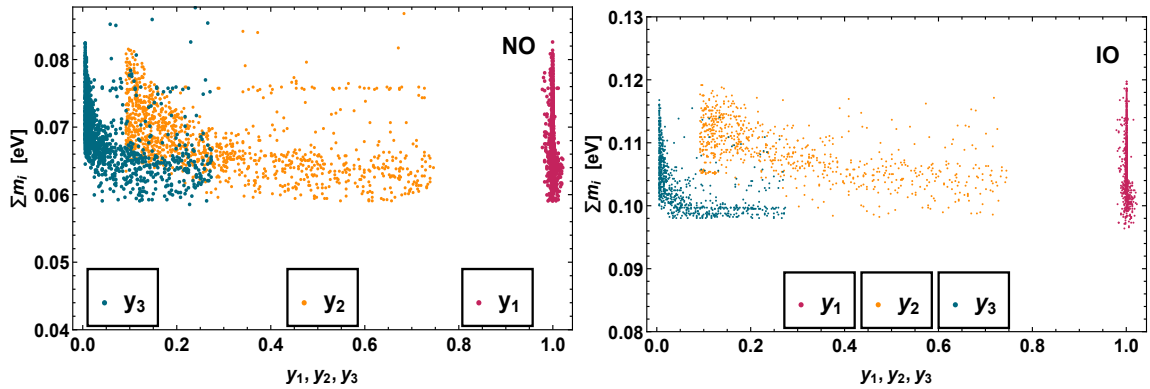

Figure 3.6: Left (right) panel reflects the alteration of sum of active neutrino masses with the modular Yukawa couplings for normal (inverted) ordering.

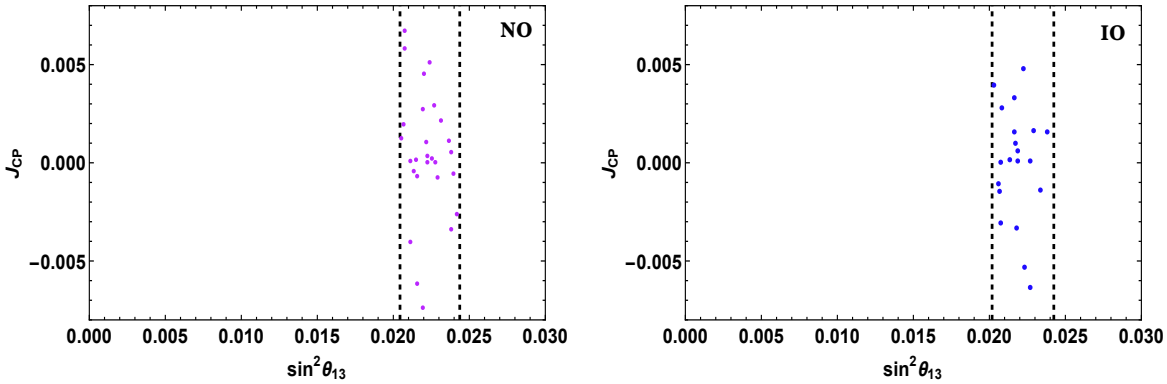

Figure 3.7: Left (right) panel shows a plot between the Jarlskog invariant with the reactor mixing angle in normal (inverted) hierarchy. Here, the vertical dashed line represents the 3σ range of $\sin^2\theta_{13}$.

3.6 Comment on LFV Decays and $\mu - e$ conversion

3.6.1 Comment on $\mu \to e\gamma$

The quest in looking for lepton flavour violating decay mode $\mu \to e\gamma$ plays an exceptionally pivotal role in the hunt for new physics beyond the SM. Many experiments are looking for this decay mode with great effort for an improved sensitivity, and the current limit on its branching $\mathrm{Br}(\mu \to e\gamma) < 4.2 \times 10^{-13}$ is from MEG collaboration [103]. In the present framework, the LFV process $\mu \to e\gamma$ occur at one loop level through standard Yukawa interactions. The Feynman diagrams for this process are displayed in Fig. 3.13.

The branching ratio for the rare decay $\ell_\alpha \to \ell_\beta\gamma$ is given as [177]

$$\mathrm{Br}(\ell_\alpha \to \ell_\beta\gamma) = \frac{3(4\pi)^3\alpha_{em}}{4\,G_F^2}|\mathscr{A}_\mathscr{D}|^2 \times \mathrm{Br}(\ell_\alpha \to \ell_\beta\nu_\alpha\bar{\nu}_\beta), \tag{3.27}$$

where, $G_F \approx 10^{-5}\ GeV^{-2}$ (i.e. Fermi constant) and α being the electromagnetic fine structure constant and

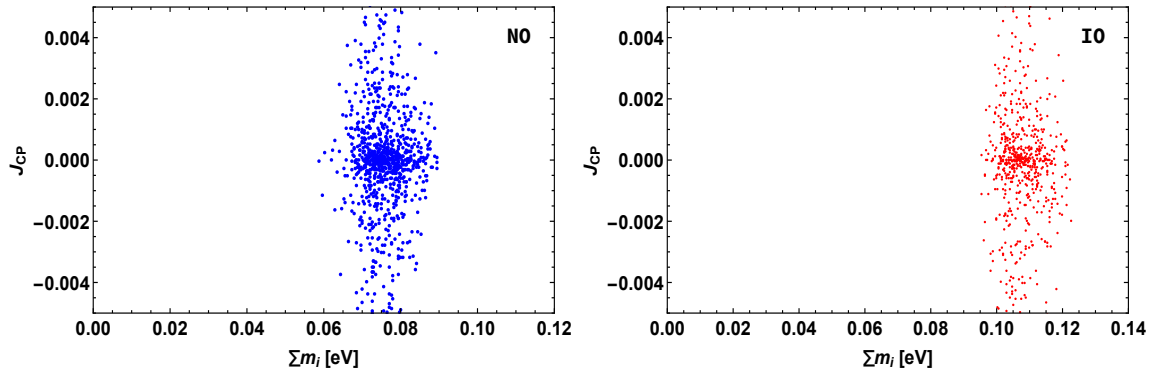

Figure 3.8: Left (right) panel above depicts the plot of Jarlskog invariant with the sum of active neutrino masses in normal (inverted) ordering.

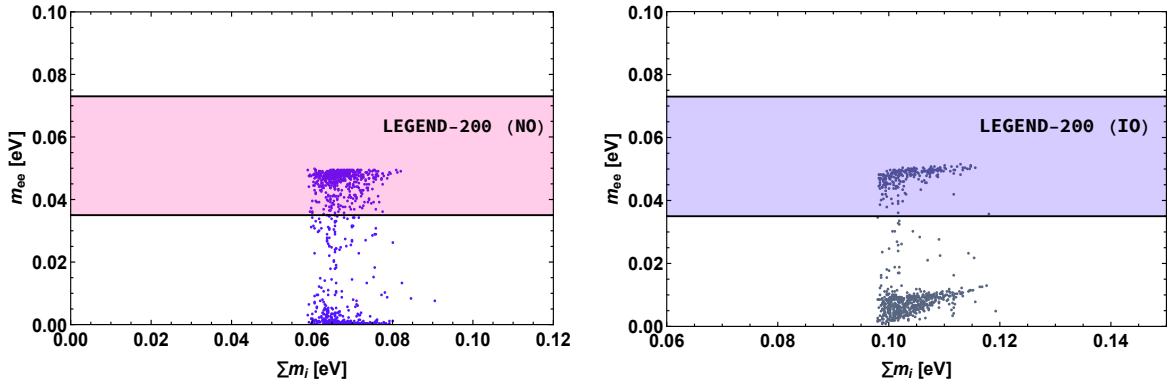

Figure 3.9: Left (right) panel above project the interdependence of effective neutrino mass of NDBD with the sum of active neutrino masses for normal (inverted) ordering.

$\mathscr{A}_{\mathscr{D}}$ is the dipole contribution, hence, expressed as

$$\mathscr{A}_{\mathscr{D}} = \sum_k \frac{(Y_D)_{k\alpha}\,(Y_{LS}{}^*)_{k\beta}\,\mathscr{G}_1(\xi_k)}{2(4\pi)^2 M^2_{\eta^+}}. \tag{3.28}$$

Here, Y_D & Y_{LS} being the Yukawa coupling matrices as shown in eqn.(3.20) and (3.21), $\xi_k = \frac{M_k^2}{M^2_{\eta^+}}$ and $\mathscr{G}_1(x)$ is the loop function provided in Appendix B.3.

In the left of Fig. 3.14, we have represented the dependence of the branching fraction of $\mu \to e\gamma$ on the inert charged scalar mass, which are found to lie within the experimental limits. In the right panel of Fig. 3.14 the variation of $\mu \to e\gamma$ branching fraction with the modular Yukawa couplings is consistent with neutrino mass constraints as displayed.

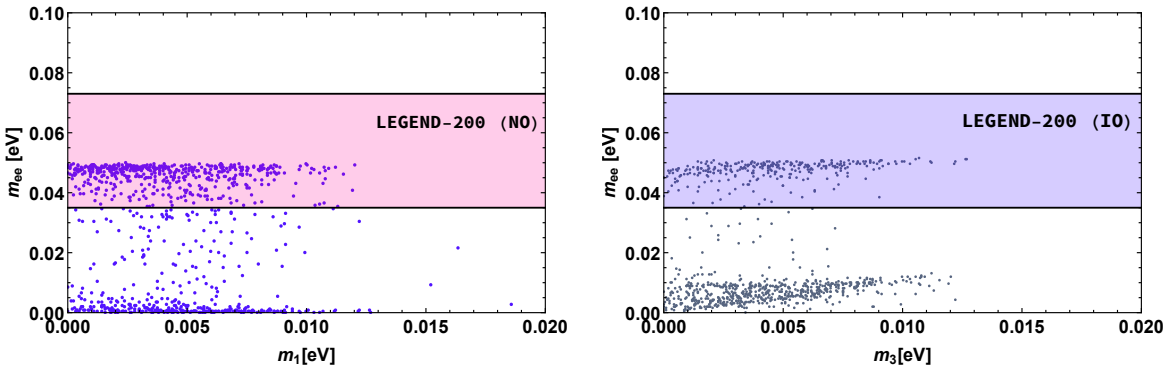

Figure 3.10: Left (right) panel above project the interdependence of effective neutrino mass of NDBD with the lightest neutrino mass $m_1(m_3)$ for normal (inverted) ordering.

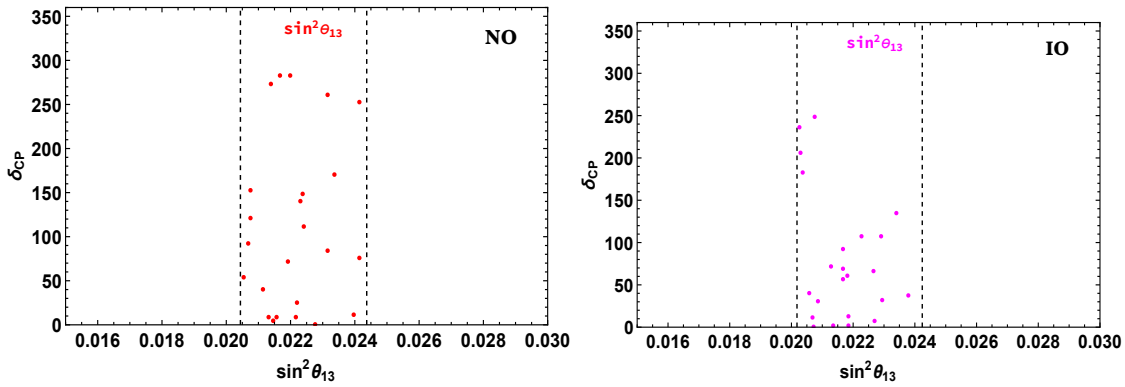

Figure 3.11: Above plots depicts the variation of δ_{CP} with respect to the mixing angles i.e. $\sin^2\theta_{13}$ for normal ordering (left panel) and for inverted ordering (right panel).

3.6.2 Comment on $\mu \to 3e$

The three body LFV decay processes $\ell_\alpha \to \ell_\beta \overline{\ell_\beta} \ell_\beta$ can proceed through penguin and box diagrams, which are shown in Fig. 3.15. The corresponding branching ratio can be expressed as [177, 178]

$$\begin{aligned} \mathrm{BR}\left(\ell_\alpha \to \ell_\beta \overline{\ell_\beta} \ell_\beta\right) \;=\; & \frac{3(4\pi)^2 \alpha_{\mathrm{em}}^2}{8 G_F^2} \left[|\mathcal{A}_{\mathcal{ND}}|^2 + |\mathcal{A}_{\mathcal{D}}|^2 \left(\frac{16}{3} \log\left(\frac{m_\alpha}{m_\beta}\right) - \frac{22}{3} \right) \right. \\ & \left. + \frac{1}{6} |\mathcal{B}|^2 + \left(-2 \mathcal{A}_{\mathcal{ND}} \mathcal{A}_{\mathcal{D}}^* + \frac{1}{3} \mathcal{A}_{\mathcal{ND}} \mathcal{B}^* - \frac{2}{3} \mathcal{A}_{\mathcal{D}} \mathcal{B}^* + \mathrm{h.c.} \right) \right] \\ & \times \mathrm{Br}\left(\ell_\alpha \to \ell_\beta \nu_\alpha \overline{\nu_\beta}\right) . \end{aligned} \tag{3.29}$$

The form factor $\mathcal{A}_{\mathcal{D}}$ is dipole contribution and is given in Eqn. (3.28). Regarding the other form factors, $\mathcal{A}_{\mathcal{ND}}$, given by

$$\mathcal{A}_{\mathcal{ND}} = \sum_i \frac{(Y_{LS}^*)_{i\beta} (Y_D)_{i\alpha}}{6(4\pi)^2} \frac{1}{m_{\eta^+}^2} \mathcal{G}_2(\xi_i), \tag{3.30}$$

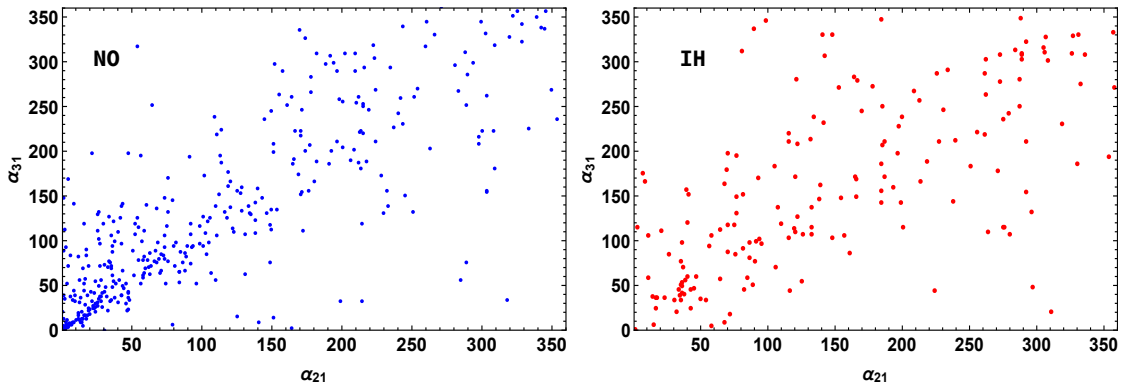

Figure 3.12: Left (right) panel depicts the correlation between the Majorana phases α_{21} with α_{31} for normal (inverted) ordering respectively.

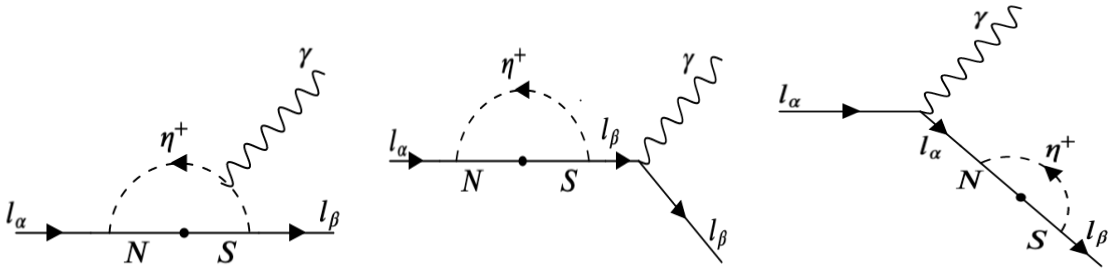

Figure 3.13: Feynman diagrams depicting the LFV rare decay processes $\ell_\alpha \to \ell_\beta \gamma$. Here, the blob corresponds to mixing of the right handed neutrinos N_R & S_L.

is generated by non-dipole contribution, whereas $\mathscr{B}$, induced by box diagrams, is

$$\begin{aligned}\mathscr{B} &= \frac{1}{(4\pi e)^2 m^2_{\eta^+}} \sum_{i,j} \Big[\frac{1}{2} \mathscr{D}_1(\xi_i,\xi_j)(Y^*_{LS})_{j\beta}(Y_D)_{j\beta}(Y_{LS})_{i\beta}(Y^*_D)_{i\alpha} \\ &\quad + \sqrt{\xi_i \xi_j}\, \mathscr{D}_2(\xi_i,\xi_j)(Y_{LS})_{j\beta}(Y_D)_{j\beta}(Y^*_{LS})_{i\beta}(Y^*_D)_{i\alpha} \Big] . \end{aligned} \tag{3.31}$$

The loops functions $\mathscr{G}_2(x)$, $\mathscr{D}_1(x,y)$ and $\mathscr{D}_2(x,y)$ are presented in Appendix B.3. Upper left panel of Fig. 3.16 represents the variation of the branching fraction of $\mu \to 3e$ with the mass of inert doublet. Here, we find the branching fraction is obtained below the present upper limit $\mathrm{Br}(\mu \to e^- e^+ e^-) < 1.0 \times 10^{-12}$ [179]. Similarly, in the upper right panel, we display the variation of $\mathrm{Br}(\mu \to 3e)$ with dark matter mass, while the lower panel represents the correlation of modular Yukawa couplings with the $\mu \to 3e$ branching fraction.

3.6.3 $\mu - e$ conversion in Nuclei

The most stringent constraint on LFV decays are favored by the $\mu \to e\gamma$, however, the improved sensitivity is expected from the $\mu - e$ conversion in the nucleus in coming decades. Several experiments like Mu2e,

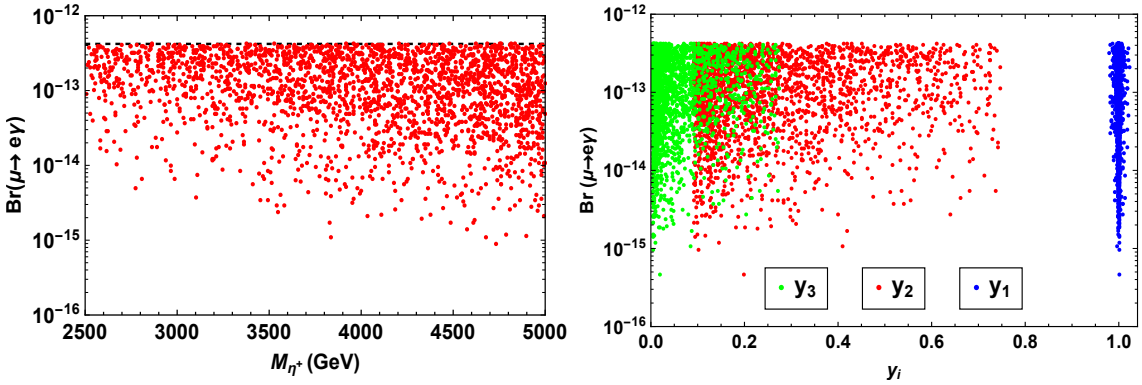

Figure 3.14: The left panel represents the variation of the branching ratio of LFV process $\mu \to e\gamma$ with the charged inert scalar mass, whereas the right panel represents the variation with modular Yukawa couplings, which are consistent with neutrino mass.

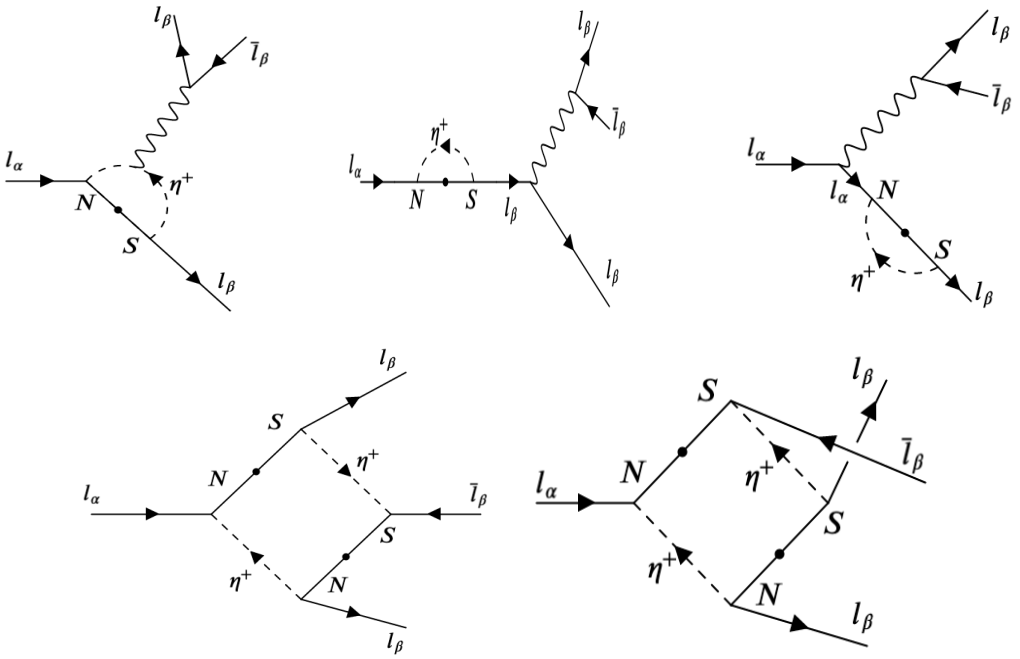

Figure 3.15: Feynman diagrams to represent the $\mu \to 3e$ conversion in the nucleus mediated by the gauge bosons and photon.

DeeMe, COMET and PRISM/PRIME [180–182] are on its peak to reach an upper limit of 4.3×10^{-14} (for Ti Nucleus) to future sensitivity upto 10^{-18}. We briefly discuss the contribution from $\mu - e$ conversion in

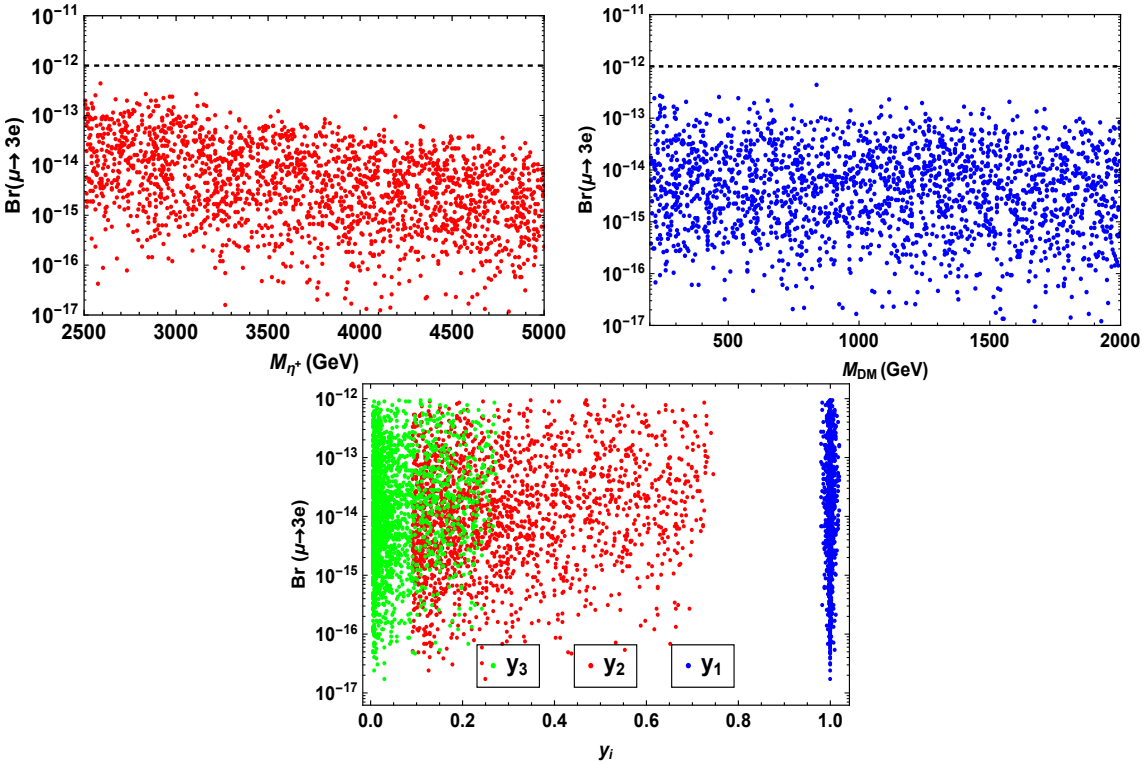

Figure 3.16: In the upper panel, left plot represents the variation of the branching ratio of LFV process $\mu \to 3e$ with the charged inert scalar mass, whereas the right plot represents the variation with dark matter mass. Plot in lower panel depicts the variation with Yukawa couplings.

nucleus [183, 184] shown in Fig. 3.17. The conversion rate for $\mu - e$ in the nucleus is provided as

$$\begin{aligned} CR(\mu\text{-}e,\text{Nucleus}) = & \frac{p_e E_e m_\mu^3 G_F^2 \alpha_{\rm em}^3 Z_{eff}^4 F_p^2}{8\pi^2 Z \Gamma_{capt}} \\ & \times \left\{ \left| (Z+N)\left(g_{LV}^{(0)} + g_{LS}^{(0)}\right) + Z - N\left(g_{LV}^{(1)} + g_{LS}^{(1)}\right) \right|^2 + \right. \\ & \left. \left| (Z+N)\left(g_{RV}^{(0)} + g_{RS}^{(0)}\right) + (Z-N)\left(g_{RV}^{(1)} + g_{RS}^{(1)}\right) \right|^2 \right\}. \end{aligned} \tag{3.32}$$

Here, the proton and neutron numbers inside the nucleus are expressed by Z and N, Z_{eff} represents the effective atomic charge [185], F_p & $\Gamma_{\rm capt}$ denote the nuclear matrix element and the total muon capture rate respectively. These parameters can be determined based on the choice of nucleus. Other parameters used in the above equation are provided below [184], where $X = L, R$ and $K = V, S$,

$$\begin{aligned} g_{XK}^{(0)} &= \frac{1}{2} \sum_{q=u,d,s} \left(g_{XK(q)} G_K^{(q,p)} + g_{XK(q)} G_K^{(q,n)} \right), \\ g_{XK}^{(1)} &= \frac{1}{2} \sum_{q=u,d,s} \left(g_{XK(q)} G_K^{(q,p)} - g_{XK(q)} G_K^{(q,n)} \right). \end{aligned} \tag{3.33}$$

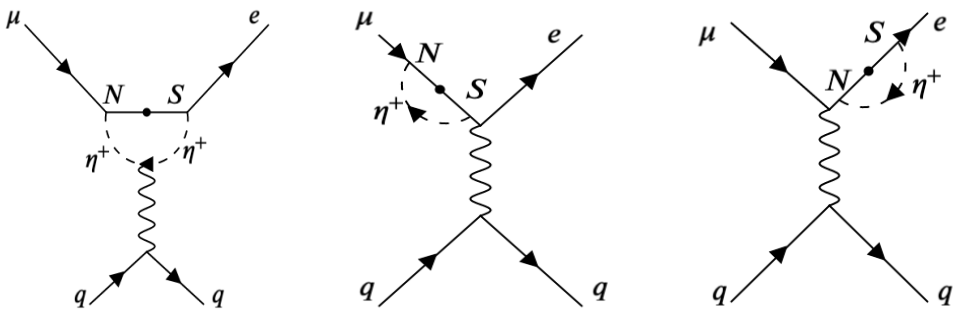

Figure 3.17: Feynman diagrams to represent the μ-e conversion in the nucleus mediated by the gauge bosons and photon.

The numerical values of G_K coefficients are taken from [183, 184, 186]. Here, $g_{XK(q)}$ being the effective couplings, given as follows

$$\begin{aligned} g_{LS(q)} &\approx 0\,, \\ g_{RS(q)} &\approx 0\,, \\ g_{RV(q)} &= g_{LV(q)}\big|_{L\leftrightarrow R}\,, \\ g_{LV(q)} &\approx g^{\gamma}_{LV(q)}\,, \end{aligned} \tag{3.34}$$

where, $g^{\gamma}_{LV(q)} = \frac{\sqrt{2}}{G_F} e^2 \mathcal{Q}_q \left(\mathcal{A}_{\mathcal{N}\mathcal{D}} - \mathcal{A}_{\mathcal{D}}\right)$ is generated from photon penguins, $\mathcal{Q}_q$ represents electric charge of the corresponding quark.

We compute the conversion rate of $\mu - e$ in Titanium ($^{48}_{22}$Ti) nucleus (relevant details can be found in [184]). Left panel of Fig. 3.18, projects the conversion rate versus M_{η^+} and right panel signifies its correlation with Br($\mu \to e\gamma$). Horizontal dashed line corresponds to the upper bound [187].

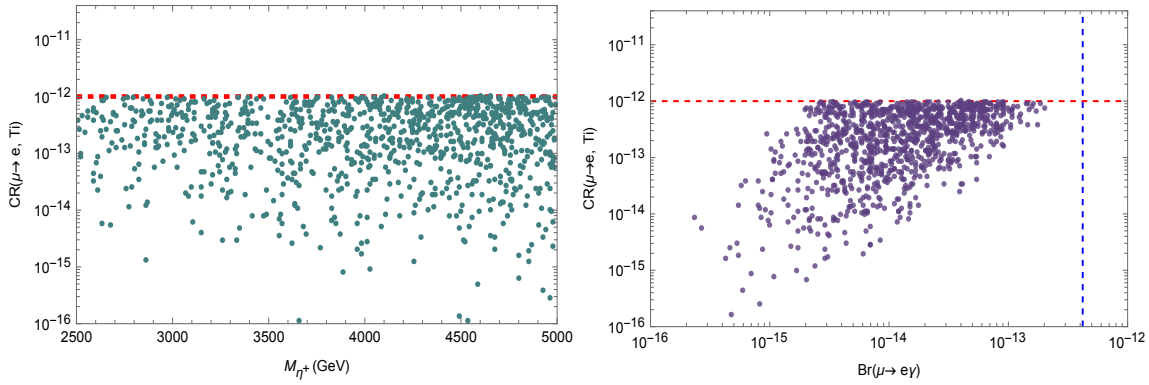

Figure 3.18: The left panel represents the variation of the conversion ratio of $\mu - e$ for Ti nuclei with the charged inert scalar mass, whereas the right panel represents the variation with branching ratio Br($\mu \to e\gamma$). Here the horizontal (red) and vertical (blue) dashed line represents the upper bound [187].

3.7 A brief discussion on Fermionic dark matter

In this section, we give a brief discussion on fermionic dark matter. The model includes three heavy Dirac neutrinos, out of which the lightest one (N_{D_1}) can serve as a dark matter candidate, provided the inert scalar particles are heavier. The DM can have scalar mediated annihilations and can also annihilate via Z', which arises due the kinetic term,

$$\mathscr{L}_{\rm kin} \supset \overline{N}_{D_1}\gamma^{\mu}\left(\partial_{\mu} + i\, g_{\rm BL} Z'_{\mu}\right) N_{D_1}\,. \tag{3.35}$$

The DM abundance can be estimated by the formula [188]

$$\Omega h^2 = \frac{1.07\times 10^9\ {\rm GeV}^{-1}}{{g_*}^{1/2} M_{\rm Pl}}\frac{1}{J(x_f)}, \tag{3.36}$$

where, $M_{\rm Pl} = 1.22\times 10^{19}$ GeV, $g_\star$ is effective relativistic degrees of freedom, x_f is the freeze-out parameter and $J(x_f)$ reads as

$$J(x_f) = \int_{x_f}^{\infty} \frac{\langle\sigma v\rangle(x)}{x^2} dx. \tag{3.37}$$

The thermally averaged annihilation cross section $\langle\sigma v\rangle$ can be computed by [189]

$$\langle\sigma v\rangle(x) = \frac{x}{8M_{\rm DM}^5 K_2^2(x)}\int_{4M_{\rm DM}^2}^{\infty} \sigma\times(s-4M_{\rm DM}^2)\,\sqrt{s}\,K_1\left(\frac{x\sqrt{s}}{M_{\rm DM}}\right) ds. \tag{3.38}$$

In the above, σ stands for annihilation cross section, s stands for center of mass energy, K_1 and K_2 denote the modified Bessel functions. We have implemented the model in LanHEP package [190] and then extracted the results from micrOMEGAs [191–193].

The parameters that alter DM abundance include the mediator mass i.e., of η and Z', and their couplings with DM particle. Choosing equal values ($\alpha_{\rm DM}$) for the couplings $\alpha_D, \beta_D, \gamma_D$ and $\alpha'_D, \beta'_D, \gamma'_D$, we project the DM relic density as a function of its mass in left panel of Fig. 3.19. The benchmark is suitably chosen, which also meets the DM scattering experiments and stringent ATLAS constraints (to be discussed in the next section). Once kinematically allowed, the annihilation channels (shown in Fig. 3.20) with lepton and anti-lepton pair i.e., $\bar{\ell}\ell, \bar{\nu}\nu$ in the final state in η-portal (t-channel), SM fermion anti-fermion pair i.e., $\bar{q}q, \bar{\ell}\ell, \bar{\nu}\nu$ in Z'-portal (s-channel), contribute to relic density. One can see that the s-channel contribution gives resonance on the either side of $M_{\rm DM} = M_{Z'}/2$ [194]. Furthermore, for the chosen benchmarks with large α_{DM} and small gauge coupling g_{BL}, the t-channel processes in η-portal completely dominate and dictate the shape of the relic density curve. To support this argument, we have plotted the thermally averaged annihilation cross section in dual portals for one of the benchmark values in the right panel of Fig. 3.19.

Moving to detection prospects, the Dirac fermion can scatter off the nucleus via Z' with the effective interaction of the form

$$\mathscr{L}_{\rm SI} \supset \frac{g_{\rm BL}^2}{M_{Z'}^2}(\overline{N_{D1}}\gamma^{\mu}N_{D1})(\overline{q}\gamma_{\mu}q)\,. \tag{3.39}$$

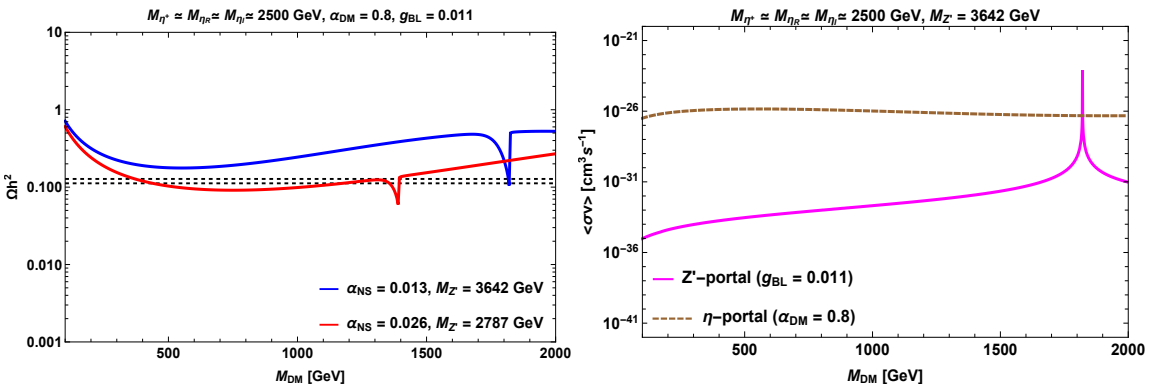

Figure 3.19: Left panel projects the variation of abundance of fermionic DM as a function of its mass for two sets of values assigned to model parameters. Black horizontal dashed lines stand for the 3σ bound of Planck satellite data [40]. Right panel shows the thermally averaged annihilation cross section in dual portals.

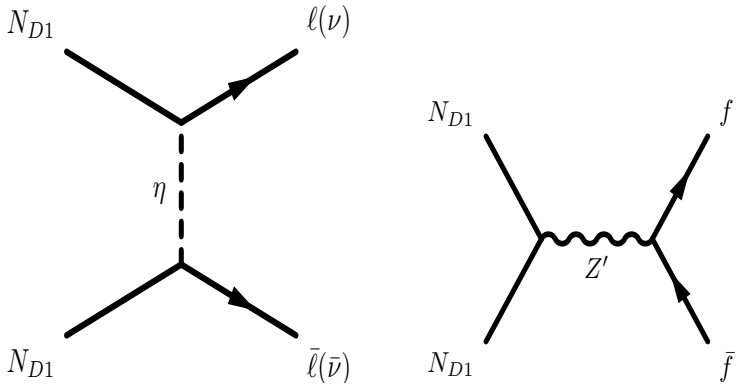

Figure 3.20: Feynman diagrams for t and s-channel annihilation of DM N_{D1}, whose contribution is towards the relic density.

The above interaction provides spin-independent (SI) WIMP-nucleon cross section [195], which is tightly constrained from current stringent upper bound set by PandaX-4T experiment [196].

3.8 Collider studies

For collider studies, we have used CalcHEP [197, 198] to compute the cross section of $pp \to Z' \to ee(\mu\mu)$ as a function Z' mass, projected in the upper panel of Fig. 3.21 for a representative set of values for $g_{\rm BL}$, provided with the bound from ATLAS collaboration [199]. It is clear from the figure that, for $g_{\rm BL} = 0.01$, the region $M_{Z'} < 1.2$ TeV is excluded and for $g_{\rm BL} = 0.03$, the favorable region is $M_{Z'} \gtrsim 3.15$ TeV. For $g_{\rm BL} = 0.1$, the $M_{Z'}$ should be over 4.2 TeV.

We have run a scan over the model parameters displayed in Table. 3.3 that alter the annihilation cross section and in turn the relic density of fermionic dark matter. In the process, no new constraint is obtained

on the Yukawas y_i. The constraint on the gauge parameters obtained from Planck relic density limit upto 3σ is projected in the lower left panel of Fig. 3.21, with the exclusion limits of ATLAS and LEP-II $\left(\frac{M_{Z'}}{g_{BL}} > 6.9 \text{ TeV}\right)$. The favourable region turns out to be below both the exclusion limits. Furthermore, green data points violate the PandaX-4T limit [196], which is made clear from the lower right panel of Fig. 3.21. We notice that there is a parameter region (orange data points) consistent with both Planck [40], PandaX-4T as well as ATLAS dilepton constraints [199].

Parameter	$g_{\mu\tau}$	$\alpha_{\rm DM}$	$M_{Z'}$ [GeV]	$M_{\eta^+}, M_{\eta_R}, M_{\eta_I}$ [GeV]
Range	$0.001-0.1$	$0.1-1$	$500-4000$	2500

Table 3.3: Parameter scan for DM study.

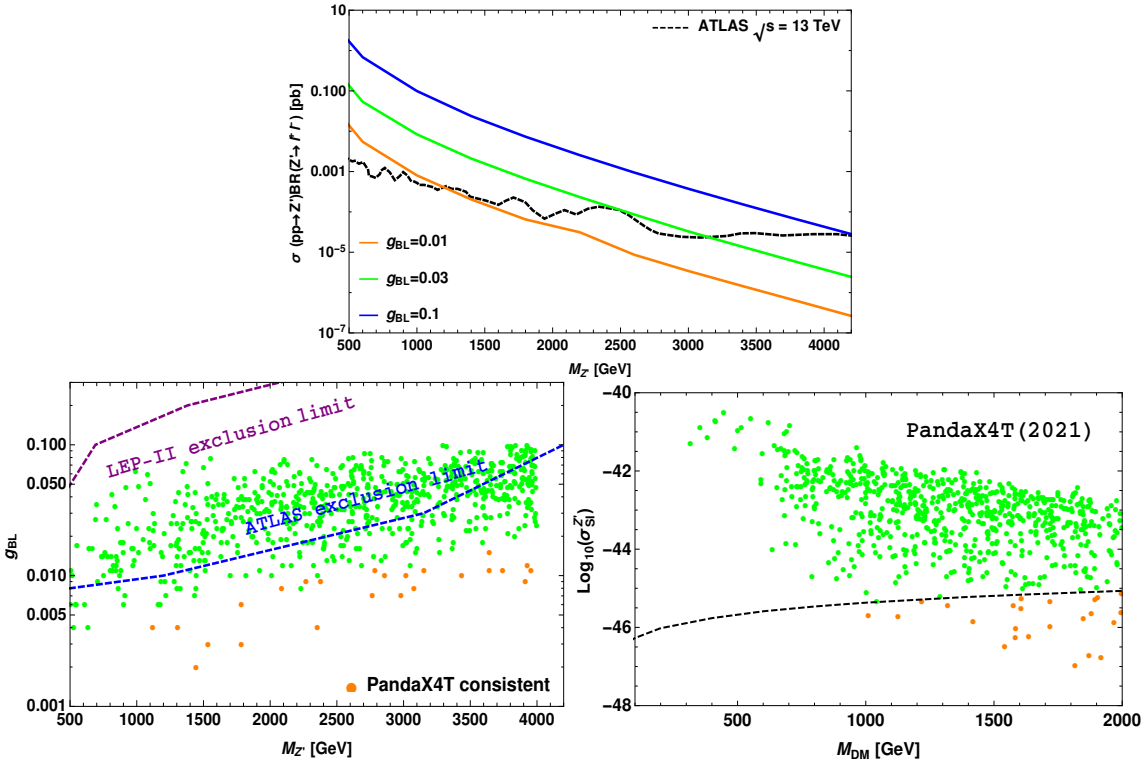

Figure 3.21: Colored lines in the upper panel correspond to the dilepton signal cross section as a function of $M_{Z'}$ for a set of values assigned to $g_{\rm BL}$ and the black dashed line points to ATLAS bound [199]. Lower left panel projects the Planck data consistent gauge parameter space with ATLAS and LEP-II [200] bounds. Lower right panel projects the SI cross section for the parameters corresponding to the lower left panel. Black dashed line stands for the bound from PandaX-4T [196]. Orange data points are consistent with Planck, PandaX-4T and collider constraints.

Moving onto the Z' width, in the regime $M_{Z'} > 2M_{\rm DM}$, the dark matter can contribute to invisible width apart from $\nu\bar{\nu}$ mode. The $B-L$ charge of dark matter comes into act in rescaling this width and the

decay to pair of all other heavy fermions is kinematically forbidden. The precise measurement of invisible width can distinguish the present model from other frameworks.

3.9 Conclusion

The major goal of this research is utilization of scotogenic framework to establish A_4 modular symmetry and explore how it affects neutrino phenomenology. Establishment of neutrino mass at one loop level is made possible by introducing six heavy fermions (N_R and S_L) assigned as triplets under A_4 symmetry and having modular weights of -1 and $+1$ respectively. Alongside an inert scalar is accommodated as a A_4 doublet and modular weight of -2. The charm of A_4 modular symmetry is prominently seen when the Yukawa couplings acquire triplet charge ($\mathbf{Y}$) with modular weight 2, and the scalar couplings for terms involving η as A_4 singlets (λ_η, λ'_η) with weights $4, 8$ respectively. A $B-L$ gauge symmetry i.e. $U(1)_{B-L}$ is also introduced to avoid unwanted Majorana mass terms and a complex scalar singlet ρ is accommodated for breaking of the gauge symmetry so introduced.

Modular symmetry not only prevents the addition of new flavon fields for neutrino phenomenology but also safeguard dark matter stability. A specific flavor structure for the neutrino mass matrix is established along with neutrino mixing. We make use of numerical diagonalization for the neutrino mass matrix and fixed the model parameters in such a way that they remain compatible with present 3σ range of oscillation data both in normal and inverted orderings. Proceeding in this way, we were also able to establish the present model's contribution towards lepton flavor violating decay $\mu \to e\gamma$, conversion compatible with upper bound set by MEG collaboration. We have thoughtfully checked for $\mu \to 3e$ and $\mu - e$ conversion in the nuclei for the present model. Lastly, we looked at the phenomenology of the lightest stable fermion in dark matter. We determined the relic density compatible with Planck data for a certain benchmark of model parameter values using stringent restrictions on Yukawa couplings constraining dark matter mass. According to our findings the annihilations with lepton-anti lepton pair in the final state via η and Z' ($U(1)_{B-L}$ associated) portal contribute to relic density. Tree-level direct detection mediated by η is not possible as η does not couple to quarks directly. While, the Dirac dark matter scatter off the nucleus via Z', providing spin-independent cross section. We have shown the favorable parameter space, consistent with Planck, PandaX-4T, ATLAS dilepton searches and LEP-II. Finally, A_4 modular symmetry stands out, enabling rich neutrino phenomenology while eliminating the flavon fields utilised in traditional frameworks and stabilising dark matter candidates. The current work serves as an example, addressing the aforementioned issues in the context of modular symmetry.

CHAPTER 4

INVERSE SEESAW UNDER A_5' MODULAR SYMMETRY

4.1 Introduction

The results from various neutrino oscillation experiments have unambiguously established the fact that neutrinos posses very small but non-zero masses contradicting their vanishing mass concept presumed in the Standard Model (SM). Therefore, understanding the origin of the neutrino mass necessitates to employ physics beyond the SM. One of the conventional ways to generate the light neutrino masses is through the canonical seesaw mechanism [47, 201–203], where three heavy right handed (RH) neutrinos $\mathcal{N}_{R_i}$ are introduced on top of the SM particle spectrum. The inclusion of right-handed neutrinos not only generates the Dirac mass term but also leads to Majorana mass for $\mathcal{N}_{Ri}$'s, of the form $\overline{\mathcal{N}_{Ri}}\mathcal{N}_{Ri}^c$ which violates the lepton number by two units. The master formula for generating the masses of the active neutrinos is governed by $m_\nu \approx -\mathcal{M}_D\mathcal{M}_R^{-1}\mathcal{M}_D^T$, where $\mathcal{M}_D$ is the Dirac neutrino mass matrix and $\mathcal{M}_R$ being the Majorana neutrino mass matrix of the heavy RH neutrinos, satisfying the relation $\mathcal{M}_D \ll \mathcal{M}_R$. However, myriad literature on seesaw models show work on other extensions like type-II, with the inclusion of a scalar triplet [204–209], type-III [210–215], where a fermion triplet is added to the SM particle content. In these approaches, the masses of the new heavy particles are quite heavy and are beyond the access of the present and future generation experiments.

Many other alternative approaches were proposed, e.g., linear seesaw [19, 86, 87, 117], inverse seesaw [171, 216–221], where the new physics scale responsible for neutrino mass generation can be brought down to TeV scale, at the expense of the inclusion of new additional fermion fields (S_{L_i}), which are SM singlets. The inverse seesaw formalism is implemented by including three additional left-handed (LH)

singlet fermions $\mathscr{S}_{L_i}$ and hence, the basis that involves for the neutrino mass generation is $(\nu_L^c, \mathscr{N}_{R_i}, \mathscr{S}_{L_i})^T$. This leads to the neutrino mass matrix structure as $m_\nu \approx (\mathscr{M}_D/\mathscr{M}_{RS})\,\mathscr{M}_\mu\,(\mathscr{M}_D/\mathscr{M}_{RS})^T$, where $\mathscr{M}_\mu$ is the Majorana mass term for the heavy singlet fermion $\mathscr{S}_{Li}$. For inverse seesaw, the various mass terms satisfy the relation $\mathscr{M}_\mu \ll \mathscr{M}_D < \mathscr{M}_{RS}$, and hence, the neutrino mass is given by $m_\nu \approx \mathscr{M}_D^2 \mathscr{M}_\mu/\mathscr{M}_{RS}^2$. So to get the correct order of the light neutrino masses, the typical values of different mass scales are: $\mathscr{M}_D \sim 10$ GeV, $\mathscr{M}_{RS} \sim 10$ TeV, and $\mathscr{M}_\mu \sim 1$ keV.

Genearally, to implement inverse seesaw certain symmtries are assumed, like discrete flavour symmetries S_3 [222, 223], A_4 [62, 88, 172, 224, 225], S_4 [226–228] etc., to avoid certain unwanted terms in the extended neutrino mass matrix of $(\nu_L^c, \mathscr{N}_{R_i}, \mathscr{S}_{L_i})^T$ basis. However, a number of flavon fields are required for the breaking of these flavor symmetries as well as to accommodate the observed neutrino oscillation data and the vacuum alignment of these flavon fields pose a challenging task. But in recent times, modular symmetry [59, 229–232] has gained pace and is in the limelight. Modular symmetry removes the usage of excess flavon fields, where, the role of flavons is performed by Yukawa couplings, which are holomorphic function of modulus τ. When this modulus acquires the vacuum expectation value (VEV), it breaks the flavor symmetry. Exploration of myriad text shows work on modular groups S_3 [233–235], S_4 [70, 236, 237], A_4 [69, 74, 156, 238–244], A_5 [75, 159], double covering of A_4 [245], double covering of A_5 [158]. These modular groups help to accurately calculate the neutrino oscillation parameters at 3σ level along with other observables.

In this work, we intend to focus on the double covering modular group $\Gamma_5' \simeq A_5'$ and its implications on neutrino phenomenology in the inverse seesaw framework. The inverse seesaw mechanism in the context of A_4 modular symmetry has been explored in Ref. [69]. In the past, quite a few works in the literature have been discussed the significace of finite groups, which comprehend the basic properties of A_5' group [246–248]. The phenomenology of neutrino masses and mixing has been investigated using the double covering modular group $\Gamma_3' \cong T'$ in the canonical seesaw model in Ref. [245], where they have shown that for suitable choice of model parameters, the lepton masses and mixing parameters can be successfully accommodated. The implications of the double covering group $\Gamma_5' \cong A_5'$ on leptonic masses and mixing pattern have been investigated in Ref. [158] in the minimal seesaw scenario. Hence, for the sake of completeness, here we mention only the essential points regarding A_5' modular symmetry group. The A_5' group has 120 elements, which can be constructed by three generators S, T and R, which satisy the identities $S^2 = R$, $(ST)^3 = \mathbb{I}$, $R^2 = \mathbb{I}$ and $RT = TR$ [158]. These 120 elements are categorized into nine conjugacy classes, which classifies them as the nine distinct irreducible representations, symbolized as $\mathbf{1}$, $\widehat{\mathbf{2}}$, $\widehat{\mathbf{2}}'$, $\mathbf{3}$, $\mathbf{3}'$, $\mathbf{4}$, $\widehat{\mathbf{4}}$, $\mathbf{5}$ and $\widehat{\mathbf{6}}$ by their dimensions. Moreover, conjugacy classes and character table of A_5', as well as the representation matrices of all three generators S, T and R in the irreducible representations, are presented in Appendix [158]. It should be noted that the $\mathbf{1}$, $\mathbf{3}$, $\mathbf{3}'$, $\mathbf{4}$ and $\mathbf{5}$ representations with $R = \mathbb{I}$ coincide with those for A_5, whereas $\widehat{\mathbf{2}}$, $\widehat{\mathbf{2}}'$, $\widehat{\mathbf{4}}$ and $\widehat{\mathbf{6}}$ are unique for A_5' with $R = -\mathbb{I}$. As we are working in the

modular space of $\Gamma(5)$, hence, its dimension is $5k+1$, where, k is the modular weight. A brief discussion concerning the modular space of $\Gamma(5)$ is presented in Appendix C.1. For $k=1$, the modular space $M_1[\Gamma(5)]$ will have six basis vectors i.e ($\widehat{e}_i$, where $i=1,2,3,4,5,6$) whose q-expansion are given below and they are used in expressing the Yukawa coupling $Y^{(1)}_{\widehat{\mathbf{6}}}$ as shown in Appendix C.3:

$$\begin{aligned}
\widehat{e}_1 &= 1+3q+4q^2+2q^3+q^4+3q^5+6q^6+4q^7-q^9+\cdots\,,\\
\widehat{e}_2 &= q^{1/5}\left(1+2q+2q^2+q^3+2q^4+2q^5+2q^6+q^7+2q^8+2q^9+\cdots\right),\\
\widehat{e}_3 &= q^{2/5}\left(1+q+q^2+q^3+2q^4+q^6+q^7+2q^8+q^9+\cdots\right),\\
\widehat{e}_4 &= q^{3/5}\left(1+q^2+q^3+q^4-q^5+2q^6+2q^8+q^9+\cdots\right),\\
\widehat{e}_5 &= q^{4/5}\left(1-q+2q^2+2q^6-2q^7+2q^8+q^9+\cdots\right),\\
\widehat{e}_6 &= q\left(1-2q+4q^2-3q^3+q^4+2q^5-2q^6+3q^8-2q^9+\cdots\right). \qquad (4.1)
\end{aligned}$$

Structure of this chapter is as follows. In Sec. 4.2, we discuss the model framework for generating the light neutrino masses using inverse seesaw mechanism with discrete A'_5 modular flavor symmetry. This A'_5 modular symmetry is double covered, hence, there are more number of irreducible representation as compared to A_5 modular symmetry. This helps us to construct charged leptons and neutral lepton mass matrices. In Sec. 4.3, numerical correlational study between the observables of neutrino sector and the model input parameters is established. A brief discussion on the non-unitarity effect is presented in Sec. 4.4. In addition, lepton flavor violation (LFV) in the context of the present model is presented in Sec. 4.5 and collider bound on the mass of new gauge boson Z' is provided in section 4.6. Finally, in Sec. 4.7, we conclude our results.

4.2 Model Framework

We consider a scenario in which inverse seesaw is implemented in the context of supersymmetry (SUSY) to study the neutrino phenomenology, where the SM is extended with a discrete A'_5 modular symmetry. An additional local $U(1)_{B-L}$ symmetry is added to prohibit certain undesirable terms in the superpotential. The SM particle spectrum is supplemented with three extra RH singlet fermion superfields ($\mathscr{N}_{R_i}$), three LH singlet fermion superfields ($\mathscr{S}_{L_i}$) and one weighton (ζ). The added fermion superfields of the model transform as $3'$ under the A'_5 modular group, whereas, the $U(1)_{B-L}$ charges assigned to them are -1 ($\mathscr{N}_{R_i}$) and 0 ($\mathscr{S}_{L_i}$). Also RH neutrinos are assigned modular weight 6 and LH neutrinos with 0. The particle content and their charges under various groups are provided in Table 4.1. The A'_5 and $U(1)_{B-L}$ symmetries are considered to be broken at a scale much higher than the electroweak symmetry breaking [89]. The $U(1)_{B-L}$ symmetry is spontaneously broken by assigning non-zero vacuum expectation value (VEV) to the singlet weighton ζ, and consequently the additional singlet fermion superfields acquire their masses. The Z' boson associated with $U(1)_{B-L}$ acquires its mass by the singlet VEV v_ζ, and we will show that its mass

and gauge coupling satisfy the present experimental bounds in section 4.6. In addition to above, several higher order Yukawa couplings are introduced which obey the rule: $k_Y = k_{I_1} + k_{I_2} + \cdots + k_{I_n}$, where k_Y is the weight on the Yukawa couplings and $k_{I_i} (i = 1,2,3,4\cdots)$ are the weights on the superfields. These higher order Yukawa couplings implicitly depend on $Y^{(1)}_{\widehat{\mathbf{6}}}$ whose complete forms are shown in Appendix C.3.

Fields	e_R	μ_R	τ_R	$\overline{L}_L$	$\mathcal{N}_R$	$\mathcal{S}_L$	$\mathcal{H}_{u,d}$	ζ
$SU(2)_L$	1	1	1	2	1	1	2	1
$U(1)_Y$	-1	-1	-1	$\frac{1}{2}$	0	0	$-\frac{1}{2}, \frac{1}{2}$	0
A_5'	1	1	1	3	$3'$	$3'$	1	1
$U(1)_{B-L}$	-1	-1	-1	1	-1	0	0	1
k_I	2	4	6	0	6	0	0	0

Table 4.1: Particle content of the model and their charges under $SU(2)_L \times U(1)_Y \times A_5' \times U_{B-L}$ group and their modular weights k_I.

The superpotential of the model is given by

$$\begin{aligned} \mathcal{W} &= A_{\mathcal{M}_l}\left[(\overline{L}_l l_R))_{\mathbf{3}} Y^{k_I}_{\mathbf{3}}\right]\mathcal{H}_d + \mu \mathcal{H}_u \mathcal{H}_d + G_D\left[(\overline{L}_L \mathcal{N}_R))_{\mathbf{4}} \sum_{i=1}^{2} Y^{(6)}_{\mathbf{4},i}\right]\mathcal{H}_u \\ &+ B_{\mathcal{M}_{RS}}\left[(\overline{\mathcal{S}}_L \mathcal{N}_R)_{\mathbf{5}} \sum_{i=1}^{2} Y^{(6)}_{\mathbf{5},i}\right]\zeta + \mu_0 \overline{\mathcal{S}^C_L}\mathcal{S}_L\,, \end{aligned} \tag{4.2}$$

where, $A_{\mathcal{M}_l}, G_D$ and $B_{\mathcal{M}_{RS}}$ are 3×3 diagonal matrices given as $A_{\mathcal{M}_l} = \mathrm{diag}\left(\alpha_{\mathcal{M}_l}, \beta_{\mathcal{M}_l}, \gamma_{\mathcal{M}_l}\right)$, $G_D = \mathrm{d}iag\left(g_{D_1}, g_{D_2}, g_{D_3}\right)$, and $B_{\mathcal{M}_{RS}} = \mathrm{d}iag\left(\alpha_{RS_1}, \alpha_{RS_2}, \alpha_{RS_3}\right)$, characterizing the coupling strengths of various interaction terms. The modular weight k_I in the first term takes the values $k_I = (2,4,6)$ for $l = (e,\mu,\tau)$.

4.2.1 Dirac mass term for charged leptons

To establish charged leptons mass matrix, the left-handed doublet superfields i.e., $\overline{L}_L$, transform as triplets under the A_5' symmetry with $B-L$ charge -1. The Higgsinos $\mathcal{H}_{u,d}$ are given charges 0, 1 under the U_{B-L} and A_5' symmetries respectively with zero modular weight. The VEVs of these Higgsinos $\mathcal{H}_u$ and $\mathcal{H}_d$ are given as $v_u/\sqrt{2}$ and $v_d/\sqrt{2}$ respectively. Moreover, Higgsino VEVs are associated to SM Higgs VEV as $v_H = \frac{1}{2}\sqrt{v_u^2 + v_d^2}$ and the ratio of their VEVs is expressed as $\tan\beta = (v_u/v_d) = 5$. Hence, the relevant superpotential term for charged leptons is given as

$$\mathcal{W}_{\mathcal{M}_l} = \alpha_{\mathcal{M}_l}\left[(\overline{L_L} e_R)_{\mathbf{3}} Y^{(2)}_{\mathbf{3}}\right]\mathcal{H}_d + \beta_{\mathcal{M}_l}\left[(\overline{L_L}\mu_R)_{\mathbf{3}} Y^{(4)}_{\mathbf{3}}\right]\mathcal{H}_d + \gamma_{\mathcal{M}_l}\left[(\overline{L_L}\tau_R)_{\mathbf{3}}\left\{\sum_{i=1}^{2} Y^{(6)}_{\mathbf{3},i}\right\}\right]\mathcal{H}_d\,. \tag{4.3}$$

After the spontaneous symmetry breaking, it is evident that the charged lepton mass matrix isn't diagonal and is expressed as

$$\mathscr{M}_l = \frac{v_d}{\sqrt{6}} \begin{bmatrix} \left(Y^{(2)}_{\mathbf{3}}\right)_1 & \left(Y^{(4)}_{\mathbf{3}}\right)_1 & \left(\sum_{i=1}^{2} Y^{(6)}_{\mathbf{3},i}\right)_1 \\ \left(Y^{(2)}_{\mathbf{3}}\right)_3 & \left(Y^{(4)}_{\mathbf{3}}\right)_3 & \left(\sum_{i=1}^{2} Y^{(6)}_{\mathbf{3},i}\right)_3 \\ \left(Y^{(2)}_{\mathbf{3}}\right)_2 & \left(Y^{(4)}_{\mathbf{3}}\right)_2 & \left(\sum_{i=1}^{2} Y^{(6)}_{\mathbf{3},i}\right)_2 \end{bmatrix}_{LR} \cdot \begin{bmatrix} \alpha_{\mathscr{M}_l} & 0 & 0 \\ 0 & \beta_{\mathscr{M}_l} & 0 \\ 0 & 0 & \gamma_{\mathscr{M}_l} \end{bmatrix} . \tag{4.4}$$

The charged lepton mass matrix $\mathscr{M}_l$ can be diagonalised by the unitary matrix U_l, giving rise to the physical masses of e, μ and τ as

$$U_l^{\dagger} \mathscr{M}_l \mathscr{M}_l^{\dagger} U_l = \text{diag}(m_e^2, m_\mu^2, m_\tau^2) \,. \tag{4.5}$$

In addition, it also satisfies the following identities, which will be used for numerical analysis in section 4.3:

$$\begin{aligned} \text{Tr}\left(\mathscr{M}_l \mathscr{M}_l^{\dagger}\right) &= m_e^2 + m_\mu^2 + m_\tau^2 \,, \\ \text{Det}\left(\mathscr{M}_l \mathscr{M}_l^{\dagger}\right) &= m_e^2 m_\mu^2 m_\tau^2 \,, \\ \frac{1}{2}\left[\text{Tr}\left(\mathscr{M}_l \mathscr{M}_l^{\dagger}\right)\right]^2 - \frac{1}{2}\text{Tr}\left[(\mathscr{M}_l \mathscr{M}_l^{\dagger})^2\right] &= m_e^2 m_\mu^2 + m_\mu^2 m_\tau^2 + m_\tau^2 m_e^2 \,. \end{aligned} \tag{4.6}$$

4.2.2 Dirac mass term for neutrinos

The right-handed neutrino superfields $\mathscr{N}_{R_i}$ are $3'$ under A_5' modular group with a $B-L$ charge of -1 and modular weight 6. Therefore, the invariant superpotential, describing the Dirac mass term for the neutrinos can be written as,

$$\mathscr{W}_D = G_D \left[(\overline{L}_L \, \mathscr{N}_R)_{\mathbf{4}} \sum_{i=1}^{2} Y^{(6)}_{\mathbf{4},i} \right] \mathscr{H}_u \,. \tag{4.7}$$

Here, the subscript for the operator $\overline{L}_L \mathscr{N}_R$ indicates A_5' representation constructed by the Kronecker product rule (see Appendix C.2) which further leads in obtaining a invariant superpotential. The resulting Dirac neutrino mass matrix is found to be

$$\mathscr{M}_D = \frac{v_u}{2\sqrt{6}} \begin{bmatrix} 0 & -\sqrt{2}\left(\sum_{i=1}^{2} Y^{(6)}_{\mathbf{4},i}\right)_3 & -\sqrt{2}\left(\sum_{i=1}^{2} Y^{(6)}_{\mathbf{4},i}\right)_2 \\ \sqrt{2}\left(\sum_{i=1}^{2} Y^{(6)}_{\mathbf{4},i}\right)_4 & \left(\sum_{i=1}^{2} Y^{(6)}_{\mathbf{4},i}\right)_2 & -\sqrt{2}\left(\sum_{i=1}^{2} Y^{(6)}_{\mathbf{4},i}\right)_1 \\ \sqrt{2}\left(\sum_{i=1}^{2} Y^{(6)}_{\mathbf{4},i}\right)_1 & \left(\sum_{i=1}^{2} Y^{(6)}_{\mathbf{4},i}\right)_4 & -\left(\sum_{i=1}^{2} Y^{(6)}_{\mathbf{4},i}\right)_3 \end{bmatrix}_{LR} \cdot \begin{bmatrix} g_{D_1} & 0 & 0 \\ 0 & g_{D_2} & 0 \\ 0 & 0 & g_{D_3} \end{bmatrix} , \tag{4.8}$$

where $(g_{D_1}, g_{D_2}, g_{D_3})$ are the free parameters of the diagonal matrix G_D.

4.2.3 Mixing between the heavy fermions $\mathcal{N}_R$ and $\mathcal{S}_L$

The mixing between heavy fermion superfields $\mathcal{N}_R$ and $\mathcal{S}_L$ can be expressed as follows,

$$\mathcal{W}_{\mathcal{M}_{RS}} = B_{\mathcal{M}_{RS}}\left[(\overline{\mathcal{S}}_L\mathcal{N}_R)_{\mathbf{5}}\sum_{i=1}^{2}Y^{(6)}_{\mathbf{5},i}\right]\zeta \tag{4.9}$$

where, the choice of Yukawa coupling depends on the sum of the modular weight of the superfields and the Kronecker product rule as given in Appendix C.2. Using $\langle\zeta\rangle = v_\zeta/\sqrt{2}$, the resulting mass matrix is found to be

$$\mathcal{M}_{RS} = \frac{v_\zeta}{2\sqrt{15}}\begin{bmatrix} 2\left(\sum_{i=1}^{2}Y^{(6)}_{\mathbf{5,i}}\right)_1 & -\sqrt{3}\left(\sum_{i=1}^{2}Y^{(6)}_{\mathbf{5,i}}\right)_4 & -\sqrt{3}\left(\sum_{i=1}^{2}Y^{(6)}_{\mathbf{5,i}}\right)_3 \\ -\sqrt{3}\left(\sum_{i=1}^{2}Y^{(6)}_{\mathbf{5,i}}\right)_4 & -\sqrt{6}\left(\sum_{i=1}^{2}Y^{(6)}_{\mathbf{5,i}}\right)_2 & -\left(\sum_{i=1}^{2}Y^{(6)}_{\mathbf{5,i}}\right)_1 \\ -\sqrt{3}\left(\sum_{i=1}^{2}Y^{(6)}_{\mathbf{5,i}}\right)_3 & -\left(\sum_{i=1}^{2}Y^{(6)}_{\mathbf{5,i}}\right)_1 & -\sqrt{6}\left(\sum_{i=1}^{2}Y^{(6)}_{\mathbf{5,i}}\right)_5 \end{bmatrix}_{LR}\cdot\begin{bmatrix}\alpha_{RS_1} & 0 & 0\\ 0 & \alpha_{RS_2} & 0\\ 0 & 0 & \alpha_{RS_3}\end{bmatrix}, \tag{4.10}$$

where $(\alpha_{RS_1},\alpha_{RS_2},\alpha_{RS_3})$ are the free paramaters of the diagonal matrix $B_{\mathcal{M}_{RS}}$.

4.2.4 Majorana mass term for $\mathcal{S}_L$

Under A_5' singlet heavy fermions $\mathcal{S}_L$ transform as triplet $3'$ having zero modular weight. Hence, its Majorana mass term can be written as,

$$\mathcal{W}_\mu = \mu_0\mathcal{S}_L\mathcal{S}_L, \tag{4.11}$$

leading to the mass matrix ($\mathcal{M}_\mu$) of the form

$$\mathcal{M}_\mu = \mu_0\begin{bmatrix}1 & 0 & 0\\ 0 & 0 & 1\\ 0 & 1 & 0\end{bmatrix}. \tag{4.12}$$

4.2.5 Inverse Seesaw mechanism for light neutrino Masses

In the present model constructed using A_5' modular symmetry, the complete 9×9 neutral fermion mass matrix in the flavor basis of $\left(\nu_L,\mathcal{N}_R,\mathcal{S}_L^c\right)^T$ is given as

$$\mathbb{M} = \left(\begin{array}{c|ccc} & \nu_L & \mathcal{N}_R & \mathcal{S}_L^c \\ \hline \nu_L & 0 & \mathcal{M}_D & 0 \\ \mathcal{N}_R & \mathcal{M}_D^T & 0 & \mathcal{M}_{RS} \\ \mathcal{S}_L^c & 0 & \mathcal{M}_{RS}^T & \mathcal{M}_\mu \end{array}\right). \tag{4.13}$$

In the limit $\mathscr{M}_\mu \ll \mathscr{M}_D < \mathscr{M}_{RS}$, the above mass matrix (4.13) provides the inverse seesaw mass formula for the light neutrinos as

$$m_\nu \;=\; \mathscr{M}_D\, \mathscr{M}_{RS}^{-1}\, \mathscr{M}_\mu\, (\mathscr{M}_{RS}^{-1})^T\, (\mathscr{M}_D)^T . \tag{4.14}$$

Thus, diagonalization of the light neutrino mass matrix (4.14) yields the masses of the active neutrinos. Apart from determining the small neutrino masses, other observables, which are of great use, are the Jarlskog invariant (J_{CP}) and the effective neutrino mass $\langle m_{ee}\rangle$ describing the neutrinoless double beta decay. These observables related to the mixing angles and phases of PMNS matrix through

$$J_{CP} = \mathrm{Im}[U_{e1}U_{\mu 2}U_{e2}^* U_{\mu 1}^*] = s_{23}c_{23}s_{12}c_{12}s_{13}c_{13}^2 \sin\delta_{CP}\,, \tag{4.15}$$

$$\langle m_{ee}\rangle = |m_{\nu_1}\cos^2\theta_{12}\cos^2\theta_{13} + m_{\nu_2}\sin^2\theta_{12}\cos^2\theta_{13}e^{i\alpha_{21}} + m_{\nu_3}\sin^2\theta_{13}e^{i(\alpha_{31}-2\delta_{CP})}|. \tag{4.16}$$

The effective Majorana mass parameter $\langle m_{ee}\rangle$ is expected to have improved sensitivity measured by KamLAND-Zen experiment in coming future [97].

4.3 Numerical Analysis

Numerical analysis is performed by considering experimental data at 3σ interval [173] as follows:

$$\begin{aligned} &\mathrm{NO}: \Delta m^2_{\mathrm{atm}} = [2.47, 2.63]\times 10^{-3}\ \mathrm{eV}^2,\ \Delta m^2_{\mathrm{sol}} = [6.94, 8.14]\times 10^{-5}\ \mathrm{eV}^2, \\ &\sin^2\theta_{13} = [0.0200, 0.02405],\ \sin^2\theta_{23} = [0.434, 0.610],\ \sin^2\theta_{12} = [0.271, 0.369]\,. \end{aligned} \tag{4.17}$$

Here, numerical diagonalization of the light neutrino mass matrix as given in eqn.(4.14) is done through $U_\nu^\dagger \mathscr{M} U_\nu = \mathrm{diag}(m_1^2, m_2^2, m_3^2)$, where $\mathscr{M} = m_\nu m_\nu^\dagger$ and U_ν is an unitary matrix. Thus, the lepton mixing matrix is given as $U = U_l^\dagger U_\nu$, from which the neutrino mixing angles can be extracted using the standard relations:

$$\sin^2\theta_{13} = |U_{13}|^2\,, \quad \sin^2\theta_{12} = \frac{|U_{12}|^2}{1-|U_{13}|^2}\,, \quad \sin^2\theta_{23} = \frac{|U_{23}|^2}{1-|U_{13}|^2}\,. \tag{4.18}$$

In order to demonstrate the current neutrino oscillation data, the values of model parameters are chosen to be in the following ranges:

$$\begin{aligned} &\mathrm{Re}[\tau]\in[0,0.5],\ \ \mathrm{Im}[\tau]\in[0.5,2],\ \ \{g_{D_1}, g_{D_2}, g_{D_3}\}\in\ [10^{-4}, 10^{-1}]\,, \\ &\{\alpha_{RS_1}, \alpha_{RS_2}, \alpha_{RS_3}\}\in[0.1,1], \quad v_\zeta \in [10,100]\ \mathrm{TeV}\,. \end{aligned} \tag{4.19}$$

For diagonalizing the charged lepton mass matrix $\mathscr{M}_l$ eqn.(4.4), we use the values of the free parameters as: $\alpha_{\mathscr{M}_l} \approx \mathscr{O}(10^{-6})$, $\beta_{\mathscr{M}_l} \approx \mathscr{O}(10^{-2})$ and $\gamma_{\mathscr{M}_l} \approx \mathscr{O}(10^{-4})$, and scanning over the allowed ranges of real and imaginary parts of the modulus τ, i.e., $0 \lesssim \mathrm{Re}[\tau] \lesssim 0.5$ and $0.5 \lesssim \mathrm{Im}[\tau] \lesssim 2$, we numerically obtain the diagonalizing matrix U_l, that gives the charged-lepton masses as $m_e = 0.511$ MeV, $m_\mu = 105.66$ MeV, $m_\tau = 1776.86$ MeV.

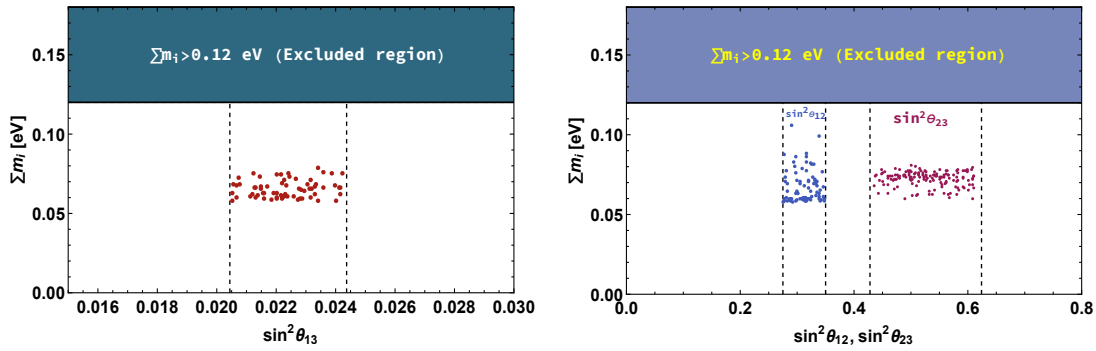

Figure 4.1: Left (right) panel signify the correlation of the mixing angles i.e. $\sin^2\theta_{13}$ ($\sin^2\theta_{12}$, $\sin^2\theta_{23}$) respectively with the sum of neutrino masses $\sum m_i$ (eV).

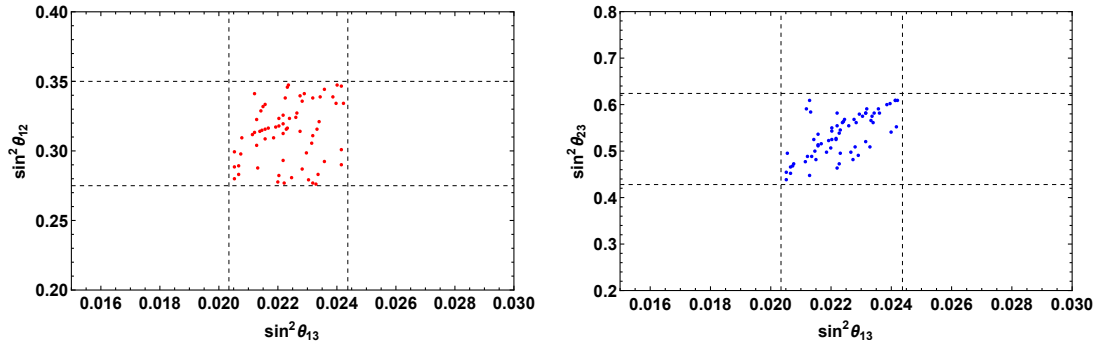

Figure 4.2: Left (right) panel signify the correlation of the mixing angles i.e. $\sin^2\theta_{13}$ ($\sin^2\theta_{12}$, $\sin^2\theta_{23}$) respectively with the sum of neutrino masses $\sum m_i$ (eV).

In order to make appropriate predictions of the neutrino mixing angles and other parameters within their 3σ ranges, the input parameters are generated in a random fashion. The allowed ranges of solar and atmospheric mass squared differences at 3σ level used as constraints to calculate other neutrino oscillation parameters in their 3σ ranges [173]. Here, we have kept the range of modulus τ as: $0 \lesssim \text{Re}[\tau] \lesssim 0.5$ and $0.5 \lesssim \text{Im}[\tau] \lesssim 2$ and also the estimated range for $\mu_0 \in [10^{-5}, 10]$ keV for obtaining the neutrino masses in normal ordering (NO). With these values, the neutrino mixing angles are then extracted using eqn. (4.18). The variation of the mixing angles $\sin^2\theta_{13}$ (left panel) and $\sin^2\theta_{12}$, $\sin^2\theta_{23}$ (right panel) w.r.t sum of the active neutrino mass $\sum m_i < 0.12$ eV [40] are shown in Fig. 4.2. From these plots, it can be inferred that the allowed range of the sum of active neutrino masses to be in the range $(0.058 - 0.1)$ eV. Further, the variation of δ_{CP} with respect to mixing angles $\sin^2\theta_{13}$ (left panel) and $\sin^2\theta_{12}$, $\sin^2\theta_{23}$ (right panel) is shown in Fig. 4.3, where the vertical dashed lines represent the in 3σ ranges of the mixing angles. These plots suggest δ_{CP} should be in the range $(100 - 250)^\circ$. Fig. 4.4 focuses on the correlation between the Majorana phases i.e., α_{21} and α_{31}, and they are seen to be unconstrained and lie within the range of $(0 - 360)^\circ$. The left panel of Fig. 4.5, signifies the correlation between the effective neutrinoless double beta

decay mass parameter (m_{ee}) and the lightest neutrino mass m_1 as well as with the sum of active neutrino masses ($\sum m_i$). It can be inferred from the plot that the model predicts the lightest neutrino mass m_1 to be less that 0.015 eV and m_{ee} to be in the range $(0.001 - 0.025)$ eV, satisfying the current upper limits from KamLAND-ZEN experiment [97]. In the right panel of Fig. 4.5, we show the correlation of Jarsklog CP invariant allowed by the neutrino data, with the reactor mixing angle, which is found to be of the order of $\mathcal{O}(10^{-3})$. In Fig. 4.6, we represent the correlations between the heavy fermion masses, where, left panel is the plot expressing M_1 with M_2 while the right panel is for M_2 versus M_3 in TeV scale.

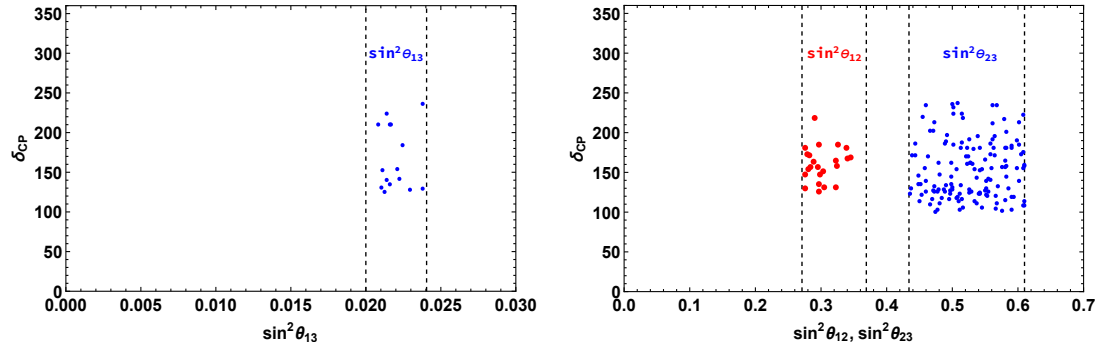

Figure 4.3: Left (right) panel displays the correlation between δ_{CP} w.r.t $sin^2\theta_{13}$ ($sin^2\theta_{12}$ and $sin^2\theta_{23}$).

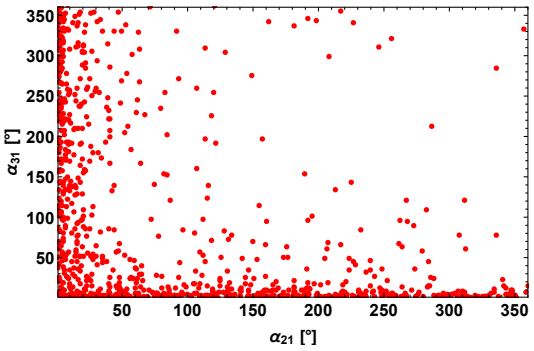

Figure 4.4: The above panel shows the plot between the Majorana phases i.e., α_{21} and α_{31}.

4.4 Comments on non-unitarity

In the section, we briefly comment on non-unitarity of neutrino mixing matrix U'_{PMNS} which basically arises due to the mixing between the active neutrinos and the heavy neutral fermions. The form for the deviation from unitarity is expressed as follows [99]

$$U'_{\text{PMNS}} \equiv \left(1 - \frac{1}{2}\mathscr{F}\mathscr{F}^{\dagger}\right) U_{\text{PMNS}} \,. \tag{4.20}$$

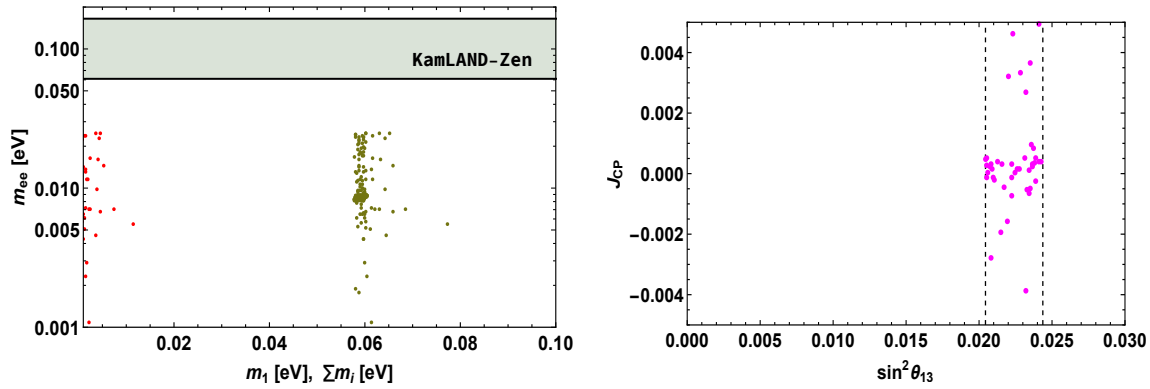

Figure 4.5: Left panel shows the correlation of effective neutrino mass of neutrinoless double beta decay with the lightest neutrino mass m_1 (red points) and sum of active neutrino masses (dark green points). The right panel represents a correlation between J_{CP} with respect to the reactor mixing angle.

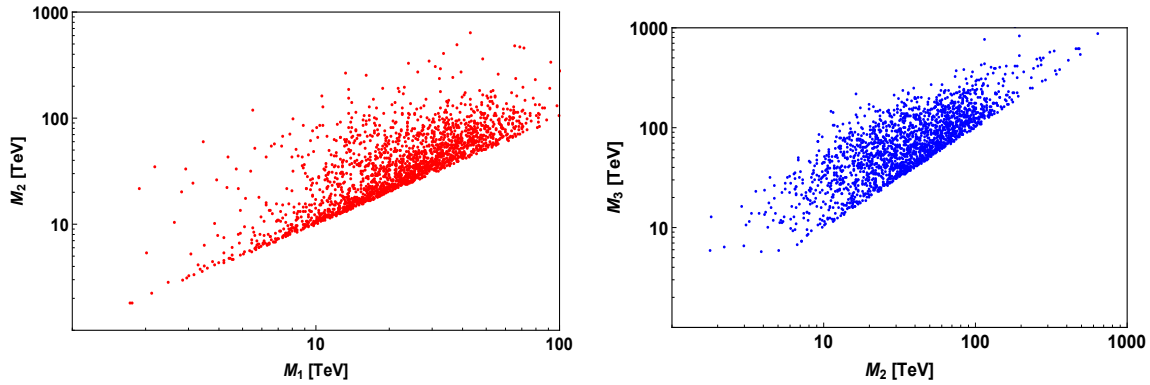

Figure 4.6: Left panel shows the correlation of heavy fermion masses M_1 versus M_2 and right panel represents a correlation of heavy fermion masses M_2 versus M_3 in TeV scale.

Here, U_{PMNS} is the PMNS mixing matrix, used in diagonalising the mass matrix of the three light neutrinos and $\mathscr{F}$ represents the mixing of active neutrinos with the heavy fermions and its form is given by

$$\mathscr{F} \equiv (\mathscr{M}_{RS}^{T})^{-1}\mathscr{M}_D \approx (g_D v_u/\alpha_{RS} v_\zeta)\,, \tag{4.21}$$

which is hermitian in nature. The global constraints on the non-unitarity parameters [100–102], come from several experimental results such as the W boson mass M_W, the Weinberg angle θ_W, several ratios of fermionic Z boson decays as well as its invisible decay, electroweak universality, CKM unitarity bounds, and lepton flavor violations. As mentioned earlier, in the inverse seesaw framework, the light neutrino mass matrix eqn.(4.14) can be expressed as

$$m_\nu = \left(\frac{\mathscr{M}_D}{\mathscr{M}_{RS}}\right)\mathscr{M}_\mu\left(\frac{\mathscr{M}_D}{\mathscr{M}_{RS}}\right)^{T}. \tag{4.22}$$

Thus, in the context of the present model, we consider the following approximated mass values for the Dirac, Majorana mass for $\mathscr{S}_L$ and the pseudo-Dirac mass for the heavy fermions to correctly generate the observed mass square differences of the desired order as:

$$\left(\frac{m_\nu}{0.1\text{ eV}}\right) \approx \left(\frac{\mathscr{M}_D}{10^2\text{ GeV}}\right)^2 \left(\frac{\mathscr{M}_\mu}{\text{keV}}\right)\left(\frac{10^4\text{ GeV}}{\mathscr{M}_{RS}}\right)^2 . \tag{4.23}$$

With these benchmark values and using eqn.(4.21), we obtain the approximated non-unitary mixing for the present model as given below:

$$|\mathscr{F}\mathscr{F}^\dagger| \leq \begin{bmatrix} 1.1\times10^{-5} & 8.3\times10^{-7} & 3.8\times10^{-6} \\ 8.3\times10^{-7} & 9.5\times10^{-8} & 5.02\times10^{-7} \\ 3.8\times10^{-6} & 5.02\times10^{-7} & 3.05\times10^{-7} \end{bmatrix} . \tag{4.24}$$

4.5 Comments on LFV

Lepton flavour violation is one of the most fascinating probes for new physics beyond the SM, therefore, here we investigate decay mode $\mu \to e\gamma$. Several experiments are looking for this decay mode with great effort for an improved sensitivity, and the current limit on its branching ratio is from MEG collaboration as $\text{Br}(\mu \to e\gamma) < 4.2\times10^{-13}$ [103]. There is a sizeable contribution in the present model using the A_5' inverse seesaw mechanism, due to the allowed light-heavy neutrino mixing. The branching ratio for the $\mu \to e\gamma$ in our model framework is given by

$$\text{Br}(\mu \to e\gamma) = \frac{3}{16}\left(\frac{\alpha}{2\pi}\right)\sum_{i=1}^{3} f\left(\mathscr{M}_i^2/\mathscr{M}_W^2\right)\left|\mathscr{F}_{\mu i}^*\,\mathscr{F}_{ei}\right|^2 . \tag{4.25}$$

Here, $\mathscr{M}_i$ represents the heavy fermion masses and $f(\mathscr{M}_i^2/\mathscr{M}_W^2)$ is the loop-function [249] and $\mathscr{F}_{ai}$ are the non-unitary parameters defined in eqn (4.21).

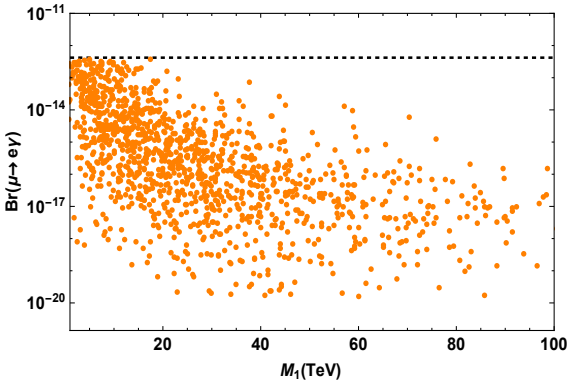

Figure 4.7: Plot above represents the correlation between $\text{Br}(\mu \to e\gamma)$ with respect to (lightest heavy fermion) M_1.

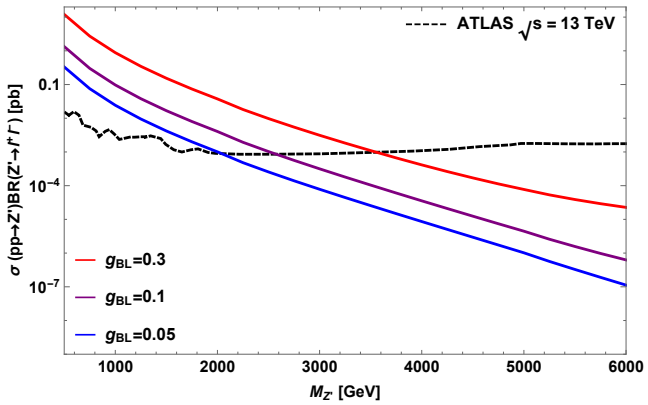

Figure 4.8: The colored lines represent the dilepton signal cross sections for $pp \to Z' \to ee(\mu\mu)$ as a function of $M_{Z'}$ for a representative set of g_{BL} values and the black dashed line symbolizes the ATLAS bound [199].

The branching ratio plot for the lepton flavor violating decay $\mu \to e\gamma$ is presented against lightest heavy fermion mixing mass M_1 in Fig. 4.7. From the figure, it is evident that the predicted branching ratio is well below the current upper limit mentioned above.

4.6 Collider Bound on Z' mass

As discussed earlier in Sec 4.2, the $U(1)_{B-L}$ gauge symmetry is spontaneously broken by assigning the vacuum expectation value v_ζ to the singlet scalar ζ. Consequently, the neutral gauge boson Z' associated with this symmetry becomes massive by absorbing the massless pseudoscalar component of ζ and its mass is given as

$$M_{Z'} = g_{BL} v_\zeta \,, \tag{4.26}$$

where g_{BL} is the gauge coupling constant of $U(1)_{B-L}$. The LEP-II provides the constraint on the ratio of mass of Z' boson to its coupling as $M_{Z'}/g_{BL} > 6.9$ TeV [250]. Hence, in this work we have considered the range of the v_ζ as [10-100] TeV eqn.(4.19), consistent with the LEP-II bound.

The ATLAS and CMS collaborations have performed extensive searches for the new resonances in both dilepton and dijet channels. In the absence of any excess events over the SM background, they put lower bounds on the mass of Z' boson. These bounds are usually limited to a specific model, and typically the experiments report their results assuming simplified models, like the Sequential Standard Model (SSM) or GUT-inspired E_6 models.

Recent results from ATLAS [199], provide the lower limits on the Z' mass from the dilepton search using Run 2 data, collected with the center of mass energy $\sqrt{s} = 13$ TeV. In this work, we use CalcHEP [197] to compute the production cross section of Z', i.e., $pp \to Z' \to ee(\mu\mu)$. In Fig. 4.8, we show the Z' production cross section times the branching fraction of Z' decaying to dilepton $(ee, \mu\mu)$ signal as a function

of $M_{Z'}$, for some representative values of the gauge coupling $g_{BL} = 0.05, 0.1, 0.3$. The black dashed line denotes the dilepton bound from ATLAS [199]. It can be noticed from the figure that the region below $M_{Z'} \simeq 3.6$ TeV is excluded for $g_{BL} = 0.3$. For $g_{BL} = 0.1$, $M_{Z'} < 2.6$ TeV is ruled out and the mass region of $M_{Z'} > 2.1$ TeV is allowed for $g_{BL} = 0.05$. Thus, one can generalize these observations as the lower limits on $M_{Z'}$ increases with the increase of the gauge couplings.

4.7 Conclusion

In the context of the inverse seesaw framework, we studied the consequences of modular A_5' flavour symmetry on neutrino phenomenology. To account for the inverse seesaw process, the present model comprises three right-handed and three left-handed heavy neutral fermions. The singlet scalar ζ is crucial in breaking the $U(1)_{B-L}$ symmetry spontaneously and providing masses to the heavy fermions. We have considered higher order Yukawa couplings that follow the rule $k_Y = k_{I_1} + k_{I_2} + \cdots + k_{I_n}$, where k_Y is the weight on the Yukawa coupling and $k_{I_i} (i = 1, 2, 3, 4 \cdots)$ are the weights on the superfields under A_5' symmetry. Due to this we were able to attain a specific flavor structure for neutrino mass matrix as needed by the inverse seesaw formalism. Moving on, we numerically diagonalize the mass matrix and obtain a valid model parameter-space that allows us to produce results that are compatible with the 3σ limit of oscillation data for normal ordering. Furthermore, our model predictions suggests that the CP violating phase δ_{CP} to be in the range of $(100^\circ - 250^\circ)$, whereas the Majorana phases remain unconstrained. The sum of active neutrino masses is found to be in the range $0.058 \text{ eV} \leq \Sigma m_i \leq 0.1$ eV and the mass of the light neutrino mass as $m_1 \leq 0.015$ eV. We also determined the effective neutrinoless double beta decay mass parameter m_{ee} as $(0.001 - 0.025)$ eV, which is significantly lower than the existing maximum limits from KamLAND-Zen experiment i.e., $< (61 - 165)$ meV. We also looked at the lepton flavour violating decay mode $\mu \to e\gamma$ discovered that its predicted branching ratio is substantially below the current experimental upper limit 4.2×10^{-13}. Furthermore, we demonstrated that the mass of the new neutral Z' gauge boson associated with $U(1)_{B-L}$ symmetry is within the present experimental collider bounds.

CHAPTER 5

LINEAR SEESAW IN A_5' MODULAR SYMMETRY WITH LEPTOGENESIS

5.1 Introduction

There are several unsolved knots in the realm of particle physics, e.g., the baryon asymmetry of the Universe, the dark matter content, the origin of neutrino masses and mixing, etc., and the understanding of these issues is one of the prime objectives of the present day research. In the last couple of decades, several diligent attempts have been made towards comprehending and resolving the issue of dynamical origin of the fermion masses and their mixing. Present scenario has taken us few steps ahead in terms of getting a convincing explanation of the origin of mass through Higgs mechanism while being within the domain of Standard Model (SM). However, it does not provide proper grounds to explain the origin of the observed neutrino masses and their mixing. Rather, very diverse approaches are made in order to gain an insightful resolution towards the above existing problems, and obviously the answer lies in going beyond standard model (BSM) physics. It should be emphasized that, certain well-defined patterns are observed in quark masses and mixing, the appreciation of which is still an enigma. Nonetheless, there are ample amount of research work present, which make an attempt to grasp their fundamental origin. In addition, perplexity to the problem has increased due to the observation of the neutrino masses and their sizeable mixing. The reason being, the order of magnitude of the observed neutrino masses are approximately twelve order smaller than that of electroweak (EW) scale. Also, there is immense difference in the pattern of leptonic and quark mixings, the former is having large mixing angles, while the later involves smaller mixing angles. Numerous experiments [251–254] have corroborated the tininess of the neutrino masses and other parameters with high accuracy. The global fit values of the neutrino oscillation parameters are

furnished in Refs. [173, 175].

It is well-known that in the SM framework, the neutrino mass generation cannot be explained through the standard Higgs mechanism due to the absence of the right-handed (RH) components. Still, if we could manage to add the RH neutrinos into SM by hand, and allow Dirac mass terms, the values of the required Yukawa couplings to be around $\mathcal{O}(10^{-12})$, i.e., which appear as aberrant. In contrast, there exist many BSM scenarios that help to generate tiny neutrino mass through the conventional seesaw mechanism. Some of the prominent seesaw mechanisms are categorized as type-I [47, 201, 203, 255], type-II [204–209], type-III [210–215] and all of them require additional heavy fermions or scalars beyond the SM particle content. Literature survey shows there are many flavor symmetries either discrete A_4 [225, 256, 257], S_3 [258–261], S_4 [262–264] etc. or continuous $U(1)_{B-L}$ [194, 223, 265–267], $U(1)_H$ [268–270], $U(1)_{L_e-L_\tau}$ [271, 272] etc., which can generate the tiny neutrino masses and also accommodate the observed neutrino oscillation data with the help of some additional scalars and perturbation (wherever required). As aforesaid, inclusion of flavons affects the neatness of the model and the predictability of the model is hampered because of the higher dimensional operators. These drawbacks can be eliminated through the recent approach of including modular symmetry [59, 70, 74, 75, 93, 156, 159, 229–244, 273], where the Yukawa couplings transform non-trivially under the discrete flavor symmetry group and have certain modular weight.

The modular group $\Gamma_5' \simeq A_5'$ is a new and promising candidate, which corresponds to the special case of $N = 5$. People have done extensive studies on the essential properties of this A_5' finite group [246–248], so here we bring up only the important points regarding A_5' modular symmetry. The A_5' group consists of 120 elements, which are likely to be originated by the generators: S, T and R gratifying the identities for $N = 5$ [158]. So, categorization of these 120 elements are done into nine conjugacy classes which are represented by nine well defined irreducible representations, symbolized as $\mathbf{1}$, $\widehat{\mathbf{2}}$, $\widehat{\mathbf{2}}'$, $\mathbf{3}$, $\mathbf{3}'$, $\mathbf{4}$, $\widehat{\mathbf{4}}$, $\mathbf{5}$ and $\widehat{\mathbf{6}}$. Additionally, the conjugacy classes along with the character table of A_5', and the representation matrices of the generators are presented in Appendix of Ref. [158]. It ought to be noticed that the $\mathbf{1}$, $\mathbf{3}$, $\mathbf{3}'$, $\mathbf{4}$ and $\mathbf{5}$ representations with $R = \mathbb{I}$ are identical to those for A_5, while $\widehat{\mathbf{2}}$, $\widehat{\mathbf{2}}'$, $\widehat{\mathbf{4}}$ and $\widehat{\mathbf{6}}$ are different for A_5', with $R = -\mathbb{I}$. As we are working in the modular space of $\Gamma(5)$, hence, its dimension is $5k+1$, where, k is the modular weight. A brief discussion concerning the modular space of $\Gamma(5)$ is presented in Appendix C.1. For $k = 1$, the modular space $M_1[\Gamma(5)]$ will have six basis vectors i.e., ($\widehat{e}_i$, where $i = 1,2,3,4,5,6$) whose q-expansion are given

below and they are used in expressing the Yukawa coupling $Y^{(1)}_{\hat{\mathbf{6}}}$ as shown in Appendix C.3:

$$\begin{aligned}
\widehat{e}_1 &= 1+3q+4q^2+2q^3+q^4+3q^5+6q^6+4q^7-q^9+\cdots\,,\\
\widehat{e}_2 &= q^{1/5}\left(1+2q+2q^2+q^3+2q^4+2q^5+2q^6+q^7+2q^8+2q^9+\cdots\right),\\
\widehat{e}_3 &= q^{2/5}\left(1+q+q^2+q^3+2q^4+q^6+q^7+2q^8+q^9+\cdots\right),\\
\widehat{e}_4 &= q^{3/5}\left(1+q^2+q^3+q^4-q^5+2q^6+2q^8+q^9+\cdots\right),\\
\widehat{e}_5 &= q^{4/5}\left(1-q+2q^2+2q^6-2q^7+2q^8+q^9+\cdots\right),\\
\widehat{e}_6 &= q\left(1-2q+4q^2-3q^3+q^4+2q^5-2q^6+3q^8-2q^9+\cdots\right). \qquad (5.1)
\end{aligned}$$

Our aim here is to utilize the expediency of the modular A'_5 symmetry by incorporating the linear seesaw mechanism in the context of supersymmetry, as we are quite familiar with the dynamics of TeV scale seesaw frameworks from numerous [274, 275] literature. The deciding factor whether it will be linear seesaw or inverse seesaw is the position of the zero elements in the mass matrix under the basis of (ν, N_{R_i}, S_{L_i}). It is quite evident when 11 and 33 elements of the mass matrix are zero, it gives the structure of linear seesaw. As mentioned above, introduction of three left-handed (S_{L_i}) alongside three right-handed (N_{R_i}) neutral fermion superfields validates and generates the neutrino mass matrix structure of linear seesaw which has been widely studied in the context of discrete A_4 flavor symmetry [86–88]. In this work, we are interested to implement it with A'_5 modular symmetry. For this purpose, we consider the heavy fermions S_{Li} and N_{Ri} to transform as $3'$ under A'_5 symmetry and the modular form of the Yukawa couplings leads to a constrained structure. After that we perform the numerical analysis to look for the region which is acceptable in order to fit the neutrino data. Hence, prediction for the neutrino sector is done after fixing the allowed parameter space.

The outline of the chapter is as follows. In Sec. 5.2, we present the layout of the linear seesaw framework in the context of discrete A'_5 modular symmetry. Using the A'_5 product rules, we obtain the simple mass matrix structure for the charged leptons as well as the neutral fermions. After that we briefly discuss the light neutrino masses and mixing phenomena in this framework. The numerical analysis is performed in Sec. 5.3 followed by a brief comment on the non-unitarity effect. Sec. 5.4 contains the discussion on leptogenesis in the context of the present model and finally our results are summarized in Sec. 5.5.

5.2 The Model

Here we work on a model under linear seesaw scenario in the context of supersymmetry (SUSY), where Table 5.1 provided below expresses the list of particles and their respective group charges. For exploring neutrino sector beyond standard model, we extend it with the discrete A'_5 modular symmetry and a local $U(1)_{B-L}$ gauge symmetry. However, the local $U(1)_{B-L}$ becomes the auxillary symmetry which has been added to avoid certain undesirable terms in the superpotential. The advantage of working in BSM is that

we can add right-handed neutrinos and extra fields, and hence, here we have included three SM singlet right-handed superfields (N_R), three left-handed superfields (S_L) and a pair of weightons (ζ, ζ') in the particle gamut. The transformation of extra added superfields is taken as $3'$ under the modular group A_5'. The A_5' and $U(1)_{B-L}$ symmetries are assumed to be broken at a very high scale, much greater than the scale of electroweak symmetry breaking [89]. Mass acquisition by the extra singlet superfield happens by assigning the vacuum expectation value (VEV) to the weightons ζ and ζ'. All the particles are assigned definite values of modular weights denoted as k_I. One of the key point of introducing modular symmetry is the curtailment of flavon (weighton) fields, which otherwise are traditionally required while working in BSM with discrete symmetries, since the Yukawa couplings transform non-trivially under A_5' modular symmetry group, and their transformation properties are present in [158].

Fields	e_R^c	μ_R^c	τ_R^c	L_L	N_R^c	S_L	$H_{u,d}$	ζ	ζ'
$SU(2)_L$	1	1	1	2	1	1	2	1	1
$U(1)_Y$	1	1	1	$-\frac{1}{2}$	0	0	$\frac{1}{2}, -\frac{1}{2}$	0	0
$U(1)_{B-L}$	1	1	1	-1	1	0	0	1	-1
A_5'	1	1	1	3	$3'$	$3'$	1	1	1
k_I	1	3	5	1	1	4	0	1	1

Table 5.1: The particle spectrum and their charges under the symmetry groups $SU(2)_L \times U(1)_Y \times U(1)_{B-L} \times A_5'$ while k_I represents the modular weight.

The complete superpotential is given by

$$\begin{aligned} \mathcal{W} &= A_{M_l}\left[(L_L l_R^c)_{\mathbf{3}} Y_{\mathbf{3}}^{k_Y}\right] H_d + \mu H_u H_d + G_D\left[(L_L N_R^c)_{\mathbf{5}} Y_{\mathbf{5}}^{(2)}\right] H_u + \\ & G_{LS}\left[(L_L S_L)_{\mathbf{4}} H_u \sum_{i=1}^{2} Y_{\mathbf{4},i}^{(6)}\right] \frac{\zeta}{\Lambda} + B_{M_{RS}}\left[(S_L N_R^c)_{\mathbf{5}} \sum_{i=1}^{2} Y_{\mathbf{5},i}^{(6)}\right] \zeta', \end{aligned} \tag{5.2}$$

where, $A_{\mathcal{M}_l} = (\alpha_{\mathcal{M}_l}, \beta_{\mathcal{M}_l}, \gamma_{\mathcal{M}_l})$, $l_R^c = (e_R^c, \mu_R^c, \tau_R^c)$, $k_Y = (2,4,6)$, and $G_D = \text{diag}\{g_{D_1}, g_{D_2}, g_{D_3}\}$, $G_{LS} = \text{diag}\{g_{\text{LS}_1}, g_{\text{LS}_2}, g_{\text{LS}_3}\}$, $B_{M_{RS}} = \text{diag}\{\alpha_{RS_1}, \alpha_{RS_2}, \alpha_{RS_3}\}$ represent the coupling strengths of various interaction terms.

5.2.1 Mass terms for the charged leptons (M_ℓ)

For obtaining simplified and elegant structure for the mass matrix of charged leptons, we envisage that the three families of left-handed lepton doublets (L_{Li}) transform as triplets (**3**) under the A_5' modular symmetry with $U(1)_{B-L}$ charge -1. The right-handed charged leptons (l_R^c) transform as singlets under both A_5' symmetry and have $U(1)_{B-L}$ charge $+1$. However, (e_R^c, μ_R^c, τ_R^c) are given the modular weight as

1, 3, and 5 respectively. The Higgsinos $H_{u,d}$ are given charges 0 under U_{B-L} and 1 for A_5' symmetries with zero modular weights. The VEVs of these Higgsinos H_u and H_d are represented as $v_u/\sqrt{2}$ and $v_d/\sqrt{2}$ respectively. Moreover, Higgsinos VEVs are associated to SM Higgs VEV as $v_H = \frac{1}{2}\sqrt{v_u^2 + v_d^2}$ and the ratio of their VEVs is expressed as $\tan\beta = (v_u/v_d)$ and we use its value to be 5 in our analysis. The relevant superpotential terms for charged leptons are given by

$$\mathcal{W}_{M_l} = \alpha_{M_l}\left[(L_L e_R^c)_{\mathbf{3}} Y_{\mathbf{3}}^{(2)}\right] H_d + \beta_{M_l}\left[(L_L \mu_R^c)_{\mathbf{3}} Y_{\mathbf{3}}^{(4)}\right] H_d + \gamma_{M_l}\left[(L_L \tau_R^c)_{\mathbf{3}} \left\{\sum_{i=1}^{2} Y_{\mathbf{3},i}^{(6)}\right\}\right] H_d . \tag{5.3}$$

Working under A_5' modular group, its Kronecker product leaves us with a non diagonal charged lepton mass matrix after the spontaneous symmetry breaking. The mass matrix takes the form

$$M_l = \frac{v_d}{\sqrt{2}} \begin{bmatrix} \left(Y_{\mathbf{3}}^{(2)}\right)_1 & \left(Y_{\mathbf{3}}^{(4)}\right)_1 & \left(\sum_{i=1}^{2} Y_{\mathbf{3},i}^{(6)}\right)_1 \\ \left(Y_{\mathbf{3}}^{(2)}\right)_3 & \left(Y_{\mathbf{3}}^{(4)}\right)_3 & \left(\sum_{i=1}^{2} Y_{\mathbf{3},i}^{(6)}\right)_3 \\ \left(Y_{\mathbf{3}}^{(2)}\right)_2 & \left(Y_{\mathbf{3}}^{(4)}\right)_2 & \left(\sum_{i=1}^{2} Y_{\mathbf{3},i}^{(6)}\right)_2 \end{bmatrix}_{LR} \cdot \begin{bmatrix} \alpha_{M_l} & 0 & 0 \\ 0 & \beta_{M_l} & 0 \\ 0 & 0 & \gamma_{M_l} \end{bmatrix} . \tag{5.4}$$

The charged lepton mass matrix M_l can be diagonalised by the unitary matrix U_l, giving rise to the physical masses m_e, m_μ and m_τ as

$$U_l^\dagger M_l M_l^\dagger U_l = \mathrm{diag}(m_e^2, m_\mu^2, m_\tau^2) . \tag{5.5}$$

Additionally, it also satisfies the following identities, which will be used for numerical analysis in section 5.3:

$$\begin{aligned} \mathrm{Tr}\left(M_l M_l^\dagger\right) &= m_e^2 + m_\mu^2 + m_\tau^2 , \\ \mathrm{Det}\left(M_l M_l^\dagger\right) &= m_e^2 m_\mu^2 m_\tau^2 , \\ \frac{1}{2}\left[\mathrm{Tr}\left(M_l M_l^\dagger\right)\right]^2 - \frac{1}{2}\mathrm{Tr}\left[(M_l M_l^\dagger)^2\right] &= m_e^2 m_\mu^2 + m_\mu^2 m_\tau^2 + m_\tau^2 m_e^2 . \end{aligned} \tag{5.6}$$

5.2.2 Dirac as well as pseudo-Dirac mass terms for light neutrinos

In addition to lepton doublet transformation, hitherto, the heavy fermion superfields, i.e., N_R^c (S_L) transform as triplet $\mathbf{3}'$ under A_5' modular group with $U(1)_{B-L}$ charge of -1 (0) along with modular weight 1 (4) respectively. As discussed in Ref. [158], the choice of Yukawa couplings depends on the equation $k_Y = k_{I_1} + k_{I_2} + \cdots + k_{I_n}$ where k_Y is the modular weight of Yukawa couplings and $\Sigma_{i=1}^{I_n} k_{I_n}$ is sum of the modular weights of all other particles present in the definition of superpotential terms. These Yukawa couplings can be written in terms of Dedekind eta-function $\eta(\tau)$, and thus have q-expansion forms, in order to avoid the complexity in calculations. The relevant superpotential term involving the active and

right-handed heavy neutrino fields can be expressed as

$$\mathcal{W}_D = G_D \left[(L_L N_R^c)_{\mathbf{5}} Y_{\mathbf{5}}^{(2)} \right] H_u \,, \tag{5.7}$$

where, G_D is the diagonal matrix containing the free parameters and the modular weight of the Yukawa coupling is equal to the sum of the the modular weights of all other particles present in eqn.(5.7). The choice of the Yukawa coupling is made based on the Kroncker product rules for A_5' modular symmetry such that superpotential remains singlet. Consequently, the Dirac neutrino mass matrix can be given as

$$M_D = \frac{v_u}{\sqrt{3}0} G_D \begin{bmatrix} \sqrt{3}(Y_{\mathbf{5}}^{(2)})_1 & (Y_{\mathbf{5}}^{(2)})_4 & (Y_{\mathbf{5}}^{(2)})_3 \\ (Y_{\mathbf{5}}^{(2)})_5 & -\sqrt{2}(Y_{\mathbf{5}}^{(2)})_3 & -\sqrt{2}(Y_{\mathbf{5}}^{(2)})_2 \\ (Y_{\mathbf{5}}^{(2)})_2 & -\sqrt{2}(Y_{\mathbf{5}}^{(2)})_5 & -\sqrt{2}(Y_{\mathbf{5}}^{(2)})_4 \end{bmatrix}_{LR} . \tag{5.8}$$

As the transformation of the sterile fermion superfield S_L is same as N_R under A_5', it allows us to write the pseudo-Dirac mass term for the light neutrinos and the corresponding super potential can be written as

$$\mathcal{W}_{LS} = G_{LS} \left[(L_L S_L)_{\mathbf{4}} \sum_{2}^{i=1} Y_{\mathbf{4},i}^{(6)} \right] H_u \left(\frac{\zeta}{\Lambda} \right) , \tag{5.9}$$

where, G_{LS} is a diagonal matrix containing three free parameters and the choice of Yukawa coupling depends upon the idea of keeping the superpotential singlet. Thus, we obtain the pseudo-Dirac mass matrix for the neutrinos as,

$$M_{LS} = \frac{v_u}{2\sqrt{6}} \left(\frac{v_\zeta}{\sqrt{2}\Lambda} \right) G_{LS} \begin{bmatrix} 0 & -\sqrt{2}\left(\sum_{i=1}^{2} Y_{\mathbf{4,i}}^{(6)} \right)_3 & -\sqrt{2}\left(\sum_{i=1}^{2} Y_{\mathbf{4,i}}^{(6)} \right)_2 \\ \sqrt{2}\left(\sum_{i=1}^{2} Y_{\mathbf{4,i}}^{(6)} \right)_4 & -\left(\sum_{i=1}^{2} Y_{\mathbf{4,i}}^{(6)} \right)_2 & \left(\sum_{i=1}^{2} Y_{\mathbf{4,i}}^{(6)} \right)_1 \\ \left(\sum_{i=1}^{2} Y_{\mathbf{4,i}}^{(6)} \right)_1 & \left(\sum_{i=1}^{2} Y_{\mathbf{4,i}}^{(6)} \right)_4 & -\left(\sum_{i=1}^{2} Y_{\mathbf{4,i}}^{(6)} \right)_3 \end{bmatrix}_{LR} . \tag{5.10}$$

5.2.3 Mixing between the heavy fermions N_R and S_L

Introduction of extra symmetries, helps in allowing the mixing of heavy superfields but forbids the usual Majorana mass terms. Hence, below we show the mixing of these extra superfields i.e., (N_R^c, S_L) as follows

$$\mathcal{W}_{M_{RS}} \quad = \quad B_{M_{RS}} \left[(S_L N_R^c)_{\mathbf{5}} \sum_{i=1}^{2} Y_{\mathbf{5},i}^{(6)} \right] \zeta' , \tag{5.11}$$

where, $B_{M_{RS}}$ is the free parameter and $\langle \zeta' \rangle = v_\zeta'/\sqrt{2}$ is the VEV of ζ' and the superpotential is singlet under the A_5' modular symmetry product rule. Thus, considering $v_{\zeta'} \approx v_\zeta$, one can obtain the mass matrix as

follows:

$$M_{RS} = \frac{v_\zeta}{\sqrt{6}0} B_{M_{RS}} \begin{bmatrix} 2\left(\sum_{i=1}^{2} Y^{(6)}_{\mathbf{5,i}}\right)_1 & -\sqrt{3}\left(\sum_{i=1}^{2} Y^{(6)}_{\mathbf{5,i}}\right)_4 & -\sqrt{3}\left(\sum_{i=1}^{2} Y^{(6)}_{\mathbf{5,i}}\right)_3 \\ -\sqrt{3}\left(\sum_{i=1}^{2} Y^{(6)}_{\mathbf{5,i}}\right)_4 & \sqrt{6}\left(\sum_{i=1}^{2} Y^{(6)}_{\mathbf{5,i}}\right)_2 & -\left(\sum_{i=1}^{2} Y^{(6)}_{\mathbf{5,i}}\right)_1 \\ -\sqrt{3}\left(\sum_{i=1}^{2} Y^{(6)}_{\mathbf{5,i}}\right)_3 & -\left(\sum_{i=1}^{2} Y^{(6)}_{\mathbf{5,i}}\right)_1 & \sqrt{6}\left(\sum_{i=1}^{2} Y^{(6)}_{\mathbf{5,i}}\right)_5 \end{bmatrix}_{LR} . \tag{5.12}$$

The masses for the heavy superfields can be found in the basis $(N_R, S_L)^T$ as

$$M_{hf} = \begin{pmatrix} 0 & M_{RS} \\ M_{RS}^T & 0 \end{pmatrix}, \tag{5.13}$$

Hence, one can have three doubly degenerate mass eigenstates for the heavy superfields upon diagonalization.

5.2.4 Linear Seesaw framework for light neutrino mass

In the present scenario of A_5' modular symmetry, the light neutrino masses can be generated in the framework of linear seesaw. Thus, the mass matrix in the flavor basis of $\left(\nu_L, N_R^c, S_L\right)^T$, can be manifested as

$$\mathbb{M} = \begin{pmatrix} 0 & M_D & M_{LS} \\ M_D^T & 0 & M_{RS} \\ M_{LS}^T & M_{RS}^T & 0 \end{pmatrix}. \tag{5.14}$$

Assuming that $M_{RS} \gg M_D, M_{LS}$, one can write the linear seesaw mass formula for light neutrinos as

$$m_\nu = M_D M_{RS}^{-1} M_{LS}^T + \text{transpose} . \tag{5.15}$$

Besides the neutrino masses, other relevant parameters which can play important role in the understanding of neutrino physics are the Jarlskog invariant, that signifies the measure of CP violation and the effective electron neutrino mass $\langle m_{ee} \rangle$ in neutrinoless double beta decay. These parameters can be computed from the PMNS matrix elements as following:

$$J_{CP} = \text{Im}[U_{e1} U_{\mu 2} U_{e2}^* U_{\mu 1}^*] = s_{23} c_{23} s_{12} c_{12} s_{13} c_{13}^2 \sin\delta_{CP} , \tag{5.16}$$

$$\begin{aligned} \left|\langle m_{ee} \rangle\right| &= \left| m_1 |U_{e1}|^2 + m_2 |U_{e2}|^2 e^{i\alpha_{21}} + m_3 |U_{e3}|^2 e^{i(\alpha_{31} - 2\delta_{CP})} \right| , \\ &= \left| m_1 \cos^2\theta_{12} \cos^2\theta_{13} + m_2 \sin^2\theta_{12} \cos^2\theta_{13} e^{i\alpha_{21}} + m_3 \sin^2\theta_{13} e^{i(\alpha_{31} - 2\delta_{CP})} \right| . \end{aligned} \tag{5.17}$$

Many dedicated experiments are planned to measure the CP violation in neutrino sector as well as the neutrinoless double beta decay processes. Hopefully, CP violation will be precisely measured in

the upcoming DUNE and T2HK experiments and the effective Majorana mass parameter $\langle m_{ee} \rangle$ can be measured by the KamLAND-Zen experiment in the near future [97].

5.3 Numerical Results

For numerical analysis, we use the neutrino oscillation parameters from the global-fit results [98, 174, 276] obtained from various experiments, as given in Table 5.2. The numerical diagonalization of the light neutrino mass matrix given in eqn.(5.15), is done through $U_\nu^\dagger \mathcal{M} U_\nu = \text{diag}\left(m_1^2, m_2^2, m_3^2\right)$, with $\mathcal{M} = m_\nu m_\nu^\dagger$ and U_ν is the unitary matrix. Thus, one can write the lepton mixing matrix as $U = U_l^\dagger U_\nu$ and consequently obtain the mixing angles by using the standard relations:

$$\sin^2\theta_{12} = \frac{|U_{12}|^2}{1-|U_{13}|^2}, \qquad \sin^2\theta_{23} = \frac{|U_{23}|^2}{1-|U_{13}|^2}, \quad and \quad \sin^2\theta_{13} = |U_{13}|^2 \,. \tag{5.18}$$

For explaining the observed neutrino oscillation data, we vary the model parameters in the following ranges:

$$\begin{aligned} &\text{Re}[\tau] \in [0, 0.5], \;\; \text{Im}[\tau] \in [1, 3], \;\; G_D \in [10^{-7}, 10^{-6}], \;\; G_{LS} \in [10^{-4}, 10^{-3}] \quad v_\zeta \in [10, 100] \text{ TeV}, \\ &B_{M_{RS}} \in [10^{-3}, 10^{-2}], \quad \Lambda \in [10^4, 10^5] \text{ TeV}. \end{aligned} \tag{5.19}$$

Oscillation Parameters	**Best fit value** $\pm 1\sigma$	**2σ range**	**3σ range**
$\Delta m^2_{21}[10^{-5}\text{ eV}^2]$	7.56 ± 0.19	7.20–7.95	7.05–8.14
$\lvert\Delta m^2_{31}\rvert[10^{-3}\text{ eV}^2]$ (NO)	2.55 ± 0.04	2.47–2.63	2.43–2.67
$\sin^2\theta_{12}/10^{-1}$	$3.21^{+0.18}_{-0.16}$	2.89–3.59	2.73–3.79
$\sin^2\theta_{23}/10^{-1}$ (NO)	$4.30^{+0.20}_{-0.18}$	3.98–4.78 & 5.60–6.17	3.84–6.35
	$5.98^{+0.17}_{-0.15}$	4.09–4.42 & 5.61–6.27	3.89–4.88 & 5.22–6.41
$\sin^2\theta_{13}/10^{-2}$ (NO)	$2.155^{+0.090}_{-0.075}$	$1.98 - 2.31$	$2.04 - 2.43$
δ_{CP}/π (NO)	$1.08^{+0.13}_{-0.12}$	$0.84 - 1.42$	$0.71 - 1.99$

Table 5.2: The global-fit values of the oscillation parameters alongwith their $1\sigma/2\sigma/3\sigma$ ranges [98, 174, 276].

The input parameters are varied randomly in the ranges as provided in Eqn. (5.19) and constrained by imposing the 3σ bounds on neutrino oscillation data, i.e., the solar and atmospheric mass squared differences and the mixing angles as presented in Table 5.2, as well as the sum of the active neutrino masses: $\Sigma m_i < 0.12$ eV [277]. The allowed range of the modulus τ is found to be: $0 \lesssim \text{Re}[\tau] \lesssim 0.5$ and $1 \lesssim \text{Im}[\tau] \lesssim 3$, for normal ordering of neutrino masses. In Fig. 5.1, we show the variation of the sum of active neutrino masses (Σm_i) with the reactor mixing angle $\sin^2\theta_{13}$ (left panel), while the right panel demonstrates Σm_i versus $\sin^2\theta_{12}$ and $\sin^2\theta_{23}$. From these figures, it can be observed that the model predictions for the sum of neutrino masses as $\Sigma 0.058$ e$V \leq m_i \leq 0.062$ eV for the allowed 3σ ranges of the mixing angles.

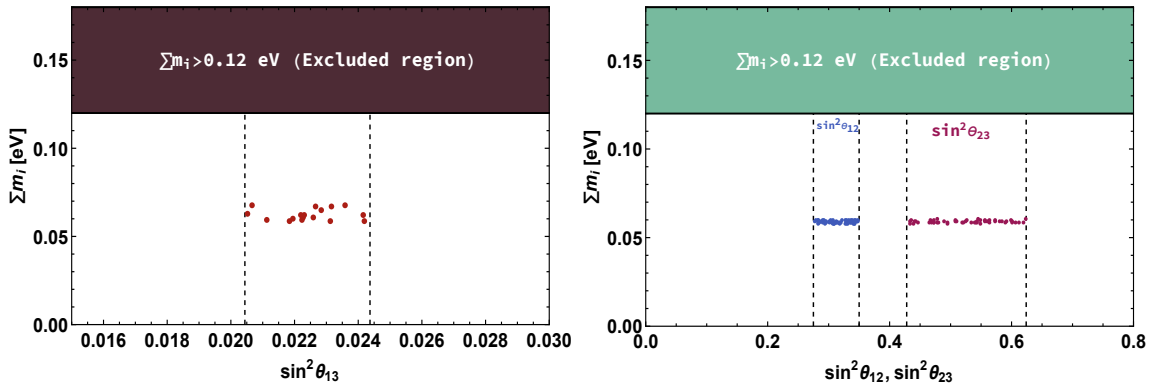

Figure 5.1: the plot in the left (right) panel demonstrates the correlation between $\sin^2\theta_{13}$ ($\sin^2\theta_{12}$ & $\sin^2\theta_{23}$) with the sum of active neutrino masses $\sum m_i$. The vertical lines represent the 3σ allowed ranges of the mixing angles.

The variation of the effective mass parameter m_{ee} of neutrinoless double beta decay with Σm_i is displayed in Fig. 5.2, from which the upper limit on m_{ee} is found to be 0.025 eV satisfying KamLAND-Zen bound. Further, we display the variation of δ_{CP} and J_{CP} w.r.t $\sin^2\theta_{13}$ in the left and right panel of Fig. 5.3 respectively, where we obtain their limits as $100^\circ \leq \delta_{CP} \leq 250^\circ$ and $|J_{CP}| \leq 0.004$.

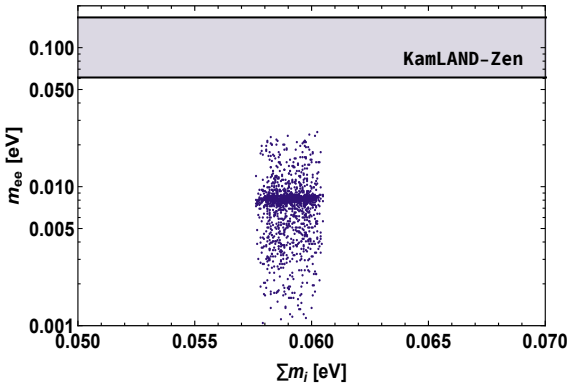

Figure 5.2: Correlation plot between the effective neutrino mass m_{ee} of neutrinoless double beta decay and the sum of active neutrino masses.

Comment on non-unitarity of leptonic mixing matrix

Here, we present a brief discussion on the non-unitarity of neutrino mixing matrix U'_{PMNS} in the context of the present model. Due to the mixing between the light and heavy fermions, there will be small deviation from unitarity of the leptonic mixing matrix, which can be expressed as follows [99]

$$U'_{\rm PMNS} \equiv \left(1 - \frac{1}{2}FF^\dagger\right) U_{\rm PMNS}. \tag{5.20}$$

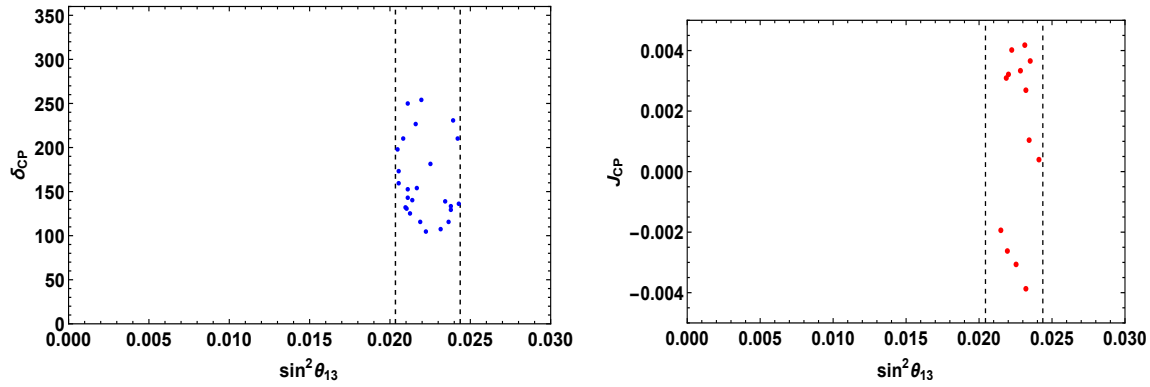

Figure 5.3: Left (right) panel shows the plot of δ_{CP} (J_{CP}) with $\sin^2\theta_{13}$ within its 3σ bound.

Here, U_{PMNS} denotes the PMNS mixing matrix that diagonalises the light neutrino mass matrix and F represents the mixing of active light neutrinos with the heavy one, which is approximated as $F \equiv (M_{NS}^T)^{-1} M_D \approx \frac{g_D v}{\alpha_{RS} v_\zeta}$, and is a hermitian matrix. The non-unitarity parameters are constrained through various electroweak precision measurements [100–102], such as the mass of W boson (M_W), Weinberg mixing angle (θ_W), ratios of various fermionic decays of Z boson and its invisible decay, lepton flavour violations and the CKM unitarity bounds. In the context of the present model, we take into account the following approximated normalized order of masses for the Dirac, pseudo-Dirac and heavy fermions for generating the observed mass-squared differences as well as the sum of active neutrino masses of desired order as

$$\left(\frac{m_\nu}{0.1\ \mathrm{eV}}\right) \approx \left(\frac{M_D}{10^{-3}\ \mathrm{GeV}}\right)\left(\frac{M_{RS}}{10^{3}\ \mathrm{GeV}}\right)^{-1}\left(\frac{M_{LS}}{10^{-4}\ \mathrm{GeV}}\right). \tag{5.21}$$

With these chosen order masses, we obtain the following approximated non-unitary mixing for the present model:

$$|FF^\dagger| \leq \begin{bmatrix} 4.5\times10^{-13} & 2.3\times10^{-13} & 6.2\times10^{-13} \\ 2.3\times10^{-13} & 2.08\times10^{-12} & 4.5\times10^{-12} \\ 6.2\times10^{-13} & 4.5\times10^{-12} & 5.6\times10^{-12} \end{bmatrix}. \tag{5.22}$$

As the mixing between the active light and heavy fermions is quite small in our model, it generates a negligible contribution for the non-unitarity.

5.4 Leptogenesis

The present universe is clearly seen to be baryon dominated, with the ratio of the measured over-abundance of baryons over anti-baryons to the entropy density is found to be

$$Y_B = (8.56 \pm 0.22)\times10^{-11}\,. \tag{5.23}$$

Considering the fact that the universe had started from an initially symmetric state of baryons and antibaryons, following three conditions have to be fulfilled for generating a non-zero baryon asymmetry. According to Sakharov [23], these three criteria are: Baryon number violation, C and CP violation and departure from thermal equilibrium during the evolution of the universe. Though the SM assures all these criteria for an expanding Universe akin ours, the extent of CP violation found in the SM is quite small to accommodate the observed baryon asymmetry of the universe. Therefore, additional sources of CP violation are absolutely essential for explaining this asymmetry. The most common new sources of CP violation possibly could arise in the lepton sector, which is however, not yet firmly established experimentally. Leptogenesis is the phenomenon that furnishes a minimal set up to correlate the CP violation in the lepton sector to the observed baryon asymmetry, as well as imposes indirect constraints on the CP phases from the requirement that it would yield the correct baryon asymmetry. It is seen that the scale of CP-asymmetry generated from the heavy neutral fermion decays can come down to as low as TeV [109–112] due to resonant enhancement. However, the present scenario is realized by involving six heavy states, which comprises three pairs of heavy neutrinos with doubly degenerate masses eqn.(5.13). Nevertheless, introduction of a higher dimensional mass terms for the Majorana fermions (N_R^c) can be made through the following superpotential

$$\mathcal{W}_{M_R} = -G_R \left[\sum_{i=1}^{2} Y_{5,i}^{(4)} N_R^c N_R^c \right] \frac{\zeta'^2}{\Lambda}\,, \tag{5.24}$$

which gives rise to a petty mass splitting amid the heavy neutral fermions, and hence provides an enhancement in the CP asymmetry for generating the required lepton asymmetry [113, 114]. Thus, from (5.24) one can construct the Majorana mass matrix for the right-handed neutrinos N_R as

$$M_R = \frac{G_R v_\zeta^2}{2\Lambda\sqrt{30}} \begin{bmatrix} 2\left(\sum_{i=1}^{2} Y_{\mathbf{5,i}}^{(4)}\right)_1 & -\sqrt{3}\left(\sum_{i=1}^{2} Y_{\mathbf{5,i}}^{(4)}\right)_4 & -\sqrt{3}\left(\sum_{i=1}^{2} Y_{\mathbf{5,i}}^{(4)}\right)_3 \\ -\sqrt{3}\left(\sum_{i=1}^{2} Y_{\mathbf{5,i}}^{(4)}\right)_4 & \sqrt{6}\left(\sum_{i=1}^{2} Y_{\mathbf{5,i}}^{(4)}\right)_2 & -\left(\sum_{i=1}^{2} Y_{\mathbf{5,i}}^{(4)}\right)_1 \\ -\sqrt{3}\left(\sum_{i=1}^{2} Y_{\mathbf{5,i}}^{(4)}\right)_3 & -\left(\sum_{i=1}^{2} Y_{\mathbf{5,i}}^{(4)}\right)_1 & \sqrt{6}\left(\sum_{i=1}^{2} Y_{\mathbf{5,i}}^{(4)}\right)_5 \end{bmatrix}_{LR}\,. \tag{5.25}$$

The coupling G_R is considered as exceptionally small to preserve the linear seesaw texture of the neutrino mass matrix eqn.(5.14), i.e., $M_D, M_{LS} \gg M_R$ and hence, inclusion of such additional term does not alter the results obtained earlier. However, this added term generates a small mass difference. Hence, the 2×2 submatrix of eqn.(5.14) in the basis of (N_R^c, S_L), becomes

$$M = \begin{pmatrix} M_R & M_{RS} \\ M_{RS}^T & 0 \end{pmatrix}, \tag{5.26}$$

which can be block diagonalized by using the unitary matrix: $\frac{1}{\sqrt{2}}\begin{pmatrix} I & -I \\ I & I \end{pmatrix}$ as

$$M' = \begin{pmatrix} M_{RS}+\frac{M_R}{2} & -\frac{M_R}{2} \\ -\frac{M_R}{2} & -M_{RS}+\frac{M_R}{2} \end{pmatrix} \approx \begin{pmatrix} M_{RS}+\frac{M_R}{2} & 0 \\ 0 & -M_{RS}+\frac{M_R}{2} \end{pmatrix}. \tag{5.27}$$

Thus, one can express the mass eigenstates ($N^{\pm}$) in terms of the flavor states (N_R, S_L) as

$$\begin{pmatrix} S_{Li} \\ N^c_{Ri} \end{pmatrix} = \begin{pmatrix} \cos\theta & -\sin\theta \\ \sin\theta & \cos\theta \end{pmatrix} \begin{pmatrix} N^+_i \\ N^-_i \end{pmatrix}. \tag{5.28}$$

Assuming the mixing to be maximal, one can have

$$N^c_{Ri} = \frac{(N^+_i + N^-_i)}{\sqrt{2}}, \;\; S_{Li} = \frac{(N^+_i - N^-_i)}{\sqrt{2}}. \tag{5.29}$$

Hence, the interaction superpotential (5.8) can be manifested in terms of the new basis. One can obtain the mass eigenvalues of the new states N^+ and N^- by diagonalizing the block-diagonal form of the heavy-fermion masses which are given as $\frac{M_R}{2}+M_{RS}$ and $\frac{M_R}{2}-M_{RS}$ from eqn.(5.27).

The Dirac (5.7) and pseudo-Dirac (5.9) terms are now modified as

$$\mathcal{W}_D = G_D L_L H_u \left[Y^{(2)}_5 \left(\frac{(N^+_i + N^-_i)}{\sqrt{2}} \right) \right], \tag{5.30}$$

and

$$\mathcal{W}_{LS} = G_{LS} L_L H_u \left[\sum_2^{i=1} Y^{(6)}_{4,i} \left(\frac{(N^+_i - N^-_i)}{\sqrt{2}} \right) \right] \frac{\zeta}{\Lambda}. \tag{5.31}$$

Thus, one can symbolically express the block-diagonal matrix for the heavy fermions (5.27) as

$$M_{RS} \pm \frac{M_R}{2} = \frac{v_\zeta}{\sqrt{6}0} B_{M_{RS}} \begin{bmatrix} 2a & d & e \\ d & b & f \\ e & f & c \end{bmatrix}_{LR} \pm \frac{G_R v_\zeta^2}{2\Lambda\sqrt{30}} \begin{bmatrix} 2a' & d' & e' \\ d' & b' & f' \\ e' & f' & c' \end{bmatrix}_{LR}, \tag{5.32}$$

where, the different matrix elements are defined as

$$\begin{aligned} a(a') &= \left(\sum_{i=1}^{2} Y^{6(4)}_{\mathbf{5,i}} \right)_1, \;\; b(b') = \sqrt{6} \left(\sum_{i=1}^{2} Y^{6(4)}_{\mathbf{5,i}} \right)_2, \;\; c(c') = \sqrt{6} \left(\sum_{i=1}^{2} Y^{6(4)}_{\mathbf{5,i}} \right)_5, \\ d(d') &= -\sqrt{3} \left(\sum_{i=1}^{2} Y^{6(4)}_{\mathbf{5,i}} \right)_4, \;\; e(e') = -\sqrt{3} \left(\sum_{i=1}^{2} Y^{6(4)}_{\mathbf{5,i}} \right)_3, \;\; f(f') = -a(a'). \end{aligned} \tag{5.33}$$

One can obtain the diagonalized mass matrix from (5.32) through rotation to the mass eigen-basis as: $(M^{\pm})_{\text{diag}} = U_{\text{TBM}} U_R \left(M_{RS} \pm \frac{M_R}{2} \right) U_R^T U_{\text{TBM}}^T$. Consequently, three sets of approximately degenerate mass states can be obtained

upon diagonalization. Further, we presume that the lightest pair among them with mass in the TeV range, contribute predominantly to the CP asymmetry. The small mass difference amid the lightest pair demonstrates that the CP asymmetry generated through the one-loop self energy contribution dominates over the vertex part in the decay of heavy particle. Thus, the CP asymmetry can be expressed as [109, 117]

$$\epsilon_{N_i^-} \approx \frac{1}{32\pi^2 A_{N_i^-}} \mathrm{Im}\left[\left(\frac{\tilde{M}_D}{v}-\frac{\tilde{M}_{LS}}{v}\right)^{\dagger}\left(\frac{\tilde{M}_D}{v}+\frac{\tilde{M}_{LS}}{v}\right)^{2}\left(\frac{\tilde{M}_D}{v}-\frac{\tilde{M}_{LS}}{v}\right)^{\dagger}\right]_{ii} \frac{r_N}{r_N^2+4A_{N_i^-}^2}, \tag{5.34}$$

where $\tilde{M}_{D(LS)} = M_{D(LS)} U_{TBM} U_R$, $\Delta M = M_i^+ - M_i^- \approx M_R$, $v = v_u$ and r_N and A_{N^-} are given as

$$r_N = \frac{(M_i^+)^2-(M_i^-)^2}{M_i^+ M_i^-} = \frac{\Delta M(M_i^+ + M_i^-)}{M_i^+ M_i^-},$$
$$A_{N^-} \approx \frac{1}{16\pi}\left[\left(\frac{\tilde{M}_D}{v}-\frac{\tilde{M}_{LS}}{v}\right)\left(\frac{\tilde{M}_D}{v}+\frac{\tilde{M}_{LS}}{v}\right)\right]_{ii}. \tag{5.35}$$

In Fig. 5.4, we depict the behavior of CP asymmetry with r_N, which satisfies both neutrino oscillation data and the CP asymmetry required for leptogenesis [118, 119], which will be discussed in the next subsection.

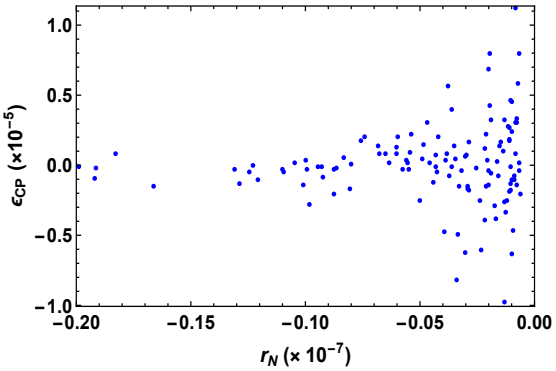

Figure 5.4: Correlation plot demonstrating the dependence of CP asymmetry with the parameter r_N.

$\epsilon^e_{N^-}$	$\epsilon^\mu_{N^-}$	$\epsilon^\tau_{N^-}$	ϵ_{N^-}	ΔM (GeV)
-1.78×10^{-5}	-2.6×10^{-5}	-4.15×10^{-5}	-8.53×10^{-5}	4×10^{-6}

Table 5.3: CP asymmetries and mass splitting obtained from the allowed range of model parameters which satisfy neutrino oscillation data.

5.4.1 Boltzmann Equations

Boltzmann equations are invoked to solve for the lepton asymmetry. It should be reiterated that, the Sakharov criteria [23] require the decay of the parent heavy fermion which ought to be out of equilibrium for generating the lepton asymmetry. In order to implement this, one needs to confront the Hubble expansion rate with the decay rate as

$$K_{N_i^-} = \frac{\Gamma_{N_i^-}}{H(T=M_i^-)}. \tag{5.36}$$

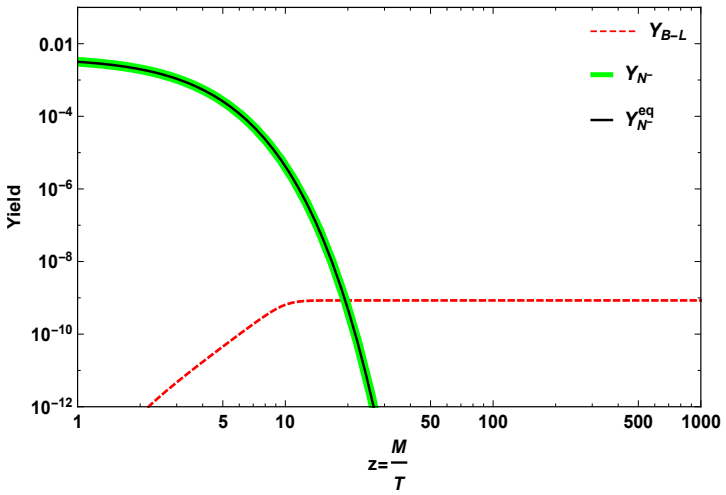

Figure 5.5: Evolution of the yield parameters Y_N and Y_{B-L} as a function of $z \equiv M_{N^-}/T$.

Here, $H = \frac{1.67\sqrt{g_\star}\ T^2}{M_{Pl}}$ is the Hubble rate, with $g_\star = 106.75$ is the number of relativistic degrees of freedom in the thermal bath and $M_{Pl} = 1.22 \times 10^{19}$ GeV is the Planck mass. Coupling strength becomes the deciding factor which assures that inverse decay would not come into thermal equilibrium. For instance, if the strength is below 10^{-7}, it gives $K_{N^-} \sim 1$. The Boltzmann equations associated with evolution of the number densities of right-handed fermion field and lepton can be articulated in terms of the yield parameters, i.e., the ratio of number densities to entropy density, and are expressed as [119–123]

$$\begin{aligned}
\frac{dY_{N^-}}{dz} &= -\frac{z}{sH(M_{N^-})}\left[\left(\frac{Y_{N^-}}{Y_{N^-}^{eq}}-1\right)\gamma_D + \left(\left(\frac{Y_{N^-}}{Y_{N^-}^{eq}}\right)^2 - 1\right)\gamma_S\right], \\
\frac{dY_{B-L}}{dz} &= -\frac{z}{sH(M_{N^-})}\left[2\frac{Y_{B-L}}{Y_\ell^{eq}}\gamma_{Ns} - \epsilon_{N^-}\left(\frac{Y_{N^-}}{Y_{N^-}^{eq}}-1\right)\gamma_D\right],
\end{aligned} \tag{5.37}$$

where $z = M_i^-/T$, s is the entropy density, and the equilibrium number densities have the form [118]

$$Y_{N^-}^{eq} = \frac{135 g_{N^-}}{16\pi^4 g_\star} z^2 K_2(z), \quad Y_\ell^{eq} = \frac{3}{4}\frac{45\zeta(3) g_\ell}{2\pi^4 g_\star}. \tag{5.38}$$

$K_{1,2}$ in Eq. (5.38) represent the modified Bessel functions, the lepton and RH fermion degrees of freedom take the values $g_\ell = 2$ and $g_{N^-} = 2$ and the decay rate γ_D is given as

$$\gamma_D = s Y_{N^-}^{eq} \Gamma_{N^-} \frac{K_1(z)}{K_2(z)}. \tag{5.39}$$

While γ_S represents the scattering rate of $N^-N^- \to \zeta\zeta$ [123] and γ_{Ns} denotes the scattering rate of $\Delta L = 2$ process. One can keep away the delicacy of the asymmetry being produced, even when the RH fermion field N^- is in thermal equilibrium, by subtracting the contribution arising from the exchange of on-shell N^-, i.e., $\frac{\gamma_D}{4}$ from the total rate γ_{Ns} and is given as $\gamma_{Ns}^{sub} = \gamma_{Ns} - \frac{\gamma_D}{4}$ [121].

The solution of Boltzmann eq. (5.37) is displayed in Fig. 5.5. For large coupling strength Y_{N^-} (green-thick curve) almost traces $Y_{N^-}^{eq}$ (black-solid curve) and the generated lepton asymmetry (red-dashed curve). The lepton asymmetry thus obtained can be converted into baryon asymmetry through the sphaleron transition process, and is given as [120]

$$Y_B = -\left(\frac{8N_f + 4N_H}{22N_f + 13N_H}\right) Y_L, \tag{5.40}$$

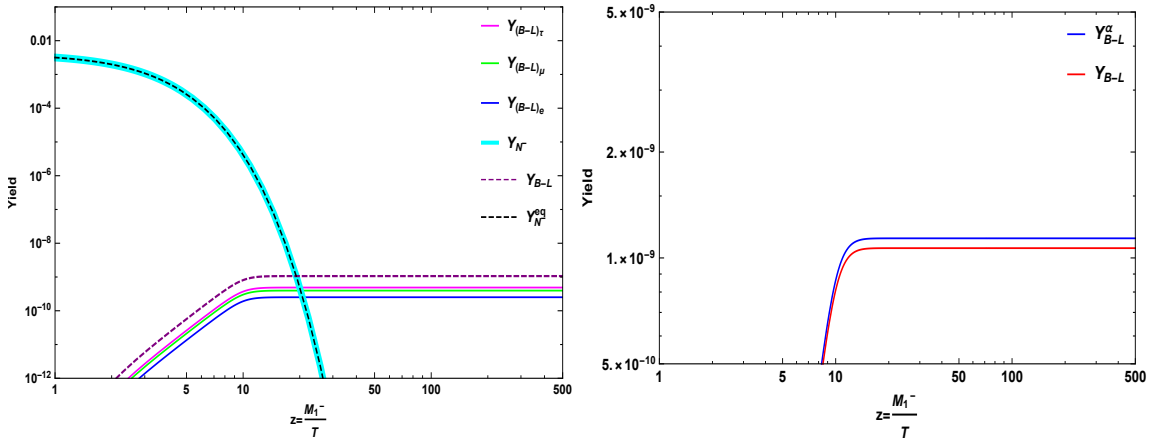

Figure 5.6: After including the flavor effects the yield is shown in left panel, whereas, right panel displays the yield enhancement due to flavor effects.

where N_f represents the number of fermion generations, N_H denotes the no. of Higgs doublets and $Y_L = Y_\ell - Y_{\bar{\ell}}$. The observed baryon asymmetry of the universe generally expressed in terms of baryon to photon ratio as [26]

$$\eta = \frac{n_b - n_{\bar{b}}}{n_\gamma} = 6.08 \times 10^{-10}. \tag{5.41}$$

The current bound on baryon asymmetry can be procured from the relation $Y_B = \eta/7.04$ as $Y_B = 8.6 \times 10^{-11}$. Using the asymptotic value of the lepton asymmetry Y_L as (8.77×10^{-10}) from Fig. 5.5, we obtain the value of baryon asymmetry as $Y_B = -\frac{28}{79}\, Y_L \sim 10^{-10}$.

5.4.2 A note on flavor consideration

In leptogenesis, one flavor approximation is sufficient when ($T > 10^{12}$ GeV), meaning all the Yukawa interactions are out of equilibrium. But for temperatures $\ll 10^8$ GeV, several charged lepton Yukawa couplings come into equilibrium making flavor effects an important consideration for generating the final lepton asymmetry. For temperatures below 10^6 GeV, all the Yukawa interactions are in equilibrium and the asymmetry is stored in the individual lepton flavor. The detailed investigation of flavor effects in type-I leptogenesis can be seen in myriad literature [125–130].

The Boltzmann equation describing the generation of lepton asymmetry in each flavor is [126]

$$\frac{dY^\alpha_{B-L_\alpha}}{dz} = -\frac{z}{sH(M_1^-)}\left[\epsilon^\alpha_{N^-}\left(\frac{Y_{N^-}}{Y^{eq}_{N^-}} - 1\right)\gamma_D - \left(\frac{\gamma^\alpha_D}{2}\right)\frac{A_{\alpha\alpha}Y^\alpha_{B-L_\alpha}}{Y^{eq}_\ell}\right], \tag{5.42}$$

where, $\epsilon^\alpha_{N^-}$ i.e. $(\alpha = e, \mu, \tau)$ represents the CP asymmetry in each lepton flavor

$$\gamma^\alpha_D = sY^{eq}_{N^-}\Gamma^\alpha_{N^-}\frac{K_1(z)}{K_2(z)}, \quad \gamma_D = \sum_\alpha \gamma^\alpha_D.$$

The matrix A is given by [127],

$$A = \begin{pmatrix} -\frac{221}{711} & \frac{16}{711} & \frac{16}{711} \\ \frac{16}{711} & -\frac{221}{711} & \frac{16}{711} \\ \frac{16}{711} & \frac{16}{711} & -\frac{221}{711} \end{pmatrix}.$$

From the benchmark considered in Table. 5.3, we estimate the $B-L$ yield with flavor consideration in the left panel of Fig. 5.6. It is quite obvious to notice that the enhancement in $B-L$ asymmetry is obtained in case of flavor consideration (blue line) over the one flavor approximation (red line), as displayed in the right panel. This is because, in one flavor approximation the decay of the heavy fermion to a particular lepton flavor final state can get washed away by the inverse decays of any flavor unlike the flavoured case [128].

5.5 Conclusion

In this paper, we looked at the effects of A_5' modular symmetry on neutrino phenomenology. The modular flavour symmetry is notable for minimising the complexities involved with using several flavon fields, which are typically associated with the usage of discrete flavour symmetries. In the current model, the SM is expanded by the A_5' modular symmetry as well as a $U(1)_{B-L}$ local gauge symmetry. To achieve the neutrino phenomenology in the linear seesaw framework, it includes three right-handed and three left-handed heavy fermion fields. It also comprises a pair of singlet scalars, which plays an important role in spontaneously breaking the $U(1)_{B-L}$ symmetry and providing masses to the heavy fermions. Another noteworthy aspect is that the Yukawa couplings are thought to transform non-trivially under the modular A_5' group, thereby replacing the role of ordinary flavon fields. As a result, the neutrino mass matrix has a distinct flavour structure, which simplifies the analysis of neutrino phenomenology. We subsequently numerically diagonalized the neutrino mass matrix and determined the allowable regions for the model parameters by comparing it to the present 3σ limit of the oscillation data. Additionally, our model predicts the CP violating phase δ_{CP} to be in the range of $(100^\circ - 250^\circ)$ and the Jarlskog invariant to be $\mathcal{O}(10^{-3})$. The sum of active neutrino masses is found to be in the range $0.058\ \text{eV} \leq \Sigma m_i \leq 0.062$ eV and the value of effective neutrinoless double beta decay mass parameter m_{ee} as $(0.001 - 0.025)$ eV, which is below the current upper limits from KamLAND-Zen experiment i.e., $< (61 - 165)$ meV. Furthermore, the flavour structure of heavy fermion masses leads to three sets of doubly-degenerate mass states, therefore in order to incorporate leptogenesis, we inserted a higher dimensional mass term for RH neutrinos in order to garner a slight mass difference between them. The non-zero CP asymmetry was then found from the lightest heavy fermion decay, where the contribution from the self-energy diagram is partially augmented due to the modest mass splitting between the two lightest heavy fermions. We solved the coupled Boltzmann equations to induce lepton asymmetry at the TeV scale using a specific benchmark of model parameters consistent with oscillation data. The obtained lepton asymmetry is found to be of the of the order $\simeq 10^{-10}$, which is adequate to accommodate the present baryon asymmetry of the universe. Besides, we have additionally shed light on the increase in asymmetry due to flavor consideration.

CHAPTER 6

SUMMARY AND CONCLUSIONS

The concluding remarks to my doctoral work is about delving into the implementation of an unique concept of modular symmetry, alongside, avoiding the excess use of flavon fields and increasing the predictability of the model by not letting non-renormalizable terms to get involved in predictions. This was made possible by introducing the modular form of the Yukawa couplings which has an explicit dependence on Dedekind eta function and an implicit dependence on modulus τ. This makes things more interesting when Yukawa couplings enact the role of flavon fields. Further, different seesaw mechanisms utilized act as catalyst to bring about the neutrino phenomenology results precisely matching the oscillation data.

Therefore, in second chapter, we showcase the linear seesaw framework utilized in making attempts to explain neutrino phenomenology by the help of A_4 modular symmetry which makes things easier and avoids unwanted auperpotential terms by having suitable charge assignments. Further, we discussed leptogenesis which is accounted in the present model by introducing a higher order term bringing a small mass splitting to have a CP asymmetry appropriate to obtain the observed baryon asymmetry of the universe. Further, it also shows the flavor effects arising because the leptogenesis discussed is of TeV scale.

Moving on, in the third chapter, we increase the complexity of the model by ensuring neutrino mass at one loop model which tests the predictability and diversity of modular symmetry by establishing an ideal match with the 3σ data extracted from oscillation experiments. We were also able to accomodate lepton flavor violation which completely explainable in our model predicting an impeccable match with the experimental data. Further, we were able to harbour fermionic dark matter in our model and showed that obtained the relic density is consistent with the observed Planck data.

In chapter four, we explored the double cover of A_5 modular symmetry i.e. $\Gamma'_5 \approx A'_5$ modular symmetry. Its advantage is there are many higher order Yukawa couplings present making it easy to choose accordingly to elaborate

and explain neutrino phenomenology in inverse seesaw framework by avoiding the unwanted term that can ruin the specific flavor structure. We were also successful in explaining the lepton flavor violation i.e. $\ell_i \to \ell_j \gamma$. As we have introduced local gauge symmetry hence the associated neutral Z' gauge boson mass is discussed in light of collider bounds.

FInally, we have extended our knowledge of double cover gained in previous work by implementing it to the linear seesaw framework in chapter five. In this work, we have shown how the phenomenology is quite different because of the involvement of many higher order Yukawa couplings and results drastically changes from that of A_4 symmetry. Here we have discussed the scenario of resonant leptogenesis to get desirable order of CP asymmetry term which then is utilized in the Boltzmann equation of both one flavor and flavored effects of the leptogenesis and yield the correct order of the baryon asymmetry.

Therefore it is evident from the work presented above that experiments and theories go hand in hand. Exploring different mechanisms and technique helps us to explain the unexplainable and at the same time verifies the existing phenomenon which in-return implies that we are on the right track. Theoretical knowledge motivate us to look beyond what is unseen and compel us to upgrade our experiments for new results and findings. At the same time experimental results pushes new ideas and concepts towards validation, provided, they can explain the existing results from the experiments.

APPENDIX

A.1 A_4 modular symmetry

$\bar{\Gamma}$ is the modular group which attains a linear fractional transformation γ which acts on modulus τ linked to the upper-half complex plane whose transformation is given by

$$\tau \longrightarrow \gamma\tau = \frac{a\tau + b}{c\tau + d}\ ,\ \ where\ \ a,b,c,d \in \mathbb{Z}\ \ and\ \ ad - bc = 1,\ \ \mathrm{I}m[\tau] > 0\ , \tag{A.1}$$

where it is isomorphic to the transformation $PSL(2,\mathbb{Z}) = SL(2,\mathbb{Z})/\{I,-I\}$. The S and T transformation helps in generating the modular transformation defined by

$$S : \tau \longrightarrow -\frac{1}{\tau}\ , \qquad\qquad T : \tau \longrightarrow \tau + 1\ , \tag{A.2}$$

and hence the algebric relations so satisfied are as follows,

$$S^2 = \mathbb{I}\ , \qquad (ST)^3 = \mathbb{I}\ . \tag{A.3}$$

Here, series of groups are introduced, $\Gamma(N)$ $(N = 1,2,3,\ldots)$ and defined as

$$\Gamma(N) = \left\{ \begin{pmatrix} a & b \\ c & d \end{pmatrix} \in SL(2,\mathbb{Z})\ ,\ \begin{pmatrix} a & b \\ c & d \end{pmatrix} = \begin{pmatrix} 1 & 0 \\ 0 & 1 \end{pmatrix}\ (\mathrm{mod}N) \right\}. \tag{A.4}$$

Definition of $\bar{\Gamma}(2) \equiv \Gamma(2)/\{I,-I\}$ for $N = 2$. Since $-I$ is not associated with $\Gamma(N)$ for $N > 2$ case, one can have $\bar{\Gamma}(N) = \Gamma(N)$, which are infinite normal subgroup of $\bar{\Gamma}$ known as principal congruence subgroups. Quotient groups come from the finite modular group defined as $\Gamma_N \equiv \bar{\Gamma}/\bar{\Gamma}(N)$. Imposition of $T^N = \mathbb{I}$, is done for these finite groups Γ_N. Thus, the groups Γ_N $(N = 2,3,4,5)$ are isomorphic to S_3, A_4, S_4 and A_5, respectively [230]. N level modular forms are holomorphic functions $f(\tau)$ which are transformed under the influence of $\Gamma(N)$ as follows:

$$f(\gamma\tau) = (c\tau + d)^k f(\tau)\ ,\ \ \gamma \in \Gamma(N)\ , \tag{A.5}$$

where k is the modular weight.

Here the discussion is all about the modular symmetric theory without applying supersymmetry explicitly. This paper comprises of A_4 ($N = 3$) modular group. A field $\phi^{(I)}$ transforms under the modular transformation of Eq.(A.1), as

$$\phi^{(I)} \to (c\tau + d)^{-k_I} \rho^{(I)}(\gamma)\phi^{(I)}, \tag{A.6}$$

where $-k_I$ represents the modular weight and $\rho^{(I)}(\gamma)$ signifies an unitary representation matrix of $\gamma \in \Gamma(2)$.

The scalar fields$'$ kinetic term is as follows

$$\sum_I \frac{|\partial_\mu \phi^{(I)}|^2}{(-i\tau + i\bar{\tau})^{k_I}} , \tag{A.7}$$

which doesn't change under the modular transformation and eventually the overall factor is absorbed by the field redefinition. Thus, the Lagrangian should be invariant under the modular symmetry.

The modular forms of the Yukawa coupling $\mathbf{Y} = (y_1, y_2, y_3)$ with weight 2, which transforms as a triplet of A_4 can be expressed in terms of Dedekind eta-function $\eta(\tau)$ and its derivative [59]:

$$\begin{aligned}
y_1(\tau) &= \frac{i}{2\pi}\left(\frac{\eta'(\tau/3)}{\eta(\tau/3)} + \frac{\eta'((\tau+1)/3)}{\eta((\tau+1)/3)} + \frac{\eta'((\tau+2)/3)}{\eta((\tau+2)/3)} - \frac{27\eta'(3\tau)}{\eta(3\tau)}\right), \\
y_2(\tau) &= \frac{-i}{\pi}\left(\frac{\eta'(\tau/3)}{\eta(\tau/3)} + \omega^2\frac{\eta'((\tau+1)/3)}{\eta((\tau+1)/3)} + \omega\frac{\eta'((\tau+2)/3)}{\eta((\tau+2)/3)}\right), \\
y_3(\tau) &= \frac{-i}{\pi}\left(\frac{\eta'(\tau/3)}{\eta(\tau/3)} + \omega\frac{\eta'((\tau+1)/3)}{\eta((\tau+1)/3)} + \omega^2\frac{\eta'((\tau+2)/3)}{\eta((\tau+2)/3)}\right).
\end{aligned} \tag{A.8}$$

It is interesting to note that the couplings those are defined as singlet under A_4 start from $-k = 4$ while they are zero if $-k = 2$.

APPENDIX B

B.1 Modular form of Yukawa Couplings

The modular forms of the Yukawa coupling $\mathbf{Y} = (y_1, y_2, y_3)$ with weight 2, which transforms as a triplet of A_4 can be expressed in terms of Dedekind eta-function $\eta(\tau)$ and its derivative [59]:

$$\begin{aligned} y_1(\tau) &= \frac{i}{2\pi}\left(\frac{\eta'(\tau/3)}{\eta(\tau/3)} + \frac{\eta'((\tau+1)/3)}{\eta((\tau+1)/3)} + \frac{\eta'((\tau+2)/3)}{\eta((\tau+2)/3)} - \frac{27\eta'(3\tau)}{\eta(3\tau)}\right), \\ y_2(\tau) &= \frac{-i}{\pi}\left(\frac{\eta'(\tau/3)}{\eta(\tau/3)} + \omega^2\frac{\eta'((\tau+1)/3)}{\eta((\tau+1)/3)} + \omega\frac{\eta'((\tau+2)/3)}{\eta((\tau+2)/3)}\right), \\ y_3(\tau) &= \frac{-i}{\pi}\left(\frac{\eta'(\tau/3)}{\eta(\tau/3)} + \omega\frac{\eta'((\tau+1)/3)}{\eta((\tau+1)/3)} + \omega^2\frac{\eta'((\tau+2)/3)}{\eta((\tau+2)/3)}\right). \end{aligned} \tag{B.1}$$

The q-expansion of $y_i(\tau)$ i.e. $(i = 1,2,3)$ is given as

$$\begin{aligned} y_1(\tau) &= 1 + 12q + 36q^2 + 12q^3 + \cdots, \\ y_2(\tau) &= -6q^{1/3}(1 + 7q + 8q^2 + \cdots), \\ y_3(\tau) &= -18q^{2/3}(1 + 2q + 5q^2 + \cdots). \end{aligned} \tag{B.2}$$

It is interesting to note that the couplings those are defined as singlet under A_4 start from $-k = 4$ while they are zero if $-k = 2$.

For, $k = 4$ [278]

$$\begin{aligned} Y_1^{(4)} &= y_1^2 + 2y_2y_3, \quad Y_{1'}^{(4)} = y_3^2 + 2y_1y_2, \quad Y_{1''}^{(4)} = y_2^2 + 2y_1y_3, \\ Y_3^{(4)} &= \begin{pmatrix} y_1^2 - y_2y_3 \\ y_3^2 - 2y_1y_2 \\ y_2^2 - y_1y_3 \end{pmatrix}. \end{aligned} \tag{B.3}$$

For, $k = 8$ [278]

$$\begin{aligned}
Y_1^{(8)} &= (y_1^2+2y_2y_3)^2,\\
Y_{1'}^{(8)} &= (y_1^2+2y_2y_3)(y_3^2+2y_1y_2),\\
Y_{1''}^{(8)} &= (y_3^2+2y_1y_2)^2,\\
Y_{3,1}^{(8)} &= (y_1^2+2y_2y_3)\begin{pmatrix} y_1^2-y_2y_3\\ y_3^2-2y_1y_2\\ y_2^2-y_1y_3\end{pmatrix},\\
Y_{3,2}^{(8)} &= (y_3^2+2y_1y_2)\begin{pmatrix} y_2^2-y_1y_3\\ y_1^2-2y_2y_3\\ y_3^2-y_1y_2\end{pmatrix}.
\end{aligned} \tag{B.4}$$

B.2 One Loop derivation $\left(M_k^2 \simeq m_0^2\right)$

$$(\mathscr{M}_\nu)_{ij} = \sum_k \frac{(Y_D)_{ik}(Y_{LS})_{jk}M_k}{32\pi^2}\left[\frac{M_{\eta_R}^2}{M_{\eta_R}^2-M_k^2}\ln\frac{M_{\eta_R}^2}{M_k^2} - \frac{M_{\eta_I}^2}{M_{\eta_I}^2-M_k^2}\ln\frac{M_{\eta_I}^2}{M_k^2}\right]. \tag{B.5}$$

where, $m_0^2 = \frac{M_{\eta_R}^2+M_{\eta_I}^2}{2}$ and $\frac{M_{\eta_R}^2-M_{\eta_I}^2}{2} = \frac{\zeta_5\lambda'_\eta v^2}{2} = \delta m^2 (say)$. So, one can write $M_{\eta_R}^2 = m_0^2+\delta m^2$ and $M_{\eta_I}^2 = m_0^2-\delta m^2$.

Let $x = M_{\eta_R}^2, M_{\eta_I}^2$ and $A = M_k^2$ and so $f(x) = \frac{x}{x-A}\ln(\frac{x}{A})$. Hence, eqn.(B.5) gets modified as

$$(\mathscr{M}_\nu)_{ij} = \sum_k \frac{(Y_D)_{ik}(Y_{LS})_{jk}M_k}{32\pi^2}\left[f(M_{\eta_R}^2)-f(M_{\eta_I}^2)\right]. \tag{B.6}$$

To express $(M_\nu)_{ij}$ interms of m_0^2 we expand the function $f(x)$ around $x_0 = m_0^2$

$$f(x) = f(x_0) + \frac{df}{dx}\Big|_{x_0}(x-x_0)+\cdots \tag{B.7}$$

And it is important to notice that upto first order expansion will be sufficient, we show the first derivative

$$\begin{aligned}
\frac{df}{dx} &= \frac{d}{dx}\left(\frac{x}{x-A}\ln\frac{x}{A}\right) &\text{(B.8)}\\
&= \frac{1}{(x-A)}\left(1-\frac{A}{x-A}\ln\left(\frac{x}{A}\right)\right) &\text{(B.9)}
\end{aligned}$$

Therefore,

$$\frac{df}{dx} = \frac{x-A-x}{(x-A)^2}\ln\left(\frac{x}{A}\right)+\frac{1}{x-A} = \frac{1}{x-A}\left(1-\frac{A\ln(\frac{x}{A})}{x-A}\right) \tag{B.10}$$

Inserting eqn.(B.7) into eqn.(B.6) we get

$$(\mathscr{M}_\nu)_{ij} = \frac{2\delta m^2}{32\pi^2}\sum_k (Y_D)_{ik}(Y_{LS})_{jk}M_k\frac{df}{dM_{\eta_R}^2}\Big|_{m_0^2}. \tag{B.11}$$

Now, inserting eqn.(B.10) in eqn.(B.11) we get

$$(\mathscr{M}_\nu)_{ij} = \frac{\zeta_5\lambda'_\eta}{32\pi^2}\left[\frac{v}{\sqrt{2}}\right]^2\sum_k (Y_D)_{ik}(Y_{LS})_{jk}\frac{M_k}{m_0^2-M_k^2}\left[1-\frac{M_k^2\ln(\frac{m_0^2}{M_k^2})}{m_0^2-M_k^2}\right]. \tag{B.12}$$

We have considered the case of $M_k^2 \approx m_0^2$, so here we take logarithimic expansion into consideration where $\ln(1+x) = x - \frac{x^2}{2} + \frac{x^3}{3} - \frac{x^4}{4} + \frac{x^5}{5} - \cdots$. So, till second order expansion will be sufficient. Let us consider $w = m_0^2$ and $z = M_k^2$ and $\Delta = w - z$ so that the summand of eqn.(B.12) becomes

$$\frac{1}{w-z}\left[1 - \frac{z}{w-z}\ln\left(\frac{w}{z}\right)\right] = \frac{1}{\Delta}\left[1 - \frac{z}{\Delta}\ln\left(\frac{z+\Delta}{z}\right)\right]. \tag{B.13}$$

In the limit $\Delta \to 0$

$$\lim_{\Delta\to 0}\frac{1}{\Delta}\left[1 - \frac{z}{\Delta}\ln\frac{z+\Delta}{z}\right] = \lim_{\Delta\to 0}\frac{1}{\Delta}\left[1 - \frac{z}{\Delta}\ln\left(\frac{z+\Delta}{z}\right)\right] \tag{B.14}$$

$$= \lim_{\Delta\to 0}\frac{1}{\Delta}\left[1 - \frac{z}{\Delta}\left(\frac{\Delta}{z} - \frac{1}{2}\frac{\Delta^2}{z^2} + \cdots\right)\right] \tag{B.15}$$

$$= \lim_{\Delta\to 0}\frac{1}{\Delta}\left[1 - 1 + \frac{\Delta}{2z} + \cdots\right] = \frac{1}{2z}. \tag{B.16}$$

Thus after substituting the above deduction in eqn.(B.12), we get

$$(\mathcal{M}_\nu)_{ij} = \frac{\zeta_5\lambda'_\eta}{32\pi^2}\left[\frac{v}{\sqrt{2}}\right]^2\sum_k (Y_D)_{ik}(Y_{LS})_{jk}\frac{1}{M_k}. \tag{B.17}$$

B.3 Loop Functions for LFV

The loop functions for the LFV decay processes $\mu \to e\gamma$ and $\mu \to 3e$ are given as

$$\mathscr{G}_1(x) = \frac{1}{6}\left[\frac{1 - 2x(3 - 1.5x - x^2 + 3xlogx)}{(1-x)^4}\right], \tag{B.18}$$

$$\mathscr{G}_2(x) = \frac{2 - 9x + 18x^2 - 11x^3 + 6x^3\log x}{6(1-x)^4}, \tag{B.19}$$

$$\mathscr{D}_1(x,y) = -\frac{1}{(1-x)(1-y)} - \frac{x^2\log x}{(1-x)^2(x-y)} - \frac{y^2\log y}{(1-y)^2(y-x)}, \tag{B.20}$$

$$\mathscr{D}_2(x,y) = -\frac{1}{(1-x)(1-y)} - \frac{x\log x}{(1-x)^2(x-y)} - \frac{y\log y}{(1-y)^2(y-x)}. \tag{B.21}$$

APPENDIX C

C.1 The modular space of $\Gamma(5)$

In order to establish the modular forms which transform non-trivially under Γ'_5, and is isomorphic to A'_5, it is first required to find out the modular space of $\Gamma(5)$. Hence, if k is an integer i.e. non-negative, the modular space $M_k[\Gamma(5)]$ bearing weight k for $\Gamma(5)$ contains $5k+1$ linearly independent modular forms, which acts like the basis vectors of the modular space. According to Ref. [279], we have

$$M_k[\Gamma(5)] = \bigoplus_{\substack{a+b=5k \\ a,b\geq 0}} \mathbf{C}\, \frac{\eta(5\tau)^{15k}}{\eta(\tau)^{3k}}\, \mathsf{k}^{a}_{\frac{1}{5},\frac{0}{5}}(5\tau)\, \mathsf{k}^{b}_{\frac{2}{5},\frac{0}{5}}(5\tau)\,, \tag{C.1}$$

below given is the Dedekind eta function $\eta(\tau)$

$$\eta(\tau) = q^{1/24} \prod_{n=1}^{\infty} \left(1-q^n\right), \tag{C.2}$$

where, $q \equiv e^{2i\pi\tau}$, and $\mathsf{k}_{r_1,r_2}(\tau)$ is the Klein form

$$\mathsf{k}_{r_1,r_2}(\tau) = q_z^{(r_1-1)/2}\left(1-q_z\right) \times \prod_{n=1}^{\infty} \left(1-q^n q_z\right)\left(1-q^n q_z^{-1}\right)\left(1-q^n\right)^{-2}, \tag{C.3}$$

where (r_1, r_2) depicts a pair of rational numbers in the domain of $\mathbf{Q}^2 - \mathbf{Z}^2$, $z \equiv \tau r_1 + r_2$ and $q_z \equiv e^{2i\pi z}$. Under the transformations of S and T, the eta function and the Klein form change as follows

$$\begin{aligned} S \quad &: \quad \eta(\tau) \to \sqrt{-i\tau}\,\eta(\tau)\,, \qquad \mathsf{k}_{r_1,r_2}(\tau) \to -\frac{1}{\tau}\,\mathsf{k}_{-r_2,r_1}(\tau)\,, \\ T \quad &: \quad \eta(\tau) \to e^{i\pi/12}\eta(\tau)\,, \qquad \mathsf{k}_{r_1,r_2}(\tau) \to \mathsf{k}_{r_1,r_1+r_2}(\tau)\,. \end{aligned} \tag{C.4}$$

More information about the properties of the Kein form $\mathsf{k}_{r_1,r_2}(\tau)$ can be found in Refs. [279, 280].

C.2 The Kronecker product rules of A_5'

Here we present only those product rules [158] which are relevant to present model .

$$\mathbf{3}\otimes\mathbf{3}=\mathbf{1}_{\rm s}\oplus\mathbf{3}_{\rm a}\oplus\mathbf{5}_{\rm s}$$

$$\begin{cases}
\mathbf{1}_{\rm s}: \dfrac{\sqrt{3}}{3}(\alpha_1\beta_1+\alpha_2\beta_3+\alpha_3\beta_2)\\
\mathbf{3}_{\rm a}: \dfrac{\sqrt{2}}{2}\begin{pmatrix}\alpha_2\beta_3-\alpha_3\beta_2\\ \alpha_1\beta_2-\alpha_2\beta_1\\ \alpha_3\beta_1-\alpha_1\beta_3\end{pmatrix}\\
\mathbf{5}_{\rm s}: \dfrac{\sqrt{6}}{6}\begin{pmatrix}2\alpha_1\beta_1-\alpha_2\beta_3-\alpha_3\beta_2\\ -\sqrt{3}\alpha_1\beta_2-\sqrt{3}\alpha_2\beta_1\\ \sqrt{6}\alpha_2\beta_2\\ \sqrt{6}\alpha_3\beta_3\\ -\sqrt{3}\left(\alpha_1\beta_3+\alpha_3\beta_1\right)\end{pmatrix}
\end{cases}$$

$$\mathbf{3}'\otimes\mathbf{3}'=\mathbf{1}_{\rm s}\oplus\mathbf{3}'_{\rm a}\oplus\mathbf{5}_{\rm s}$$

$$\begin{cases}
\mathbf{1}_{\rm s}: \dfrac{\sqrt{3}}{3}\left(\alpha_1\beta_1+\alpha_2\beta_3+\alpha_3\beta_2\right)\\
\mathbf{3}'_{\rm a}: \dfrac{\sqrt{2}}{2}\begin{pmatrix}\alpha_2\beta_3-\alpha_3\beta_2\\ \alpha_1\beta_2-\alpha_2\beta_1\\ \alpha_3\beta_1-\alpha_1\beta_3\end{pmatrix}\\
\mathbf{5}_{\rm s}: \dfrac{\sqrt{6}}{6}\begin{pmatrix}2\alpha_1\beta_1-\alpha_2\beta_3-\alpha_3\beta_2\\ \sqrt{6}\alpha_3\beta_3\\ -\sqrt{3}\left(\alpha_1\beta_2+\alpha_2\beta_1\right)\\ -\sqrt{3}\left(\alpha_1\beta_3+\alpha_3\beta_1\right)\\ \sqrt{6}\alpha_2\beta_2\end{pmatrix}
\end{cases}$$

$$\mathbf{3}\otimes\mathbf{3}'=\mathbf{4}\oplus\mathbf{5}$$

$$\begin{cases}
\mathbf{4}: \dfrac{\sqrt{3}}{3}\begin{pmatrix}\sqrt{2}\alpha_2\beta_1+\alpha_3\beta_2\\ -\sqrt{2}\alpha_1\beta_2-\alpha_3\beta_3\\ -\sqrt{2}\alpha_1\beta_3-\alpha_2\beta_2\\ \sqrt{2}\alpha_3\beta_1+\alpha_2\beta_3\end{pmatrix}\\
\mathbf{5}: \dfrac{\sqrt{3}}{3}\begin{pmatrix}\sqrt{3}\alpha_1\beta_1\\ \alpha_2\beta_1-\sqrt{2}\alpha_3\beta_2\\ \alpha_1\beta_2-\sqrt{2}\alpha_3\beta_3\\ \alpha_1\beta_3-\sqrt{2}\alpha_2\beta_2\\ \alpha_3\beta_1-\sqrt{2}\alpha_2\beta_3\end{pmatrix}
\end{cases}$$

$$\mathbf{3}\otimes\mathbf{3}'=\mathbf{4}\oplus\mathbf{5}$$

$$\begin{cases}
\mathbf{4}: \dfrac{1}{\sqrt{3}}\begin{bmatrix}\sqrt{2}\alpha_2\beta_1+\alpha_3\beta_2\\ -\sqrt{2}\alpha_1\beta_2-\alpha_3\beta_3\\ -\sqrt{2}\alpha_1\beta_3-\alpha_2\beta_2\\ \sqrt{2}\alpha_3\beta_1+\alpha_2\beta_3\text{“”}\end{bmatrix}\\
\mathbf{5}: \dfrac{1}{\sqrt{3}}\begin{bmatrix}\sqrt{3}\alpha_1\beta_1\\ \alpha_2\beta_1-\sqrt{2}\alpha_3\beta_2\\ \alpha_1\beta_2-\sqrt{2}\alpha_3\beta_3\\ \alpha_1\beta_3-\sqrt{2}\alpha_2\beta_2\\ \alpha_3\beta_1-\sqrt{2}\alpha_2\beta_3\end{bmatrix}
\end{cases}.$$

$$\mathbf{4}\otimes\mathbf{4}=\mathbf{1}_{\rm s}\oplus\mathbf{3}_{\rm a}\oplus\mathbf{3}'_{\rm a}\oplus\mathbf{4}_{\rm s}\oplus\mathbf{5}_{\rm s}$$

$$\begin{cases}
\mathbf{1}_{\rm s}: \dfrac{1}{2}\left[\alpha_1\beta_4+\alpha_2\beta_3+\alpha_3\beta_2+\alpha_4\beta_1\right]\\
\mathbf{3}_{\rm a}: \dfrac{1}{2}\begin{bmatrix}-\alpha_1\beta_4+\alpha_2\beta_3-\alpha_3\beta_2+\alpha_4\beta_1\\ \sqrt{2}\left(\alpha_2\beta_4-\alpha_4\beta_2\right)\\ \sqrt{2}\left(\alpha_1\beta_3-\alpha_3\beta_1\right)\end{bmatrix}\\
\mathbf{3}'_{\rm a}: \dfrac{1}{2}\begin{bmatrix}\alpha_1\beta_4+\alpha_2\beta_3-\alpha_3\beta_2-\alpha_4\beta_1\\ \sqrt{2}\left(\alpha_3\beta_4-\alpha_4\beta_3\right)\\ \sqrt{2}\left(\alpha_1\beta_2-\alpha_2\beta_1\right)\end{bmatrix}\\
\mathbf{4}_{\rm s}: \dfrac{1}{\sqrt{3}}\begin{bmatrix}\alpha_2\beta_4+\alpha_3\beta_3+\alpha_4\beta_2\\ \alpha_1\beta_1+\alpha_3\beta_4+\alpha_4\beta_3\\ \alpha_1\beta_2+\alpha_2\beta_1+\alpha_4\beta_4\\ \alpha_1\beta_3+\alpha_2\beta_2+\alpha_3\beta_1\end{bmatrix}\\
\mathbf{5}_{\rm s}: \dfrac{1}{2\sqrt{3}}\begin{bmatrix}\sqrt{3}\left(\alpha_1\beta_4-\alpha_2\beta_3-\alpha_3\beta_2+\alpha_4\beta_1\right)\\ -\sqrt{2}\left(\alpha_2\beta_4-2\alpha_3\beta_3+\alpha_4\beta_2\right)\\ -\sqrt{2}\left(2\alpha_1\beta_1-\alpha_3\beta_4-\alpha_4\beta_3\right)\\ \sqrt{2}\left(\alpha_1\beta_2+\alpha_2\beta_1-2\alpha_4\beta_4\right)\\ -\sqrt{2}\left(\alpha_1\beta_3-2\alpha_2\beta_2+\alpha_3\beta_1\right)\end{bmatrix}
\end{cases}.$$

$$\mathbf{5}\otimes\mathbf{5}=\mathbf{1}_{\rm s}\oplus\mathbf{3}_{\rm a}\oplus\mathbf{3}'_{\rm a}\oplus\mathbf{4}_{\rm s}\oplus\mathbf{4}_{\rm a}\oplus\mathbf{5}_{\rm s,1}\oplus\mathbf{5}_{\rm s,2}$$

$$\left\{\begin{array}{l}
\mathbf{1}_{\rm s}:\dfrac{1}{\sqrt{5}}\left[\alpha_1\beta_1+\alpha_2\beta_5+\alpha_3\beta_4+\alpha_4\beta_3+\alpha_5\beta_2\right]\\[2ex]
\mathbf{3}_{\rm a}:\dfrac{1}{\sqrt{10}}\begin{bmatrix}\alpha_2\beta_5+2\alpha_3\beta_4-2\alpha_4\beta_3-\alpha_5\beta_2\\ -\sqrt{3}\alpha_1\beta_2+\sqrt{3}\alpha_2\beta_1+\sqrt{2}\alpha_3\beta_5-\sqrt{2}\alpha_5\beta_3\\ \sqrt{3}\alpha_1\beta_5+\sqrt{2}\alpha_2\beta_4-\sqrt{2}\alpha_4\beta_2-\sqrt{3}\alpha_5\beta_1\end{bmatrix}\\[2ex]
\mathbf{3}'_{\rm a}:\dfrac{1}{\sqrt{10}}\begin{bmatrix}2\alpha_2\beta_5-\alpha_3\beta_4+\alpha_4\beta_3-2\alpha_5\beta_2\\ \sqrt{3}\alpha_1\beta_3-\sqrt{3}\alpha_3\beta_1+\sqrt{2}\alpha_4\beta_5-\sqrt{2}\alpha_5\beta_4\\ -\sqrt{3}\alpha_1\beta_4+\sqrt{2}\alpha_2\beta_3-\sqrt{2}\alpha_3\beta_2+\sqrt{3}\alpha_4\beta_1\end{bmatrix}\\[2ex]
\mathbf{4}_{\rm s}:\dfrac{1}{\sqrt{30}}\begin{bmatrix}\sqrt{6}\alpha_1\beta_2+\sqrt{6}\alpha_2\beta_1-\alpha_3\beta_5+4\alpha_4\beta_4-\alpha_5\beta_3\\ \sqrt{6}\alpha_1\beta_3+4\alpha_2\beta_2+\sqrt{6}\alpha_3\beta_1-\alpha_4\beta_5-\alpha_5\beta_4\\ \sqrt{6}\alpha_1\beta_4-\alpha_2\beta_3-\alpha_3\beta_2+\sqrt{6}\alpha_4\beta_1+4\alpha_5\beta_5\\ \sqrt{6}\alpha_1\beta_5-\alpha_2\beta_4+4\alpha_3\beta_3-\alpha_4\beta_2+\sqrt{6}\alpha_5\beta_1\end{bmatrix}\\[2ex]
\mathbf{4}_{\rm a}:\dfrac{1}{\sqrt{10}}\begin{bmatrix}\sqrt{2}\alpha_1\beta_2-\sqrt{2}\alpha_2\beta_1+\sqrt{3}\alpha_3\beta_5-\sqrt{3}\alpha_5\beta_3\\ -\sqrt{2}\alpha_1\beta_3+\sqrt{2}\alpha_3\beta_1+\sqrt{3}\alpha_4\beta_5-\sqrt{3}\alpha_5\beta_4\\ -\sqrt{2}\alpha_1\beta_4-\sqrt{3}\alpha_2\beta_3+\sqrt{3}\alpha_3\beta_2+\sqrt{2}\alpha_4\beta_1\\ \sqrt{2}\alpha_1\beta_5-\sqrt{3}\alpha_2\beta_4+\sqrt{3}\alpha_4\beta_2-\sqrt{2}\alpha_5\beta_1\end{bmatrix}\\[2ex]
\mathbf{5}_{\rm s,1}:\dfrac{1}{\sqrt{14}}\begin{bmatrix}2\alpha_1\beta_1+\alpha_2\beta_5-2\alpha_3\beta_4-2\alpha_4\beta_3+\alpha_5\beta_2\\ \alpha_1\beta_2+\alpha_2\beta_1+\sqrt{6}\alpha_3\beta_5+\sqrt{6}\alpha_5\beta_3\\ -2\alpha_1\beta_3+\sqrt{6}\alpha_2\beta_2-2\alpha_3\beta_1\\ -2\alpha_1\beta_4-2\alpha_4\beta_1+\sqrt{6}\alpha_5\beta_5\\ \alpha_1\beta_5+\sqrt{6}\alpha_2\beta_4+\sqrt{6}\alpha_4\beta_2+\alpha_5\beta_1\end{bmatrix}\\[2ex]
\mathbf{5}_{\rm s,2}:\dfrac{1}{\sqrt{14}}\begin{bmatrix}2\alpha_1\beta_1-2\alpha_2\beta_5+\alpha_3\beta_4+\alpha_4\beta_3-2\alpha_5\beta_2\\ -2\alpha_1\beta_2-2\alpha_2\beta_1+\sqrt{6}\alpha_4\beta_4\\ \alpha_1\beta_3+\alpha_3\beta_1+\sqrt{6}\alpha_4\beta_5+\sqrt{6}\alpha_5\beta_4\\ \alpha_1\beta_4+\sqrt{6}\alpha_2\beta_3+\sqrt{6}\alpha_3\beta_2+\alpha_4\beta_1\\ -2\alpha_1\beta_5+\sqrt{6}\alpha_3\beta_3-2\alpha_5\beta_1\end{bmatrix}
\end{array}\right\}.$$

C.3 Higher Order Yukawa couplings

All higher order Yukawa couplings are expressed interms of the elements of $Y^{(1)}_{\hat{\mathbf{6}}}$ Yukawa coupling expressed as

$$Y^{(1)}_{\hat{\mathbf{6}}} = \begin{bmatrix} Y_1 \\ Y_2 \\ Y_3 \\ Y_4 \\ Y_5 \\ Y_6 \end{bmatrix} = \begin{bmatrix} \hat{e}_1 - 3\hat{e}_6 \\ 5\sqrt{2}\,\hat{e}_2 \\ 10\hat{e}_3 \\ 10\hat{e}_4 \\ 5\sqrt{2}\,\hat{e}_5 \\ -3\hat{e}_1 - \hat{e}_6 \end{bmatrix}, \tag{C.5}$$

The Yukawa couplings used in our model are expressed below and the other couplings seen in the tensor product are expressed in [158]

$$Y^{(2)}_{\mathbf{3}} = \left[Y^{(1)}_{\hat{\mathbf{6}}} \otimes Y^{(1)}_{\hat{\mathbf{6}}}\right]_{\mathbf{3}_{s,1}} = -3\begin{bmatrix} \hat{e}_1^2 - 36\hat{e}_1\hat{e}_6 - \hat{e}_6^2 \\ 5\sqrt{2}\,\hat{e}_2(\hat{e}_1 - 3\hat{e}_6) \\ 5\sqrt{2}\,\hat{e}_5(3\hat{e}_1 + \hat{e}_6) \end{bmatrix} = -3\begin{bmatrix} Y_1^2 - 3Y_1Y_6 - Y_6^2 \\ Y_1Y_2 \\ -Y_5Y_6 \end{bmatrix}, \tag{C.6}$$

$$Y^{(4)}_{\mathbf{3}} = \left[Y^{(1)}_{\hat{\mathbf{6}}} \otimes Y^{(3)}_{\hat{\mathbf{6}},2}\right]_{\mathbf{3}_{s,1}} = \frac{\sqrt{3}}{4}\begin{bmatrix} \left(Y_1^2 + Y_6^2\right)\left(7Y_1^2 - 18Y_1Y_6 - 7Y_6^2\right) \\ Y_2\left(13Y_1^3 - 3Y_1^2Y_6 - 29Y_1Y_6^2 - 9Y_6^3\right) \\ -Y_5\left(9Y_1^3 - 29Y_1^2Y_6 + 3Y_1Y_6^2 + 13Y_6^3\right) \end{bmatrix}, \tag{C.7}$$

$$Y^{(6)}_{\mathbf{3},1} = \left[Y^{(1)}_{\hat{\mathbf{6}}} \otimes Y^{(5)}_{\hat{\mathbf{2}}'}\right]_{\mathbf{3}} = \frac{9\sqrt{2}}{16}\left(Y_1^2 - 4Y_1Y_6 - Y_6^2\right)\begin{bmatrix} (Y_1 - 3Y_6)(3Y_1 + Y_6)\left(3Y_1^2 - 2Y_1Y_6 - 3Y_6^2\right) \\ 2Y_2\left(2Y_1^3 - 9Y_1Y_6^2 - 3Y_6^3\right) \\ 2Y_5\left(3Y_1^3 - 9Y_1^2Y_6 + 2Y_6^3\right) \end{bmatrix}, \tag{C.8}$$

$$Y^{(6)}_{\mathbf{3},2} = \left[Y^{(1)}_{\hat{\mathbf{6}}} \otimes Y^{(5)}_{\hat{\mathbf{6}},1}\right]_{\mathbf{3}_{s,1}} = 3\sqrt{2}\left(Y_1^4 - 3Y_1^3Y_6 - Y_1^2Y_6^2 + 3Y_1Y_6^3 + Y_6^4\right)\begin{bmatrix} Y_1^2 - 3Y_1Y_6 - Y_6^2 \\ Y_1Y_2 \\ -Y_5Y_6 \end{bmatrix}, \tag{C.9}$$

$$Y^{(6)}_{\mathbf{4},1} = \left[Y^{(1)}_{\hat{\mathbf{6}}} \otimes Y^{(5)}_{\hat{\mathbf{2}}}\right]_{\mathbf{4}} = -\frac{3}{4}\left(Y_1^2 - 4Y_1Y_6 - Y_6^2\right)^2\begin{bmatrix} -\sqrt{2}Y_2(3Y_1 + Y_6) \\ Y_3(Y_1 + Y_6) \\ Y_4(Y_1 - Y_6) \\ \sqrt{2}Y_5(Y_1 - 3Y_6) \end{bmatrix}, \tag{C.10}$$

$$Y^{(6)}_{\mathbf{4},2} = \left[Y^{(1)}_{\hat{\mathbf{6}}} \otimes Y^{(5)}_{\hat{\mathbf{2}}'}\right]_{\mathbf{4}} = -\frac{\sqrt{6}}{8}\left(Y_1^2 - 4Y_1Y_6 - Y_6^2\right)\begin{bmatrix} \sqrt{2}Y_2\left(Y_1^3 + 11Y_1^2Y_6 + 19Y_1Y_6^2 + 5Y_6^3\right) \\ Y_3\left(13Y_1^3 - 31Y_1^2Y_6 - 17Y_1Y_6^2 - Y_6^3\right) \\ Y_4\left(Y_1^3 - 17Y_1^2Y_6 + 31Y_1Y_6^2 + 13Y_6^3\right) \\ \sqrt{2}Y_5\left(5Y_1^3 - 19Y_1^2Y_6 + 11Y_1Y_6^2 - Y_6^3\right) \end{bmatrix}, \tag{C.11}$$

$$Y^{(6)}_{\mathbf{5},1} = \left[Y^{(1)}_{\hat{\mathbf{6}}} \otimes Y^{(5)}_{\hat{\mathbf{4}}}\right]_{\mathbf{5},2} = \frac{\sqrt{10}}{8}\left(Y_1^2 - 4Y_1Y_6 - Y_6^2\right)\begin{bmatrix} \sqrt{3}(Y_1 - 3Y_6)(3Y_1 + Y_6)\left(Y_1^2 + Y_6^2\right) \\ -2Y_2(2Y_1 + Y_6)\left(2Y_1^2 - 3Y_1Y_6 - Y_6^2\right) \\ \sqrt{2}Y_3\left(Y_1^3 + 2Y_1^2Y_6 - 11Y_1Y_6^2 - 4Y_6^3\right) \\ \sqrt{2}Y_4\left(4Y_1^3 - 11Y_1^2Y_6 - 2Y_1Y_6^2 + Y_6^3\right) \\ 2Y_5(Y_1 - 2Y_6)\left(Y_1^2 - 3Y_1Y_6 - 2Y_6^2\right) \end{bmatrix}, \tag{C.12}$$

$$Y^{(6)}_{\mathbf{5},2} = \left[Y^{(1)}_{\hat{\mathbf{6}}} \otimes Y^{(5)}_{\hat{\mathbf{6}},1}\right]_{\mathbf{5}_s} = -\frac{1}{\sqrt{2}}\left(Y_1^4 - 3Y_1^3Y_6 - Y_1^2Y_6^2 + 3Y_1Y_6^3 + Y_6^4\right)\begin{bmatrix} \sqrt{2}\left(Y_1^2 + Y_6^2\right) \\ 2\sqrt{6}Y_2(2Y_1 + Y_6) \\ -\sqrt{3}Y_3(3Y_1 - Y_6) \\ \sqrt{3}Y_4(Y_1 + 3Y_6) \\ -2\sqrt{6}Y_5(Y_1 - 2Y_6) \end{bmatrix}. \tag{C.13}$$

BIBLIOGRAPHY

[1] S.L. Glashow, *Partial Symmetries of Weak Interactions*, *Nucl. Phys.* **22** (1961) 579.

[2] S. Weinberg, *A Model of Leptons*, *Phys. Rev. Lett.* **19** (1967) 1264.

[3] J. Goldstone, A. Salam and S. Weinberg, *Broken symmetries*, *Phys. Rev.* **127** (Aug, 1962) 965, https://link.aps.org/doi/10.1103/PhysRev.127.965.

[4] J. Goldstone, A. Salam and S. Weinberg, *Broken Symmetries*, *Phys. Rev.* **127** (1962) 965.

[5] R. Davis, D.S. Harmer and K.C. Hoffman, *Search for neutrinos from the sun*, *Phys. Rev. Lett.* **20** (May, 1968) 1205, https://link.aps.org/doi/10.1103/PhysRevLett.20.1205.

[6] J.N. Bahcall, M.H. Pinsonneault and S. Basu, *Solar models: Current epoch and time dependences, neutrinos, and helioseismological properties*, *Astrophys. J.* **555** (2001) 990 [astro-ph/0010346].

[7] SUPER-KAMIOKANDE collaboration, Y. Fukuda et al., *The Super-Kamiokande detector*, *Nucl. Instrum. Meth. A* **501** (2003) 418.

[8] SNO collaboration, A.B. McDonald et al., *Direct evidence for neutrino flavor transformation from neutral-current interactions in SNO*, *AIP Conf. Proc.* **646** (2002) 43.

[9] KAMLAND collaboration, S. Abe et al., *Precision Measurement of Neutrino Oscillation Parameters with KamLAND*, *Phys. Rev. Lett.* **100** (2008) 221803 [arXiv:0801.4589].

[10] T2K collaboration, K. Abe et al., *Indication of Electron Neutrino Appearance from an Accelerator-produced Off-axis Muon Neutrino Beam*, *Phys. Rev. Lett.* **107** (2011) 041801 [arXiv:1106.2822].

[11] DOUBLE CHOOZ collaboration, Y. Abe et al., *Indication of Reactor $\bar{\nu}_e$ Disappearance in the Double Chooz Experiment*, *Phys. Rev. Lett.* **108** (2012) 131801 [arXiv:1112.6353].

[12] DAYA BAY collaboration, F.P. An et al., *Observation of electron-antineutrino disappearance at Daya Bay*, *Phys. Rev. Lett.* **108** (2012) 171803 [arXiv:1203.1669].

[13] MINOS collaboration, P. Adamson et al., *Electron neutrino and antineutrino appearance in the full MINOS data sample*, *Phys. Rev. Lett.* **110** (2013) 171801 [arXiv:1301.4581].

[14] M. Ghosh, *Present Aspects and Future Prospects of Neutrino Mass and Oscillation*, Ph.D. thesis, Mohanlal Sukhadia U., 2015.
arXiv:1603.04514.

[15] C. Giunti and C.W. Kim, *Fundamentals of Neutrino Physics and Astrophysics* (2007).

[16] M. Czakon, M. Zralek and J. Gluza, *Are neutrinos Dirac or Majorana particles?*, *Acta Phys. Polon. B* **30** (1999) 3121 [hep-ph/9910357].

[17] E. Ma and O. Popov, *Pathways to Naturally Small Dirac Neutrino Masses*, *Phys. Lett. B* **764** (2017) 142 [arXiv:1609.02538].

[18] A.G. Dias, C.A. de S. Pires and P.S. Rodrigues da Silva, *How the inverse seesaw mechanism can reveal itself natural, canonical, and independent of the right-handed neutrino mass*, *Phys. Rev. D* **84** (Sep, 2011) 053011, https://link.aps.org/doi/10.1103/PhysRevD.84.053011.

[19] E. Ma, *Deciphering the Seesaw Nature of Neutrino Mass from Unitarity Violation*, *Mod. Phys. Lett. A* **24** (2009) 2161 [arXiv:0904.1580].

[20] H.P. Nilles, S. Ramos-Sánchez and P.K.S. Vaudrevange, *Eclectic Flavor Groups*, *JHEP* **02** (2020) 045 [arXiv:2001.01736].

[21] P.P. Novichkov, J.T. Penedo and S.T. Petcov, *Double cover of modular S_4 for flavour model building*, *Nucl. Phys. B* **963** (2021) 115301 [arXiv:2006.03058].

[22] J.M. Cline, *TASI Lectures on Early Universe Cosmology: Inflation, Baryogenesis and Dark Matter*, *PoS* **TASI2018** (2019) 001 [arXiv:1807.08749].

[23] A. Sakharov, *Violation of CP Invariance, C asymmetry, and baryon asymmetry of the universe*, *Sov. Phys. Usp.* **34** (1991) 392.

[24] M. van der Meulen, D. Sexty, J. Smit and A. Tranberg, *Chern-Simons and winding number in a tachyonic electroweak transition*, *JHEP* **02** (2006) 029 [hep-ph/0511080].

[25] WMAP collaboration, G. Hinshaw et al., *Nine-Year Wilkinson Microwave Anisotropy Probe (WMAP) Observations: Cosmological Parameter Results*, *Astrophys. J. Suppl.* **208** (2013) 19 [arXiv:1212.5226].

[26] PLANCK collaboration, N. Aghanim et al., *Planck 2018 results. VI. Cosmological parameters*, *Astron. Astrophys.* **641** (2020) A6 [arXiv:1807.06209].

[27] G. Bertone and D. Hooper, *History of dark matter*, *Rev. Mod. Phys.* **90** (Oct, 2018) 045002, https://link.aps.org/doi/10.1103/RevModPhys.90.045002.

[28] F. Zwicky, *On the Masses of Nebulae and of Clusters of Nebulae*, *apj* **86** (Oct., 1937) 217.

[29] G.R. Blumenthal, S.M. Faber, J.R. Primack and M.J. Rees, *Formation of galaxies and large-scale structure with cold dark matter.*, *nat* **311** (Oct., 1984) 517.

[30] J.F. Navarro, C.S. Frenk and S.D.M. White, *The Structure of cold dark matter halos*, *Astrophys. J.* **462** (1996) 563 [astro-ph/9508025].

[31] V.C. Rubin and W.K. Ford Jr, *Rotation of the andromeda nebula from a spectroscopic survey of emission regions*, *The Astrophysical Journal* **159** (1970) 379.

[32] K.C. Freeman, *On the disks of spiral and SO Galaxies*, *Astrophys. J.* **160** (1970) 811.

[33] V.C. Rubin, W.K. Ford, Jr. and N. Thonnard, *Extended rotation curves of high-luminosity spiral galaxies. IV. Systematic dynamical properties, Sa through Sc*, *Astrophys. J. Lett.* **225** (1978) L107.

[34] A. Faessler, *Status of the determination of the electron–neutrino mass*, *Prog. Part. Nucl. Phys.* **113** (2020) 103789.

[35] KATRIN collaboration, M. Aker et al., *Improved Upper Limit on the Neutrino Mass from a Direct Kinematic Method by KATRIN*, *Phys. Rev. Lett.* **123** (2019) 221802 [arXiv:1909.06048].

[36] F. Feruglio, *Neutrino masses and mixing angles: A tribute to Guido Altarelli*, *Frascati Phys. Ser.* **64** (2017) 174.

[37] KamLAND collaboration, T. Araki et al., *Measurement of neutrino oscillation with KamLAND: Evidence of spectral distortion*, *Phys. Rev. Lett.* **94** (2005) 081801 [hep-ex/0406035].

[38] B. Pontecorvo, *Neutrino Experiments and the Problem of Conservation of Leptonic Charge*, *Sov. Phys. JETP* **26** (1968) 984.

[39] T2K collaboration, K. Abe et al., *Search for heavy neutrinos with the T2K near detector ND280*, *Phys. Rev. D* **100** (2019) 052006 [arXiv:1902.07598].

[40] Planck collaboration, N. Aghanim et al., *Planck 2018 results. VI. Cosmological parameters*, arXiv:1807.06209.

[41] Particle Data Group collaboration, M. Tanabashi et al., *Review of Particle Physics*, *Phys. Rev.* **D98** (2018) 030001.

[42] S. Weinberg, *Varieties of Baryon and Lepton Nonconservation*, *Phys. Rev.* **D22** (1980) 1694.

[43] S. Weinberg, *Baryon and Lepton Nonconserving Processes*, *Phys. Rev. Lett.* **43** (1979) 1566.

[44] F. Wilczek and A. Zee, *Operator Analysis of Nucleon Decay*, *Phys. Rev. Lett.* **43** (1979) 1571.

[45] B. Gripaios, *Lectures on Physics Beyond the Standard Model*, arXiv:1503.02636.

[46] P. Minkowski, *$\mu \to e\gamma$ at a Rate of One Out of 10^9 Muon Decays?*, *Phys. Lett.* **67B** (1977) 421.

[47] R.N. Mohapatra and G. Senjanovic, *Neutrino Mass and Spontaneous Parity Nonconservation*, *Phys. Rev. Lett.* **44** (1980) 912.

[48] M. Gell-Mann, P. Ramond and R. Slansky, *Complex Spinors and Unified Theories*, *Conf. Proc.* **C790927** (1979) 315 [arXiv:1306.4669].

[49] A. Zee, *A Theory of Lepton Number Violation, Neutrino Majorana Mass, and Oscillation*, *Phys. Lett.* **93B** (1980) 389.

[50] K.S. Babu, *Model of 'Calculable' Majorana Neutrino Masses*, *Phys. Lett.* **B203** (1988) 132.

[51] N. Arkani-Hamed, S. Dimopoulos, G.R. Dvali and J. March-Russell, *Neutrino masses from large extra dimensions*, *Phys. Rev.* **D65** (2001) 024032 [hep-ph/9811448].

[52] R.N. Mohapatra and J.W.F. Valle, *Neutrino Mass and Baryon Number Nonconservation in Superstring Models*, *Phys. Rev.* **D34** (1986) 1642.

[53] M.C. Gonzalez-Garcia and J.W.F. Valle, *Fast Decaying Neutrinos and Observable Flavor Violation in a New Class of Majoron Models*, *Phys. Lett.* **B216** (1989) 360.

[54] A. Cárcamo Hernández, J. Marchant González and U. Saldaña Salazar, *Viable low-scale model with universal and inverse seesaw mechanisms*, *Phys. Rev. D* **100** (2019) 035024 [arXiv:1904.09993].

[55] M. Malinsky, J.C. Romao and J.W.F. Valle, *Novel supersymmetric SO(10) seesaw mechanism*, *Phys. Rev. Lett.* **95** (2005) 161801 [hep-ph/0506296].

[56] R.N. Mohapatra et al., *Theory of neutrinos: A White paper*, *Rept. Prog. Phys.* **70** (2007) 1757 [hep-ph/0510213].

[57] E. Ma and G. Rajasekaran, *Softly broken A(4) symmetry for nearly degenerate neutrino masses*, *Phys. Rev. D* **64** (2001) 113012 [hep-ph/0106291].

[58] S. Pakvasa and H. Sugawara, *Discrete Symmetry and Cabibbo Angle*, *Phys. Lett. B* **73** (1978) 61.

[59] F. Feruglio, *Are neutrino masses modular forms?*, arXiv:1706.08749.

[60] S.J. King and S.F. King, *Fermion Mass Hierarchies from Modular Symmetry*, arXiv:2002.00969.

[61] S. King, *Unified Models of Neutrinos, Flavour and CP Violation*, *Prog. Part. Nucl. Phys.* **94** (2017) 217 [arXiv:1701.04413].

[62] G. Altarelli and F. Feruglio, *Discrete Flavor Symmetries and Models of Neutrino Mixing*, *Rev. Mod. Phys.* **82** (2010) 2701 [arXiv:1002.0211].

[63] H. Ishimori, T. Kobayashi, H. Ohki, Y. Shimizu, H. Okada and M. Tanimoto, *Non-Abelian Discrete Symmetries in Particle Physics*, *Prog. Theor. Phys. Suppl.* **183** (2010) 1 [arXiv:1003.3552].

[64] S.F. King, *Models of Neutrino Mass, Mixing and CP Violation*, *J. Phys. G* **42** (2015) 123001 [arXiv:1510.02091].

[65] M. Abbas, *Flavor masses and mixing in modular A_4 Symmetry*, arXiv:2002.01929.

[66] X. Wang, *Lepton Flavor Mixing and CP Violation in the Minimal Type-(I+II) Seesaw Model with a Modular A_4 Symmetry*, arXiv:1912.13284.

[67] J.N. Lu, X.G. Liu and G.J. Ding, *Modular symmetry origin of texture zeros and quark lepton unification*, *Phys. Rev. D* **101** (2020) 115020 [arXiv:1912.07573].

[68] T. Kobayashi, T. Nomura and T. Shimomura, *Type II seesaw models with modular A_4 symmetry*, arXiv:1912.00637.

[69] T. Nomura, H. Okada and S. Patra, *An inverse seesaw model with A_4 -modular symmetry*, *Nucl. Phys. B* **967** (2021) 115395 [arXiv:1912.00379].

[70] J. Penedo and S. Petcov, *Lepton Masses and Mixing from Modular S_4 Symmetry*, *Nucl. Phys. B* **939** (2019) 292 [arXiv:1806.11040].

[71] X.G. Liu, C.Y. Yao and G.J. Ding, *Modular Invariant Quark and Lepton Models in Double Covering of S_4 Modular Group*, arXiv:2006.10722.

[72] G.J. Ding, S.F. King, X.G. Liu and J.N. Lu, *Modular S_4 and A_4 symmetries and their fixed points: new predictive examples of lepton mixing*, *JHEP* **12** (2019) 030 [arXiv:1910.03460].

[73] T. Kobayashi, Y. Shimizu, K. Takagi, M. Tanimoto and T.H. Tatsuishi, *A_4 lepton flavor model and modulus stabilization from S_4 modular symmetry*, *Phys. Rev. D* **100** (2019) 115045 [arXiv:1909.05139].

[74] G.J. Ding, S.F. King and X.G. Liu, *Modular A_4 symmetry models of neutrinos and charged leptons*, *JHEP* **09** (2019) 074 [arXiv:1907.11714].

[75] P. Novichkov, J. Penedo, S. Petcov and A. Titov, *Modular A_5 symmetry for flavour model building*, *JHEP* **04** (2019) 174 [arXiv:1812.02158].

[76] T. Kobayashi, Y. Shimizu, K. Takagi, M. Tanimoto, T.H. Tatsuishi and H. Uchida, *Finite modular subgroups for fermion mass matrices and baryon/lepton number violation*, *Phys. Lett. B* **794** (2019) 114 [arXiv:1812.11072].

[77] T. Nomura, H. Okada and O. Popov, *A modular A_4 symmetric scotogenic model*, *Phys. Lett. B* **803** (2020) 135294 [arXiv:1908.07457].

[78] E. Ma, *Neutrino mixing: A_4 variations*, *Phys. Lett. B* **752** (2016) 198 [arXiv:1510.02501].

[79] S. Mishra, M. Kumar Behera, R. Mohanta, S. Patra and S. Singirala, *Neutrino Phenomenology and Dark matter in an A_4 flavour extended B-L model*, *Eur. Phys. J. C* **80** (2020) 420 [arXiv:1907.06429].

[80] B.S. Acharya, D. Bailin, A. Love, W. Sabra and S. Thomas, *Spontaneous breaking of CP symmetry by orbifold moduli*, *Phys. Lett. B* **357** (1995) 387 [hep-th/9506143].

[81] P. Novichkov, J. Penedo, S. Petcov and A. Titov, *Generalised CP Symmetry in Modular-Invariant Models of Flavour*, *JHEP* **07** (2019) 165 [arXiv:1905.11970].

[82] A. Baur, H.P. Nilles, A. Trautner and P.K. Vaudrevange, *Unification of Flavor, CP, and Modular Symmetries*, *Phys. Lett. B* **795** (2019) 7 [arXiv:1901.03251].

[83] T. Dent, *CP violation and modular symmetries*, *Phys. Rev. D* **64** (2001) 056005 [hep-ph/0105285].

[84] J. Giedt, *CP violation and moduli stabilization in heterotic models*, *Mod. Phys. Lett. A* **17** (2002) 1465 [hep-ph/0204017].

[85] M.C. Chen, S. Ramos-Sánchez and M. Ratz, *A note on the predictions of models with modular flavor symmetries*, *Phys. Lett. B* **801** (2020) 135153 [arXiv:1909.06910].

[86] M. Sruthilaya, R. Mohanta and S. Patra, *A_4 realization of Linear Seesaw and Neutrino Phenomenology*, *Eur. Phys. J. C* **78** (2018) 719 [arXiv:1709.01737].

[87] D. Borah and B. Karmakar, *Linear seesaw for Dirac neutrinos with A_4 flavour symmetry*, *Phys. Lett. B* **789** (2019) 59 [arXiv:1806.10685].

[88] D. Borah and B. Karmakar, *A_4 flavour model for Dirac neutrinos: Type I and inverse seesaw*, *Phys. Lett. B* **780** (2018) 461 [arXiv:1712.06407].

[89] S. Dawson, *Electroweak Symmetry Breaking and Effective Field Theory*, in *Theoretical Advanced Study Institute in Elementary Particle Physics: Anticipating the Next Discoveries in Particle Physics*, p. 1, 12, 2017, arXiv:1712.07232, DOI.

[90] M. Lindner, D. Schmidt and T. Schwetz, *Dark Matter and neutrino masses from global U(1)$_{B,\grave{a}\acute{i}L}$ symmetry breaking*, *Phys. Lett. B* **705** (2011) 324 [arXiv:1105.4626].

[91] C. Garcia-Cely, A. Ibarra and E. Molinaro, *Dark matter production from Goldstone boson interactions and implications for direct searches and dark radiation*, *JCAP* **11** (2013) 061 [arXiv:1310.6256].

[92] S. Antusch and V. Maurer, *Running quark and lepton parameters at various scales*, *JHEP* **11** (2013) 115 [arXiv:1306.6879].

[93] M. Kashav and S. Verma, *Broken scaling neutrino mass matrix and leptogenesis based on A_4 modular invariance*, *JHEP* **09** (2021) 100 [arXiv:2103.07207].

[94] APPEC COMMITTEE collaboration, A. Giuliani, J. Gomez Cadenas, S. Pascoli, E. Previtali, R. Saakyan, K. Schäffner et al., *Double Beta Decay APPEC Committee Report*, arXiv:1910.04688.

[95] GERDA collaboration, M. Agostini et al., *Probing Majorana neutrinos with double-β decay*, *Science* **365** (2019) 1445 [arXiv:1909.02726].

[96] CUORE collaboration, C. Alduino et al., *First Results from CUORE: A Search for Lepton Number Violation via $0\nu\beta\beta$ Decay of ^{130}Te*, *Phys. Rev. Lett.* **120** (2018) 132501 [arXiv:1710.07988].

[97] KAMLAND-ZEN collaboration, A. Gando et al., *Search for Majorana Neutrinos near the Inverted Mass Hierarchy Region with KamLAND-Zen*, *Phys. Rev. Lett.* **117** (2016) 082503 [arXiv:1605.02889].

[98] I. Esteban, M. Gonzalez-Garcia, A. Hernandez-Cabezudo, M. Maltoni and T. Schwetz, *Global analysis of three-flavour neutrino oscillations: synergies and tensions in the determination of θ_{23}, δ_{CP}, and the mass ordering*, *JHEP* **01** (2019) 106 [arXiv:1811.05487].

[99] D.V. Forero, S. Morisi, M. Tortola and J.W.F. Valle, *Lepton flavor violation and non-unitary lepton mixing in low-scale type-I seesaw*, *JHEP* **09** (2011) 142 [arXiv:1107.6009].

[100] S. Antusch and O. Fischer, *Non-unitarity of the leptonic mixing matrix: Present bounds and future sensitivities*, *JHEP* **10** (2014) 094 [arXiv:1407.6607].

[101] M. Blennow, P. Coloma, E. Fernandez-Martinez, J. Hernandez-Garcia and J. Lopez-Pavon, *Non-Unitarity, sterile neutrinos, and Non-Standard neutrino Interactions*, *JHEP* **04** (2017) 153 [arXiv:1609.08637].

[102] E. Fernandez-Martinez, J. Hernandez-Garcia and J. Lopez-Pavon, *Global constraints on heavy neutrino mixing*, *JHEP* **08** (2016) 033 [arXiv:1605.08774].

[103] MEG collaboration, A. Baldini et al., *Search for the lepton flavour violating decay $\mu^+ \to e^+\gamma$ with the full dataset of the MEG experiment*, *Eur. Phys. J. C* **76** (2016) 434 [arXiv:1605.05081].

[104] BABAR collaboration, B. Aubert et al., *Searches for Lepton Flavor Violation in the Decays tau+- —> e+- gamma and tau+- —> mu+- gamma*, *Phys. Rev. Lett.* **104** (2010) 021802 [arXiv:0908.2381].

[105] BELLE collaboration, A. Abdesselam et al., *Search for lepton-flavor-violating tau-lepton decays to $\ell\gamma$ at Belle*, *JHEP* **10** (2021) 19 [arXiv:2103.12994].

[106] J. Bernabeu, A. Santamaria, J. Vidal, A. Mendez and J.W.F. Valle, *Lepton Flavor Nonconservation at High-Energies in a Superstring Inspired Standard Model*, *Phys. Lett. B* **187** (1987) 303.

[107] F. Deppisch and J.W.F. Valle, *Enhanced lepton flavor violation in the supersymmetric inverse seesaw model*, *Phys. Rev. D* **72** (2005) 036001 [hep-ph/0406040].

[108] A. Ilakovac and A. Pilaftsis, *Flavor violating charged lepton decays in seesaw-type models*, *Nucl. Phys. B* **437** (1995) 491 [hep-ph/9403398].

[109] A. Pilaftsis, *CP violation and baryogenesis due to heavy Majorana neutrinos*, *Phys. Rev. D* **56** (1997) 5431 [hep-ph/9707235].

[110] G. Bambhaniya, P. Bhupal Dev, S. Goswami, S. Khan and W. Rodejohann, *Naturalness, Vacuum Stability and Leptogenesis in the Minimal Seesaw Model*, *Phys. Rev. D* **95** (2017) 095016 [arXiv:1611.03827].

[111] A. Pilaftsis and T.E. Underwood, *Resonant leptogenesis*, *Nucl. Phys. B* **692** (2004) 303 [hep-ph/0309342].

[112] A. Abada, G. Arcadi, V. Domcke, M. Drewes, J. Klaric and M. Lucente, *Low-scale leptogenesis with three heavy neutrinos*, *JHEP* **01** (2019) 164 [arXiv:1810.12463].

[113] A. Pilaftsis and T.E. Underwood, *Electroweak-scale resonant leptogenesis*, *Phys. Rev. D* **72** (2005) 113001 [hep-ph/0506107].

[114] T. Asaka and T. Yoshida, *Resonant leptogenesis at TeV-scale and neutrinoless double beta decay*, *JHEP* **09** (2019) 089 [arXiv:1812.11323].

[115] P.F. Harrison, D.H. Perkins and W.G. Scott, *Tri-bimaximal mixing and the neutrino oscillation data*, *Phys. Lett.* **B530** (2002) 167 [hep-ph/0202074].

[116] P.F. Harrison and W.G. Scott, *Symmetries and generalizations of tri - bimaximal neutrino mixing*, *Phys. Lett.* **B535** (2002) 163 [hep-ph/0203209].

[117] P.H. Gu and U. Sarkar, *Leptogenesis with Linear, Inverse or Double Seesaw*, *Phys. Lett. B* **694** (2011) 226 [arXiv:1007.2323].

[118] S. Davidson, E. Nardi and Y. Nir, *Leptogenesis*, *Phys. Rept.* **466** (2008) 105 [arXiv:0802.2962].

[119] W. Buchmuller, P. Di Bari and M. Plumacher, *Leptogenesis for pedestrians*, *Annals Phys.* **315** (2005) 305 [hep-ph/0401240].

[120] M. Plumacher, *Baryogenesis and lepton number violation*, *Z. Phys. C* **74** (1997) 549 [hep-ph/9604229].

[121] G. Giudice, A. Notari, M. Raidal, A. Riotto and A. Strumia, *Towards a complete theory of thermal leptogenesis in the SM and MSSM*, *Nucl. Phys. B* **685** (2004) 89 [hep-ph/0310123].

[122] A. Strumia, *Baryogenesis via leptogenesis*, in *Les Houches Summer School on Theoretical Physics: Session 84: Particle Physics Beyond the Standard Model*, p. 655, 8, 2006, hep-ph/0608347.

[123] S. Iso, N. Okada and Y. Orikasa, *Resonant Leptogenesis in the Minimal B-L Extended Standard Model at TeV*, *Phys. Rev. D* **83** (2011) 093011 [arXiv:1011.4769].

[124] J.A. Harvey and M.S. Turner, *Cosmological baryon and lepton number in the presence of electroweak fermion number violation*, *Phys. Rev. D* **42** (1990) 3344.

[125] S. Pascoli, S.T. Petcov and A. Riotto, *Leptogenesis and Low Energy CP Violation in Neutrino Physics*, *Nucl. Phys. B* **774** (2007) 1 [hep-ph/0611338].

[126] S. Antusch, S.F. King and A. Riotto, *Flavour-Dependent Leptogenesis with Sequential Dominance*, *JCAP* **11** (2006) 011 [hep-ph/0609038].

[127] E. Nardi, Y. Nir, E. Roulet and J. Racker, *The Importance of flavor in leptogenesis*, *JHEP* **01** (2006) 164 [hep-ph/0601084].

[128] A. Abada, S. Davidson, A. Ibarra, F.X. Josse-Michaux, M. Losada and A. Riotto, *Flavour Matters in Leptogenesis*, *JHEP* **09** (2006) 010 [hep-ph/0605281].

[129] A. Granelli, K. Moffat and S.T. Petcov, *Flavoured resonant leptogenesis at sub-TeV scales*, *Nucl. Phys. B* **973** (2021) 115597 [arXiv:2009.03166].

[130] P.S.B. Dev, P. Di Bari, B. Garbrecht, S. Lavignac, P. Millington and D. Teresi, *Flavor effects in leptogenesis*, *Int. J. Mod. Phys. A* **33** (2018) 1842001 [arXiv:1711.02861].

[131] H.c. Han and Z.z. Xing, *A full parametrization of the* 9×9 *active-sterile flavor mixing matrix in the inverse or linear seesaw scenario of massive neutrinos*, *arXiv preprint arXiv:2110.12705* (2021).

[132] A. Das, P.S. Bhupal Dev and N. Okada, *Direct bounds on electroweak scale pseudo-Dirac neutrinos from* $\sqrt{s} = 8$ *TeV LHC data*, *Phys. Lett. B* **735** (2014) 364 [arXiv:1405.0177].

[133] J.A. Aguilar-Saavedra, *Heavy lepton pair production at LHC: Model discrimination with multi-lepton signals*, *Nucl. Phys. B* **828** (2010) 289 [arXiv:0905.2221].

[134] F. Zwicky, *On the Masses of Nebulae and of Clusters of Nebulae*, *Astrophys. J.* **86** (1937) 217.

[135] V.C. Rubin and W.K. Ford, Jr., *Rotation of the Andromeda Nebula from a Spectroscopic Survey of Emission Regions*, *Astrophys. J.* **159** (1970) 379.

[136] D. Clowe, A. Gonzalez and M. Markevitch, *Weak lensing mass reconstruction of the interacting cluster 1E0657-558: Direct evidence for the existence of dark matter*, *Astrophys. J.* **604** (2004) 596 [astro-ph/0312273].

[137] G. Bertone, D. Hooper and J. Silk, *Particle dark matter: Evidence, candidates and constraints*, *Phys. Rept.* **405** (2005) 279 [hep-ph/0404175].

[138] N. Arkani-Hamed, D.P. Finkbeiner, T.R. Slatyer and N. Weiner, *A Theory of Dark Matter*, *Phys. Rev. D* **79** (2009) 015014 [arXiv:0810.0713].

[139] S. Dodelson and L.M. Widrow, *Sterile-neutrinos as dark matter*, *Phys. Rev. Lett.* **72** (1994) 17 [hep-ph/9303287].

[140] S. Roy Choudhury and S. Hannestad, *Updated results on neutrino mass and mass hierarchy from cosmology with Planck 2018 likelihoods*, *JCAP* **07** (2020) 037 [arXiv:1907.12598].

[141] SUPER-KAMIOKANDE collaboration, Y. Fukuda et al., *Evidence for oscillation of atmospheric neutrinos*, *Phys. Rev. Lett.* **81** (1998) 1562 [hep-ex/9807003].

[142] E.W. Kolb and S. Wolfram, *Baryon Number Generation in the Early Universe*, *Nucl. Phys. B* **172** (1980) 224.

[143] E. Ma, *Verifiable radiative seesaw mechanism of neutrino mass and dark matter*, *Phys. Rev. D* **73** (2006) 077301 [hep-ph/0601225].

[144] L. Lopez Honorez, E. Nezri, J.F. Oliver and M.H. Tytgat, *The Inert Doublet Model: An Archetype for Dark Matter*, *JCAP* **02** (2007) 028 [hep-ph/0612275].

[145] M. Gustafsson, E. Lundstrom, L. Bergstrom and J. Edsjo, *Significant Gamma Lines from Inert Higgs Dark Matter*, *Phys. Rev. Lett.* **99** (2007) 041301 [astro-ph/0703512].

[146] E.M. Dolle and S. Su, *The Inert Dark Matter*, *Phys. Rev. D* **80** (2009) 055012 [arXiv:0906.1609].

[147] D. Suematsu, T. Toma and T. Yoshida, *Reconciliation of CDM abundance and $\mu \to e\gamma$ in a radiative seesaw model*, *Phys. Rev. D* **79** (2009) 093004 [arXiv:0903.0287].

[148] D. Schmidt, T. Schwetz and T. Toma, *Direct Detection of Leptophilic Dark Matter in a Model with Radiative Neutrino Masses*, *Phys. Rev. D* **85** (2012) 073009 [arXiv:1201.0906].

[149] S. Singirala, *Implications of Fermionic Dark Matter on recent neutrino oscillation data*, *Chin. Phys. C* **41** (2017) 043102 [arXiv:1607.03309].

[150] $Restrepo, Diego and Rivera, Andr\checkmark{\copyright}s$, *Phenomenological consistency of the singlet-triplet scotogenic model*, *JHEP* **04** (2020) 134 [arXiv:1907.11938].

[151] K. Babu, P.B. Dev, S. Jana and A. Thapa, *Non-Standard Interactions in Radiative Neutrino Mass Models*, *JHEP* **03** (2020) 006 [arXiv:1907.09498].

[152] C.H. Chen and T. Nomura, *Radiatively scotogenic type-II seesaw and a relevant phenomenological analysis*, *JHEP* **10** (2019) 005 [arXiv:1906.10516].

[153] E. Ma, *Scotogenic $U(1)_\chi$ Dirac neutrinos*, *Phys. Lett. B* **793** (2019) 411 [arXiv:1901.09091].

[154] E. Ma, *Radiative inverse seesaw mechanism for nonzero neutrino mass*, *Phys. Rev. D* **80** (2009) 013013 [arXiv:0904.4450].

[155] J.C. Criado and F. Feruglio, *Modular Invariance Faces Precision Neutrino Data*, *SciPost Phys.* **5** (2018) 042 [arXiv:1807.01125].

[156] M.K. Behera, S. Mishra, S. Singirala and R. Mohanta, *Implications of A_4 modular symmetry on Neutrino mass, Mixing and Leptogenesis with Linear Seesaw*, arXiv:2007.00545.

[157] X. Wang and S. Zhou, *The minimal seesaw model with a modular S_4 symmetry*, *JHEP* **05** (2020) 017 [arXiv:1910.09473].

[158] X. Wang, B. Yu and S. Zhou, *Double Covering of the Modular A_5 Group and Lepton Flavor Mixing in the Minimal Seesaw Model*, arXiv:2010.10159.

[159] C.Y. Yao, X.G. Liu and G.J. Ding, *Fermion Masses and Mixing from Double Cover and Metaplectic Cover of A_5 Modular Group*, arXiv:2011.03501.

[160] S. King, *Minimal see-saw model predicting best fit lepton mixing angles*, *Phys. Lett. B* **724** (2013) 92 [arXiv:1305.4846].

[161] S. King, *Neutrino Mass Models and the Implications of a Non-Zero Reactor Angle*, in *13th International Workshop on Neutrino Telescopes: Un altro modo di guardare il cielo: Tribute to Galileo*, p. 365, 4, 2009, arXiv:0904.3255.

[162] R. Bouchand and A. Merle, *Running of Radiative Neutrino Masses: The Scotogenic Model*, *JHEP* **07** (2012) 084 [arXiv:1205.0008].

[163] $Rojas, Nicol\sqrt{}$řs$and Srivastava, Rahul and Valle, Jos\sqrt{}$©$W.F.$, *Simplest Scoto-Seesaw Mechanism*, *Phys. Lett. B* **789** (2019) 132 [arXiv:1807.11447].

[164] $Hagedorn, Claudia and Herrero-Garc\sqrt{}\neq a, Juan and Molinaro, Emiliano and Schmidt, Michael A.$, *Phenomenology of the Generalised Scotogenic Model with Fermionic Dark Matter*, *JHEP* **11** (2018) 103 [arXiv:1804.04117].

[165] S. Pramanick, *Radiative generation of realistic neutrino mixing with $A4$*, arXiv:1903.04208.

[166] Y.L. Tang, *Some Phenomenologies of a Simple Scotogenic Inverse Seesaw Model*, *Phys. Rev. D* **97** (2018) 035020 [arXiv:1709.07735].

[167] T. Nomura and H. Okada, *A modular A_4 symmetric model of dark matter and neutrino*, *Phys. Lett. B* **797** (2019) 134799 [arXiv:1904.03937].

[168] H. Okada and Y. Orikasa, *A radiative seesaw model in modular A_4 symmetry*, arXiv:1907.13520.

[169] M. Lindner, M. Platscher, C.E. Yaguna and A. Merle, *Fermionic WIMPs and vacuum stability in the scotogenic model*, *Phys. Rev. D* **94** (2016) 115027 [arXiv:1608.00577].

[170] P. Escribano, M. Reig and A. Vicente, *Generalizing the Scotogenic model*, *JHEP* **07** (2020) 097 [arXiv:2004.05172].

[171] P. Dev and A. Pilaftsis, *Minimal Radiative Neutrino Mass Mechanism for Inverse Seesaw Models*, *Phys. Rev. D* **86** (2012) 113001 [arXiv:1209.4051].

[172] M. Hirsch, S. Morisi and J. Valle, *A4-based tri-bimaximal mixing within inverse and linear seesaw schemes*, *Phys. Lett. B* **679** (2009) 454 [arXiv:0905.3056].

[173] P.F. de Salas, D.V. Forero, S. Gariazzo, P. Martinez-Mirave, O. Mena, C.A. Ternes et al., *2020 global reassessment of the neutrino oscillation picture*, *JHEP* **02** (2021) 071 [arXiv:2006.11237].

[174] S. Gariazzo, M. Archidiacono, P. de Salas, O. Mena, C. Ternes and M. Tortola, *Neutrino masses and their ordering: Global Data, Priors and Models*, *JCAP* **03** (2018) 011 [arXiv:1801.04946].

[175] I. Esteban, M. Gonzalez-Garcia, M. Maltoni, T. Schwetz and A. Zhou, *The fate of hints: updated global analysis of three-flavor neutrino oscillations*, arXiv:2007.14792.

[176] PLANCK collaboration, N. Aghanim et al., *Planck 2018 results. V. CMB power spectra and likelihoods*, arXiv:1907.12875.

[177] T. Toma and A. Vicente, *Lepton Flavor Violation in the Scotogenic Model*, *JHEP* **01** (2014) 160 [arXiv:1312.2840].

[178] A. Vicente and C.E. Yaguna, *Probing the scotogenic model with lepton flavor violating processes*, *JHEP* **02** (2015) 144 [arXiv:1412.2545].

[179] PARTICLE DATA GROUP collaboration, P.A. Zyla et al., *Review of Particle Physics*, *PTEP* **2020** (2020) 083C01.

[180] MU2E collaboration, S. Miscetti, *Status of the Mu2e experiment at Fermilab*, *EPJ Web Conf.* **234** (2020) 01010.

[181] P. Dornan, *Mu to electron conversion with the COMET experiment*, *EPJ Web Conf.* **118** (2016) 01010.

[182] DEEME collaboration, H. Natori, *An experiment to search for mu-e conversion at J-PARC MLF in Japan, DeeMe experiment*, *PoS* **ICHEP2018** (2019) 642.

[183] Y. Kuno and Y. Okada, *Muon decay and physics beyond the standard model*, *Rev. Mod. Phys.* **73** (2001) 151 [hep-ph/9909265].

[184] E. Arganda, M.J. Herrero and A.M. Teixeira, *mu-e conversion in nuclei within the CMSSM seesaw: Universality versus non-universality*, *JHEP* **10** (2007) 104 [arXiv:0707.2955].

[185] H.C. Chiang, E. Oset, T.S. Kosmas, A. Faessler and J.D. Vergados, *Coherent and incoherent (mu-, e-) conversion in nuclei*, *Nucl. Phys. A* **559** (1993) 526.

[186] T.S. Kosmas, S. Kovalenko and I. Schmidt, *Nuclear muon- e- conversion in strange quark sea*, *Phys. Lett. B* **511** (2001) 203 [hep-ph/0102101].

[187] SINDRUM II collaboration, C. Dohmen et al., *Test of lepton flavor conservation in mu —> e conversion on titanium*, *Phys. Lett. B* **317** (1993) 631.

[188] K. Griest and D. Seckel, *Three exceptions in the calculation of relic abundances*, *Phys. Rev. D* **43** (1991) 3191.

[189] P. Gondolo and G. Gelmini, *Cosmic abundances of stable particles: Improved analysis*, *Nucl. Phys. B* **360** (1991) 145.

[190] A. Semenov, *LanHEP: A Package for automatic generation of Feynman rules in gauge models*, hep-ph/9608488.

[191] A. Pukhov, E. Boos, M. Dubinin, V. Edneral, V. Ilyin, D. Kovalenko et al., *CompHEP: A Package for evaluation of Feynman diagrams and integration over multiparticle phase space*, hep-ph/9908288.

[192] G. Belanger, F. Boudjema, A. Pukhov and A. Semenov, *MicrOMEGAs 2.0: A Program to calculate the relic density of dark matter in a generic model*, *Comput. Phys. Commun.* **176** (2007) 367 [hep-ph/0607059].

[193] G. Belanger, F. Boudjema, A. Pukhov and A. Semenov, *Dark matter direct detection rate in a generic model with micrOMEGAs 2.2*, *Comput. Phys. Commun.* **180** (2009) 747 [arXiv:0803.2360].

[194] S. Singirala, R. Mohanta, S. Patra and S. Rao, *Majorana Dark Matter in a new $B-L$ model*, *JCAP* **11** (2018) 026 [arXiv:1710.05775].

[195] P. Agrawal, Z. Chacko, C. Kilic and R.K. Mishra, *A Classification of Dark Matter Candidates with Primarily Spin-Dependent Interactions with Matter*, arXiv:1003.1912.

[196] PANDAX-4T collaboration, Y. Meng et al., *Dark Matter Search Results from the PandaX-4T Commissioning Run*, *Phys. Rev. Lett.* **127** (2021) 261802 [arXiv:2107.13438].

[197] A. Belyaev, N.D. Christensen and A. Pukhov, *CalcHEP 3.4 for collider physics within and beyond the Standard Model*, *Comput. Phys. Commun.* **184** (2013) 1729 [arXiv:1207.6082].

[198] K. Kong, *TASI 2011: CalcHEP and PYTHIA Tutorials*, in *The Dark Secrets of the Terascale: Proceedings, TASI 2011, Boulder, Colorado, USA, Jun 6 - Jul 11, 2011*, p. 161, 2013, arXiv:1208.0035, DOI.

[199] ATLAS collaboration, G. Aad et al., *Search for high-mass dilepton resonances using 139 fb^{-1} of pp collision data collected at $\sqrt{s}$ =13 TeV with the ATLAS detector*, *Phys. Lett. B* **796** (2019) 68 [arXiv:1903.06248].

[200] DELPHI, OPAL, LEP ELECTROWEAK, ALEPH, L3 collaboration, S. Schael et al., *Electroweak Measurements in Electron-Positron Collisions at W-Boson-Pair Energies at LEP*, *Phys. Rept.* **532** (2013) 119 [arXiv:1302.3415].

[201] V. Brdar, A.J. Helmboldt, S. Iwamoto and K. Schmitz, *Type-I Seesaw as the Common Origin of Neutrino Mass, Baryon Asymmetry, and the Electroweak Scale*, *Phys. Rev. D* **100** (2019) 075029 [arXiv:1905.12634].

[202] G.C. Branco, J.T. Penedo, P.M.F. Pereira, M.N. Rebelo and J.I. Silva-Marcos, *Type-I Seesaw with eV-Scale Neutrinos*, *JHEP* **07** (2020) 164 [arXiv:1912.05875].

[203] S. Bilenky, *Introduction to the physics of massive and mixed neutrinos*, vol. 817 (2010), 10.1007/978-3-642-14043-3.

[204] P.H. Gu, H. Zhang and S. Zhou, *A Minimal Type II Seesaw Model*, *Phys. Rev. D* **74** (2006) 076002 [hep-ph/0606302].

[205] S. Luo and Z.z. Xing, *The Minimal Type-II Seesaw Model and Flavor-dependent Leptogenesis*, *Int. J. Mod. Phys. A* **23** (2008) 3412 [arXiv:0712.2610].

[206] S. Antusch and S.F. King, *Type II Leptogenesis and the neutrino mass scale*, *Phys. Lett. B* **597** (2004) 199 [hep-ph/0405093].

[207] W. Rodejohann, *Type II seesaw mechanism, deviations from bimaximal neutrino mixing and leptogenesis*, *Phys. Rev. D* **70** (2004) 073010 [hep-ph/0403236].

[208] P.H. Gu, *Double type II seesaw mechanism accompanied by Dirac fermionic dark matter*, *Phys. Rev. D* **101** (2020) 015006 [arXiv:1907.10019].

[209] J. McDonald, N. Sahu and U. Sarkar, *Type-II Seesaw at Collider, Lepton Asymmetry and Singlet Scalar Dark Matter*, *JCAP* **04** (2008) 037 [arXiv:0711.4820].

[210] Y. Liao, J.Y. Liu and G.Z. Ning, *Radiative Neutrino Mass in Type III Seesaw Model*, *Phys. Rev. D* **79** (2009) 073003 [arXiv:0902.1434].

[211] E. Ma, *Pathways to naturally small neutrino masses*, *Phys. Rev. Lett.* **81** (1998) 1171 [hep-ph/9805219].

[212] R. Foot, H. Lew, X.G. He and G.C. Joshi, *Seesaw Neutrino Masses Induced by a Triplet of Leptons*, *Z. Phys. C* **44** (1989) 441.

[213] I. Dorsner and P. Fileviez Perez, *Upper Bound on the Mass of the Type III Seesaw Triplet in an SU(5) Model*, *JHEP* **06** (2007) 029 [hep-ph/0612216].

[214] R. Franceschini, T. Hambye and A. Strumia, *Type-III see-saw at LHC*, *Phys. Rev. D* **78** (2008) 033002 [arXiv:0805.1613].

[215] X.G. He and S. Oh, *Lepton FCNC in Type III Seesaw Model*, *JHEP* **09** (2009) 027 [arXiv:0902.4082].

[216] A. Das and N. Okada, *Inverse seesaw neutrino signatures at the LHC and ILC*, *Phys. Rev. D* **88** (2013) 113001 [arXiv:1207.3734].

[217] E. Arganda, M.J. Herrero, X. Marcano and C. Weiland, *Imprints of massive inverse seesaw model neutrinos in lepton flavor violating Higgs boson decays*, *Phys. Rev. D* **91** (2015) 015001 [arXiv:1405.4300].

[218] E. Ma and R. Srivastava, *Dirac or inverse seesaw neutrino masses from gauged B,ÄìL symmetry*, *Mod. Phys. Lett. A* **30** (2015) 1530020 [arXiv:1504.00111].

[219] A.G. Dias, C.A. de S. Pires, P.S. Rodrigues da Silva and A. Sampieri, *A Simple Realization of the Inverse Seesaw Mechanism*, *Phys. Rev. D* **86** (2012) 035007 [arXiv:1206.2590].

[220] A.G. Dias, C.A. de S. Pires and P.S.R. da Silva, *How the Inverse See-Saw Mechanism Can Reveal Itself Natural, Canonical and Independent of the Right-Handed Neutrino Mass*, *Phys. Rev. D* **84** (2011) 053011 [arXiv:1107.0739].

[221] F. Bazzocchi, *Minimal Dynamical Inverse See Saw*, *Phys. Rev. D* **83** (2011) 093009 [arXiv:1011.6299].

[222] A.E. Cárcamo Hernández, R. Martinez and F. Ochoa, *Fermion masses and mixings in the 3-3-1 model with right-handed neutrinos based on the S_3 flavor symmetry*, *Eur. Phys. J. C* **76** (2016) 634 [arXiv:1309.6567].

[223] E. Ma and R. Srivastava, *Dirac or inverse seesaw neutrino masses with $B-L$ gauge symmetry and S_3 flavor symmetry*, *Phys. Lett. B* **741** (2015) 217 [arXiv:1411.5042].

[224] A.E. Cárcamo Hernández and H.N. Long, *A highly predictive A_4 flavour 3-3-1 model with radiative inverse seesaw mechanism*, *J. Phys. G* **45** (2018) 045001 [arXiv:1705.05246].

[225] R. Kalita and D. Borah, *Constraining a type I seesaw model with A_4 flavor symmetry from neutrino data and leptogenesis*, *Phys. Rev. D* **92** (2015) 055012 [arXiv:1508.05466].

[226] E. Ma, *Neutrino mass matrix from S(4) symmetry*, *Phys. Lett. B* **632** (2006) 352 [hep-ph/0508231].

[227] L. Dorame, S. Morisi, E. Peinado, J.W.F. Valle and A.D. Rojas, *A new neutrino mass sum rule from inverse seesaw*, *Phys. Rev. D* **86** (2012) 056001 [arXiv:1203.0155].

[228] A.E. Cárcamo Hernández and S.F. King, *Littlest Inverse Seesaw Model*, *Nucl. Phys. B* **953** (2020) 114950 [arXiv:1903.02565].

[229] T. Kobayashi, K. Tanaka and T.H. Tatsuishi, *Neutrino mixing from finite modular groups*, *Phys. Rev. D* **98** (2018) 016004 [arXiv:1803.10391].

[230] R. de Adelhart Toorop, F. Feruglio and C. Hagedorn, *Finite Modular Groups and Lepton Mixing*, *Nucl. Phys. B* **858** (2012) 437 [arXiv:1112.1340].

[231] E. Dudas, S. Pokorski and C.A. Savoy, *Soft scalar masses in supergravity with horizontal U(1)-x gauge symmetry*, *Phys. Lett. B* **369** (1996) 255 [hep-ph/9509410].

[232] G.K. Leontaris and N.D. Tracas, *Modular weights, U(1)'s and mass matrices*, *Phys. Lett. B* **419** (1998) 206 [hep-ph/9709510].

[233] X. Du and F. Wang, *SUSY breaking constraints on modular flavor S_3 invariant SU(5) GUT model*, *JHEP* **02** (2021) 221 [arXiv:2012.01397].

[234] S. Mishra, *Neutrino mixing and Leptogenesis with modular S_3 symmetry in the framework of type III seesaw*, arXiv:2008.02095.

[235] H. Okada and Y. Orikasa, *Modular S_3 symmetric radiative seesaw model*, *Phys. Rev. D* **100** (2019) 115037 [arXiv:1907.04716].

[236] P. Novichkov, J. Penedo, S. Petcov and A. Titov, *Modular S_4 models of lepton masses and mixing*, *JHEP* **04** (2019) 005 [arXiv:1811.04933].

[237] H. Okada and Y. Orikasa, *Neutrino mass model with a modular S_4 symmetry*, arXiv:1908.08409.

[238] M. Abbas, *Modular A_4 Invariance Model for Lepton Masses and Mixing*, *Phys. Atom. Nucl.* **83** (2020) 764.

[239] K.I. Nagao and H. Okada, *Lepton sector in modular A_4 and gauged $U(1)_R$ symmetry*, arXiv:2010.03348.

[240] T. Asaka, Y. Heo and T. Yoshida, *Lepton flavor model with modular A_4 symmetry in large volume limit*, *Phys. Lett. B* **811** (2020) 135956 [arXiv:2009.12120].

[241] T. Nomura and H. Okada, *A linear seesaw model with A_4-modular flavor and local $U(1)_{B-L}$ symmetries*, arXiv:2007.04801.

[242] H. Okada and Y. Shoji, *A radiative seesaw model with three Higgs doublets in modular A_4 symmetry*, *Nucl. Phys. B* **961** (2020) 115216 [arXiv:2003.13219].

[243] M.K. Behera, S. Singirala, S. Mishra and R. Mohanta, *A modular A_4 symmetric Scotogenic model for Neutrino mass and Dark Matter*, arXiv:2009.01806.

[244] G. Altarelli and F. Feruglio, *Tri-bimaximal neutrino mixing, A(4) and the modular symmetry*, *Nucl. Phys. B* **741** (2006) 215 [hep-ph/0512103].

[245] X.G. Liu and G.J. Ding, *Neutrino Masses and Mixing from Double Covering of Finite Modular Groups*, *JHEP* **08** (2019) 134 [arXiv:1907.01488].

[246] L.L. Everett and A.J. Stuart, *The Double Cover of the Icosahedral Symmetry Group and Quark Mass Textures*, *Phys. Lett. B* **698** (2011) 131 [arXiv:1011.4928].

[247] K. Hashimoto and H. Okada, *Lepton Flavor Model and Decaying Dark Matter in The Binary Icosahedral Group Symmetry*, arXiv:1110.3640.

[248] C.S. Chen, T.W. Kephart and T.C. Yuan, *Binary Icosahedral Flavor Symmetry for Four Generations of Quarks and Leptons*, *PTEP* **2013** (2013) 103B01 [arXiv:1110.6233].

[249] A. Ibarra, E. Molinaro and S. Petcov, *Low Energy Signatures of the TeV Scale See-Saw Mechanism*, *Phys. Rev. D* **84** (2011) 013005 [arXiv:1103.6217].

[250] ALEPH, DELPHI, L3, OPAL, LEP ELECTROWEAK collaboration, S. Schael et al., *Electroweak Measurements in Electron-Positron Collisions at W-Boson-Pair Energies at LEP*, *Phys. Rept.* **532** (2013) 119 [arXiv:1302.3415].

[251] T2K collaboration, C. Bronner, *Details of T2K Oscillation Analysis*, *PoS* **NuFact2019** (2020) 037.

[252] RENO collaboration, M.Y. Pac, *Recent Results from RENO*, *PoS* **NuFact2017** (2018) 038 [arXiv:1801.04049].

[253] DAYA BAY collaboration, Z. Yu, *Recent Results from the Daya Bay Experiment*, *J. Phys. Conf. Ser.* **888** (2017) 012011.

[254] DOUBLE CHOOZ collaboration, H. de Kerret et al., *Double Chooz θ_{13} measurement via total neutron capture detection*, *Nature Phys.* **16** (2020) 558 [arXiv:1901.09445].

[255] G.C. Branco, J.T. Penedo, P.M.F. Pereira, M.N. Rebelo and J.I. Silva-Marcos, *Type-I Seesaw with eV-Scale Neutrinos*, *JHEP* **07** (2020) 164 [arXiv:1912.05875].

[256] S.F. King and M. Malinsky, *A(4) family symmetry and quark-lepton unification*, *Phys. Lett. B* **645** (2007) 351 [hep-ph/0610250].

[257] G. Altarelli, *Lectures on models of neutrino masses and mixings*, *Soryushiron Kenkyu Electron.* **116** (2008) A29 [arXiv:0711.0161].

[258] T. Kimura, *The minimal S(3) symmetric model*, *Prog. Theor. Phys.* **114** (2005) 329.

[259] S. Mishra, *Majorana dark matter and neutrino mass with S_3 symmetry*, *Eur. Phys. J. Plus* **135** (2020) 485 [arXiv:1911.02255].

[260] D. Meloni, S. Morisi and E. Peinado, *Fritzsch neutrino mass matrix from S_3 symmetry*, *J. Phys. G* **38** (2011) 015003 [arXiv:1005.3482].

[261] S. Pramanick, *Scotogenic S3 symmetric generation of realistic neutrino mixing*, *Phys. Rev. D* **100** (2019) 035009 [arXiv:1904.07558].

[262] R. Krishnan, P.F. Harrison and W.G. Scott, *Simplest Neutrino Mixing from S4 Symmetry*, *JHEP* **04** (2013) 087 [arXiv:1211.2000].

[263] M. Chakraborty, R. Krishnan and A. Ghosal, *Predictive S_4 flavon model with TM_1 mixing and baryogenesis through leptogenesis*, *JHEP* **09** (2020) 025 [arXiv:2003.00506].

[264] V.V. Vien, *Lepton mass and mixing in a neutrino mass model based on S_4 flavor symmetry*, *Int. J. Mod. Phys. A* **31** (2016) 1650039 [arXiv:1603.03933].

[265] S. Kanemura, T. Matsui and H. Sugiyama, *Neutrino mass and dark matter from gauged $U(1)_{B-L}$ breaking*, *Phys. Rev. D* **90** (2014) 013001 [arXiv:1405.1935].

[266] S. Kanemura, T. Nabeshima and H. Sugiyama, *Radiative type-I seesaw model with dark matter via U(1)$_{B-L}$ gauge symmetry breaking at future linear colliders*, *Phys. Rev. D* **87** (2013) 015009 [arXiv:1207.7061].

[267] S. Mishra, S. Singirala and S. Sahoo, *Scalar dark matter, Neutrino mass, Leptogenesis and rare B decays in a* $\mathrm{U(1)_{B-L}}$ *model*, arXiv:1908.09187.

[268] H. Cai, T. Nomura and H. Okada, *A neutrino mass model with hidden $U(1)$ gauge symmetry*, *Nucl. Phys. B* **949** (2019) 114802 [arXiv:1812.01240].

[269] T. Nomura, H. Okada and P. Sanyal, *A radiatively induced inverse seesaw model with hidden $U(1)$ gauge symmetry*, arXiv:2103.09494.

[270] U.K. Dey, T. Nomura and H. Okada, *Inverse seesaw model with global $U(1)_H$ symmetry*, *Phys. Rev. D* **100** (2019) 075013 [arXiv:1902.06205].

[271] A. Esmaili and Y. Farzan, *Explaining the ANITA events by a $L_e - L_\tau$ gauge model*, *JCAP* **12** (2019) 017 [arXiv:1909.07995].

[272] M.K. Behera, P. Panda, P. Mishra, S. Singirala and R. Mohanta, *Exploring Neutrino Masses and Mixing in the Seesaw Model with $L_e - L_\tau$ Gauged Symmetry*, arXiv:2108.04066.

[273] M.K. Behera and R. Mohanta, *Inverse seesaw in A_5' modular symmetry*, *J. Phys. G* **49** (2022) 045001 [arXiv:2108.01059].

[274] W. Grimus, *Theory of Neutrino Masses and Mixing*, *Phys. Part. Nucl.* **42** (2011) 566 [arXiv:1101.0137].

[275] E. Ma, *Neutrino Mass: Mechanisms and Models*, arXiv:0905.0221.

[276] P. de Salas, D. Forero, C. Ternes, M. Tortola and J. Valle, *Status of neutrino oscillations 2018: 3σ hint for normal mass ordering and improved CP sensitivity*, *Phys. Lett. B* **782** (2018) 633 [arXiv:1708.01186].

[277] PLANCK collaboration, N. Aghanim et al., *Planck 2018 results. V. CMB power spectra and likelihoods*, *Astron. Astrophys.* **641** (2020) A5 [arXiv:1907.12875].

[278] D. Zhang, *A modular A_4 symmetry realization of two-zero textures of the Majorana neutrino mass matrix*, *Nucl. Phys. B* **952** (2020) 114935 [arXiv:1910.07869].

[279] D. Schultz, *Notes on modular forms*, https://faculty.math.illinois.edu/šchult25/ModFormNotes.pdf.

[280] G.J. Ding, S.F. King and X.G. Liu, *Neutrino mass and mixing with A_5 modular symmetry*, *Phys. Rev. D* **100** (2019) 115005 [arXiv:1903.12588].

Thesis Publications

1. **M. K. Behera**, S. Mishra, S. Singirala and R. Mohanta, **"Implications of A4 modular symmetry on neutrino mass, mixing and leptogenesis with linear seesaw",** Phys. Dark Univ. **36**, 101027 (2022) doi:10.1016/j.dark.2022.101027 [arXiv:2007.00545 [hep-ph]].
2. **M. K. Behera**, S. Singirala, S. Mishra and R. Mohanta, **"A modular $\mathbf{A_4}$ symmetric scotogenic model for neutrino mass and dark matter",** J. Phys. G **49**, no.3, 035002 (2022) doi:10.1088/1361-6471/ac3cc2 [arXiv:2009.01806 [hep-ph]].
3. **M. K. Behera** and R. Mohanta, **"Inverse seesaw in A_5' modular symmetry",** J. Phys. G **49**, no.4, 045001 (2022) doi:10.1088/1361-6471/ac4d7a [arXiv:2108.01059 [hep-ph]].
4. **M. K. Behera** and R. Mohanta, **"Linear Seesaw in A_5' Modular Symmetry With Leptogenesis",** Front. in Phys. **10**, 854595 (2022) doi:10.3389/fphy.2022.854595 [arXiv:2201.10429 [hep-ph]].

Other Publications

1. S. Mishra, **M. K. Behera**, R. Mohanta, S. Patra and S. Singirala, **"Neutrino phenomenology and dark matter in an A_4 flavour extended $B-L$ model",** Eur. Phys. J. C **80**, no.5, 420 (2020) doi:10.1140/epjc/s10052-020-7968-9 [arXiv:1907.06429 [hep-ph]].
2. **M. K. Behera**, P. Panda, P. Mishra, S. Singirala and R. Mohanta, **"Exploring Neutrino Masses and Mixing in the Seesaw Model with $L_e - L_j$ Gauged Symmetry",** [arXiv:2108.04066 [hep-ph]].
3. P. Panda, P. Mishra, **M. K. Behera** and R. Mohanta, "Neutrino phenomenology, muon and electron (g-2) under $U(1)$ gauged symmetries in an extended inverse seesaw model", [arXiv:2203.14536 [hep-ph]].
4. P. Mishra, **M. K. Behera**, P. Panda and R. Mohanta, **"Type III seesaw under A_4 modular symmetry with leptogenesis and muon $g-2$",** [arXiv:2204.08338 [hep-ph]].

Conference Proceedings

1. **M. K. Behera** and R. Mohanta, **"eV Scale Sterile Neutrinos in A_4 Symmetric Model",** Springer Proc. Phys. **261**, 963-967 (2021) doi:10.1007/978-981-33-4408-2_139

Phenomenological aspects of modular symmetry on neutrino mass models

by Mitesh Kumar Behera

Rukmani Mohanta

Dr. Rukmani Mohanta
Professor
School of Physics
UNIVERSITY OF HYDERABAD
Hyderabad-500 046.

Submission date: 05-Sep-2022 02:13PM (UTC+0530)
Submission ID: 1892991419
File name: ological_aspects_of_modular_symmetry_on_neutrino_mass_models.pdf (18.36M)
Word count: 39924
Character count: 179076

Phenomenological aspects of modular symmetry on neutrino mass models

ORIGINALITY REPORT

54%	38%	42%	2%
SIMILARITY INDEX	INTERNET SOURCES	PUBLICATIONS	STUDENT PAPERS

PRIMARY SOURCES

1	arxiv.org Internet Source	20%
2	Mitesh Kumar Behera, Shivaramakrishna Singirala, Subhasmita Mishra, R Mohanta. " A modular symmetric scotogenic model for neutrino mass and dark matter ", Journal of Physics G: Nuclear and Particle Physics, 2021 Publication	12%
3	Mitesh Kumar Behera, Subhasmita Mishra, Shivaramakrishna Singirala, Rukmani Mohanta. " Implications of modular symmetry on neutrino mass, mixing and leptogenesis with linear seesaw ", Physics of the Dark Universe, 2022 Publication	7%
4	Mitesh Kumar Behera, R Mohanta. "Inverse seesaw in A'_5 modular symmetry", Journal of Physics G: Nuclear and Particle Physics, 2022 Publication	7%

Rukmani Mohanta
Dr. Rukmani Mohanta
Professor
School of Physics
UNIVERSITY OF HYDERABAD
Hyderabad-500 046.

Rukmani Mohanta
Dr. Rukmani Mohanta
Professor
School of Physics
UNIVERSITY OF HYDERABAD
Hyderabad-500 046.

Rukmani Mohanta
Dr. Rukmani Mohanta
Professor
School of Physics
UNIVERSITY OF HYDERABAD
Hyderabad-500 046.

Rukmani Mohanta
Dr. Rukmani Mohanta
Professor
School of Physics
UNIVERSITY OF HYDERABAD
Hyderabad-500 046.

5	Mitesh Kumar Behera, Rukmani Mohanta. "Inverse seesaw in A5' modular symmetry", Journal of Physics G: Nuclear and Particle Physics, 2022 Publication	3%
6	www.frontiersin.org Internet Source	2%
7	docplayer.net Internet Source	<1%
8	Submitted to University of Hyderabad, Hyderabad Student Paper	<1%
9	publikationen.bibliothek.kit.edu Internet Source	<1%
10	Xin Wang, Bingrong Yu, Shun Zhou. " Double covering of the modular group and lepton flavor mixing in the minimal seesaw model ", Physical Review D, 2021 Publication	<1%
11	Submitted to KTH - The Royal Institute of Technology Student Paper	<1%
12	export.arxiv.org Internet Source	<1%
13	hdl.handle.net Internet Source	<1%

Rukmani Mohanta
Dr. Rukmani Mohanta
Professor
School of Physics
UNIVERSITY OF HYDERABAD
Hyderabad-500 046.

Rukmani Mohanta
Dr. Rukmani Mohanta
Professor
School of Physics
UNIVERSITY OF HYDERABAD
Hyderabad-500 046.

14	www.iir.berkeley.edu Internet Source	<1 %
15	mafiadoc.com Internet Source	<1 %
16	epdf.pub Internet Source	<1 %
17	theor.jinr.ru Internet Source	<1 %
18	Purushottam Sahu, Sudhanwa Patra, Prativa Pritimita. "Neutrino mass and lepton flavor violation in A4-based left–right symmetric model with linear seesaw", International Journal of Modern Physics A, 2022 Publication	<1 %
19	Dong Woo Kang, Jongkuk Kim, Takaaki Nomura, Hiroshi Okada. "Natural mass hierarchy among three heavy Majorana neutrinos for resonant leptogenesis under modular A4 symmetry", Journal of High Energy Physics, 2022 Publication	<1 %
20	Monal Kashav, Surender Verma. "Broken scaling neutrino mass matrix and leptogenesis based on A4 modular invariance", Journal of High Energy Physics, 2021 Publication	<1 %

21	Submitted to International Institute of Social Studies - Erasmus University Rotterdam Student Paper	<1 %
22	coek.info Internet Source	<1 %
23	repositorio.ufrn.br Internet Source	<1 %
24	repositorio.uam.es Internet Source	<1 %
25	G. C. Branco, R. González Felipe, F. R. Joaquim. " Leptonic violation ", Reviews of Modern Physics, 2012 Publication	<1 %
26	dro.dur.ac.uk Internet Source	<1 %
27	www.guspepper.net Internet Source	<1 %
28	vetiver.com Internet Source	<1 %
29	Submitted to University of Bucharest Student Paper	<1 %
30	amsdottorato.unibo.it Internet Source	<1 %
31	nozdr.ru Internet Source	<1 %

32	M. Sruthilaya, Rukmani Mohanta, Sudhanwa Patra. "$$A_4$$ A 4 realization of linear seesaw and neutrino phenomenology", The European Physical Journal C, 2018 Publication	<1 %
33	Submitted to University of Melbourne Student Paper	<1 %
34	dare.ubvu.vu.nl Internet Source	<1 %
35	discovery.researcher.life Internet Source	<1 %
36	link.springer.com Internet Source	<1 %
37	portal.tpu.ru Internet Source	<1 %
38	www.tara.tcd.ie Internet Source	<1 %
39	"XXIII DAE High Energy Physics Symposium", Springer Science and Business Media LLC, 2021 Publication	<1 %
40	d-nb.info Internet Source	<1 %
41	Helda.helsinki.fi Internet Source	<1 %

42	authors.library.caltech.edu Internet Source	<1%
43	onlinepubs.trb.org Internet Source	<1%
44	Mitesh Kumar Behera, Rukmani Mohanta. "Linear Seesaw in A5' Modular Symmetry With Leptogenesis", Frontiers in Physics, 2022 Publication	<1%
45	Submitted to University College London Student Paper	<1%
46	refubium.fu-berlin.de Internet Source	<1%

Exclude quotes	On	Exclude matches	< 14 words
Exclude bibliography	On		

PLAGIARISM FREE STATEMENT

This is to certify that the thesis entitled "**Phenomenological aspects of modular symmetry on neutrino mass models**" has been screened by the Turnitin software at the Indira Gandhi Memorial Library (IGML), University of Hyderabad. The software shows **54%** similarity index out of which, **20%** came from the candidate's pre-published version of research articles related to this thesis. Also, **22%**, **7%** and **2%** similarity index came from his published research articles in **Journal of Physics G: Nuclear and Particle Physics, 2021**, **Physics of the Dark Universe, 2022** and **Frontiers in Physics, 2022** respectively. The remaining effective similarity index of **3%** after excluding his research articles is below **10%** stipulated by the University guidelines. These similarities came from sources or articles in which the software detected mostly generic terms, standard notations, standard equations, standard symbols and common terminologies frequently used in the field. Therefore, this thesis is free from plagiarism.

Rukmani Mohanta

Prof. Rukmani Mohanta
Thesis Supervisor

Dr. Rukmani Mohanta
Professor
School of Physics
UNIVERSITY OF HYDERABAD
Hyderabad-500 046.